Assessment and stabilization of micaceous soils

By

Jiahe Zhang BSc (Hons)

Thesis submitted in fulfillment of the requirements for the degree of Doctor of Philosophy

The University of Adelaide

Faculty of Engineering, Computer and Mathematical Sciences

School of Civil, Environmental and Mining Engineering

Summary

Mica is a mineral widely distributed around the world. This mineral generally occurs in igneous, sedimentary and certain metamorphic rocks and, if breaks down from the parent rocks, shows a unique platy structure and high elasticity. These features may affect performance of soils adversely which mica lies in, causing instability concerns to construction work or infrastructure systems involving the micaceous soils. One of the solutions is to assess the adversities arising from occurrence of mica and, using chemical and mechanical techniques, to stabilize the micaceous soils. The research presented in this thesis was conducted to develop the solution and to provide suitable guidance to implement it. The research was divided into three important aspects: i) assessing the effect of mica content on the mechanical properties of clays, ii) stabilizing the micaceous soils mechanically or chemically with jute fiber, lime, granulated blast furnace slag (GBFS), and slag-lime, and iii) formulating the stabilization outcomes using the surface response methodology and optimizing the stabilization.

Different contents of mica were added to the soils to form the micaceous soils for testing. The experimental program consisted of consistency limits, standard Proctor compaction, unconfined compression (UC), direct shear and scanning electron microscopy tests. The test results suggested that the liquid and plastic limits exhibited a linearly increasing trend with an increase in the mica content. The rate of increase in the plastic limit, however, was observed to be greater than that of the liquid limit, thereby leading to a gradual transition towards a non-plastic behavior. The spongy nature and high-water demand of the mica minerals led to higher optimum water contents and lower maximum dry unit weights with an increase in the mica content. Under low confinement conditions, the strength properties were adversely affected by mica. However, the closer packing of the clay and mica components in the matrix under high confinement conditions offsets the adverse effects of mica by inducing the frictional resistance at the shearing interface.

A series of soil stabilization attempts were made to reinforce the micaceous soils. The combined capacity of mechanical stabilizer, jute fiber and different cementitious binders such as lime, GBFS and slag-lime, were examined towards ameliorating the inferior properties of micaceous clays. The test results indicated that the inclusion of fiber consistently improved the

ductility and toughness of the composite, and the addition of cementitious binders into soil-fiber composite further improved the connection interface, and thus led to the improvements in the composites' strength, stiffness and toughness. Moreover, a non-linear, multivariable regression model was developed to quantify the peak UC strength as a function of the fiber content, slag content and the curing time, and the predictive capacity of the proposed models was examined and further validated by statistical techniques. A sensitivity analysis was also carried out to assess the relative impacts of the independent regression variables on the UC strength. The proposed regression model contained a limited number of fitting parameters, all of which can be calibrated by a standard experimental effort, as well as simple explicit calculations, and hence implemented for preliminary design assessments and predictive purposes.

Response surface methodology (RSM) was employed to design the experiments, to evaluate the results and finally to optimize the binders' content. The results showed that slag exhibited a noticeable synergistic effect and greatly contributed to the stabilization of micaceous soils with the presence of fiber or polyacrylamide. The RSM-based optimization was able to determine the additives dosage in terms of targeted UC strength values, and based on the developed models, to identify the most efficient dosage of improving micaceous soils for backfilling or other construction works.

This research has delivered important outcomes for publications. The publications are listed below:

J-H Zhang, A Soltani, A Deng and M Jaksa, 2019. Mechanical performance of jute fiber-reinforced micaceous clay composites treated with ground-granulated blast-furnace slag. *Materials*. DOI: 10.3390/ma12040576

J-H Zhang, A Soltani, A Deng and M Jaksa, 2019. Mechanical behavior of micaceous clays. *J Rock Mech Geotech Eng*. DOI: 10.1016/j.jrmge.2019.04.001

J-H Zhang, A Deng and M Jaksa, 2019. Mechanical behaviour of micaceous soils stabilized by lime, slag-lime with fibers. Written in manuscript style for submission in one month

J-H Zhang, A Deng and M Jaksa, 2019. Optimization of slag and fiber/polymeric agent to reinforce micaceous soils using response surface methodology. Written in manuscript style for submission in one month

Keywords: Geotechnical engineering; micaceous clays; strength and testing of materials; scanning electron microscopy; multivariable regression; jute fibers; ground-granulated blast-furnace slag; polyacrylamide; polypropylene fibers; central composite design; response surface methodology

Statement of Originality

I certify that this work contains no material which has been accepted for the award of any other degree or diploma in my name, in any university or other tertiary institution and, to the best of my knowledge and belief, contains no material previously published or written by another person, except where due reference has been made in the text. In addition, I certify that no part of this work will, in the future, be used in a submission in my name, for any other degree or diploma in any university or other tertiary institution without the prior approval of the University of Adelaide and where applicable, any partner institution responsible for the joint–award of this degree.

I acknowledge that copyright of published works contained within this thesis resides with the copyright holder(s) of those works.

I also give permission for the digital version of my thesis to be made available on the web, via the University's digital research repository, the Library Search and also through web search engines, unless permission has been granted by the University to restrict access for a period of time.

I acknowledge the support I have received for my research through the provision of an Australian Government Research Training Program Scholarship.

Jiahe Zhang BSc (Hons)

Signature: __ __ **Date:** 02/05/2019

Acknowledgements

This Ph.D. research began in October 2015 and has been carried out on a full-time basis ever since. I would like to express my sincere gratitude to my supervisor, Dr. An Deng and Prof. Mark Jaksa, of the School of Civil, Environmental and Mining Engineering, for the patience, motivation, and continuous support throughout this Ph.D. study. Their guidance and encouragement have been of great value to me, and I could not have imagined

Besides my supervisors, I would like to thank my fellow Dr. Amin Soltani, not only for his invaluable contribution to this research, but also the encouragement, and kind support in life throughout the period of my candidature.

I am thankful to the School of Civil, Environmental and Mining Engineering, particularly the laboratory staff, Mr. Gary Bowman, Mr. Dale Hodson and Mr. Simon Golding, for their kind assistance with the experimental work.

Last but not the least, I would like to thank my family, especially my mother, for supporting me spiritually throughout this Ph.D. study, and the sacrifice she made throughout my life. She is the most important person in my world and I dedicate this thesis to her.

Table of Contents

Summary I
Statement of Originality IV
Acknowledgements V
Chapter 1: Thesis Overview 1
1.1. Problem Statement 1
1.2. Research Gaps 2
1.3. Research Objectives and Thesis Layout 3
1.4. Concluding Remarks 4
References 8
Chapter 2: Mechanical Behavior of Micaceous Clays 9
Abstract 9
Abbreviations 11
Notation 11
2.1. Introduction 13
2.2. Materials 14
2.2.1. Clay Soil 14
2.2.2. Ground Mica 14
2.3. Experimental Work 15
2.3.1. Sample Preparations 15
2.3.2. Unconfined Compression Test 16
2.3.3. Direct Shear Test 17
2.3.4. Scanning Electron Microscopy Studies 17
2.4. Results and Discussion 18
2.4.1. Effect of Mica Content on Soil Consistency 18
2.4.2. Effect of Mica Content on Soil Compaction 19
2.4.3. Effect of Mica Content on UC Strength 20
2.4.4. Effect of Mica Content on Shear Strength 21
2.4.5. Clay–Mica Interactions and SEM Analysis 23
2.5. Conclusions 24

Acknowledgments....25
Conflicts of Interest....25
References....26
List of Tables....30
List of Figures....34
Published copy....48
Chapter 3: Mechanical Performance of Jute Fiber-Reinforced Micaceous Clay Composites Treated with Ground-Granulated Blast-Furnace Slag....61
Abstract....61
3.1. Introduction....63
3.2. Materials....65
3.2.1. Micaceous Clay....65
3.2.2. Jute Fibers....66
3.2.3. Ground-Granulated Blast-Furnace Slag....67
3.3. Experimental Program....67
3.3.1. Mix Designs and Sample Preparations....67
3.3.2. Unconfined Compression Test....69
3.3.3. Scanning Electron Microscopy Studies....69
3.4. Results and Discussion....69
3.4.1. Effect of JF on UC Strength....69
3.4.2. Effect of JF + GBFS on UC Strength....71
3.4.3. Stabilization Mechanisms and Microstructure Analysis....73
3.5. Modeling....76
3.5.1. Model Development....76
3.5.2. Sensitivity Analysis....78
3.6. Conclusions....80
Author Contributions....81
Acknowledgments:....81
Conflicts of Interest....81
References....82
List of Tables....89
List of Figures....98
Published copy....111

Chapter 4: Mechanical Behavior of Micaceous Clays stabilized by Lime, Slag-lime with Fibers 134
Abstract 134
4.1. Introduction 136
4.2. Materials 137
4.2.1. Micaceous clay 137
4.2.2. Jute fibers 138
4.2.3. Cementitious binders 138
4.3. Overview of Experimentation 138
4.3.1. Sample preparation 138
4.3.2. Unconfined compression test 139
4.4. Results and Discussion 140
4.4.1. Effect of fibers on UC strength 140
4.4.2. Effect of fibers and lime on UC strength 141
4.4.3. Effect of fibers and slag-lime on UC strength 142
4.4.4. Discussion 143
4.5. Conclusions 144
Acknowledgments 145
Conflicts of Interest 145
References 146
List of Tables 149
List of Figures 154
Chapter 5: Optimization of slag and fiber/polymeric agent to reinforce micaceous soils using response surface methodology 162
Abstract 162
5.1. Introduction 164
5.2. Materials and methods 165
5.2.1. Soils 165
5.2.2. Ground Mica 165
5.2.3. Ground-Granulated Blast-Furnace Slag 166
5.2.4. Fibers 166
5.2.5. Polymeric agent 166

5.2.6. Response surface modelling 167
5.2.7. Sample preparations and experimental tests 168
5.3. Results and discussion 168
5.3.1. Determination of the regression model and statistical analysis 168
5.3.2. Effect of addition of slag and fiber on the UCS of micaceous soils 169
5.3.3. Effect of addition of slag and polymer on the UCS of micaceous soils 171
5.3.4. Optimization study 172
5.4. Conclusions 173
Acknowledgments 174
Conflicts of Interest 174
References 175
List of Tables 179
List of Figures 188

Chapter 1

Thesis Overview

1.1. Problem Statement

Mica is a mineral widely distributed around the world. The mineral generally occurs in igneous, sedimentary and certain metamorphic rocks and, if break down from the parent rocks, shows the unique platy structure and high elasticity. Due to the extremely-elastic properties of mica minerals, micaceous soils, and micaceous clays in particular, may deform remarkably under applied loads and hence affect the bulk compressibility of such soils. Mica minerals, although rather resilient, may gradually recover their initial shape due to the elastic rebound (or springy action), thereby reducing the efficiency of compactive effort and hence potentially compromising the performance of various facilities constructed on micaceous clays (Weinert 1980). When such soils are unloaded, the elastic rebound is likely to occur, resulting in undesirable volumetric expansions in the matrix. During compression, tension or shearing, the mica particles tend to rotate and orient themselves in a somewhat parallel fashion (attributed to mica's platy shape), thereby resulting in low strength resistance in micaceous soils (Harris *et al.* 1984). Over the past decades, the adverse effects of micaceous soils haven raised concerns in many countries around the world, such as South Africa (Paige-Green and Semmelink 2002), Malawi (Netterberg et al. 2011), Nigeria (Gogo 1984) and the U.K. (Northmore 1996).

The majority of documented studies have addressed the mechanical response of coarse-grained micaceous soils (e.g., Tubey 1961; Tubey and Bulman 1964; Moore 1971; Tubey and Webster 1978; Harris *et al.* 1984; Ballantine and Rossouw 1989; Clayton *et al.* 2004; Mshali and Visser 2012). There are limited studies involving the mechanical behavior of fine-grained micaceous soils. Of those examining fine-grained micaceous soils, no relationship was developed between the mica content and the mechanical behavior of these soils. Meanwhile, the ever-increasing need to expand urban areas to satisfy population growth and industrialization has required additional land, and in some cases, land with suboptimal soil properties. The utilization of local materials, one being micaceous clays, may eliminate the costs associated with transporting new materials from other locations. Therefore, the potential reuse of micaceous soils, and micaceous

clays in particular, need to be highly considered with the stabilization techniques to improve the performance against various engineering applications.

Common stabilization solutions to counteract the adversities associated with problematic soils include soil replacement and/or soil stabilization. In general, soil stabilization is preferred since the soil replacement is often impractical due to the costs associated with transporting new materials from other locations. Soil stabilization technique can be divided into chemical, mechanical or a combination of both techniques. The chemical technique generally includes the use of chemical agents, such as cement, limes, fly ashes, slags and more recently non-conventional agents such as polymers and resins. The addition of such binders into the soils fabric creates a series of short- and long-term chemical reactions in the soil-water system and thus results in materials with lower compressibility and higher strength in comparison with natural soils. The combination of chemical and mechanical stabilization techniques can be characterized as the optimum solution to reinforce the problematic soils in order to meet the intended engineering criteria. Conventional cementitious binders such as cement and lime, though proven effective, may bring some disadvantages: i) reduction in material ductility; and ii) environmental concerns due to greenhouse gas emissions. The inclusion of fibers can significantly improve the soil-binders bonding, improving the ductility) of such soils. Moreover, the amount of cementitious binders can be reduced due to the additional strength improvement by the fibers. Therefore, comprehensive studies on the utilizing the combination of chemical and mechanical techniques are highly encouraging.

1.2. Research Gaps

The contents presented in this thesis have addressed the following research gaps:

1) The mechanical response of micaceous clays has not well documented in the previous literature. The in-depth understanding of such soils, especially the influence of different mica content on the geotechnical properties of clay soils, needs to be studied. Therefore, the systematic investigation of clay characteristics (e.g., compaction characteristics, consistency limits, strength test and micro-structure analysis) of micaceous clays needs to be conducted.

2) The stabilization scheme on the micaceous clays remains rather limited, as the majority of literature sources have mainly emphasized on stabilization of the coarse-grained

micaceous soils. Moreover, those previous studies have shown that the traditional cementitious binders would improve the strength and soil density of coarse-grained micaceous soils. However, it would also compromise the ductility and residual strength. The use of traditional cementitious binders (lime) and sustainable binders (slag-lime and slag) as well as incorporating different fibers (jute fiber and polypropylene fibers) is highly recommended. These studies would understand the influence of the combination of fiber and cementitious binders on the mechanical behavior of micaceous clays, especially the interfacial interactions between fiber and reinforced soil matrix.

3) With the stabilization binders gaining viable improvement on the micaceous soils, the need for an efficient and simple tool to adequately predict the performance under field conditions, in terms of strength, arises as an inevitable necessity. The predict toolbox, if established, would help the geotechnical engineer arrive at qualified design without the time-consuming experimental tests. In this regards, response surface methodology (RSM) was employed to design the experiments, to evaluate the results and finally to optimize the binders' content in order to meet the design criteria.

1.3. Research Objectives and Thesis Layout

The thesis consists of fiver chapters and is presented in the format of a **thesis by publication**. The current chapter, **Chapter 1**, provides an introduction to this research, and includes topics such as problem statement, research gaps, research objectives, these layouts and concluding remarks. **Chapters 2** to **5** include 4 published, accepted for publication and unpublished/unsubmitted work written in a manuscript style, which intend to address the three research gaps outlined in the previous section. A brief description of **Chapters 2** to **5** is provided as follows:

- **Chapter 2** includes an accepted journal paper entitled "Mechanical Behavior of Micaceous Clays", which intends to address **Research Gap #1** (see **section 2**). The details of this publication are as follows:

> **Zhang J**, Soltani, A, Deng A and Jaksa M **(2019)** Mechanical behavior of micaceous clays. ***Journal of Rock Mechanics and Geotechnical Engineering***, https://doi.org/10.1016/j.jrmge.2019.04.001

- **Chapter 3** includes a published journal paper entitled "Mechanical Performance of Jute-Reinforced Micaceous Clay Composites Treated with Ground-Granulated Blast-Furnace Slag", which intends to address **Research Gap #2** (see **section 2**). The details of this publication are as follows:

> **Zhang J**, Soltani, A, Deng A and Jaksa M **(2019)** Mechanical Performance of Jute-Reinforced Micaceous Clay Composites Treated with Ground-Granulated Blast-Furnace Slag. ***Materials***, 12(4), 576:1-23. http://doi.org/10.3390/ma12040576

- **Chapter 4** includes an unpublished/unsubmitted work written in a manuscript style paper entitled "Mechanical Behavior of Micaceous Clays stabilized by Lime, Slag-lime with Fibers", which intends to address **Research Gap #2** (see **section 2**). The details of this potential publication are as follows:

> **Zhang J**, Deng A and Jaksa M **(2019)** Mechanical behavior of micaceous soils stabilized by lime and slag-lime with fibers, x(x):x-x, http://doi.org/x[1]

- **Chapter 5** includes an unpublished/unsubmitted work written in a manuscript style paper entitled "Optimization of slag and fiber/polymeric agent to reinforce micaceous soils using response surface methodology", which intends to address **Research Gap #3** (see **section 2**). The details of this potential publication are as follows:

> **Zhang J**, Deng A and Jaksa M **(2019)** Optimization of slag and fiber/polymeric agent to reinforce micaceous soils using response surface methodology, x(x):x-x, http://doi.org/x[2]

1.4. Concluding Remarks

The following conclusions can be drawn from this study:

- The liquid and plastic limits exhibited a linear, monotonically-increasing trend with an increase in the mica content. The rate of increase in the plastic limit with respect to mica content was observed to be approximately three-fold greater than that of the liquid limit.

[1] **Unpublished and unsubmitted work written in a manuscript style**
[2] **Unpublished and unsubmitted work written in a manuscript style**

As a result, the plasticity index experienced a linear, monotonically-decreasing trend with respect to mica content, thereby indicating a gradual transition towards a non-plastic, cohesionless character. [see **chapter 2**]

- The mica content influenced the optimum water content of the clay soil, following a linear, monotonically-increasing trend. In contrast, the maximum dry unit weight exhibited a linear, monotonically-decreasing trend with respect to mica content. Compaction problems associated with micaceous soils was attributed to mica's high water demand, as well as its soft, spongy fabric which promotes a rebound response to compaction energy. [see **chapter 2**]

- As a result of mica inclusion, the stress-strain response, under unconfined compression (UC) loading conditions, progressively transitioned towards a strain-softening character and hence a more dramatic, brittle failure. The UC parameters — strength, ductility, toughness and stiffness — were all adversely affected by mica, with higher mica contents exhibiting lower UC parameters, following an exponential tendency for reduction. [see **chapter 2**]

- In most cases, the stress-displacement response, under direct shear (DS) testing conditions, exhibited a strain-hardening behavior. This effect, however, was slightly less pronounced for samples with higher mica contents, such as 25% and 30%, at higher normal stresses. At normal stresses equal to or less than 200 kPa, the shear strength decreased with an increase in the mica content, while the opposite occurred at higher normal stresses of 300 kPa and 400 kPa. The latter was attributed to the compact packing of the clay and mica components in the matrix under high confinement conditions, which offsets the adverse effects of mica by inducing frictional resistance at the shearing interface. [see **chapter 2**]

- The apparent shear strength parameters, namely the cohesion and the angle of internal friction, were also dependent on the mica content. In terms of cohesion, higher mica contents led to lower cohesion values, following an exponentially-decreasing trend. In contrast, higher mica contents led to increased angles of internal friction; this behavior justifies the observed improvement in shear strength at high confinement conditions. [see **chapter 2**]

- For any given granulated blast furnace slag (GBFS) content and curing time, the greater the jute fiber (JF) content the higher the developed strength and stiffness up to Fc = 1%; beyond

1% JF, the effect of JF-reinforcement adversely influenced the development of strength and stiffness. The composite's ductility and toughness, however, were consistently in favor of JF-reinforcement, meaning that the greater the JF content the higher the developed ductility and toughness. [see **chapter 3**]

- For any given JF content, the greater the GBFS content and/or the longer the curing period, the higher the developed strength, stiffness and toughness, following monotonically-increasing trends. The composite's ductility, however, was adversely influenced by GBFS-treatment, meaning that the greater the GBFS content and/or the longer the curing period, the lower the developed ductility. [see **chapter 3**]

- A non-linear, multivariable regression model was developed to quantify the peak UC strength q_u as a function of the composite's basic index properties, i.e., JF content F_c, GBFS content S_c, and curing time T_c. The predictive capacity of the suggested model was examined and further validated by statistical techniques. A sensitivity analysis was also carried out to quantify the relative impacts of the independent regression variables, namely F_c, S_c and T_c, on the dependent variable q_u. The proposed regression model contained a limited number of fitting parameters, all of which can be calibrated by little experimental effort, as well as simple explicit calculations, and hence implemented for preliminary design assessments, predictive purposes and/or JF + GBFS optimization studies. [see **chapter 3**]

- The inclusion of JF can increase the UC strength of micaceous soils, and the greater the JF, the higher the developed strength and stiffness. However, the largest peak strength was reached at the fiber content of 1.0% and that, considering the JF content of 1.0% as a threshold, and then the strength had a slight decrease on the strength of the soils with 1.5% of fibers. At any given content of JF, the compressive strength of reinforced soil increased with the addition of lime or slag-lime, and the improvement is more significant with the inclusion of slag-lime. The greater the cementitious binders and/or the longer the curing time, the higher the developed strength, stiffness and toughness. However, the ductility of the samples decreased with the cementitious binders and/or the longer period time. [see **chapter 4**]

- The response surface methodology (RSM), together with the central composite design (CCD), is one of the suitable methods enabling optimization of additives dosage in soil

stabilization. Models were developed as a tool to predict the UC strength of the micaceous soils which were stabilized by the combinations of slag and fiber/slag and polymer. Excellent agreement was obtained between the model prediction results and actual test results, for the samples tested in this study. [see **chapter 5**]

- The additions of slag and fiber/slag and polymer were able to stabilize the micaceous soils. The additives exhibited varied effects on the stabilization. Slag exhibited a noticeable synergistic effect and greatly contributed to the stabilization of micaceous soils with the presence of fiber or polycom. [see **chapter 5**]

- The RSM-based optimization was able to determine the additives dosage in terms of the targeted UC strength value, and based on the developed models, identified the most efficient dosage of improving micaceous soils for backfilling or comparable construction work. The performance of the model optimization was verified in additional laboratory tests. The test results agreed with the prediction results, suggesting that the optimization process was feasible. [see **chapter 5**]

References

Ballantine, R.W., & Rossouw, A.J. (1989) *Stabilization of Soils*. PPC Lime Ltd, Pretoria, South Africa.

Clayton, C.R., Theron, M., & Vermeulen, N. (2004) The effect of particle shape on the behaviour of gold tailings. In *Advances in Geotechnical Engineering: The Skempton Conference* (Jardine RJ, Potts DM and Higgins KG (eds)). ICE Publishing, London, UK, pp. 393–404, http://doi.org/10.1680/aigev1.32644.0017

Gogo, J.O. (1984) Compaction and strength characteristics of decomposed mica schist. *In: Proceedings of the 8th Regional Conference for Africa on Soil Mechanics and Foundation Engineering*. Harare, Zimbabwe: A.A. Balkema; p. 275–284. ISBN:9061915325

Harris,W.G., Parker, J.C., & Zelazny, L.W. (1984) Effects of mica content on engineering properties of sand. *Soil Science Society America Jouranal.*;48(3):501–5. http://doi.org/10.2136/sssaj1984.03615995004800030006x

Moore, C.A. (1971) Effect of mica on K_0 compressibility of two soils. *Journal of the Soil Mechanics and Foundations Division* 97(SM9): 1275–1291.

Mshali, M.R., & Visser, A.T. (2012) Influence of mica on unconfined compressive strength of a cement–treated weathered granite gravel. *Journal of the South African Institution of Civil Engineering* 54(2): 71–77.

Netterberg, F., Hefer, A. & Preez, H.D. (2011). Cracking and staining of an airport asphalt. *In: Proceedings of the 10th Conference on Asphalt Pavements for South Africa (CAPSA 11): Roads of the Future. KwaZulu KwaZulu–Natal*, South Africa: International Road Federation (IRF), 1–17.

Northmore, K.J., Bell, F.G., & Culshaw, M.G. (1996). The engineering properties and behaviour of the brickearth of south Essex. *Q J Eng Geol Hydrogeol*.; 29(2):147–61. http://doi.org/10.1144/gsl.qjegh.1996.029.p2.04

Paige-Green, P., & Semmelink, C.J. (2002) Road compaction problems related to the presence of biotite. *In: Proceedings of the 9th Congress of the International Association of Engineering Geology and the Environment*. Durban, KwaZulu–Natal, South Africa, p. 2605–2610.

Tubey, L.W. (1961) *A Laboratory Investigation to Determine the Effect of Mica on the Properties of Soils and Stabilized Soils*. Research Note 4077, Road Research Laboratory (RRL), Wokingham, Berkshire, UK.

Tubey, L.W., & Bulman, J.N. (1964) Micaceous soils: Methods of determining mica content and the use of routine tests in the evaluation of such soils. *Proceedings of the Australian Road Research Board (ARRB)*, 2(2): 880–901.

Tubey, L.W., & Webster, D.C. (1978) *The Effects of Mica on the Roadmaking Properties of Materials*. Supplementary Report 408, Transport and Road Research Laboratory, Wokingham, Berkshire, UK, ISBN:03051315.

Weinert, H.H. (1980) The Natural Road Construction Materials of Southern Africa (1st Ed). Cape Town, Western Cape, South Africa: H&R Academica, ISBN:0860740470

Chapter 2

Mechanical Behavior of Micaceous Clays

Jiahe Zhang [1,*] , Amin Soltani [2] , An Deng [3] , Mark B. Jaksa [4]

[1] **PhD Student** — School of Civil, Environmental and Mining Engineering, The University of Adelaide, Adelaide SA 5005, Australia | **Email:** Jiahe.Zhang@adelaide.edu.au

[2] **Research Academic** — School of Civil, Environmental and Mining Engineering, The University of Adelaide, Adelaide SA 5005, Australia | **Email:** Amin.Soltani@adelaide.edu.au ; **ORCID:** 0000-0002-0483-7487

[3] **Senior Lecturer** — School of Civil, Environmental and Mining Engineering, The University of Adelaide, Adelaide SA 5005, Australia | **Email:** An.Deng@adelaide.edu.au ; **ORCID:** 0000-0002-3897-9803

[4] **Professor** — School of Civil, Environmental and Mining Engineering, The University of Adelaide, Adelaide SA 5005, Australia | **Email:** Mark.Jaksa@adelaide.edu.au

* Corresponding Author.

Zhang J, Soltani A, Deng A and Jaksa M. B. **(2019)** Mechanical behavior of micaceous clays. ***Journal of Rock Mechanics and Geotechnical Engineering***, https://doi.org/10.1016/j.jrmge.2019.04.001

Abstract

This study investigates the effect of mica content on the mechanical properties of clays. Commercially-available ground mica was blended with a locally-available clay soil, at varying mica contents of 5%, 10%, 15%, 20%, 25% and 30% (by mass), to artificially prepare various micaceous clay blends. The preliminary testing phase included consistency limits and standard Proctor compaction tests. The primary testing program consisted of Unconfined Compression (UC), Direct Shear (DS) and Scanning Electron Microscopy (SEM) tests. The liquid and plastic limits exhibited a linear, monotonically-increasing trend with increase in the mica content. The

rate of increase in the plastic limit, however, was found to be greater than that of the liquid limit, thereby leading to a gradual transition towards a non-plastic, cohesionless character. The soft, spongy fabric and high water demand of the mica mineral led to higher optimum water contents and lower maximum dry unit weights with increase in the mica content. Under low confinement conditions, i.e., the UC test and the DS test at low normal stresses, the shear strength was adversely affected by mica. However, the closer packing of the clay and mica components in the matrix under high confinement conditions offsets the adverse effects of mica by inducing frictional resistance at the shearing interface, thus leading to improved strength resistance.

Keywords: Micaceous clay; mica content; consistency limits; compaction; shear strength; confinement; frictional resistance.

Abbreviations

AS	Australian standard
CI	Clay with intermediate plasticity
CV	Coefficient of variation
DS	Direct shear
DUW	Dry unit weight
MDUW	Maximum dry unit weight
MH	Silt with high plasticity
MI	Silt with intermediate plasticity
NP	Non-plastic
OWC	Optimum water content
SD	Standard deviation
SEM	Scanning electron microscopy
UC	Unconfined compression
USCS	Unified soil classification system
UU	Unconsolidated undrained
WC	Water content

Notation

c	Cohesion (DS test)
E_{50}	Elastic stiffness modulus (UC test)
e_{opt}	Optimum void ratio
E_u	Strain energy at peak (UC test)
G_s^M	Specific gravity of ground mica
G_s^S	Specific gravity of soil solids
I_P	Plasticity index
M_c	Mica content (by mass)
q_u	Peak UC strength
R^2	Coefficient of determination
S_a	Specific surface area
S_R	Degree of saturation
w_L	Liquid limit
w_{opt}	Optimum water content
w_P	Plastic limit
γ_{dmax}	Maximum dry unit weight
$\Delta\delta$	Horizontal displacement
ε_u	Failure axial strain (UC test)
η	Rate of increase/decrease in shear strength with respect to mica content

$\boldsymbol{\sigma_n}$	Normal stress (DS test)
$\boldsymbol{\tau_p}$	Shear strength (DS test)
$\boldsymbol{\varphi}$	Angle of internal friction (DS test)

2.1. Introduction

The mica group of sheet silicates are among the most widely distributed minerals around the world; they generally occur in igneous, sedimentary and certain metamorphic rocks (Harvey 1982; Galán and Ferrell 2013). Although the compositions and properties of mica minerals vary depending on their geological formation and climatic conditions, the unique platy structure, high elasticity and nearly-perfect basal cleavage (owing to the hexagonal sheet-like arrangement of mica atoms) are the common features which demand further attention (Zhang *et al.* 2019). Where mica minerals are separated from their host rocks, these features may affect naturally-weathered soils, thus leading to some adverse changes in the mechanical behavior of such soils.

Due to the extremely-elastic properties of mica minerals, attributed to mica's soft, spongy fabric, micaceous soils, and micaceous clays in particular, may deform remarkably under applied load and hence affect the bulk compressibility of such soils. Mica minerals, although rather resilient, may gradually recover their initial shape due to the elastic rebound (or springy action), thereby reducing the efficiency of compactive effort and hence potentially compromising the performance of various facilities constructed on micaceous clays (Weinert 1980). When such soils are unloaded, elastic rebound is likely to occur, resulting in undesirable volumetric expansion in the matrix. During compression, tension or shearing, the mica particles tend to rotate and orient themselves in a somewhat parallel fashion (attributed to mica's platy shape), thereby resulting in low strength resistance in micaceous soils (Harris *et al.* 1984). Therefore, micaceous soils are characterized by high compressibility, poor compactibility and low shear strength; such attributes present significant challenges for road construction, building foundations, earth dams and other geotechnical engineering systems, as reported in several countries around the world (e.g., Mitchell *et al.* 1975; Gogo 1984; Northmore *et al.* 1996; Paige-Green and Semmelink 2002; Netterberg *et al.* 2011).

The majority of documented studies have addressed the mechanical response of coarse-grained micaceous soils (e.g., Tubey 1961; Tubey and Bulman 1964; Moore 1971; Tubey and Webster 1978; Harris *et al.* 1984; Ballantine and Rossouw 1989; Clayton *et al.* 2004; Mshali and Visser 2012, 2014; Zhang *et al.* 2019). To the authors' knowledge, however, there are still limited studies involving the mechanical behavior of fine-grained micaceous soils. Of those examining fine-grained micaceous soils, no relationship was developed between the mica content and the mechanical behavior of these soils. Meanwhile, the ever-increasing need to expand urban areas

to satisfy population growth and industrialization has required additional land, and in some cases, land with suboptimal soil properties. The utilization of local materials, one being micaceous clays, may eliminate the costs associated with transporting new materials from other locations. Therefore, the potential reuse of micaceous soils, and micaceous clays in particular, can lead to improved efficiencies and enhanced infrastructure performance, if an in-depth understanding of their geotechnical properties can be obtained.

The present study seeks to investigate the effect of mica content on the mechanical properties of clays. A test program was designed and conducted, which consisted of two phases, namely preliminary and primary tests. The preliminary testing phase included consistency (Atterberg) limits and standard Proctor compaction tests, and the primary tests consisted of Unconfined Compression (UC) and Direct Shear (DS) tests. Moreover, Scanning Electron Microscopy (SEM) studies were carried out to observe the evolution of fabric in response to the mica inclusions, and thus perceive clay–mica interactions.

2.2. Materials

2.2.1. Clay Soil

Locally-available reddish-brown clay was used for this study; it was sourced from a landfill site located near Adelaide, South Australia. The physical and mechanical properties of the clay soil, hereafter simply referred to as the natural soil, were determined as per relevant ASTM and Australian (AS) standards, and the results are summarized in **Table 1**. The conventional grain-size analysis (ASTM D422–07) indicated a clay fraction (< 2 μm) of 37%, along with 32% silt (2–75 μm) and 32% sand (0.075–4.75 mm). In terms of consistency, the liquid limit and plasticity index were, respectively, measured as w_L = 46.21% and I_P = 28.10%; the soil was hence classified as *clay with intermediate plasticity* (CI) in accordance with the Unified Soil Classification System (USCS). The standard Proctor compaction test carried out as per ASTM D698–12, indicated an optimum water content of w_{opt} = 22.04% corresponding to a maximum dry unit weight of γ_{dmax} = 16.21 kN/m^3.

2.2.2. Ground Mica

Commercially-available ground mica, sourced from a local distributor, was used to artificially prepare various micaceous clay blends. The physical and chemical properties of the ground mica, as supplied by the manufacturer, are summarized in **Table 2**. In terms of grain-size

distribution, the ground mica consisted of a fines fraction (< 75 μm) of 93%, along with 7% sand (0.075–4.75 mm). The specific gravity of the mica particles was found to be $G_s^M = 2.80$, which is quite similar to that of natural fine-grained soils including the one used in the present study, i.e., $G_s^S = 2.74$. Other physical properties included a specific surface area of $S_a = 5.30$ m^2/g. The chemical composition of the ground mica was found to be dominated by silicon dioxide (SiO_2) and aluminum trioxide (Al_2O_3) with mass fractions of 49.5% and 29.2%, respectively. In terms of acidity, the ground mica slurry was classified as a neutral substance corresponding to a pH of 7.8.

2.3. Experimental Work

In this study, a total of seven soil–mica mix designs consisting of one control, the natural soil, and six micaceous clay blends were examined (see **Table 3**). Hereafter, the coding system M_x — where x is the mica content or M_c, and x = {0, 5, 10, 15, 20, 25, 30} — is used to designate the various mix designs; the mica content was defined as the ground mica to the natural soil mass ratio. As such, 'M_0' refers to the natural soil with no mica inclusion (or $M_c = 0$), and 'M_{30}', for instance, refers to a soil–mica blend containing 30% mica by dry mass of the natural soil (or $M_c = 30\%$). The experimental program was carried out in two phases consisting of preliminary and primary tests. The preliminary testing phase included a series of consistency (Atterberg) limits (as per AS 1289.3.9.1–15, AS 1289.3.2.1–09 and AS 1289.3.3.1–09) and standard Proctor compaction (as per ASTM D698–12) tests, and the results are partially summarized in **Table 3**. The primary testing program consisted of Unconfined Compression (UC), Direct Shear (DS) and Scanning Electron Microscopy (SEM) tests. The methodologies associated with each component of the primary testing program, as well as the sample preparation techniques, are discussed in detail below.

2.3.1. Sample Preparations

Samples for the UC and DS tests were prepared by the static compaction technique, as commonly adopted in the literature for fine-grained geomaterials (e.g., Estabragh *et al.* 2016[a]; Soltani *et al.* 2018[a], 2018[b]), at the corresponding standard Proctor optimum condition of each mixture, i.e., the optimum water content and the maximum dry unit (see w_{opt} and γ_{dmax} **Table 3**). The natural soil and ground mica were blended in dry form as per the selected mix designs outlined in **Table 3**, i.e., M_x where x = {0, 5, 10, 15, 20, 25, 30}. Mixing was carried out for approximately 5 minutes to gain visible homogeneity of the soil and mica particles. The

required volume of water corresponding to the desired optimum water content (see w_{opt} in **Table 3**) was added to each blend and thoroughly mixed by hand for approximately 15 minutes; extensive care was dedicated to pulverizing the clumped particles, targeting homogeneity of the moist mixtures. The moist mixtures were then sealed in plastic bags and were allowed to cure for approximately 24 hours to ensure an even distribution of moisture throughout the mixtures' mass. It should be noted that the artificial soil–mica blends exhibited the same typical texture, sheen and friability properties as natural micaceous soils reported in the literature, and thus may well provide a basis for systematically studying the effect of mica content on the mechanical behavior of fine-grained soils. A conventional split mold, similar to that described by the authors in Soltani *et al.* (2017[b]) and Zhang *et al.* (2019), was designed and fabricated from stainless steel to accomplish static compaction. The split mold consisted of three sections, i.e., the top collar, the middle section and the bottom collar. The middle section measures 50 mm in diameter and 100 mm in height; it accommodates the compacted sample for the UC test (see **Section 3.2**). Each of the seven moist mixtures was statically compressed in the mold (at a constant displacement rate of 1.5 mm/min) in five layers to a specific compaction load, each layer having attained its target maximum dry unit weight (see γ_{dmax} in **Table 3**). Samples for the DS tests (see **Section 3.3**) were prepared in a similar fashion to that described above; however, the moist mixtures were directly compacted in the shear box (measuring 60 mm × 60 mm in plane and 20 mm in height) in three layers (Soltani *et al.* 2019[a], 2019[b]).

To ensure consistency in void ratio (or porosity) and hence uniformity of fabric, particularly with regard to the samples prepared for the UC tests, the variations of Dry Unit Weight (DUW) and Water Content (WC) should be measured along the height of the compacted samples (Estabragh and Javadi 2008; Zhang *et al.* 2019). In this regard, representative samples, namely M_0 (natural soil), M_{10}, M_{20} and M_{30} were examined, and the results are provided in **Figure 1**. For all four cases, the variations of both DUW and WC were found to be rather marginal, as is evident with the low standard deviations (SD), which in turn corroborates the suitability and hence repeatability of the implemented static compaction technique.

2.3.2. Unconfined Compression Test

Unconfined Compression (UC) tests were carried out on the natural soil (M_0) and various soil–mica blends — M_x where x = {5, 10, 15, 20, 25, 30} — in accordance with the ASTM D2166–16 standard. The samples, prepared as per **Section 3.1**, were axially compressed at a constant displacement rate of 1 mm/min (= 1%/min), as suggested in the literature (e.g., Estabragh *et al.*

2016[b]; Soltani *et al.* 2017[a], 2017[b]). For each sample, the axial strains and the corresponding axial stresses were recorded at various time intervals to a point at which the maximum axial stress required for sample failure, the peak UC strength, and its corresponding axial strain, a measure of the sample's ductility, were achieved. To ensure sufficient accuracy, triplicate samples were tested for each mix design, and the median value was considered for further analyses. The standard deviation (SD) and the coefficient of variation (CV) for the triplicate peak UC strength data were found to range between SD = 3.37 kPa (for M_0) and 7.65 kPa (for M_{20}), and CV = 1.82% (for M_0) and 8.06% (for M_{30}); the low SD and CV values corroborate the repeatability of the adopted sample preparation technique (particularly the static compaction), as well as the implemented UC testing procedure (Zhao *et al.* 2019; Zhang *et al.* 2019). On account of the three replicates adopted for each mixture, a total of 21 UC tests were carried out to address the seven mix designs outlined in **Table 3**.

2.3.3. Direct Shear Test

Unconsolidated Undrained (UU) Direct Shear (DS) tests were carried out on the natural soil (M_0) and various soil–mica blends — M_x where x = {5, 10, 15, 20, 25, 30} — in accordance with the AS 1289.6.2.2–98 standard. As outlined in **Section 3.1**, the various mixtures were statically compacted in the shear box, measuring 60 mm × 60 mm in plane and 20 mm in height, at their respective standard Proctor optimum condition (see w_{opt}, γ_{dmax} and e_{opt} in **Table 3**); they were then tested for shear strength at varying normal stresses of σ_n = 100 kPa, 200 kPa, 300 kPa and 400 kPa. A high shear rate of 1 mm/min (= 1.67%/min) was adopted for the shearing phase to minimize both drainage and excess pore-water pressure effects (Sezer *et al.* 2006; Bai and Liu 2012; Qu and Zhao 2016). For each DS testing scenario, the shear stresses were recorded as a function of the horizontal displacements up to a total displacement of 10 mm to quantify and hence perceive the stress–displacement response at both peak and post-peak conditions. Finally, the conventional Mohr–Coulomb failure criterion, using a total stress approach, was implemented to arrive at the apparent shear strength parameters, namely the cohesion and the angle of internal friction (Al-Aqtash and Bandini 2015; Soltani *et al.* 2019[a], 2019[b]). On account of the four normal stresses applied for each mixture, a total of 28 DS tests were carried out to address the seven mix designs outlined in **Table 3**.

2.3.4. Scanning Electron Microscopy Studies

The Scanning Electron Microscopy (SEM) technique was implemented to observe the evolution of fabric in response to the mica inclusions. In this regard, typical mix designs

consisting of the natural soil (M_0), M_5 and M_{30} were examined. The desired samples — which were prepared in a similar fashion to that described for the UC test (see **Section 3.1**) — were first air-dried for approximately 14 days. The desiccated samples were carefully fractured into small cubic-shaped pieces measuring approximately 1 cm^3 in volume, as suggested in the literature (e.g., Mirzababaei *et al.* 2009; Estabragh *et al.* 2016[b]; Soltani *et al.* 2018[b]). The fractured samples were then scanned by means of the Philips XL20 scanning electron microscope (Amsterdam, The Netherlands) at various magnification ratios ranging from 250× to 20,000×. It should be mentioned that the microstructure analyses were carried out using an SEM characterization scheme developed by the authors in Soltani *et al.* (2018[b]) and Zhang *et al.* (2019).

2.4. Results and Discussion

2.4.1. Effect of Mica Content on Soil Consistency

Figure 2 illustrates the variations of the consistency limits — liquid limit w_L, plastic limit w_P, and plasticity index I_P (= $w_L - w_P$) — against mica content M_c for the tested mix designs. The mica content was positively proportional to the liquid and plastic limits, and both consistency limits followed a linear, monotonically-increasing trend with respect to mica content. Interestingly, the rate of increase in w_P (with respect to M_c) was found to be approximately three-fold greater than that of w_L, i.e., $\Delta w_P/\Delta M_c = +0.899$ compared with $\Delta w_L/\Delta M_c = +0.263$. As a result, the plasticity index experienced a linear, monotonically-decreasing trend with respect to mica content (decrease rate was $\Delta I_P/\Delta M_c = -0.635$), thereby signifying a gradual transition towards a non-plastic, cohesionless character. In terms of the plastic limit, for instance, the natural soil (M_0) resulted in w_P = 18.11%, while the inclusion of 5%, 10%, 15%, 20%, 25% and 30% mica (M_5 to M_{30}) resulted in higher values of w_P = 20.61%, 24.01%, 29.71%, 32.18%, 38.92% and 45.11%, respectively. The soft, spongy fabric (and hence high elasticity) of mica minerals make for a rather difficult, if not impossible, implementation (and hence reproducibility) of the rolling thread method for plastic limit measurements. Even though mica inclusion would theoretically lead to an increased plastic limit, one cannot arrive at a certain/unique value with confidence by following the current methodology (Tubey and Bulman 1964). Despite several attempts by different operators, a notable variability, as much as ±8% water content, seemed to dominate the plastic limit measurements, thereby suggesting the inapplicability of the current consistency limits framework, the rolling thread method in particular, for fine-grained micaceous soils. The plasticity index often serves as a measure of

the soil's apparent cohesion, with higher values manifesting a more cohesive character (Sridharan and Prakash 1999). As such, a decrease in the plasticity index, as is the case with mica inclusion, signifies a potential reduction in the soil's apparent cohesion and hence its undrained shear strength. This hypothesis will be further examined (and confirmed) by means of the UC and DS tests, the results of which will be presented in **Sections 4.3** and **4.4**, respectively.

Figure 3 illustrates the location of the seven soil–mica mixtures on Casagrande's plasticity chart. As demonstrated in the figure, the variations of I_P against w_L follows a linear path, diagonal to the 'A' and 'U' lines of the plasticity chart (see the arrowed line in **Figure 3**); the linear relationship can be expressed as $I_P = -2.37\ (w_L - 57.54)$ where $R^2 = 0.988$. Most documented studies in this context, such as Tubey (1961), have noted a non-linear transition over the I_P:w_L space, which contradicts that observed in the present study. The natural soil (M_0) was characterized as CI "*clay with intermediate plasticity*". An increase in the mica content, however, gradually translated the soil towards the MI "*silt with intermediate plasticity*" and MH "*silt with high plasticity*" categories, as shown by the arrowed line in **Figure 3**. In this case, the inclusion of 5%, 10%, 15%, 20%, 25% and 30% mica (M_5 to M_{30}) changed the original CI classification to CI, CI, MI, MI, MH and MH, respectively. Given the observed trend, a further increase in the mica content could potentially result in w_P values equal to or greater than w_L, and thus give rise to null or negative I_P ($= w_L - w_P$) values, implying a non-plastic, cohesionless (NP) behavior. It should be noted that the gradual transition towards the NP character has also been recognized by previous researchers such as Tubey (1961) and Mshali and Visser (2012, 2014).

2.4.2. Effect of Mica Content on Soil Compaction

Standard Proctor compaction curves, along with representative saturation lines (for $G_s^S = 2.74$), are illustrated in **Figure 4a** for the tested mix designs. With an increase in the mica content, the compaction curve experienced a notable downward–rightward shift, thus suggesting an increase in the optimum water content w_{opt} and a decrease in the maximum dry unit weight γ_{dmax}. The peak (or optimum) point for all mixtures was found to lie between the $S_R = 80\%$ and 100% saturation lines (see **Figure 4b**), which is consistent with that commonly reported in the literature for natural fine-grained soils (e.g., Pandian *et al.* 1997; Sridharan and Nagaraj 2005; Soltani *et al.* 2018[c]). Moreover, the peak points followed a linear decreasing trend with an

increase in the mica content M_c (see the arrowed line in **Figure 4b**), thereby signifying the existence of a linear relationship for both w_{opt} and γ_{dmax} with M_c.

Figure 5 presents the variations of the compaction characteristics — w_{opt} and γ_{dmax} — against mica content M_c for the tested mix designs. An increase in the mica content resulted in higher optimum water contents, which followed a linear, monotonically-increasing trend with an increase rate of $\Delta w_{opt}/\Delta M_c$ = +0.154. In contrast, the maximum dry unit weight exhibited a linear, monotonically-decreasing trend with a decrease rate of $\Delta\gamma_{dmax}/\Delta M_c$ = –0.052. The natural soil (M_0) resulted in w_{opt} = 22.04% (corresponding to γ_{dmax} = 16.21 kN/m^3), while the addition of 5%, 10%, 15%, 20%, 25% and 30% mica (M_5 to M_{30}) resulted in w_{opt} = 22.52%, 23.33%, 24.33%, 25.00%, 25.80% and 26.50% (corresponding to γ_{dmax} = 15.94 kN/m^3, 15.63 kN/m^3, 15.25 kN/m^3, 15.01 kN/m^3, 14.89 kN/m^3 and 14.70 kN/m^3), respectively. Compaction problems associated with micaceous soils can be attributed to mica's high water demand, as well as its soft, spongy fabric (Tubey 1961; Tubey and Webster 1978; Ballantine and Rossouw 1989; Mshali and Visser 2012, 2014). Mica minerals rebound when unloaded and hence offset a portion of the compaction energy applied to the mixtures, thus yielding a lower maximum dry unit weight (or higher void ratio). The higher void ratio, which is proportional to the mica content, suggests the existence of a series of inter- and intra-assemblage pore-spaces, respectively, formed between and within the clay aggregates; these pore-spaces facilitate the adsorption of water by clay particles, and thus may potentially result in some adverse behaviors, e.g., increased swelling, low strength resistance and high permeability.

2.4.3. Effect of Mica Content on UC Strength

Stress–strain curves, obtained from the UC tests, are provided in **Figure 6** for the tested samples. The stress–strain locus for the natural soil sample exhibited a strain-hardening behavior and hence a rather robust, non-brittle failure. As a result of mica inclusion, the stress–strain response progressively transitioned towards a strain-softening character and hence a more dramatic, brittle failure. The peak UC strength was inversely dependent to the mica content, with higher mica contents exhibiting lower peak UC strength values. The natural soil (M_0) resulted in a peak UC strength of q_u = 186.17 kPa, while the addition of 5%, 10%, 15%, 20%, 25% and 30% mica (M_5 to M_{30}) resulted in lower values of 144.90 kPa, 126.41 kPa, 102.89 kPa, 98.05 kPa, 94.11 kPa and 93.12 kPa, respectively. Interestingly, low mica contents, as low as M_c = 5%, could raise serious strength concerns when present in the soil matrix. The failure axial strain, denoted as ε_u, is an indication of the material's ductility, with higher values

suggesting a more ductile character (Estabragh *et al.* 2017; Soltani *et al.* 2017[a]; Zhao *et al.* 2019). Much like q_u, ε_u was also adversely affected by mica content, thus indicating a major reduction in the soil's ductility when paired with the mica mineral. As a typical case, the natural soil sample or M_0 yielded at ε_u = 11.09%, while the sample M_{30} led to ε_u = 5.48%, which signifies a notable two-fold reduction in the soil's ductility.

The area under a typical UC stress–strain curve up to the failure/peak point, denoted as E_u, is defined as strain energy at peak (or energy adsorption capacity); it serves as a measure of the material's toughness (Maher and Ho 1994; Mirzababaei *et al.* 2013). **Figure 7a** illustrates the variations of E_u, along with the corresponding q_u values, for the tested samples. The strain energy at peak followed a trend similar to that observed for the peak UC strength, meaning that the greater the mica content the lower the E_u value. As demonstrated in **Figure 7a**, both q_u and E_u exhibited an exponential tendency for reduction with respect to M_c. Lower strain energy at peak values suggests a decrease in the failure axial strain and/or the peak UC strength (Soltani *et al.* 2019[b]). With regard to various soil–mica blends, both parameters ε_u and q_u decrease with an increase in the mica content and hence contribute to lower E_u values. As a typical case, the natural soil sample (M_0) resulted in E_u = 16.52 kJ/m^3, while the sample M_{30} resulted in E_u = 3.24 kJ/m^3, which indicates a major five-fold reduction in the soil's energy adsorption capacity or toughness.

The secant modulus at 50% of the peak UC strength, commonly referred to as the elastic stiffness modulus and denoted as E_{50} (Radovic *et al.* 2004; Iyengar *et al.* 2013; Zhao *et al.* 2019), was also calculated for the tested samples, and the results are provided in **Figure 7b**. All mica-blended samples exhibited lower E_{50} values compared with that of the natural soil, thus indicating a reduced material stiffness as a result of mica inclusion. Much like q_u and E_u, the tendency for reduction in E_{50} followed an exponential trend with respect to M_c. The natural soil (M_0) resulted in E_{50} = 6.65 MPa, while mica inclusions of 5%, 10%, 15%, 20%, 25% and 30% (M_5 to M_{30}) resulted in lower values of 5.70 MPa, 4.68 MPa, 4.08 MPa, 3.03 MPa, 2.78 MPa and 2.65 MPa, respectively.

2.4.4. Effect of Mica Content on Shear Strength

Stress–displacement curves, obtained from the DS tests at varying normal stresses, are provided in **Figures 8a–8g** for the natural soil (M_0) and various mica-blended samples containing 5%, 10%, 15%, 20%, 25% and 30% mica (M_5 to M_{30}), respectively. In most cases,

the stress–displacement response exhibited a rise–plateau behavior without visually-detectable peak points, thereby signifying a strain-hardening behavior. This effect, however, was slightly less pronounced for samples of higher mica contents, such as M_{25} and M_{30}, particularly at higher normal stresses, e.g., see σ_n = 300 kPa and 400 kPa in **Figures 8f and 8g**. Much like natural fine-grained soils, the stress–displacement response for a given mica content was dependent on the applied normal stress, with higher normal stresses exhibiting higher shear strength values. It should be noted that the shear strength, denoted as τ_p, was defined as the maximum shear stress attained within the 6–10 mm displacement region (Liu and Evett 2009). At a normal stress of σ_n = 100 kPa, for instance, the natural soil (M_0) and the samples blended with 5% and 30% mica (M_5 and M_{30}) resulted in τ_p = 97.44 kPa, 94.61 kPa and 81.42 kPa, respectively. Where σ_n = 400 kPa, these values increased to 145.84 kPa, 144.07 kPa and 191.16 kPa, respectively.

Figure 9 illustrates the variations of shear strength, at varying normal stresses, against mica content for the tested samples. At a given normal stress, the variations of shear strength followed a nearly-linear path with respect to mica content M_c. At normal stresses equal to or less than 200 kPa, τ_p exhibited a linear, monotonically-decreasing trend with respect to M_c, while the opposite occurred at higher normal stresses of 300 kPa and 400 kPa. The former, σ_n = 100 kPa and 200 kPa, is consistent with the results obtained from the UC tests which, in essence, is a low-confinement strength test (see **Figure 6**). The rate of decrease or increase in τ_p with respect to M_c, i.e., $\eta = \Delta\tau_p/\Delta M_c$, was strongly dependent on the applied normal stress; the higher the applied normal stress the higher the value of η. As demonstrated in **Figure 9**, at σ_n = 100 kPa and 200 kPa, η was obtained as –0.463 and –0.041, respectively. Where σ_n = 300 kPa and 400 kPa, however, η transitioned towards the positive values of +1.173 and +1.767, respectively. Interestingly, micaceous soils, though inherently characterized as low-grade, problematic soils, may be deemed suitable under high-confinement conditions. At σ_n = 100 kPa, for instance, the natural soil (M_0) and the sample blended with 30% mica (M_{30}) resulted in τ_p = 97.44 kPa and 81.42 kPa, respectively (i.e., 16.44% reduction in τ_p). Where σ_n = 400 kPa, these values changed to 145.84 kPa (for M_0) and 191.16 kPa (for M_{30}), which suggest a 31.08% increase in τ_p. Improvement in the shear strength due to confinement can be attributed to the closer packing of the clay and mica components in the matrix. An increase in normal stress (or confinement) leads to a greater contact level between the clay and mica particles, which contributes to an induced frictional resistance at the shearing interface (owing to the

difference of mica and clay in terms of surface roughness), thereby leading to higher shear strength values.

The conventional Mohr–Coulomb failure criterion — $\tau_p = c + \sigma_n \tan\varphi$, where c = cohesion and φ = angle of internal friction — was implemented using a total stress approach to arrive at the apparent shear strength parameters c and φ, and the results are presented in **Figure 10**. In terms of cohesion, the greater the mica content the lower the apparent cohesion, following an exponentially-decreasing trend. In contrast, the greater the mica content the higher the apparent angle of internal friction, which in turn justifies the observed improvements in the shear strength at higher normal stresses (see **Figure 9**). The natural soil (M_0) resulted in c = 81.35 kPa (φ = 9.40°), while the inclusion of 5%, 10%, 15%, 20%, 25% and 30% mica (M_5 to M_{30}) resulted in c = 76.08 kPa, 74.64 kPa, 66.94 kPa, 60.86 kPa, 49.61 kPa and 39.80 kPa (φ = 9.50°, 11.97°, 13.57°, 17.30°, 19.11° and 20.90°), respectively.

2.4.5. Clay–Mica Interactions and SEM Analysis

Figures 11a–**11c** present SEM micrographs for the natural soil (M_0) and the samples blended with 5% and 30% mica (M_5 and M_{30}), respectively. The natural soil sample exhibited a fully-dense, uniform matrix, which was accompanied by a limited number of rather small inter- and intra-assemblage voids/pore-spaces, respectively, formed between and within the soil aggregates; these morphological features warrant the presence of an edge-to-face flocculated fabric (see **Figure 11a**). The inter-assemblage voids were formed during sample preparation, or static compaction, and thus are proportional to the sample's initial/as-compacted void ratio, as presented in **Table 3**. However, the shape and extension of these voids may have changed during the drying process of the SEM sample fabrication (see **Section 3.4**), owing to the development of tensile stresses within the fabric during desiccation (Soltani *et al.* 2018[b]). The sample blended with 5% mica (M_5) manifested a relatively loose, partly-uniform matrix, which was accompanied by a notable number of more pronounced voids distributed along the soil–mica interfaces; such attributes indicate a transition towards an edge-to-edge dispersed fabric (see **Figure 11b**). As opposed to a flocculated fabric, a dispersed fabric offers less resistance to external loading and/or shear (Mitchell and Soga 2005; Kim and Palomino 2009); this is consistent with the results obtained from the UC and DS (at low normal stresses) tests outlined in in **Sections 4.3** and **4.4**. In the case of 30% mica inclusion (M_{30}), an edge-to-edge dispersed character clearly dominated the fabric, as is evident with the presence of a fully-loose, non-uniform matrix accompanied by an increased number of relatively larger pore-spaces (see

Figure 11c). As such, the degree of fabric dispersion is proportional to the mica content, with higher mica contents resulting in a more dispersed fabric and hence lower strength resistance. The above discussion, however, only holds provided that the mica-blended sample is tested under low-confinement conditions. As is evident from the DS test results outlined in **Figure 9**, high confinements (or normal stresses) can alter the fabric by providing a closer packing of the clay and mica particles, thereby inducing frictional resistance at the shearing interface, owing to an induced clay–mica contact level, and thus improving the shear strength performance.

2.5. Conclusions

The present study has arrived at the following conclusions:

- The liquid and plastic limits exhibited a linear, monotonically-increasing trend with increase in the mica content. The rate of increase in the plastic limit with respect to mica content was observed to be approximately three-fold greater than that of the liquid limit. As a result, the plasticity index experienced a linear, monotonically-decreasing trend with respect to mica content, thereby indicating a gradual transition towards a non-plastic, cohesionless character.

- The mica content influenced the optimum water content of the clay soil, following a linear, monotonically-increasing trend. In contrast, the maximum dry unit weight exhibited a linear, monotonically-decreasing trend with respect to mica content. Compaction problems associated with micaceous soils was attributed to mica's high water demand, as well as its soft, spongy fabric which promotes a rebound response to compaction energy.

- As a result of mica inclusion, the stress–strain response, under Unconfined Compression (UC) loading conditions, progressively transitioned towards a strain-softening character and hence a more dramatic, brittle failure. The UC parameters — strength, ductility, toughness and stiffness — were all adversely affected by mica, with higher mica contents exhibiting lower UC parameters, following an exponential tendency for reduction.

- In most cases, the stress–displacement response, under Direct Shear (DS) testing conditions, exhibited a strain-hardening behavior. This effect, however, was slightly less pronounced for samples with higher mica contents, such as 25% and 30%, at higher normal stresses. At normal stresses equal to or less than 200 kPa, the shear strength decreased with an increase in the

- mica content, while the opposite occurred at higher normal stresses of 300 kPa and 400 kPa. The latter was attributed to the compact packing of the clay and mica components in the matrix under high confinement conditions, which offsets the adverse effects of mica by inducing frictional resistance at the shearing interface.

- The apparent shear strength parameters, namely the cohesion and the angle of internal friction, were also dependent on the mica content. In terms of cohesion, higher mica contents led to lower cohesion values, following an exponentially-decreasing trend. In contrast, higher mica contents led to increased angles of internal friction; this behavior justifies the observed improvement in shear strength at high confinement conditions.

Acknowledgments

This research was made possible through the provision of an Australian Government Research Training Program Scholarship; this support is gratefully acknowledged

Conflicts of Interest

The authors wish to confirm that there are no known conflicts of interest associated with this publication, and there has been no significant financial support for this work that could have influenced its outcome.

References

Al-Aqtash U, Bandini P. Prediction of unsaturated shear strength of an adobe soil from the soil–water characteristic curve. Constr Build Mater. **2015**;98:892–9. http://doi.org/10.1016/j.conbuildmat.2015.07.188

Bai FQ, Liu SH. Measurement of the shear strength of an expansive soil by combining a filter paper method and direct shear tests. Geotech Test J. **2012**;35(3):451–9. http://doi.org/10.1520/gtj103342

Ballantine RW, Rossouw AJ. Stabilization of Soils. Pretoria, Gauteng, South Africa: PPC Lime Ltd.; **1989**. p. 25–7, 42–51.

Clayton CR., Theron M, Vermeulen N. The effect of particle shape on the behaviour of gold tailings. In: Jardine RJ, Potts DM, Higgins KG, editors. Advances in Geotechnical Engineering: The Skempton Conference. London, England, UK: ICE Publishing; **2004**. p. 393–404. http://doi.org/10.1680/aigev1.32644.0017

Estabragh AR, Javadi AA. Critical state for overconsolidated unsaturated silty soil. Can Geotech J. **2008**;45(3):408–20. http://doi.org/10.1139/t07-105

Estabragh AR, Khatibi M, Javadi AA. Effect of cement on treatment of a clay soil contaminated with glycerol. J Mater Civ Eng. **2016[b]**;28(4):04015157:1–10. http://doi.org/10.1061/(asce)mt.1943-5533.0001443

Estabragh AR, Ranjbari S, Javadi AA. Properties of clay soil and soil cement reinforced with polypropylene fibers. ACI Mater J. **2017**;114(2):195–205. http://doi.org/10.14359/51689469

Estabragh AR, Soltani A, Javadi AA. Models for predicting the seepage velocity and seepage force in a fiber reinforced silty soil. Comput Geotech. **2016[a]**;75:174–181. http://doi.org/10.1016/j.compgeo.2016.02.002

Galán E, Ferrell RE. Chapter 3 – Genesis of clay minerals. Dev Clay Sci. **2013**;5:83–126. http://doi.org/10.1016/b978-0-08-098258-8.00003-1

Gogo JO. Compaction and strength characteristics of decomposed mica schist. In: Proceedings of the 8th Regional Conference for Africa on Soil Mechanics and Foundation Engineering. Harare, Zimbabwe: A.A. Balkema; **1984**. p. 275–284. ISBN:9061915325

Harris WG, Parker JC, Zelazny LW. Effects of mica content on engineering properties of sand. Soil Sci Soc Am J. **1984**;48(3):501–5. http://doi.org/10.2136/sssaj1984.03615995004800030006x

Harvey JC. Geology for Geotechnical Engineers (1st Ed). Cambridge, CambridgeshireEngland, UK: Cambridge University Press; **1982**. ISBN:9780521288620

Iyengar SR, Masad E, Rodriguez AK, Bazzi HS, Little D, Hanley HJM. Pavement subgrade stabilization using polymers: Characterization and performance. J Mater Civ Eng. **2013**;25(4):472–83. http://doi.org/10.1061/(asce)mt.1943-5533.0000612

Kim S, Palomino AM. Polyacrylamide–treated kaolin: A fabric study. Appl Clay Sci. **2009**;45(4):270–279. http://doi.org/10.1016/j.clay.2009.06.009

Liu C, Evett J. Soil Properties: Testing, Measurement, and Evaluation (6th Ed). Upper Saddle River, New Jersey, USA: Pearson/Prentice Hall; **2009**. ISBN:9780136141235

Maher MH, Ho YC. Mechanical properties of kaolinite/fiber soil composite. J Geotech Eng. **1994**;120(8):1381–93. http://doi.org/10.1061/(asce)0733-9410(1994)120:8(1381)

Mirzababaei M, Miraftab M, Mohamed M, McMahon P. Unconfined compression strength of reinforced clays with carpet waste fibers. J Geotech Geoenvironmental Eng. **2013**;139(3):483–93. http://doi.org/10.1061/(asce)gt.1943-5606.0000792

Mirzababaei M, Yasrobi SS, Al-Rawas AA. Effect of polymers on swelling potential of expansive soils. Proc Inst Civ Eng – Gr Improv. **2009**;162(3):111–9. http://doi.org/10.1680/grim.2009.162.3.111

Mitchell JK, Soga K. Soil–water–chemical interactions. In: Fundamentals of Soil Behavior (3rd Ed). Hoboken, New Jersey, USA: John Wiley & Sons; **2005**. p. 143–72. http://doi.org/10.2136/sssaj1976.03615995004000040003x, ISBN:9780471463023

Mitchell RL, Van der Merwe CP, Geel HK. Standardised Flexible Pavement Design for Rural Roads with Light to Medium Traffic. Salisbury, Zimbabwe: Special Report, Rhodesian Government Central Laboratory; **1975**.

Moore CA. Effect of mica on K_0 compressibility of two soils. J Soil Mech Found Div. **1971**;97(SM9):1275–91.

Mshali MR, Visser AT. Influence of mica on compactability and moisture content of cement–treated weathered granite gravel. In: Proceedings of the 33rd Southern African Transport Conference (SATC 2014). Pretoria, Gauteng, South Africa: Minister of Transport, South Africa; **2014**. p. 546–55. ISBN:9781920017613

Mshali MR, Visser AT. Influence of mica on unconfined compressive strength of a cement–treated weathered granite gravel. J South African Inst Civ Eng. **2012**;54(2):71–7.

Netterberg F, Hefer A, Preez HD. Cracking and staining of an airport asphalt. In: Proceedings of the 10th Conference on Asphalt Pavements for South Africa (CAPSA 11): Roads of the Future. KwaZulu KwaZulu–Natal, South Africa: International Road Federation (IRF); **2011**. p. 1–17.

Northmore KJ, Bell FG, Culshaw MG. The engineering properties and behaviour of the brickearth of south Essex. Q J Eng Geol Hydrogeol. **1996**;29(2):147–61. http://doi.org/10.1144/gsl.qjegh.1996.029.p2.04

Paige-Green P, Semmelink CJ. Road compaction problems related to the presence of biotite. In: Proceedings of the 9th Congress of the International Association of Engineering Geology and the Environment. Durban, KwaZulu–Natal, South Africa; **2002**. p. 2605–2610.

Pandian NS, Nagaraj TS, Manoj M. Re–examination of compaction characteristics of fine–grained soils. Géotechnique. **1997**;47(2):363–6. http://doi.org/10.1680/geot.1997.47.2.363

Qu J, Zhao D. Stabilising the cohesive soil with palm fibre sheath strip. Road Mater Pavement Des. **2016**;17(1):87–103. http://doi.org/10.1080/14680629.2015.1064010

Radovic M, Lara-Curzio E, Riester L. Comparison of different experimental techniques for determination of elastic properties of solids. Mater Sci Eng A. **2004**;368(1–2):56–70. http://doi.org/10.1016/j.msea.2003.09.080

Sezer A, İnan G, Recep Yılmaz H, Ramyar K. Utilization of a very high lime fly ash for improvement of Izmir clay. Build Environ. **2006**;41(2):150–5. http://doi.org/10.1016/j.buildenv.2004.12.009

Soltani A, Deng A, Taheri A, Mirzababaei M, Nikraz H. Interfacial shear strength of rubber–reinforced clays: A dimensional analysis perspective. Geosynth Int. **2019[a]**;in press. http://doi.org/10.1680/jgein.18.00045

Soltani A, Deng A, Taheri A, Mirzababaei M. A sulphonated oil for stabilisation of expansive soils. Int J Pavement Eng. **2017[b]**;in press. http://doi.org/10.1080/10298436.2017.1408270

Soltani A, Deng A, Taheri A, Mirzababaei M. Rubber powder–polymer combined stabilization of South Australian expansive soils. Geosynth Int. **2018[b]**;25(3):304–21. http://doi.org/10.1680/jgein.18.00009

Soltani A, Deng A, Taheri A, Sridharan A. Consistency limits and compaction characteristics of clay soils containing rubber waste. Proc Inst Civ Eng – Geotech Eng. **2018[c]**;in press. http://doi.org/10.1680/jgeen.18.00042

Soltani A, Deng A, Taheri A. Swell–compression characteristics of a fiber–reinforced expansive soil. Geotext Geomembranes. **2018[a]**;46(2):183–9. http://doi.org/10.1016/j.geotexmem.2017.11.009

Soltani A, Taheri A, Deng A, Nikraz H. Tyre rubber and expansive soils: Two hazards, one solution. Proc Inst Civ Eng – Constr Mater. **2019[b]**;in press. http://doi.org/10.1680/jcoma.18.00075

Soltani A, Taheri A, Khatibi M, Estabragh AR. Swelling potential of a stabilized expansive soil: A comparative experimental study. Geotech Geol Eng. **2017[a]**;35(4):1717–1744. http://doi.org/10.1007/s10706-017-0204-1

Sridharan A, Nagaraj HB. Plastic limit and compaction characteristics of fine–grained soils. Proc Inst Civ Eng – Gr Improv. **2005**;9(1):17–22. http://doi.org/10.1680/grim.2005.9.1.17

Sridharan A, Prakash K. Mechanisms controlling the undrained shear strength behaviour of clays. Can Geotech J. **1999**;36(6):1030–8. http://doi.org/10.1139/t99-071

Tubey LW, Bulman JN. Micaceous soils: Methods of determining mica content and the use of routine tests in the evaluation of such soils. Proc Aust Road Res Board (ARRB). **1964**;2(2):880–901.

Tubey LW, Webster DC. The Effects of Mica on the Roadmaking Properties of Materials. CrowthorneWokingham, Berkshire, UK: Supplementary Report 408, Transport and Road Research Laboratory (TRL); **1978**. ISBN:03051315

Tubey LW. A Laboratory Investigation to Determine the Effect of Mica on the Properties of Soils and Stabilized Soils. Wokingham, Berkshire, UK: Research Note 4077, Road Research Laboratory (RRL); **1961**.

Weinert HH. The Natural Road Construction Materials of Southern Africa (1st Ed). Cape Town, Western Cape, South Africa: H&R Academica; **1980**. ISBN:0860740470

Zhang J, Soltani A, Deng A, Jaksa MB. Mechanical performance of jute fiber–reinforced micaceous clay composites treated with ground–granulated blast–furnace slag. Materials. **2019**;12(4),576:1–23. http://doi.org/10.3390/ma12040576

Zhao Y, Soltani A, Taheri A, Karakus M, Deng A. Application of slag–cement and fly ash for strength development in cemented paste backfills. Minerals. **2019**;9(1),22:1–19. http://doi.org/10.3390/min9010022

List of Tables

Table 1. Physical and mechanical properties of the natural soil.

Table 2. Physical and chemical properties of ground mica.

Table 3. Soil–mica mix designs and their properties.

Table 1. Physical and mechanical properties of the natural soil.

Properties	Value	Standard Designation
Specific gravity of solids, G_s [S]	2.74	ASTM D854–14
Grain-Size Distribution		
Clay [< 2 μm] (%)	37	ASTM D422–07
Silt [2–75 μm] (%)	32	ASTM D422–07
Sand [0.075–4.75 mm] (%)	32	ASTM D422–07
Consistency Limits and Classifications		
Liquid limit, w_L (%)	46.21	AS 1289.3.9.1–15 [a]
Plastic limit, w_P (%)	18.11	AS 1289.3.2.1–09 [b]
Plasticity index, I_P (%)	28.10	AS 1289.3.3.1–09
USCS classification	CI	ASTM D2487–11
Compaction Characteristics		
Optimum water content, w_{opt} (%)	22.04	ASTM D698–12
Maximum dry unit weight, γ_{dmax} (kN/m^3)	16.21	ASTM D698–12

[a] Cone penetration method; and [b] Rolling thread method.

Table 2. Physical and chemical properties of ground mica.

Properties	Value
Physical Properties	
Appearance	Fine white powder
Specific gravity of solids, G_s^M	2.80
Fines [< 75 μm] (%)	93
Sand [0.075–4.75 mm] (%)	7
Particle diameter D_{90} (μm)	53.60
Specific surface area, S_a (m^2/g)	5.30
Natural water content, w_N (%)	0.41
Hardness (Mohs)	2.50
Chemical Properties	
SiO_2 (%)	49.5
Al_2O_3 (%)	29.2
K_2O (%)	8.9
Fe_2O_3 (%)	4.6
TiO_2 (%)	0.8
MgO (%)	0.7
Na_2O (%)	0.5
CaO (%)	0.4
Acidity, pH [20% slurry]	7.8
Oil absorption (mL/100 g)	36.0
Loss on Ignition, LoI [at 1000 ^oC] (%)	< 6.0

Table 3. Soil–mica mix designs and their properties.

Group	**Mica Content, M_c (%)**	**Designation**	**w_{opt} (%) [a]**	**γ_{dmax} (kN/m^3) [a]**	**e_{opt} [a]**
Control [b]	0	M_0	22.04	16.21	0.658
Mica-blended	5	M_5	22.52	15.94	0.688
	10	M_{10}	23.33	15.63	0.723
	15	M_{15}	24.33	15.25	0.768
	20	M_{20}	25.00	15.01	0.798
	25	M_{25}	25.80	14.89	0.815
	30	M_{30}	26.50	14.70	0.841

w_{opt} = Optimum water content; γ_{dmax} = Maximum dry unit weight; e_{opt} = Optimum void ratio; [a] Initial placement condition for the UC, DS and SEM tests; and [b] Natural soil.

List of Figures

Figure 1. Variations of the Dry Unit Weight (DUW) along the height of the statically compacted samples: **(a)** M_0; **(b)** M_{10}; **(c)** M_{20}; and **(d)** M_{30}.

Figure 2. Variations of the consistency limits — liquid limit, plastic limit and plasticity index — against mica content for the tested mix designs.

Figure 3. Soil–mica mix designs illustrated on Casagrande's plasticity chart.

Figure 4. Standard Proctor compaction results for the tested mix designs: **(a)** Compaction curves; and **(b)** Path of optimums.

Figure 5. Variations of the Optimum Water Content (OWC) and the Maximum Dry Unit Weight (MDUW) against mica content for the tested mix designs.

Figure 6. UC stress–strain curves for the natural soil and various soil–mica blends.

Figure 7. Variations of the **(a)** strain energy at peak E_u and the **(b)** elastic stiffness modulus E_{50}, along with the corresponding peak UC strength values q_u, against mica content for the tested samples.

Figure 8. DS stress–displacement curves for the tested mix designs: **(a)** M_0; **(b)** M_5; **(c)** M_{10}; **(d)** M_{15}; **(e)** M_{20}; **(f)** M_{25}; and **(g)** M_{30}.

Figure 9. Variations of the shear strength, at varying normal stresses, against mica content for the tested samples.

Figure 10. Variations of the shear strength parameters — cohesion c and angle of internal friction φ — against mica content for the tested samples.

Figure 11. SEM micrographs for the tested samples: **(a)** M_0; **(b)** M_5; and **(c)** M_{30}.

Figure 1. Variations of the Dry Unit Weight (DUW) along the height of the statically compacted samples: **(a)** M_0; **(b)** M_{10}; **(c)** M_{20}; and **(d)** M_{30}.

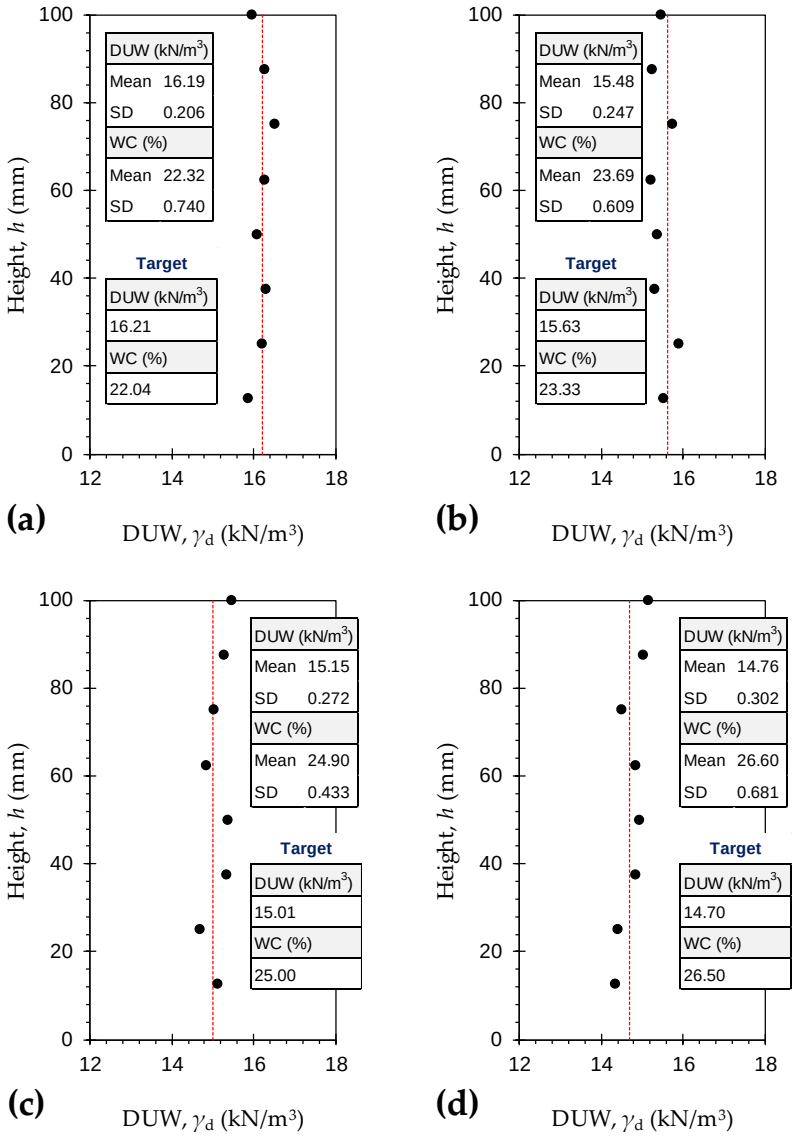

Figure 2. Variations of the consistency limits — liquid limit, plastic limit and plasticity index — against mica content for the tested mix designs.

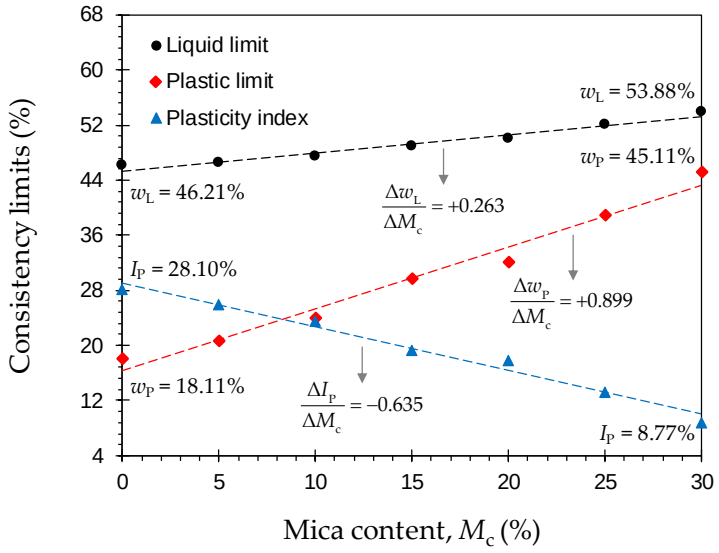

Figure 3. Soil–mica mix designs illustrated on Casagrande's plasticity chart.

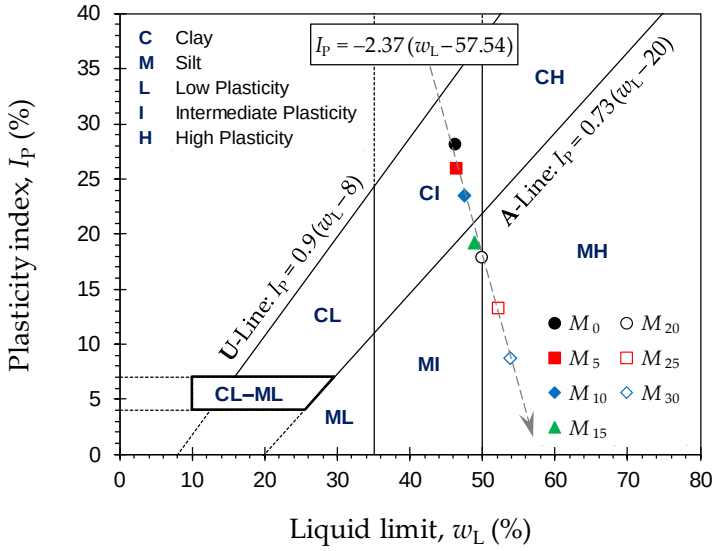

Figure 4. Standard Proctor compaction results for the tested mix designs: **(a)** Compaction curves; and **(b)** Path of optimums.

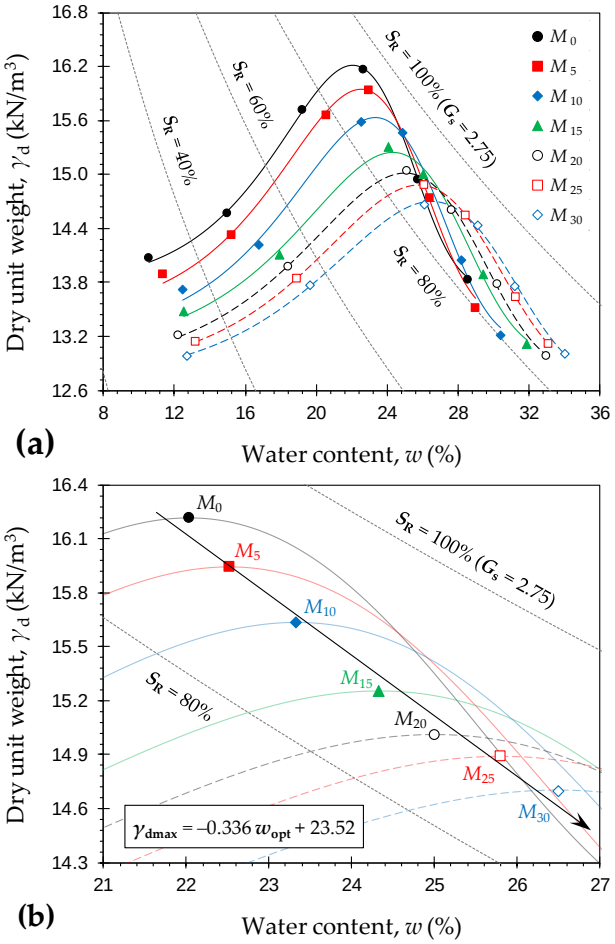

Figure 5. Variations of the Optimum Water Content (OWC) and the Maximum Dry Unit Weight (MDUW) against mica content for the tested mix designs.

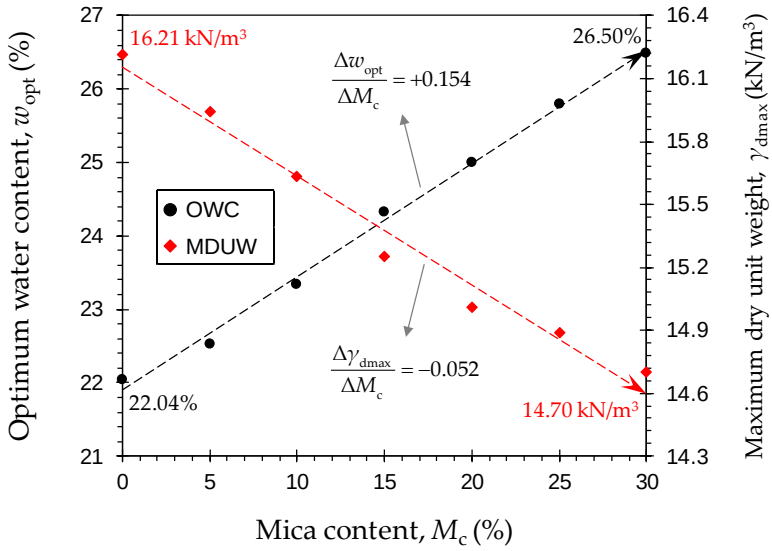

Figure 6. UC stress–strain curves for the natural soil and various soil–mica blends.

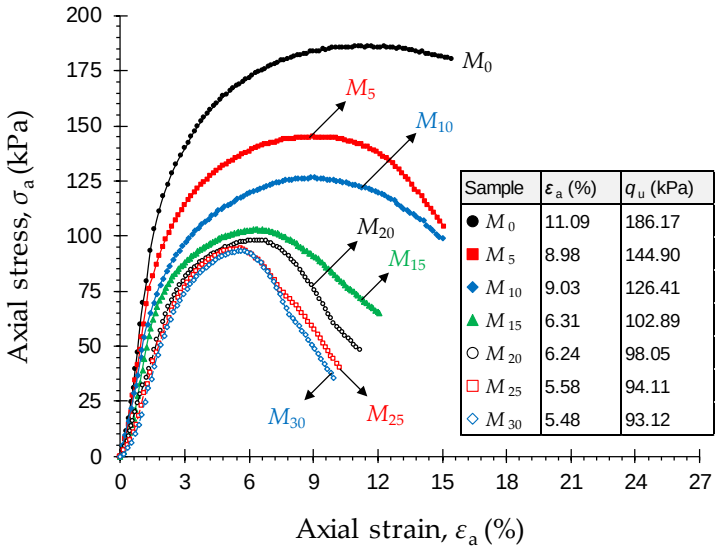

Figure 7. Variations of the **(a)** strain energy at peak E_u and the **(b)** elastic stiffness modulus E_{50}, along with the corresponding peak UC strength values q_u, against mica content for the tested samples.

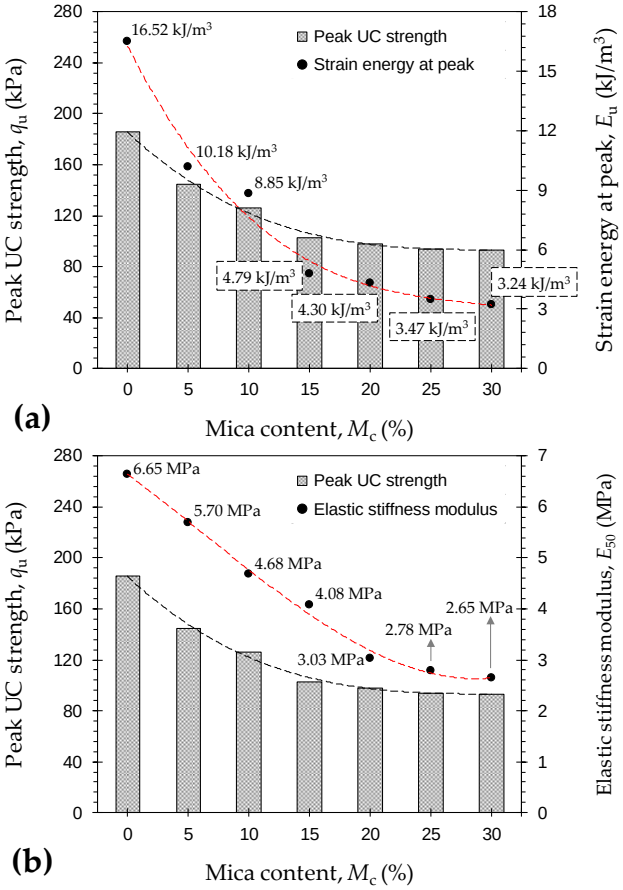

Figure 8. DS stress–displacement curves for the tested mix designs: **(a)** M_0; **(b)** M_5; **(c)** M_{10}; **(d)** M_{15}; **(e)** M_{20}; **(f)** M_{25}; and **(g)** M_{30}.

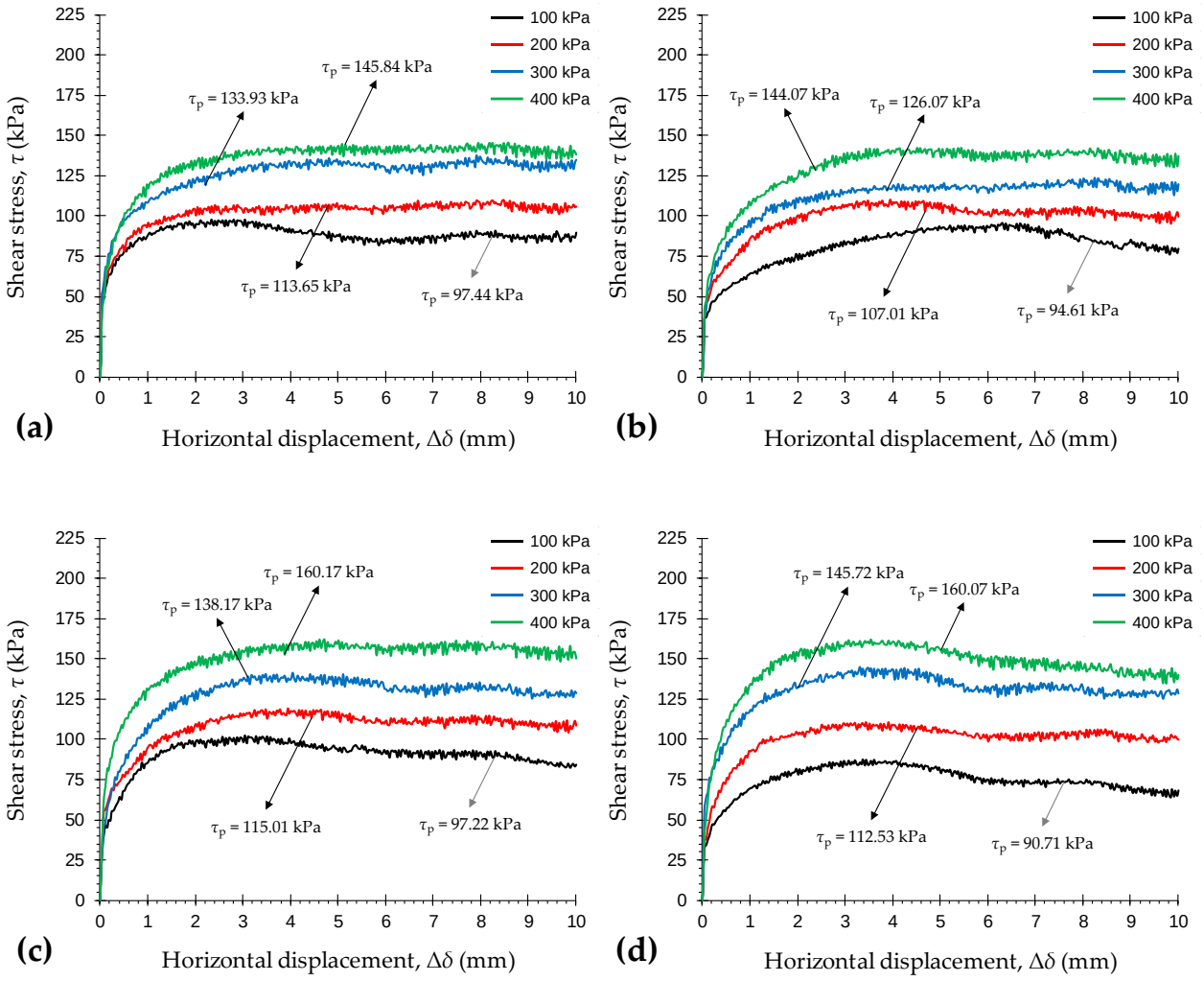

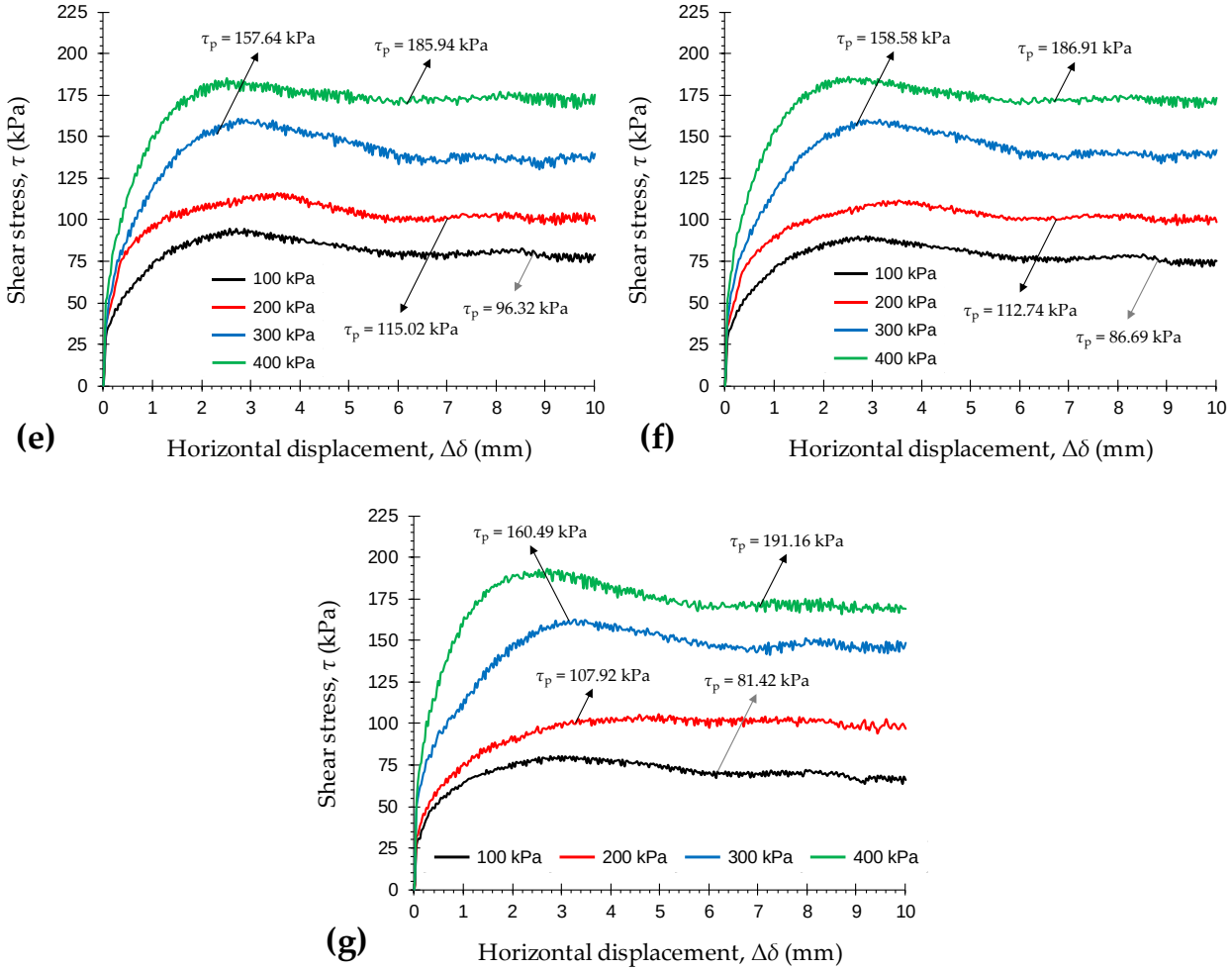
(e)
Shear stress, τ (kPa)
Horizontal displacement, Δδ (mm)
τp = 157.64 kPa
τp = 185.94 kPa
τp = 115.02 kPa
τp = 96.32 kPa
100 kPa
200 kPa
300 kPa
400 kPa
(f)
Shear stress, τ (kPa)
Horizontal displacement, Δδ (mm)
τp = 158.58 kPa
τp = 186.91 kPa
τp = 112.74 kPa
τp = 86.69 kPa
100 kPa
200 kPa
300 kPa
400 kPa
(g)
Shear stress, τ (kPa)
Horizontal displacement, Δδ (mm)
τp = 160.49 kPa
τp = 191.16 kPa
τp = 107.92 kPa
τp = 81.42 kPa
100 kPa
200 kPa
300 kPa
400 kPa

Figure 9. Variations of the shear strength, at varying normal stresses, against mica content for the tested samples.

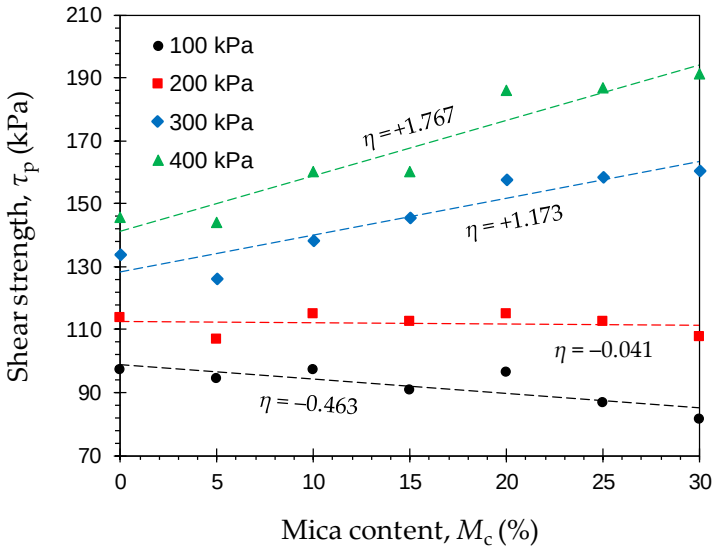

Figure 10. Variations of the shear strength parameters — cohesion c and angle of internal friction φ — against mica content for the tested samples.

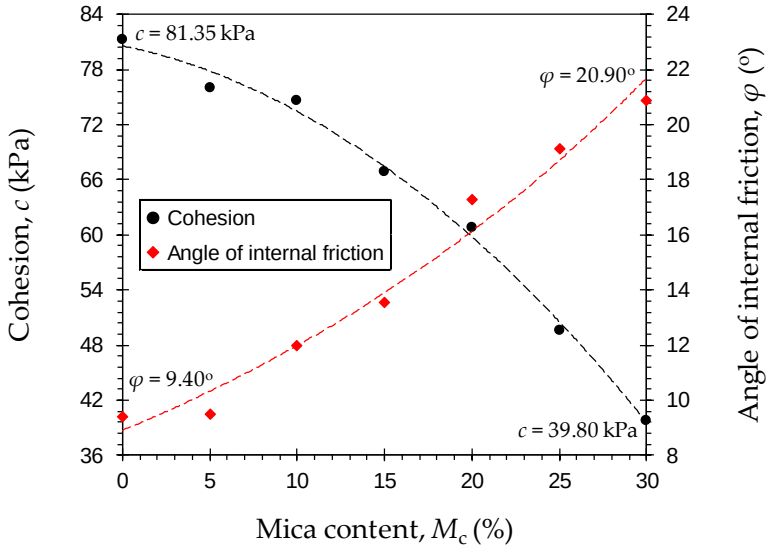

Figure 11. SEM micrographs for the tested samples: **(a)** M_0; **(b)** M_5; and **(c)** M_{30}.

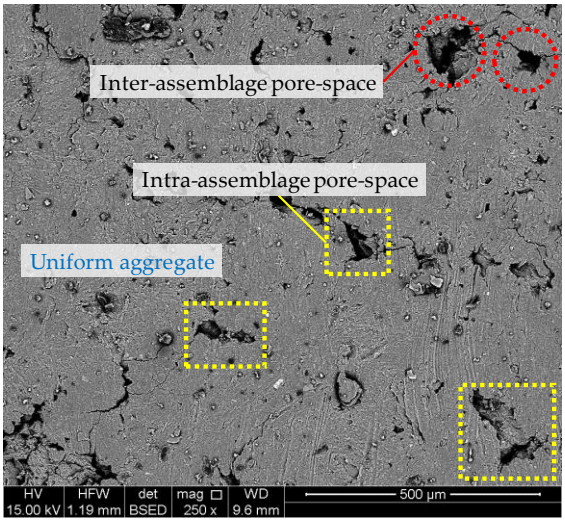

(a)

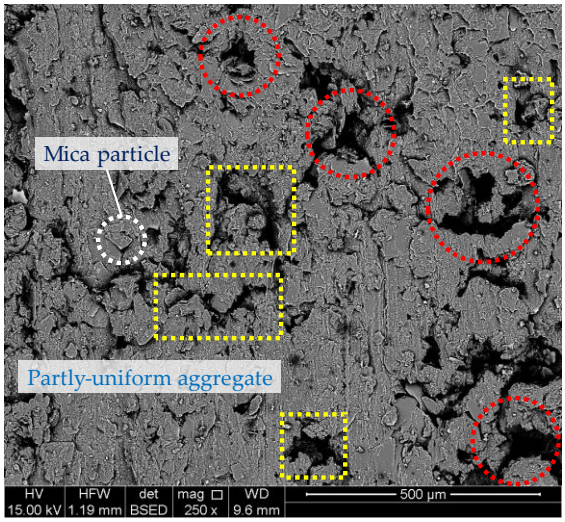

(b)

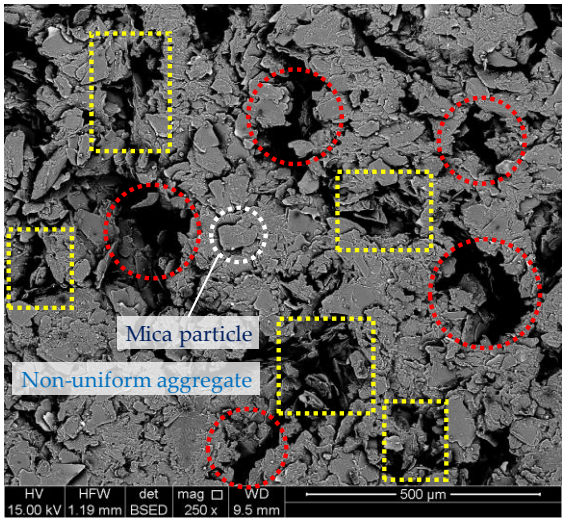

(c)

Statement of Authorship

Title of Paper	Mechanical Behavior of Micaceous Clays
Publication Status	☐Published ☐Submitted for Publication ■Accepted for Publication ☐Unpublished and Unsubmitted work written in manuscript style
Publication Details	**Zhang J**, Soltani A, Deng A, Jaksa M **(2019)** Mechanical behavior of micaceous clays. ***Journal of Rock Mechanics and Geotechnical Engineering***, x(x):x-x, http://doi.org/x

Principal Author

Name of Principal Author (Candidate)	Jiahe Zhang (**Email**: Jiahe.Zhang@adelaide.edu.au)		
Contribution to the Paper	Overall paper preparation		
Overall percentage (%)	85%		
Certification:	This paper reports on original research I conducted during the period of my Higher Degree by Research candidature and is not subject to any obligations or contractual agreements with a third party that would constrain its inclusion in this thesis. I am the primary author of this paper.		
Signature		Date	01/05/2019

Co-Author Contributions

By signing the Statement of Authorship, each author certifies that:

i. the candidate's stated contribution to the publication is accurate (as detailed above);
ii. permission is granted for the candidate in include the publication in the thesis; and
iii. the sum of all co-author contributions is equal to 100% less the candidate's stated contribution.

Name of Co-Author	An Deng **Senior Lecturer**, School of Civil, Environmental and Mining Engineering, The University of Adelaide, Adelaide, SA 5005, Australia (**Email**: An.Deng@adelaide.edu.au)		
Contribution to the Paper	Methodology, paper review and revision		
Signature		Date	1/05/2019

Name of Co-Author	Mark Jaksa **Professor**, School of Civil, Environmental and Mining Engineering, The University of Adelaide, Adelaide, SA 5005, Australia (**Email**: Mark.Jaksa@adelaide.edu.au)		
Contribution to the Paper	Paper review and revision		
Signature		Date	2/05/2019

Name of Co-Author	Amin Soltani Former: **Research Academic**, School of Civil, Environmental and Mining Engineering, The University of Adelaide, Adelaide, SA 5005, Australia (**Email**: Amin.Soltani@adelaide.edu.au) Current: **Research Fellow in Geotechnical Engineering**, Department of Infrastructure Engineering, Melbourne School of Engineering, the University of Melbourne, Parkville VIC 3010, (Email: Amin.Soltani@unimelb.edu.au)		
Contribution to the Paper	Paper review and revision		
Signature		Date	2/05/2019

Published copy

ARTICLE IN PRESS

Journal of Rock Mechanics and Geotechnical Engineering xxx (xxxx) xxx

Contents lists available at ScienceDirect

Journal of Rock Mechanics and Geotechnical Engineering

journal homepage: www.rockgeotech.org

Full Length Article

Mechanical behavior of micaceous clays

Jiahe Zhang [a,*], Amin Soltani [b], An Deng [a], Mark B. Jaksa [a]

[a] School of Civil, Environmental and Mining Engineering, The University of Adelaide, Adelaide, SA 5005, Australia
[b] Department of Infrastructure Engineering, The University of Melbourne, Parkville, VIC 3010, Australia

ARTICLE INFO

Article history:
Received 6 October 2018
Received in revised form
28 February 2019
Accepted 26 April 2019
Available online xxx

Keywords:
Micaceous clay
Mica content
Consistency limits
Compaction
Shear strength
Confinement
Frictional resistance

ABSTRACT

This study aims to investigate the effect of mica content on the mechanical properties of clays. Commercially available ground mica was blended with a locally available clayey soil, at varying mica contents by mass of 5%, 10%, 15%, 20%, 25% and 30%, to artificially prepare various micaceous clay blends. The preliminary testing phase included consistency limits and standard Proctor compaction tests. The primary testing program consisted of unconfined compression (UC), direct shear (DS) and scanning electron microscopy (SEM) tests. The test results showed that the liquid and plastic limits exhibited a linear, monotonically increasing trend with increase in mica content. The rate of increase in the plastic limit, however, was found to be greater than that of the liquid limit, thereby leading to a gradual transition towards a non-plastic, cohesionless character. The soft, spongy fabric and high water demand of the mica mineral led to higher optimum water contents and lower maximum dry unit weights with increasing mica content. Under low confinement conditions, i.e. the UC test and the DS test at low normal stresses, the shear strength was adversely affected by mica. However, the closer packing of the clay and mica components in the matrix under high confinement conditions offsets the adverse effects of mica by inducing frictional resistance at the shearing interface, thus leading to improved strength resistance.

1. Introduction

The mica group of sheet silicates is among the most widely distributed minerals around the world; they generally occur in igneous, sedimentary and certain metamorphic rocks (Harvey, 1982; Galán and Ferrell, 2013). Although the compositions and properties of mica minerals vary depending on their geological formation and climatic conditions, the unique platy structure, high elasticity and nearly-perfect basal cleavage (owing to the hexagonal sheet-like arrangement of mica atoms) are the common features which demand further attention (Zhang et al., 2019). Where mica minerals are separated from their host rocks, these features may affect naturally weathered soils, thus leading to some adverse changes in the mechanical behavior of such soils.

Due to the extremely elastic properties of mica minerals, attributed to mica's soft, spongy fabric, the micaceous soils in particular micaceous clays may deform remarkably under applied load and hence affect the bulk compressibility of such soils. Mica minerals, although rather resilient, may gradually recover their initial shape due to the elastic rebound (or springy action), thereby reducing the efficiency of compactive effort and hence potentially compromising the performance of various facilities constructed on micaceous clays (Weinert, 1980). When such soils are unloaded, elastic rebound is likely to occur, resulting in undesirable volumetric expansion in the matrix. During compression, tension or shearing, the mica particles tend to rotate and orient themselves in a somewhat parallel fashion (attributed to mica's platy shape), thereby resulting in low strength resistance in micaceous soils (Harris et al., 1984). In this instance, micaceous soils are basically characterized by high compressibility, poor compactibility and low shear strength; such attributes present significant challenges for road construction, building foundations, earth dams and other geotechnical engineering systems, as reported in several countries around the world (e.g. Mitchell et al., 1975; Gogo, 1984; Northmore et al., 1996; Paige-Green and Semmelink, 2002; Netterberg et al., 2011).

The majority of documented studies have addressed the mechanical responses of coarse-grained micaceous soils (e.g. Tubey, 1961; Tubey and Bulman, 1964; Moore, 1971; Tubey and Webster, 1978; Harris et al., 1984; Ballantine and Rossouw, 1989; Clayton et al., 2004; Mshali and Visser, 2012, 2014; Zhang et al., 2019). To

* Corresponding author.
E-mail address: Jiahe.Zhang@adelaide.edu.au (J. Zhang).
Peer review under responsibility of Institute of Rock and Soil Mechanics, Chinese Academy of Sciences.

https://doi.org/10.1016/j.jrmge.2019.04.001

the authors' knowledge, however, there are still limited studies involving the mechanical behaviors of fine-grained micaceous soils. Of those examining fine-grained micaceous soils, no relationship was developed between the mica content and the mechanical behavior of these soils. Meanwhile, the ever-increasing need to expand urban areas to satisfy population growth and industrialization has required additional land, and in some cases, land with suboptimal soil properties. The utilization of local materials, one being micaceous clays, may eliminate the costs associated with transporting new materials from other locations. Therefore, the potential reuse of micaceous soils, and micaceous clays in particular, can lead to improved efficiencies and enhanced infrastructure performance, if an in-depth understanding of their geotechnical properties can be obtained.

The present study seeks to investigate the effect of mica content on the mechanical properties of clays. A test program was designed and conducted, which consisted of two phases, namely preliminary and primary tests. The preliminary testing phase included consistency (Atterberg) limits and standard Proctor compaction tests, and the primary tests consisted of unconfined compression (UC) and direct shear (DS) tests. Moreover, scanning electron microscopy (SEM) studies were carried out to observe the evolution of fabric in response to the mica inclusions, and thus perceive clay–mica interactions.

2. Materials

2.1. Clayey soil

Locally available reddish-brown clay was used for this study; it was sourced from a landfill site located near Adelaide, South Australia. The physical properties of the clay soil, hereafter simply referred to as the natural soil, were determined as per relevant American Society for Testing Materials (ASTM) and Australian Standards (AS), and the results are summarized in Table 1. The conventional grain size analysis (ASTM D422–63(2007)e2, 2007) indicated a clay fraction (<2 μm) of 37%, along with 32% silt (2–75 μm) and 32% sand (0.075–4.75 mm). In terms of consistency, the liquid limit and plasticity index were, respectively, measured as $w_L = 46.21\%$ and $I_P = 28.1\%$; the soil was hence classified as *clay with intermediate plasticity* (CI) in accordance with the Unified Soil Classification System (USCS). The standard Proctor compaction test, carried out as per ASTM D698–12e2 (2012), indicated an optimum water content of $w_{opt} = 22.04\%$ corresponding to a maximum dry unit weight of $\gamma_{dmax} = 16.21$ kN/m^3.

Table 1
Physical properties of the natural soil.

Properties		Value	Standard designation
Specific gravity of solids, G_s^S		2.74	ASTM D854–14 (2014)
Grain size distribution	Clay (<2 μm) (%)	37	ASTM D422–63(2007)e2 (2007)
	Silt (2–75 μm) (%)	32	ASTM D422–63(2007)e2 (2007)
	Sand (0.075–4.75 mm) (%)	32	ASTM D422–63(2007)e2 (2007)
Consistency limits and classifications	Liquid limit, w_L (%)	46.21	AS 1289.3.9.1–15 (2015)[a]
	Plastic limit, w_P (%)	18.11	AS 1289.3.2.1–09 (2009)[b]
	Plasticity index, I_p (%)	28.1	AS 1289.3.3.1–09 (2009)
	USCS classification	CI	ASTM D2487–11 (2011)
Compaction characteristics	Optimum water content, w_{opt} (%)	22.04	ASTM D698–12e2 (2012)
	Maximum dry unit weight, γ_{dmax} (kN/m^3)	16.21	ASTM D698–12e2 (2012)

[a] Cone penetration method.
[b] Rolling thread method.

Table 2
Physical and chemical properties of ground mica.

Properties		Value
Physical	Appearance	Fine white powder
	Specific gravity of solids, G_s^M	2.8
	Fines (<75 μm) (%)	93
	Sand (0.075–4.75 mm) (%)	7
	Particle diameter, D_{50} (μm)	53.6
	Specific surface area, S_a (m^2/g)	5.3
	Natural water content, w_N (%)	0.41
	Hardness (Mohs)	2.5
Chemical	SiO_2 (%)	49.5
	Al_2O_3 (%)	29.2
	K_2O (%)	8.9
	Fe_2O_3 (%)	4.6
	TiO_2 (%)	0.8
	MgO (%)	0.7
	Na_2O (%)	0.5
	CaO (%)	0.4
	Acidity, pH value (20% slurry)	7.8
	Oil absorption (mL/100 g)	36
	Loss on ignition, loi (at 1000 °C) (%)	<6

2.2. Ground mica

Commercially available ground mica, sourced from a local distributor, was used to artificially prepare various micaceous clay blends. The physical and chemical properties of the ground mica, as supplied by the manufacturer, are summarized in Table 2. In terms of grain size distribution, the ground mica consisted of a fines fraction (<75 μm) of 93%, along with 7% sand (0.075–4.75 mm). The specific gravity of the mica particles was found to be $G_s^M = 2.8$, which is quite similar to that of natural fine-grained soils including the one used in the present study, i.e. $G_s^S = 2.74$. Other physical properties included a specific surface area of $S_a = 5.3$ m^2/g. The chemical composition of the ground mica was found to be dominated by silicon dioxide (SiO_2) and aluminum trioxide (Al_2O_3) with mass fractions of 49.5% and 29.2%, respectively. In terms of acidity, the ground mica slurry was classified as a neutral substance corresponding to a pH value of 7.8.

3. Experimental work

In this study, a total of seven soil–mica mix designs consisting of one control, the natural soil, and six micaceous clay blends were examined (see Table 3). Hereafter, the coding system M_x, where x is the mica content or M_C and $x = \{0, 5, 10, 15, 20, 25, 30\}$, is used to designate the various mix designs; the mica content was defined as the ground mica to the natural soil mass ratio. As such, 'M_0' refers to

Table 3
Soil–mica mix designs and their properties.

Group	Mica content, M_C (%)	Designation	w_{opt} (%)[a]	γ_{dmax} (kN/m^3)[a]	e_{opt}[a]
Control[b]	0	M_0	22.04	16.21	0.658
Mica-blended	5	M_5	22.52	15.94	0.688
	10	M_{10}	23.33	15.63	0.723
	15	M_{15}	24.33	15.25	0.768
	20	M_{20}	25	15.01	0.798
	25	M_{25}	25.8	14.89	0.815
	30	M_{30}	26.5	14.7	0.841

Note: e_{opt} = Optimum void ratio.
[a] Initial placement condition for the UC, DS and SEM tests.
[b] Natural soil.

Please cite this article as: Zhang J et al., Mechanical behavior of micaceous clays, Journal of Rock Mechanics and Geotechnical Engineering, https://doi.org/10.1016/j.jrmge.2019.04.001

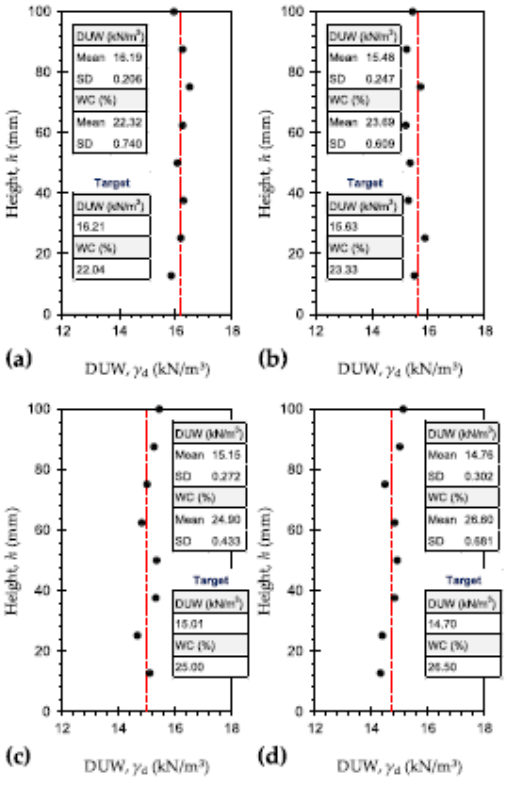

Fig. 1. Variations of the dry unit weight (DUW) along the height of the statically compacted samples: (a) M_0; (b) M_{10}; (c) M_{20}; and (d) M_{30}.

the natural soil with no mica inclusion (or $M_c = 0$), and 'M_{30}', for instance, refers to a soil–mica blend containing 30% mica by dry mass of the natural soil (or $M_c = 30\%$). The preliminary testing phase included a series of consistency (Atterberg) limits (as per AS 1289.3.9.1–15 (2015), AS 1289.3.2.1–09 (2009) and AS 1289.3.3.1–09 (2009)) and standard Proctor compaction (as per ASTM D698–12e2 (2012)) tests, and the results are partially summarized in Table 3. The primary testing program consisted of UC, DS and SEM tests. The methodologies associated with each component of the primary testing program, as well as the sample preparation techniques, are discussed in detail below.

3.1. Sample preparation

Samples used for the UC and DS tests were prepared by the static compaction technique, as commonly adopted in the literature for fine-grained geomaterials (e.g. Estabragh et al., 2016a; Soltani et al., 2018a, b), at the corresponding standard Proctor optimum condition of each mixture, i.e. the optimum water content and the maximum dry unit (see w_{opt} and γ_{dmax} in Table 3). The natural soil and ground mica were blended in dry form as per the selected mix designs outlined in Table 3, i.e. M_x where $x = \{0, 5, 10, 15, 20, 25, 30\}$. Mixing was carried out for approximately 5 min to gain visible homogeneity of the soil and mica particles. The required volume of water corresponding to the desired optimum water content (see w_{opt} in Table 3) was added to each blend and thoroughly mixed by hand for approximately 15 min; extensive care was dedicated to pulverizing the clumped particles, targeting homogeneity of the moist mixtures. The moist mixtures were then sealed in plastic bags and were allowed to cure for approximately 24 h to ensure an even distribution of moisture throughout the mixtures' mass. It should be noted that the artificial soil–mica blends exhibited the same typical texture, sheen and friability properties as natural micaceous soils reported in the literature, and thus may well provide a basis for systematically studying the effect of mica content on the mechanical behavior of fine-grained soils. A conventional split mold, similar to that described by Soltani et al. (2017a) and Zhang et al. (2019), was designed and fabricated from stainless steel to accomplish static compaction. The split mold consisted of three sections, i.e. the top collar, the middle section and the bottom collar. The middle section measures 50 mm in diameter and 100 mm in height; it accommodates the compacted sample for the UC test (see Section 3.2). Each of the seven moist mixtures was statically compressed in the mold (at a constant displacement rate of 1.5 mm/min) in five layers to a specific compaction load, each layer having attained its target maximum dry unit weight (see γ_{dmax} in Table 3). Samples for the DS tests (see Section 3.3) were prepared in a similar fashion to that described above; however, the moist mixtures were directly compacted in the shear box (measuring 60 mm × 60 mm in plane and 20 mm in height) in three layers (Soltani et al., 2019a, b).

To ensure consistency in void ratio (or porosity) and hence uniformity of fabric, particularly with regard to the samples prepared for the UC tests, the variations of dry unit weight (DUW) and water content (WC) should be measured along the height of the compacted samples (Estabragh and Javadi, 2008; Zhang et al., 2019). In this regard, representative samples, namely M_0 (natural soil), M_{10}, M_{20} and M_{30} were examined, and the results are provided in Fig. 1. For all four cases, the variations of both DUW and WC were found to be rather marginal, as is evident with the low standard deviations (SDs), which in turn corroborates the suitability and hence repeatability of the implemented static compaction technique.

3.2. Unconfined compression test

UC tests were carried out on the natural soil (M_0) and various soil–mica blends, M_x where $x = \{5, 10, 15, 20, 25, 30\}$, in accordance with the ASTM D2166/D2166M–16 (2016) standard. The samples,

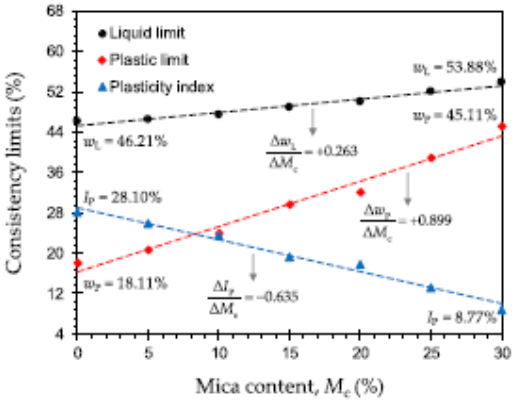

Fig. 2. Variations of the consistency limits, including liquid limit, plastic limit and plasticity index, against mica content for the tested mix designs.

Please cite this article as: Zhang J et al., Mechanical behavior of micaceous clays, Journal of Rock Mechanics and Geotechnical Engineering, https://doi.org/10.1016/j.jrmge.2019.04.001

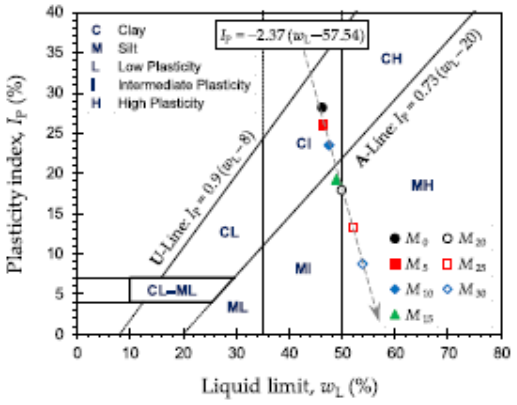

Fig. 3. Soil–mica mix designs illustrated on Casagrande's plasticity chart.

prepared as per Section 3.1, were axially compressed at a constant displacement rate of 1 mm/min (= 1%/min), as suggested in the literature (e.g. Estabragh et al., 2016b; Soltani et al., 2017a, b). For each sample, the axial strains and the corresponding axial stresses were recorded at various time intervals to a point at which the maximum axial stress required for sample failure, the peak UC strength, and its corresponding axial strain, a measure of the sample's ductility, were achieved. To ensure sufficient accuracy, triplicate samples were tested for each mix design, and the median value was considered for further analyses. The standard deviation (SD) and the coefficient of variation (CV) for the triplicate peak UC strength data were found to range between SD = 3.37 kPa (for M_0) and 7.65 kPa (for M_{20}), and CV = 1.82% (for M_0) and 8.06% (for M_{30}); the low SD and CV values corroborate the repeatability of the adopted sample preparation technique (particularly the static compaction), as well as the implemented UC testing procedure (Zhao et al., 2019; Zhang et al., 2019). On account of the three replicates adopted for each mixture, a total of 21 UC tests were carried out to address the seven mix designs outlined in Table 3.

3.3. Direct shear test

Unconsolidated undrained (UU) DS tests were carried out on the natural soil (M_0) and various soil–mica blends, M_x where $x = \{5, 10, 15, 20, 25, 30\}$, in accordance with the AS 1289.6.2.2–98 (1998) standard. As outlined in Section 3.1, the various mixtures were statically compacted in the shear box, measuring 60 mm × 60 mm in plane and 20 mm in height, at their respective standard Proctor optimum condition (see w_{opt}, γ_{dmax} and e_{opt} in Table 3); they were then tested for shear strength at varying normal stresses of σ_n = 100 kPa, 200 kPa, 300 kPa and 400 kPa. A high shear rate of 1 mm/min (= 1.67%/min) was adopted for the shearing phase to minimize both drainage and excess pore water pressure effects (Sezer et al., 2006; Bai and Liu, 2012; Qu and Zhao, 2016). For each DS testing scenario, the shear stresses were recorded as a function of the horizontal displacements up to a total displacement of 10 mm to quantify and hence perceive the stress–displacement response at both peak and post-peak conditions. Finally, the conventional Mohr–Coulomb failure criterion, using a total stress approach, was implemented to arrive at the apparent shear strength parameters, namely the cohesion and the angle of internal friction (Al-Aqtash and Bandini, 2015; Soltani et al., 2019a, b). On account of the four normal stresses applied for each mixture, a total of 28 DS tests were carried out to address the seven mix designs outlined in Table 3.

3.4. Scanning electron microscopy studies

The SEM technique was implemented to observe the evolution of fabric in response to the mica inclusions. In this regard, typical mix designs consisting of the natural soil (M_0), M_5 and M_{30} were examined. The desired samples, which were prepared in a similar fashion to that described for the UC test (see Section 3.1), were first air-dried for approximately 14 d. The desiccated samples were carefully fractured into small cubic-shaped pieces measuring approximately 1 cm^3 in volume, as suggested in the literature (e.g. Mirzababaei et al., 2009; Estabragh et al., 2016b; Soltani et al., 2018b). The fractured samples were then scanned by means of the Philips XL20 scanning electron microscope (Amsterdam, the Netherlands) at various magnification ratios ranging from 250× to 20,000×. It should be mentioned that the microstructure analyses were carried out using a SEM characterization scheme developed by Soltani et al. (2018b) and Zhang et al. (2019).

4. Results and discussion

4.1. Effect of mica content on soil consistency

Fig. 2 illustrates the variations of the consistency limits, including liquid limit w_L, plastic limit w_P, and plasticity index I_P (= $w_L - w_P$), against mica content M_c for the tested mix designs. The

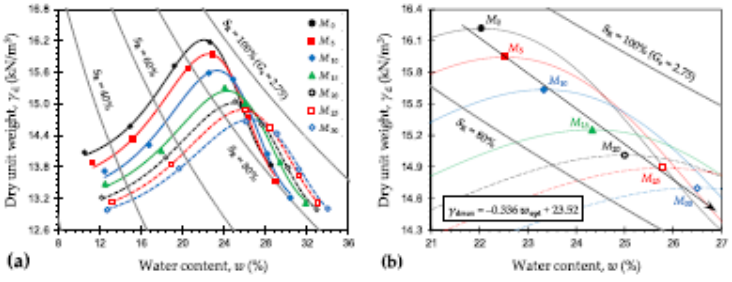

Fig. 4. Standard Proctor compaction results for the tested mix designs: (a) Compaction curves; and (b) Path of optimums.

Please cite this article as: Zhang J et al., Mechanical behavior of micaceous clays, Journal of Rock Mechanics and Geotechnical Engineering, https://doi.org/10.1016/j.jrmge.2019.04.001

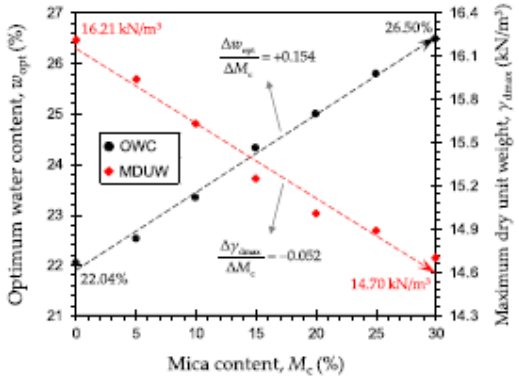

Fig. 5. Variations of the optimum water content (OWC) and the maximum dry unit weight (MDUW) against mica content for the tested mix designs.

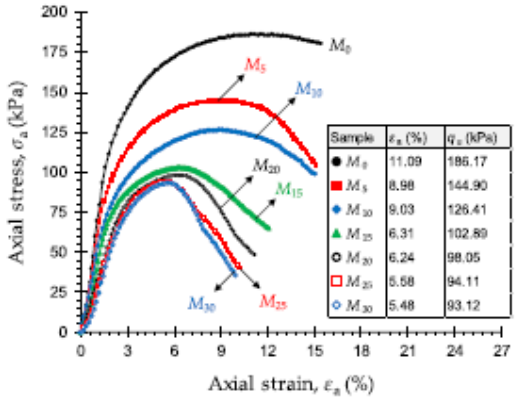

Fig. 6. UC stress–strain curves for the natural soil and various soil–mica blends.

mica content was positively proportional to the liquid and plastic limits, and both consistency limits followed a linear, monotonically increasing trend with respect to mica content. Interestingly, the rate of increase in w_P (with respect to M_c) was found to be approximately three-fold greater than that of w_L, i.e. $\Delta w_P/\Delta M_c = 0.899$ compared with $\Delta w_L/\Delta M_c = 0.263$. As a result, the plasticity index experienced a linear, monotonically decreasing trend with respect to mica content (decrease rate was $\Delta I_P/\Delta M_c = -0.635$), thereby signifying a gradual transition towards a non-plastic, cohesionless (NP) character. In terms of the plastic limit, for instance, the natural soil (M_0) resulted in $w_P = 18.11\%$, while the inclusion of 5%, 10%, 15%, 20%, 25% and 30% mica (M_5 to M_{30}) resulted in higher values of $w_P = 20.61\%$, 24.01%, 29.71%, 32.18%, 38.92% and 45.11%, respectively. The soft, spongy fabric (and hence high elasticity) of mica minerals makes for a rather difficult, if not impossible, implementation (and hence reproducibility) of the rolling thread method for plastic limit measurements. Even though mica inclusion would theoretically lead to an increased plastic limit, one cannot arrive at a certain/unique value with confidence by following the current methodology (Tubey and Bulman, 1964). Despite several attempts by different operators, a notable variability, as much as ±8% water content, seemed to dominate the plastic limit measurements, thereby suggesting the inapplicability of the current consistency limits framework, the rolling thread method in particular, for fine-grained micaceous soils. The plasticity index often serves as a measure of the soil's apparent cohesion, with higher values manifesting a more cohesive character (Sridharan and Prakash, 1999). As such, a decrease in the plasticity index, as is the case with mica inclusion, signifies a potential reduction in the soil's apparent cohesion and hence its undrained shear strength. This hypothesis will be further examined (and confirmed) by means of the UC and DS tests, and the results of which will be presented in Sections 4.3 and 4.4, respectively.

Fig. 3 illustrates the location of the seven soil–mica mixtures on Casagrande's plasticity chart. As demonstrated in the figure, the variations of I_P against w_L follows a linear path, diagonal to the 'A' and 'U' lines of the plasticity chart (see the arrowed line in Fig. 3); the linear relationship can be expressed as $I_P = -2.37\,(w_L - 57.54)$ where coefficient of determination is $R^2 = 0.988$. Most documented studies in this context, such as Tubey (1961), have noted a nonlinear transition over the I_P–w_L space, which contradicts that observed in the present study. The natural soil (M_0) was characterized as CI "*clay with intermediate plasticity*". An increase in mica content, however, gradually transitioned the soil towards the MI "*silt with intermediate plasticity*" and MH "*silt with high plasticity*" categories, as shown by the arrowed line in Fig. 3. In this case, the inclusion of 5%, 10%, 15%, 20%, 25% and 30% mica (M_5 to M_{30}) changed the original CI classification to CI, CI, MI, MI, MH and MH, respectively. Given the observed trend, a further increase in mica content could potentially result in w_P values equal to or greater than w_L, and thus give rise to null or

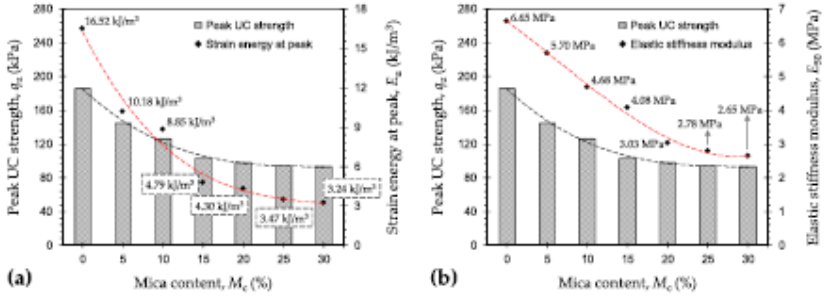

Fig. 7. Variations of (a) the strain energy at peak E_u and (b) the elastic stiffness modulus E_{50}, along with the corresponding peak UC strength values q_u, against mica content for the tested samples.

Please cite this article as: Zhang J et al., Mechanical behavior of micaceous clays, Journal of Rock Mechanics and Geotechnical Engineering, https://doi.org/10.1016/j.jrmge.2019.04.001

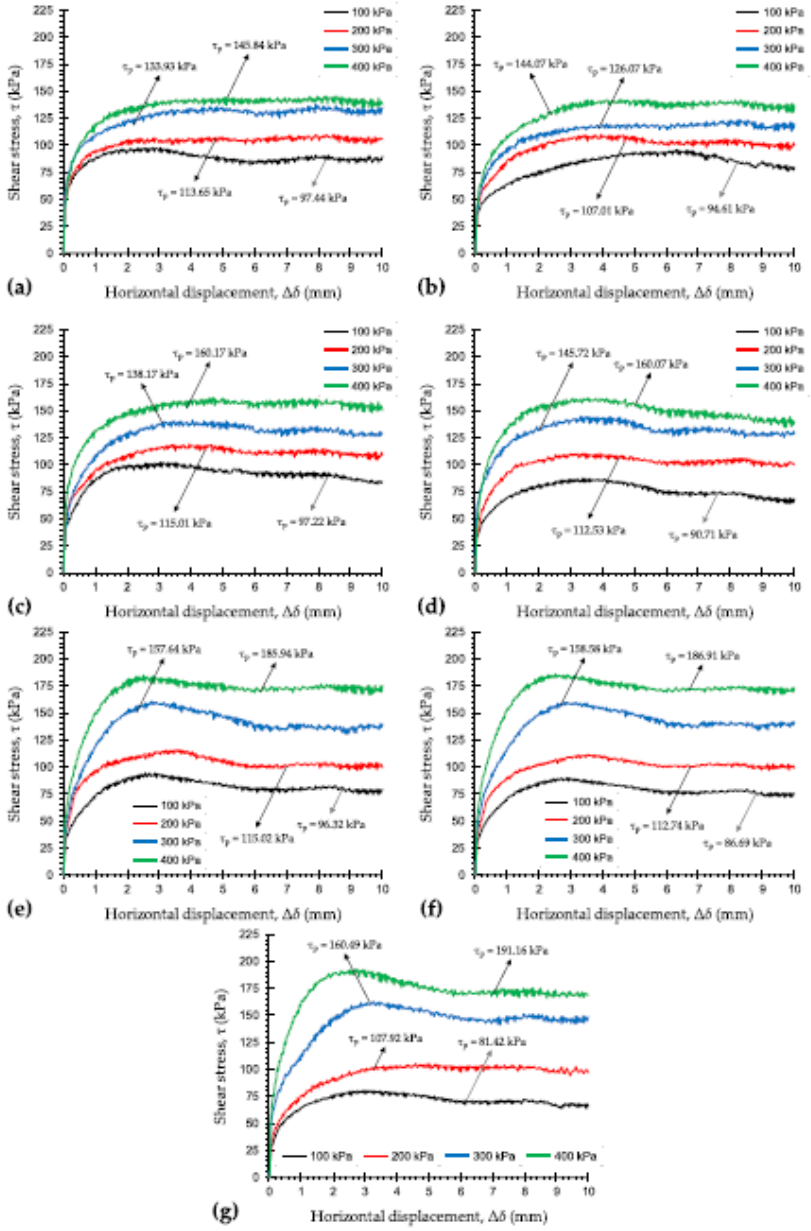

Fig. 8. DS stress–displacement curves for the tested mix designs: (a) M_0; (b) M_5; (c) M_{10}; (d) M_{15}; (e) M_{20}; (f) M_{25}; and (g) M_{30}.

negative I_P ($= w_L - w_P$) values, implying an NP behavior. It should be noted that the gradual transition towards the NP character has also been recognized by previous researchers such as Tubey (1961) and Mshali and Visser (2012, 2014).

4.2. Effect of mica content on soil compaction

Standard Proctor compaction curves, along with representative saturation lines (for $G_s^S = 2.74$), are illustrated in Fig. 4a for the

Please cite this article as: Zhang J et al., Mechanical behavior of micaceous clays, Journal of Rock Mechanics and Geotechnical Engineering, https://doi.org/10.1016/j.jrmge.2019.04.001

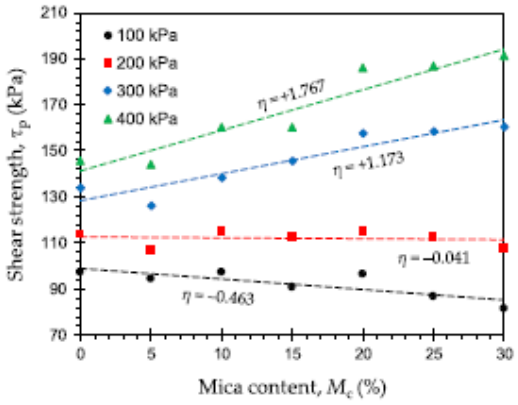

Fig. 9. Variations of the shear strength, at varying normal stresses, against mica content for the tested samples.

tested mix designs. With an increase in mica content, the compaction curve experienced a notable downward–rightward shift, suggesting an increase in the optimum water content w_{opt} and a decrease in the maximum dry unit weight γ_{dmax}. The peak (or optimum) point for all mixtures was found to lie between $S_R = 80\%$ and 100% saturation lines (see Fig. 4b), which is consistent with that commonly reported in the literature for natural fine-grained soils (e.g. Pandian et al., 1997; Sridharan and Nagaraj, 2005; Soltani et al., 2019c). Moreover, the peak points followed a linear decreasing trend with an increase in mica content M_c (see the arrowed line in Fig. 4b), thereby signifying the existence of a linear relationship for both w_{opt} and γ_{dmax} with M_c.

Fig. 5 presents the variations of the compaction characteristics (w_{opt} and γ_{dmax}) against mica content M_c for the tested mix designs. An increase in mica content resulted in higher optimum water contents, which followed a linear, monotonically increasing trend with an increase rate of $\Delta w_{opt}/\Delta M_c = 0.154$. In contrast, the maximum dry unit weight exhibited a linear, monotonically decreasing trend with a decrease rate of $\Delta \gamma_{dmax}/\Delta M_c = -0.052$. The natural soil ($M_0$) resulted in $w_{opt} = 22.04\%$ (corresponding to $\gamma_{dmax} = 16.21$ kN/m^3), while the addition of 5%, 10%, 15%, 20%, 25% and 30% mica (M_5 to M_{30}) resulted in $w_{opt} = 22.52\%$, 23.33%, 24.33%, 25%, 25.8% and 26.5% (corresponding to $\gamma_{dmax} = 15.94$ kN/m^3, 15.63 kN/m^3, 15.25 kN/m^3, 15.01 kN/m^3, 14.89 kN/m^3 and 14.7 kN/m^3), respectively. Compaction problems associated with micaceous soils can be attributed to mica's high water demand, as well as its soft, spongy fabric (Tubey, 1961; Tubey and Webster, 1978; Ballantine and Rossouw, 1989; Mshali and Visser, 2012, 2014). Mica minerals rebound when unloaded and hence offset a portion of the compaction energy applied to the mixtures, thus yield a lower maximum dry unit weight (or higher void ratio). The higher void ratio, which is proportional to the mica content, suggests the existence of a series of inter- and intra-assemblage pore-spaces, respectively, formed between and within the clay aggregates; these pore-spaces facilitate the adsorption of water by clay particles, and thus may potentially result in some adverse behaviors, e.g. increased swelling, low strength resistance and high permeability.

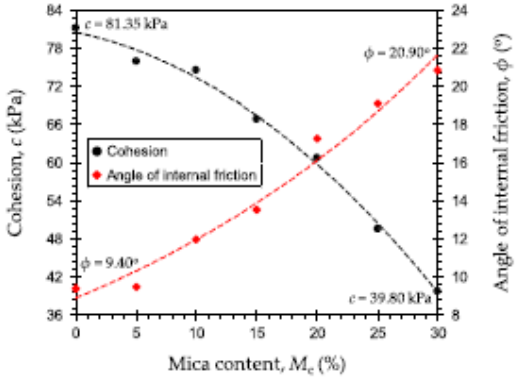

Fig. 10. Variations of the shear strength parameters (cohesion c and angle of internal friction ϕ) against mica content for the tested samples.

4.3. Effect of mica content on UC strength

Stress–strain curves, obtained from the UC tests, are provided in Fig. 6 for the tested samples. The stress–strain locus for the natural soil sample exhibited a strain-hardening behavior and hence a rather robust, non-brittle failure. As a result of mica inclusion, the stress–strain response progressively transitioned towards a strain-softening character and hence a more dramatic, brittle failure. The peak UC strength was inversely dependent on the mica content, with higher mica contents exhibiting lower peak UC strength values. The natural soil (M_0) resulted in a peak UC strength of $q_u = 186.17$ kPa, while the addition of 5%, 10%, 15%, 20%, 25% and 30% mica (M_5 to M_{30}) resulted in lower values of 144.9 kPa, 126.41 kPa, 102.89 kPa, 98.05 kPa, 94.11 kPa and 93.12 kPa, respectively. Interestingly, low mica contents, as low as $M_c = 5\%$, could raise serious strength concerns when presented in the soil matrix. The failure axial strain, denoted as ε_u, is an indicator of the material's ductility, with higher values suggesting a more ductile character (Estabragh et al., 2017; Soltani et al., 2017b; Zhao et al., 2019). Much like q_u, ε_u was also adversely affected by mica content, indicating a major reduction in the soil's ductility when paired with the mica mineral. As a typical case, the natural soil sample or M_0 yielded at $\varepsilon_u = 11.09\%$, while the sample M_{30} led to $\varepsilon_u = 5.48\%$, which signifies a notable two-fold reduction in the soil's ductility.

The area under a typical UC stress–strain curve up to the failure/peak point, denoted as E_u, is defined as strain energy at peak (or energy adsorption capacity); it serves as a measure of the material's toughness (Maher and Ho, 1994; Mirzababaei et al., 2013). Fig. 7a illustrates the variations of E_u, along with the corresponding q_u values, for the tested samples. The strain energy at peak followed a trend similar to that observed for the peak UC strength, meaning that the greater the mica content, the lower the E_u value. As demonstrated in Fig. 7a, both q_u and E_u exhibited an exponential tendency for reduction with respect to M_c. Lower strain energy at peak values suggests a decrease in the failure axial strain and/or the peak UC strength (Soltani et al., 2019b). With regard to various soil–mica blends, both parameters ε_u and q_u decrease with an increase in mica content and hence contribute to lower E_u values. As a typical case, the natural soil sample (M_0) resulted in $E_u = 16.52$ kJ/m^3, while the sample M_{30} resulted in $E_u = 3.24$ kJ/m^3, which indicates a five-fold reduction in the soil's energy adsorption capacity or toughness.

The secant modulus at 50% of the peak UC strength, commonly referred to as the elastic stiffness modulus and denoted as E_{50} (Radovic et al., 2004; Iyengar et al., 2013; Zhao et al., 2019), was also calculated for the tested samples, and the results are provided in Fig. 7b. All mica-blended samples exhibited lower E_{50} values

Please cite this article as: Zhang J et al., Mechanical behavior of micaceous clays, Journal of Rock Mechanics and Geotechnical Engineering, https://doi.org/10.1016/j.jrmge.2019.04.001

compared with that of the natural soil, indicating a reduced material stiffness as a result of mica inclusion. Much like q_u and E_u, the tendency for reduction in E_{50} followed an exponential trend with respect to M_c. The natural soil (M_0) resulted in E_{50} = 6.65 MPa, while mica inclusions of 5%, 10%, 15%, 20%, 25% and 30% (M_5 to M_{30}) resulted in lower values of 5.7 MPa, 4.68 MPa, 4.08 MPa, 3.03 MPa, 2.78 MPa and 2.65 MPa, respectively.

4.4. Effect of mica content on shear strength

Stress–displacement curves, obtained from the DS tests at varying normal stresses, are provided in Fig. 8a–g for the natural soil (M_0) and various mica-blended samples containing 5%, 10%, 15%, 20%, 25% and 30% mica (M_5 to M_{30}), respectively. In most cases, the stress–displacement response exhibited a rise–plateau behavior without visually detectable peak points, thereby signifying a strain-hardening behavior. This effect, however, was slightly less pronounced for samples of higher mica contents, such as M_{25} and M_{30}, particularly at higher normal stresses, e.g. see σ_n = 300 kPa and 400 kPa in Fig. 8f and g. Much like natural fine-grained soils, the stress–displacement response for a given mica content was dependent on the applied normal stress, with higher normal stresses exhibiting higher shear strength values. It should be noted that the shear strength, denoted as τ_p, was defined as the maximum shear stress attained within the 6–10 mm displacement region (Liu and Evett, 2009). At a normal stress of σ_n = 100 kPa, for instance, the natural soil (M_0) and the samples blended with 5% and 30% mica (M_5 and M_{30}) resulted in τ_p = 97.44 kPa, 94.61 kPa and 81.42 kPa, respectively. Where σ_n = 400 kPa, these values increased to 145.84 kPa, 144.07 kPa and 191.16 kPa, respectively.

Fig. 9 illustrates the variations of shear strength, at varying normal stresses, against mica content for the tested samples. At a given normal stress, the variations of shear strength followed a nearly linear path with respect to mica content M_c. At normal stresses equal to or less than 200 kPa, τ_p exhibited a linear, monotonically decreasing trend with respect to M_c, while the opposite occurred at higher normal stresses of 300 kPa and 400 kPa. The former, σ_n = 100 kPa and 200 kPa, is consistent with the results obtained from the UC tests which, in essence, is a low-confinement strength test (see Fig. 6). The rate of decrease or increase in τ_p with respect to M_c, i.e. $\eta = \Delta\tau_p/\Delta M_c$, was strongly dependent on the applied normal stress; the higher the applied normal stress, the higher the value of η. As demonstrated in Fig. 9, at σ_n = 100 kPa and 200 kPa, η was obtained as −0.463 and −0.041, respectively. When σ_n = 300 kPa and 400 kPa, however, η transitioned towards the positive values of 1.173 and 1.767, respectively. Interestingly, micaceous soils, though inherently characterized as low-grade, problematic soils, may be deemed suitable under high confinement conditions. At σ_n = 100 kPa, for instance, the natural soil (M_0) and the sample blended with 30%

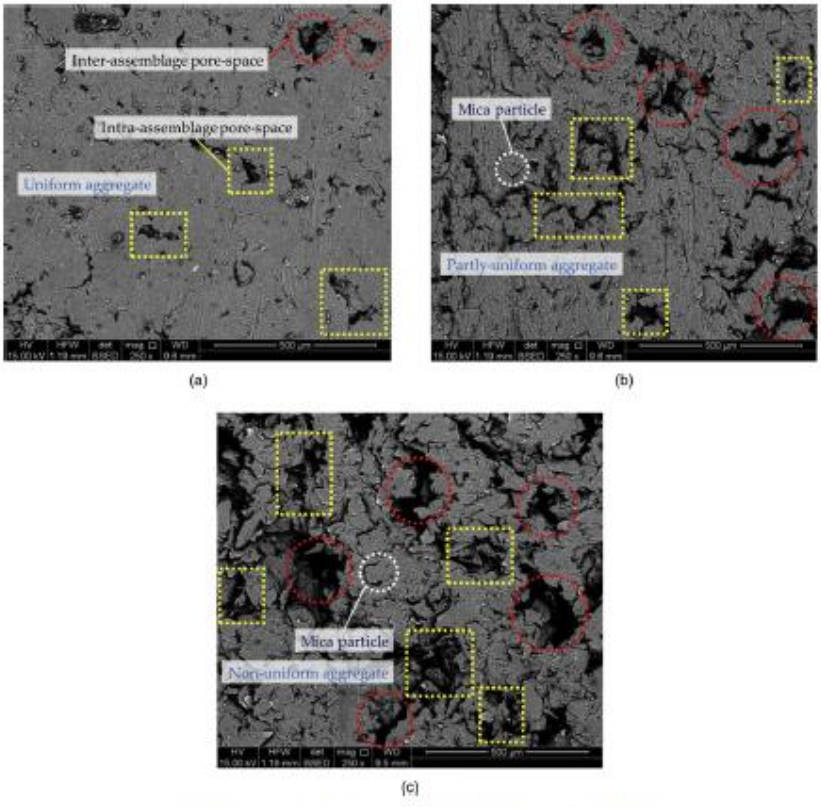

Fig. 11. SEM micrographs for the tested samples: (a) M_0; (b) M_5; and (c) M_{30}.

Please cite this article as: Zhang J et al., Mechanical behavior of micaceous clays, Journal of Rock Mechanics and Geotechnical Engineering, https://doi.org/10.1016/j.jrmge.2019.04.001

mica (M_{30}) resulted in $\tau_p = 97.44$ kPa and 81.42 kPa, respectively (i.e. 16.44% reduction in τ_p). When $\sigma_n = 400$ kPa, these values changed to 145.84 kPa (for M_0) and 191.16 kPa (for M_{30}), which suggested a 31.08% increase in τ_p. Improvement in the shear strength due to confinement can be attributed to the closer packing of the clay and mica components in the matrix. An increase in normal stress (or confinement) leads to a greater contact level between the clay and mica particles, which contributes to an induced frictional resistance at the shearing interface (owing to the difference of mica and clay in terms of surface roughness), thereby leading to higher shear strength values.

The conventional Mohr–Coulomb failure criterion, $\tau_p = c + \sigma_n \tan\phi$, where c is the cohesion and ϕ is the angle of internal friction, was implemented using a total stress approach to arrive at the apparent shear strength parameters c and ϕ, and the results are presented in Fig. 10. In terms of cohesion, the greater the mica content, the lower the apparent cohesion, following an exponentially decreasing trend. In contrast, the greater the mica content, the higher the apparent angle of internal friction, which in turn justifies the observed improvements in the shear strength at higher normal stresses (see Fig. 9). The natural soil (M_0) resulted in $c = 81.35$ kPa ($\phi = 9.4°$), while the inclusion of 5%, 10%, 15%, 20%, 25% and 30% mica (M_5 to M_{30}) resulted in $c = 76.08$ kPa, 74.64 kPa, 66.94 kPa, 60.86 kPa, 49.61 kPa and 39.8 kPa ($\phi = 9.5°$, 11.97°, 13.57°, 17.3°, 19.11° and 20.9°), respectively.

4.5. Clay–mica interactions and scanning electron microscopy analysis

Fig. 11a–c presents the SEM micrographs for the natural soil (M_0) and the samples blended with 5% and 30% mica contents (M_5 and M_{30}), respectively. The natural soil sample exhibited a fully dense, uniform matrix, which was accompanied by a limited number of rather small inter- and intra-assemblage voids/pore-spaces, respectively, formed between and within the soil aggregates; these morphological features warrant the presence of an edge-to-face flocculated fabric (see Fig. 11a). The inter-assemblage voids were formed during sample preparation, or static compaction, and thus are proportional to the sample's initial/as-compacted void ratio, as presented in Table 3. However, the shape and extension of these voids may have changed during the drying process of the SEM sample fabrication (see Section 3.4), owing to the development of tensile stresses within the fabric during desiccation (Soltani et al., 2018b). The sample blended with 5% mica (M_5) manifested a relatively loose, partly uniform matrix, which was accompanied by a notable number of more pronounced voids distributed along the soil–mica interfaces; such attributes indicate a transition towards an edge-to-edge dispersed fabric (see Fig. 11b). As opposed to a flocculated fabric, a dispersed fabric offers less resistance to external loading and/or shear (Mitchell and Soga, 2005; Kim and Palomino, 2009); this is consistent with the results obtained from the UC and DS (at low normal stresses) tests outlined in Sections 4.3 and 4.4. In the case of 30% mica inclusion (M_{30}), an edge-to-edge dispersed character clearly dominated the fabric, as is evident with the presence of a fully loose, non-uniform matrix accompanied by an increased number of relatively larger pore-spaces (see Fig. 11c). As such, the degree of fabric dispersion is proportional to the mica content, with higher mica contents resulting in a more dispersed fabric and hence lower strength resistance. The above discussion, however, only holds provided that the mica-blended sample is tested under low confinements. As is evident from the DS test results outlined in Fig. 9, high confinements (or normal stresses) can alter the fabric by providing a closer packing of the clay and mica particles, thereby inducing frictional resistance at the shearing interface, owing to an induced clay–mica contact level, and thus improving the shear strength performance.

5. Conclusions

The present study has arrived at the following conclusions:

(1) The liquid and plastic limits exhibited a linear, monotonically increasing trend with increase in mica content. The rate of increase in the plastic limit with respect to mica content was observed to be approximately three-fold greater than that of the liquid limit. As a result, the plasticity index experienced a linear, monotonically decreasing trend with respect to mica content, indicating a gradual transition towards an NP character.

(2) The mica content influenced the optimum water content of the clay soil, following a linear, monotonically increasing trend. In contrast, the maximum dry unit weight exhibited a linear, monotonically decreasing trend with respect to mica content. Compaction problems associated with micaceous soils was attributed to mica's high water demand, as well as its soft, spongy fabric which promotes a rebound response to compaction energy.

(3) As a result of mica inclusion, the stress–strain response, under UC loading conditions, progressively transitioned towards a strain-softening character and hence a more dramatic, brittle failure. The UC parameters including strength, ductility, toughness and stiffness were all adversely affected by mica, with higher mica contents exhibiting lower UC parameters, following an exponential tendency for reduction.

(4) In most cases, the stress–displacement response, under DS testing conditions, exhibited a strain-hardening behavior. This effect, however, was slightly less pronounced for samples with higher mica contents, such as 25% and 30%, at higher normal stresses. At normal stresses equal to or less than 200 kPa, the shear strength decreased with an increase in mica content, while the opposite occurred at higher normal stresses of 300 kPa and 400 kPa. The latter was attributed to the compact packing of the clay and mica components in the matrix under high confinement, which offsets the adverse effects of mica by inducing frictional resistance at the shearing interface.

(5) The apparent shear strength parameters, namely the cohesion and the angle of internal friction, were also dependent on the mica content. In terms of cohesion, higher mica contents led to lower cohesion values, following an exponentially decreasing trend. In contrast, higher mica contents led to increased angles of internal friction; this behavior justifies the observed improvement in shear strength at high confinements.

Conflicts of interest

The authors wish to confirm that there are no known conflicts of interest associated with this publication, and there has been no significant financial support for this work that could have influenced its outcome.

Acknowledgments

This research was made possible through the provision of an Australian Government Research Training Program Scholarship; this support is gratefully acknowledged.

Please cite this article as: Zhang J et al., Mechanical behavior of micaceous clays, Journal of Rock Mechanics and Geotechnical Engineering, https://doi.org/10.1016/j.jrmge.2019.04.001

Abbreviations

AS	Australian standards
CI	Clay with intermediate plasticity
CV	Coefficient of variation
DS	Direct shear
DUW	Dry unit weight
MDUW	Maximum dry unit weight
MH	Silt with high plasticity
MI	Silt with intermediate plasticity
NP	Non-plastic
OWC	Optimum water content
SD	Standard deviation
SEM	Scanning electron microscopy
UC	Unconfined compression
USCS	Unified soil classification system
UU	Unconsolidated undrained
WC	Water content

Notation

C	Cohesion (DS test)
E_{50}	Elastic stiffness modulus (UC test)
e_{opt}	Optimum void ratio
E_u	Strain energy at peak (UC test)
G_S^M	Specific gravity of ground mica
G_S^S	Specific gravity of soil solids
I_P	Plasticity index
M_c	Mica content (by mass)
q_u	Peak UC strength
R^2	Coefficient of determination
S_a	Specific surface area
S_R	Degree of saturation
w_L	Liquid limit
w_{opt}	Optimum water content
w_P	Plastic limit
γ_{dmax}	Maximum dry unit weight
$\Delta\delta$	Horizontal displacement
ε_u	Failure axial strain (UC test)
η	Rate of increase/decrease in shear strength with respect to mica content
σ_n	Normal stress (DS test)
τ_p	Shear strength (DS test)
φ	Angle of internal friction (DS test)

References

ASTM D2166/D2166M−16. Standard test method for unconfined compressive strength of cohesive soil. West Conshohocken, PA, USA: ASTM International; 2016.
ASTM D422−63(2007)e2. Standard test method for particle-size analysis of soils. West Conshohocken, PA, USA: ASTM International; 2007.
ASTM D698−12e2. Standard test methods for laboratory compaction characteristics of soil using standard effort (12,400 ft−lbf/ft3 (600 kN−m/m3). West Conshohocken, PA, USA: ASTM International; 2012.
Al-Aqtash U, Bandini P. Prediction of unsaturated shear strength of an adobe soil from the soil–water characteristic curve. Construction and Building Materials 2015;98:892–9.
AS 1289.3.2.1–09. Methods of testing soils for engineering purposes: soil classification tests—determination of the plastic limit of a soil. Sydney, NSW, Australia: Standards Australia; 2009.
AS 1289.3.3.1–09. Methods of testing soils for engineering purposes: soil classification tests—calculation of the plasticity index of a soil. Sydney, NSW, Australia: Standards Australia; 2009.
AS 1289.3.9.1–15. Methods of testing soils for engineering purposes: soil classification tests—determination of the cone liquid limit of a soil. Sydney, NSW, Australia: Standards Australia; 2015.
AS 1289.6.2.2–98. Methods of testing soils for engineering purposes: soil strength and consolidation tests—determination of shear strength of a soil—direct shear test using a shear box. Sydney, NSW, Australia: Standards Australia; 1998.
ASTM D2487-11. Standard practice for classification of soils for engineering purposes (unified soil classification system). West Conshohocken, PA, USA: ASTM International; 2011.
ASTM D854-14. Standard test methods for specific gravity of soil solids by water pycnometer. West Conshohocken, PA, USA: ASTM International; 2014.
Bai FQ, Liu SH. Measurement of the shear strength of an expansive soil by combining a filter paper method and direct shear tests. Geotechnical Testing Journal 2012;35(3):451–9.
Ballantine RW, Rossouw AJ. Stabilization of soils. Pretoria, Gauteng, South Africa: PPC Lime Ltd.; 1989.
Clayton CR, Theron M, Vermeulen N. The effect of particle shape on the behaviour of gold tailings. In: Jardine RJ, Potts DM, Higgins KG, editors. Advances in geotechnical engineering: the skempton conference. London, England, UK: ICE Publishing; 2004. p. 393–404.
Estabragh AR, Javadi AA. Critical state for overconsolidated unsaturated silty soil. Canadian Geotechnical Journal 2008;45(3):408–20.
Estabragh AR, Soltani A, Javadi AA. Models for predicting the seepage velocity and seepage force in a fiber reinforced silty soil. Computers and Geotechnics 2016a;75:174–81.
Estabragh AR, Khatibi M, Javadi AA. Effect of cement on treatment of a clay soil contaminated with glycerol. Journal of Materials in Civil Engineering 2016b;28(4). https://doi.org/10.1061/(ASCE)MT.1943-5533.0001443.
Estabragh AR, Ranjbari S, Javadi AA. Properties of clay soil and soil cement reinforced with polypropylene fibers. ACI Materials Journal 2017;114(2):195–205.
Galán E, Ferrell RE. Chapter 3 – genesis of clay minerals. Developments in Clay Science 2013;5:83–126.
Gogo JO. Compaction and strength characteristics of decomposed mica schist. In: Proceedings of the 8th regional conference for africa on soil mechanics and foundation engineering. Harare, Zimbabwe: A.A. Balkema; 1984. p. 275–84.
Harris WG, Parker JC, Zelazny LW. Effects of mica content on engineering properties of sand. Soil Science Society of America Journal 1984;48(3):501–5.
Harvey JC. Geology for geotechnical engineers. 1st ed. Cambridge, UK: Cambridge University Press; 1982.
Iyengar SR, Masad E, Rodriguez AK, Bazzi HS, Little D, Hanley HJM. Pavement subgrade stabilization using polymers: characterization and performance. Journal of Materials in Civil Engineering 2013;25(4):472–83.
Kim S, Palomino AM. Polyacrylamide–treated kaolin: a fabric study. Applied Clay Science 2009;45(4):270–9.
Liu C, Evett J. Soil properties: testing, measurement, and evaluation. 6th ed. Upper Saddle River, New Jersey, USA: Pearson/Prentice Hall; 2009.
Maher MH, Ho YC. Mechanical properties of kaolinite/fiber soil composite. Journal of Geotechnical Engineering 1994;120(8):1381–93.
Mirzabahaei M, Yasrobi SS, Al-Rawas AA. Effect of polymers on swelling potential of expansive soils. Proceedings of the Institution of Civil Engineers - Ground Improvement 2009;162(3):111–9.
Mirzabahaei M, Miraftab M, Mohamed M, McMahon P. Unconfined compression strength of reinforced clays with carpet waste fibers. Journal of Geotechnical and Geoenvironmental Engineering 2013;139(3):483–93.
Mitchell JK, Soga K. Soil–water–chemical interactions. In: Fundamentals of soil behavior.3rd ed. Hoboken, New Jersey, USA: John Wiley & Sons; 2005. p. 143–72.
Mitchell RI, Van der Merwe CP, Geel HK. Standardised flexible pavement design for rural roads with light to medium traffic. Special Report. Salisbury, Zimbabwe: Rhodesian Government Central Laboratory; 1975.
Moore CA. Effect of mica on K_0 compressibility of two soils. Journal of the Soil Mechanics and Foundations Division 1971;97(9):1275–91.
Mshali MR, Visser AT. Influence of mica on unconfined compressive strength of a cement–treated weathered granite gravel. Journal of the South African Institution of Civil Engineering 2012;54(2):71–7.
Mshali MR, Visser AT. Influence of mica on compactability and moisture content of cement–treated weathered granite gravel. In: Proceedings of the 33rd southern African transport conference (SATC 2014). Pretoria, gauteng, South Africa. Minister of Transport; 2014. p. 546–55.
Netterberg F, Hefer A, Preez HD. Cracking and staining of an airport asphalt. In: Proceedings of the 10th conference on asphalt pavements for South Africa (CAPSA 11): roads of the future. KwaZulu, KwaZulu–Natal. South Africa: International Road Federation (IRF); 2011. p. 1–17.
Northmore KJ, Bell FG, Culshaw MG. The engineering properties and behaviour of the brickearth of south Essex. Quarterly Journal of Engineering Geology and Hydrogeology 1996;29(2):147–61.
Paige-Green P, Semmelink CJ. Road compaction problems related to the presence of biotite. In: Proceedings of the 9th congress of the International association of engineering geology and the environment. Durban, KwaZulu–Natal, South Africa; 2002. p. 2605–10.
Pandian NS, Nagaraj TS, Manoj M. Re-examination of compaction characteristics of fine–grained soils. Géotechnique 1997;47(2):363–6.
Qu J, Zhao D. Stabilising the cohesive soil with palm fibre sheath strip. Road Materials and Pavement Design 2016;17(1):87–103.
Radovic M, Lara-Curzio E, Riester L. Comparison of different experimental techniques for determination of elastic properties of solids. Materials Science and Engineering: A 2004;368(1–2):56–70.
Sezer A, İnan G, Recep Yılmaz H, Ramyar K. Utilization of a very high lime fly ash for improvement of Izmir clay. Building and Environment 2006;41(2):150–5.

Please cite this article as: Zhang J et al., Mechanical behavior of micaceous clays, Journal of Rock Mechanics and Geotechnical Engineering, https://doi.org/10.1016/j.jrmge.2019.04.001

Soltani A, Deng A, Taheri A, Mirzababaei M. A sulphonated oil for stabilisation of expansive soils. International Journal of Pavement Engineering 2017. in press, http://doi.org/10.1080/10298436.2017.1408270.

Soltani A, Taheri A, Khatibi M, Estabragh AR. Swelling potential of a stabilized expansive soil: a comparative experimental study. Geotechnical and Geological Engineering 2017b;35(4):1717–44.

Soltani A, Deng A, Taheri A. Swell–compression characteristics of a fiber–reinforced expansive soil. Geotextiles and Geomembranes 2018a;46(2):183–9.

Soltani A, Deng A, Taheri A, Mirzababaei M. Rubber powder–polymer combined stabilization of South Australian expansive soils. Geosynthetics International 2018b;25(3):304–21.

Soltani A, Deng A, Taheri A, Mirzababaei M, Nikraz H. Interfacial shear strength of rubber–reinforced clays: a dimensional analysis perspective. Geosynthetics International 2019a;26(2):164–83.

Soltani A, Taheri A, Deng A, Nikraz H. Tyre rubber and expansive soils: two hazards, one solution. Proceedings of the Institution of Civil Engineers - Construction Materials 2019. in press, http://doi.org/10.1680/jcoma.18.00075.

Soltani A, Deng A, Taheri A, Sridharan A. Consistency limits and compaction characteristics of clay soils containing rubber waste. Proceedings of the Institution of Civil Engineers - Geotechnical Engineering 2019c;172(2):174–88.

Sridharan A, Nagaraj HB. Plastic limit and compaction characteristics of fine-grained soils. Proceedings of the Institution of Civil Engineers - Ground Improvement 2005;9(1):17–22.

Sridharan A, Prakash K. Mechanisms controlling the undrained shear strength behaviour of clays. Canadian Geotechnical Journal 1999;36(6):1030–8.

Tubey LW. A laboratory investigation to determine the effect of mica on the properties of soils and stabilized soils. Research Note 4077. Wokingham, Berkshire, UK: Road Research Laboratory (RRL); 1961.

Tubey LW, Bulman JN. Micaceous soils: methods of determining mica content and the use of routine tests in the evaluation of such soils. In: Proceedings of the 2nd Australian road research board (ARRB) conference. ARRB; 1964. p. 880–901.

Tubey LW, Webster DC. The effects of mica on the roadmaking properties of materials. Supplementary Report 408. CrowthorneWokingham. Berkshire, UK: Transport and Road Research Laboratory (TRL); 1978.

Weinert HH. The natural road construction materials of Southern Africa. 1st ed. Cape Town, Western Cape, South Africa: H&R Academica; 1980.

Zhang J, Soltani A, Deng A, Jaksa MB. Mechanical performance of jute fiber-reinforced micaceous clay composites treated with ground-granulated blast-furnace slag. Materials 2019;12(4). https://doi.org/10.3390/ma12040576.

Zhao Y, Soltani A, Taheri A, Karakus M, Deng A. Application of slag–cement and fly ash for strength development in cemented paste backfills. Minerals 2019;9(1). https://doi.org/10.3390/min9010022.

Please cite this article as: Zhang J et al., Mechanical behavior of micaceous clays, Journal of Rock Mechanics and Geotechnical Engineering. https://doi.org/10.1016/j.jrmge.2019.04.001

Chapter 3

Mechanical Performance of Jute Fiber-Reinforced Micaceous Clay Composites Treated with Ground-Granulated Blast-Furnace Slag

Jiahe Zhang [1] , Amin Soltani [2,*] , An Deng [3] , Mark B. Jaksa [4]

[1] **PhD Student** — School of Civil, Environmental and Mining Engineering, The University of Adelaide, Adelaide SA 5005, Australia | **Email:** Jiahe.Zhang@adelaide.edu.au

[2] **Research Academic** — School of Civil, Environmental and Mining Engineering, The University of Adelaide, Adelaide SA 5005, Australia | **Email:** Amin.Soltani@adelaide.edu.au ; **ORCID:** 0000-0002-0483-7487

[3] **Senior Lecturer** — School of Civil, Environmental and Mining Engineering, The University of Adelaide, Adelaide SA 5005, Australia | **Email:** An.Deng@adelaide.edu.au ; **ORCID:** 0000-0002-3897-9803

[4] **Professor** — School of Civil, Environmental and Mining Engineering, The University of Adelaide, Adelaide SA 5005, Australia | **Email:** Mark.Jaksa@adelaide.edu.au

* Corresponding Author.

Zhang J, Deng A, Soltani, A and Jaksa MB **(2019)** Mechanical Performance of Jute-Reinforced Micaceous Clay Composites Treated with Ground-Granulated Blast-Furnace Slag. ***Materials***, 12(4), 576:1-23. http://doi.org/10.3390/ma12040576

Abstract

The combined capacity of Jute Fibers (JF), the reinforcement, and Ground-Granulated Blast-Furnace Slag (GBFS), the binder, was examined as a sustainable solution towards ameliorating the inferior engineering properties of micaceous clays. A total of sixteen JF + GBFS mix designs, i.e., JF (% by total mass) = {0, 0.5, 1.0, 1.5} and GBFS (% by total mass) = {0, 3, 6,

9}, were tested for unconfined compression (UC) strength; for those mix designs containing GBFS, curing was allowed for 7 and 28 days prior to testing. Scanning electron microscopy (SEM) studies were also carried out to observe the evolution of fabric in response to JF, GBFS and JF + GBFS amendments. The greater the JF content the higher the developed strength and stiffness up to 1% JF, beyond of which the effect of JF-reinforcement led to some adverse results. The JF inclusions, however, consistently improved the ductility and toughness of the composite. The addition of GBFS to the JF-reinforced samples improved the soil–fiber connection interface, and thus led to further improvements in the composite's strength, stiffness and toughness. The mix design "1% JF + 9% GBFS" managed to satisfy ASTM's strength criterion and hence was deemed as the optimum choice in this investigation. Finally, a non-linear, multivariable regression model was developed and validated to quantify the peak UC strength as a function of the composite's index properties. The proposed model contained a limited number of fitting parameters, all of which can be calibrated by little experimental effort, and thus implemented for preliminary design assessments.

Keywords: micaceous clay; jute fibers; ground-granulated blast-furnace slag; unconfined compression; strength; stiffness; scanning electron microscopy; multivariable regression

3.1. Introduction

Soils are the most common and readily accessible of all materials encountered in construction operations. Most soils, however, are characterized as problematic, as their intrinsic mechanical features, e.g., strength and bearing capacity, are often less than ideal for common civil engineering applications (Wei *et al.* 2018; Yin *et al*. 2018). Meanwhile, shortage of land for development, as well as increasing costs associated with construction and raw materials, necessitates maximum utilization of local materials, one being problematic soils; among others, micaceous soils have been less publicized and hence demand further attention. The mica group of sheet silicates are among the most widely distributed minerals around the world; they naturally occur in igneous, sedimentary and certain metamorphic rocks (Harvey 1982; Galán and Ferrell 2013). Common physical features of mica include its unique platy structure, high elasticity (owing to its soft, spongy fabric) and nearly perfect basal cleavage; the latter, the nearly perfect cleavage, is attributed to the hexagonal sheet-like arrangement of mica atoms (Frempong 1994; Fleet 2003). The presence of excessive mica minerals such as muscovite in weathered soils, particularly sands, adversely influence the soil's mechanical properties. Mica minerals, although rather resilient, may gradually recover their initial shape due to the elastic rebound (or springy action), thereby reducing the efficiency of compactive effort and hence compromising the performance of facilities founded on micaceous soils (Weinert 1980). During loading, i.e., compression, tension or shearing, mica minerals tend to rotate and orient themselves in a somewhat parallel fashion, which in turn leads to low strength resistance in micaceous soils (Harries *et al.* 1984). Therefore, micaceous soils are characterized by poor compactibility, high compressibility and low shear strength, all of which present significant challenges for road construction, building foundations, earth dams and other geotechnical engineering systems (Gilboy 1928; Tubey 1961; McCarthy *et al.* 1963; Tubey and Bulman 1964; Moore 1971; Tubey and Webster 1978; Hight *et al.* 1998; Lee *et al*. 2007; Ekblad and Isacsson 2008; Schmidt 2008; Cabalar and Cevik 2011; Seethalakshmi and Sachan 2018[a],2018[b]). Consequently, micaceous soils demand engineering solutions to alleviate the associated socio-economic impacts on human life.

Common solutions to counteract the adversities associated with problematic soils, and most likely micaceous clays, include soil replacement or attempting to amend the low-graded soil by means of stabilization (Soltani *et al.* 2019). The former involves replacing a portion of the problematic host soil with suitable quarried/burrowed materials capable of satisfying the

desired mechanical performance; this approach is often impractical due to long-haul distances, as well as other economic considerations (Estabragh *et al.* 2013). The latter, soil stabilization, refers to any chemical, physical, biological or combined practice of altering the soil fabric to meet the intended engineering criteria (Winterkorn and Pamukcu 1991). The chemical stabilization scheme makes use of chemical binders and/or additives — Portland cements, limes, fly ashes and slags, and more recently non-conventional agents such as polymers, resins and sulfonated oils — which initiate a series of short- and long-term chemical reactions in the soil–water medium, thereby amending the soil fabric into a coherent matrix of improved mechanical performance (Miller and Azad 2000; Mirzababaei *et al.* 2009; Estabragh *et al.* 2013[a], 2013[b]; Onyejekwe and Ghataora 2015; Alazigha et al. 2016; Keramatikerman et al. 2016; Sharma and Sivapullaiah 2016; Vakili et al. 2016; Soltani et al. 2017[a], 2017[b]; Phanikumar and Nagaraju 2018; Sekhar and Nayak 2018; Zhao *et al.* 2019). Physical stabilization often involves the placement of random or systematically-engineered reinforcements in the soil regime, thus engendering a spatial three-dimensional reinforcement network in favor of weaving/interlocking the soil particles into a unitary mass of induced strength resistance and improved ductility. Common reinforcements include fibers and geogrids of natural (e.g., bamboo, coir, hemp, jute and sisal) or synthetic (e.g., nylon, polyester, polyethylene, polypropylene and steel) origin, and more recently other sustainable geosynthetics such as waste textiles and recycled tire rubbers, all of which have been well documented in the literature (Kim *et al.* 2008; Sivakumar And Vasudevan 2008; Tang et al. 2010; Mirzababaei *et al.* 2013; Qu *et al.* 2013; Estabragh *et al.* 2016; Qu and Zhao 2016; Soltani *et al.* 2017; Wang *et al.* 2017; Mirzababaei *et al.* 2017[a],2017[b]; Soltani *et al.* 2018[a], 2018[b], 2018[c]). Recent studies indicate that the use of chemical agents, particularly cementitious binders such as Portland cement and lime, alongside physical reinforcements may significantly improve the soil–reinforcement connection interface or bonding, thereby promoting further fabric enhancements (Wei *et al.* 2018; Tang *et al.* 2007; Arpitha *et al.* 2017; Olgun 2013; Estabragh *et al.* 2017; Shahbazi *et al.* 2017; Yadav and Tiwari 2017; Mirzababaei *et al.* 2018; Soltani *et al.* 2018; Tran *et al.* 2018).

A sustainable soil stabilization scheme can be characterized as one that maintains a perfect balance between infrastructure performance and the social, economic and ecological processes required to maintain human equity, diversity, and the functionality of natural systems. Traditional stabilization agents including cementitious binders and synthetic reinforcements, although proven effective, are not financially competitive in terms of materials procurement, labor and equipment usage. Furthermore, these solutions often suffer from serious

environmental drawbacks attributed to their significant energy and carbon emissions footprints (Soltani *et al.* 2018, 2019) As such, the transition towards sustainable soil stabilization necessitates utilizing natural reinforcements and/or industrial by-products as part of the infrastructure system, and more specifically as replacements for traditional stabilization materials. Although the adverse effects of mica content on soils, particularly gravels and sands, have been well documented in the literature, systematic stabilization studies on micaceous soils, and micaceous clays in particular, are still limited (Tubey and Bulman 1964; Frempong 1995; Mshali and Visser 2012, 2013). More importantly, the adopted stabilization materials have been limited to Portland cement and lime, while sustainable agents commonly practiced for other problematic soils, e.g., natural fibers and industrial by-products such as fly ashes and slags, have not yet been examined and hence demand further attention.

The present study examines the combined capacity of Jute Fibers (JF), the reinforcement, and Ground-Granulated Blast-Furnace Slag (GBFS), the binder, as a sustainable solution towards ameliorating the inferior engineering characteristics of micaceous clays. A series of unconfined compression (UC) tests were carried out on various mix designs to evaluate the effects of JF-reinforcement and/or GBFS-treatment on the strength, ductility, stiffness and toughness of the micaceous clay. Scanning electron microscopy (SEM) studies were also carried out to observe the evolution of soil fabric in response to JF, GBFS and JF + GBFS amendments. Finally, a non-linear, multivariable regression model was developed and validated to quantify the peak UC strength as a function of the composite's index properties. A sensitivity analysis was also carried out to quantify the relative impacts of the independent regression variables, namely JF content, GBFS content and curing time, on the composite's strength.

3.2. Materials

3.2.1. Micaceous Clay

Commercially-available Kaolin (K) and Ground Mica (GM), sourced from local distributors, were used to artificially prepare a desired Micaceous Clay (MC) blend for further experimental work. The choice of GM content for the MC blend was selected as 20% (by dry mass of K), as it represents an upper boundary prerequisite to simulate adverse mechanical attributes commonly exhibited by natural micaceous clays, i.e., compactability issues and low shear strength/bearing capacity (Tubey 1961; McCarthy and Lonard 1963; Lee *et al.* 2007). The artificial MC blend manifested the same typical texture, sheen and friability features as natural

micaceous clays commonly reported in the literature, and thus may well provide a basis for systematic stabilization studies. The physical and mechanical properties of K, GM and the MC blend (hereafter simply referred to as natural soil) were determined as per relevant ASTM and Australian (AS) standards, and the results are summarized in Table 1. The conventional gradation analysis, carried out in accordance with ASTM D422–07, indicated a clay fraction (< 2 μm) of 51%, along with 48% silt (2–75 μm) and 1% sand (0.075–4.75 mm) for K. As a result of 20% GM inclusion, the aforementioned values changed to 39%, 55% and 6%, respectively. The liquid limit and plasticity index were measured as LL = 44.67% and PI = 20.95% for K, and LL = 48.67% and PI = 11.28% for MC, from which these soils were, respectively, characterized as *clay with intermediate plasticity* (CI) and *silt with intermediate plasticity* (MI) in accordance with the Unified Soil Classification System (USCS). The standard Proctor compaction test (ASTM D698–12) indicated optimum water contents of w_{opt} = 19.84% and 23.52%, along with maximum dry densities of ρ_{dmax} = 1.63 g/cm^3 and 1.56 g/cm^3, for K and MC, respectively. Such trends can be attributed to the spongy nature (i.e., elastic/rebound response to compaction energy) and high water demand of the mica mineral (Tubey and Bulman 1964; Ballantine and Rossouw 1989; Seethalakshmi and Sachan 2018).

The chemical compositions of K and GM, as supplied by the manufacturers, are outlined in Table 2. The chemical composition of both K and GM is mainly dominated by silicon dioxide (SiO_2) and aluminum trioxide (Al_2O_3) with mass fractions of 64.9% and 22.2% for K, and 49.5% and 29.2% for GM, respectively. The pH for slurries of K and GM was, respectively, found to be 7.4 and 7.8, from which both materials were classified as neutral substances. Other material properties included a specific surface area of SSA = 11.2 m^2/g and 5.3 m^2/g for K and GM, respectively.

3.2.2. Jute Fibers

Commercially-available Jute Fibers (JF), manufactured from *Corchorus capsularis* (a shrub species in the Malvaceae family), was used as the reinforcing agent. Its biochemical composition, as commonly reported in the literature, consists of 56–71% cellulose, 29–35% hemicellulose and 11–14% lignin (Gowthaman *et al.* 2018). The raw fibers had a diameter of F_D = 30–40 μm; they were cut into segments of approximately F_L = 15 mm, thus resulting in an aspect ratio of $F_{AR} = F_L/F_D$ = 375–500 (see Figures 1a and 1b). The scanning electron microscopy (SEM) technique was used to observe the fiber's surface morphology, and the results are illustrated in Figure 1c. The fiber's surface embodies a highly-irregular shape

comprising of a series of peaks and troughs of varying heights, depths and spacing, thus signifying a rough surface texture. Such surface features may potentially promote adhesion and/or induce frictional resistance at the soil–fiber interface, and thus amend the soil fabric into a coherent matrix of induced strength and improved ductility (see Section 4.3). The physical and mechanical properties of JF, as supplied by the distributor, are provided in Table 3. The specific gravity of JF was found to be 1.30–1.46, which is approximately two-fold less than that of the MC blend.

3.2.3. Ground-Granulated Blast-Furnace Slag

A large quantity of Ground-Granulated Blast-Furnace Slag (GBFS) was sourced from a local manufacturer in South Australia, and was used as the cementitious binder. The physical properties and chemical composition of GBFS, as supplied by the manufacturer, are outlined in Table 4. The particles of GBFS were mainly finer than 75 μm in size; its fines and sand fractions were found to be 96% and 4%, respectively. Other properties included a basic pH of 9.6 and a specific surface area of SSA = 0.7 m^2/g; the latter is approximately two-fold greater than that of ordinary Portland cement (Kosmatka *et al.* 2002). The chemical composition of GBFS is mainly dominated by calcium oxide or lime (CaO) and silicon dioxide (SiO_2) with mass fractions of 44.7% and 27.1%, respectively. The former, the calcium oxide, acts as a precursor agent, initiating a series of short- and long-term chemical reactions in the soil–water medium, i.e., cation exchange, flocculation–agglomeration and pozzolanic reactions, thereby amending the soil fabric into a unitary mass of enhanced mechanical performance (see Section 4.3).

3.3. Experimental Program

3.3.1. Mix Designs and Sample Preparations

In this study, a total of sixteen mix designs consisting of one control (natural soil), three JF-reinforced, three GBFS-treated and nine JF + GBFS blends were examined (see Table 5). Hereafter, the following coding system is adopted to designate the various mix designs:

$$F_x S_y T_z \tag{1}$$

where F_x = x% JF; S_y = y% GBFS; and T_z = z days of curing.

The JF, GBFS and water contents were, respectively, defined as:

$$(\%)\ F_c = \frac{m_{JF}}{m_{JF} + m_{GBFS} + m_{MC}} \times 100 \quad (2)$$

$$(\%)\ S_c = \frac{m_{GBFS}}{m_{GBFS} + m_{JF} + m_{MC}} \times 100 \quad (3)$$

$$(\%)\ w_c = \frac{m_W}{m_{JF} + m_{GBFS} + m_{MC}} \times 100 \quad (4)$$

where F_c = JF content; S_c = GBFS content; w_c = water content; m_{JF} = mass of JF; m_{GBFS} = mass of GBFS; m_{MC} = mass of micaceous clay (or natural soil); and m_W = mass of water.

The natural soil, JF and GBFS were blended in dry form as per the selected mix designs outlined in Table 5. Mixing was carried out for approximately 5 minutes to gain visible homogeneity of the ingredients. The required volume of water corresponding to a water content of w_c = 23.52%, the standard Proctor optimum water content of the natural soil (ASTM D698–12), was added to each blend and thoroughly mixed by hand for approximately 15 minutes. Extensive care was taken to pulverize the clumped particles, targeting homogeneity of the mixtures. A special split mold, similar to that described in the literature, was designed and fabricated from stainless steel to accomplish static compaction (Estabragh *et al.* 2016; Soltani *et al.* 2017, 2018). The mold consisted of three segments, namely the top collar, the middle section, and the bottom collar. The middle section measures 50 mm in diameter and 100 mm in height, and accommodates the sample for the unconfined compression test (see Section 3.2). The moist blends were statically compacted in the mold in five layers; each layer achieved a dry density of ρ_d = 1.56 g/cm^3 (i.e., the standard Proctor maximum dry density of the natural soil, obtained as per ASTM D698–12). The surface of the first to fourth compacted layers was scarified to ensure adequate bonding between adjacent layers of the mixture. Samples containing GBFS were enclosed in multiple layers of cling wrap and transferred to a humidity chamber, maintained at 70% relative humidity and a temperature of 25 ± 2 ^{o}C, where curing was allowed for 7 and 28 days prior to testing.

To ensure uniformity of fabric and hence consistency in behavior, the variations of dry density and water content should be measured along the height of the compacted samples (Estabragh and Javadi 2008). In this regard, typical cases including $F_0S_0T_0$ (natural soil), $F_{1.0}S_0T_0$, $F_0S_6T_0$ and $F_{1.0}S_6T_0$ were examined, and the results are provided in Figure 2. The variations of both dry density and water content were found to be marginal, as evident with the low standard deviations (SD), thus corroborating the suitability of the adopted sample preparation technique.

3.3.2. Unconfined Compression Test

Unconfined compression (UC) tests were carried out in accordance with ASTM D2166–16. The prepared samples (see Section 3.1) were axially compressed at a constant displacement rate of 1 mm/min (equivalent to 1%/min), as commonly adopted in the literature (Ang and Loehr 2003; Soltani *et al.* 2017, 2019). Axial strains and the corresponding axial stresses were recorded at various time intervals to a point at which the maximum axial stress required for sample failure, denoted as the peak UC strength, was achieved. On account of the two curing times adopted for the samples containing GBFS, a total of 28 UC tests, i.e., one for control (natural soil), three for JF-reinforced, six for GBFS-treated and eighteen for JF + GBFS blends, were conducted to address the sixteen mix designs outlined in Table 5. To ensure sufficient accuracy, triplicate samples were tested for typical mix designs, i.e., $F_0S_0T_0$ (natural soil), $F_{1.0}S_0T_0$, $F_0S_6T_{28}$ and $F_{1.0}S_6T_{28}$. In this regard, the standard deviation (SD) and the coefficient of variation (CV) for the triplicate peak UC strength data were found to range between SD = 3.74 kPa and 11.19 kPa, and CV = 3.23% and 5.15%; these low values corroborate the repeatability of the adopted sample preparation technique, as well as the implemented UC testing procedure.

3.3.3. Scanning Electron Microscopy Studies

The scanning electron microscopy (SEM) technique was implemented to investigate the evolution of fabric in response to JF, GBFS and JF + GBFS amendments. SEM imaging was carried out by means of the Philips XL20 scanning electron microscope. Apparatus specifications included a resolution of 4 μm and a maximum magnification ratio of 50,000×. In this regard, typical mix designs consisting of $F_0S_0T_0$ (natural soil), $F_{1.0}S_0T_0$, $F_0S_6T_{28}$ and $F_{1.0}S_6T_{28}$ were examined. The desired samples, prepared as per Section 3.1, were first air-dried for approximately 14 days. The desiccated samples were then carefully fractured into small cubic-shaped pieces measuring approximately 1,000 mm^3 in volume, and were further subjected to SEM imaging at various magnification ratios ranging from 250× to 20,000×.

3.4. Results and Discussion

3.4.1. Effect of JF on UC Strength

Stress–strain curves for the natural soil and various JF-reinforced samples — $F_xS_yT_z$ where x = {0, 0.5, 1.0, 1.5}, y = {0}, and z = {0} — are provided in Figure 3. The stress–strain relationship for the natural soil sample demonstrated a rise–fall response with a visually-detectable peak

point, thereby indicating a strain-softening behavior accompanied by a brittle sample failure. As a result of JF-reinforcement, the stress–strain locus progressively transitioned towards a strain-hardening character. In this case, the greater the JF content the more prominent the strain-hardening effect and hence the less dramatic (or the more ductile) the failures.

As demonstrated in Figure 3, the greater the JF content the higher the peak UC strength up to F_c = 1%, beyond of which JF-reinforcement was found to adversely influence strength development in the composite. The natural soil exhibited a peak UC strength of q_u = 82.15 kPa, while the samples reinforced with F_c = 0.5% and 1% resulted in higher values of q_u = 119.35 kPa and 138.21 kPa, respectively. The higher JF inclusion of 1.5% changed the peak UC strength to 132.24 kPa, which still holds a notable advantage over the natural soil, as well as the sample reinforced with 0.5% JF. The axial strain at failure, denoted as ε_u, is an indication of the material's ductility; higher ε_u values manifest a more ductile (or a less brittle) character. Improvement in ductility is often quantified by means of the deformability index I_D (Park 2011):

$$I_D = \frac{\varepsilon_u^{\ S}}{\varepsilon_u^{\ N}} \tag{5}$$

where $\varepsilon_u^{\ S}$ = axial strain at failure for the stabilized soil sample; and $\varepsilon_u^{\ N}$ = axial strain at failure for the control (or natural soil) sample.

The deformability index exhibited a monotonically-increasing trend with JF content, thus indicating that the greater the JF content the more ductile the sample's response to compression. By definition, the natural soil corresponds to a deformability index of unity ($\varepsilon_u^{\ N}$ = 4.73%). As a result of JF-reinforcement, the deformability index exhibited a monotonically-increasing trend, and resulted in I_D = 1.24, 1.39 and 1.81 ($\varepsilon_u^{\ S}$ = 5.88%, 6.57% and 8.55%) for F_c = 0.5%, 1% and 1.5%, respectively.

The secant modulus at 50% of the peak UC strength, denoted as E_{50}, is a measure of the material's stiffness in the elastic compression domain (Radovic *et al.* 2004; Soltani *et al.* 2019). The variations of E_{50}, as given in Figure 3, exhibited a trend similar to that observed for the peak UC strength, peaking at F_c = 1% and then slightly decreasing for the higher JF content of 1.5%. The natural soil and samples reinforced with 0.5%, 1% and 1.5% JF resulted in E_{50} = 2.27 MPa, 3.35 MPa, 3.70 MPa and 3.67 MPa, respectively. The area under a typical stress–strain curve up to the peak point, defined as the energy stored by a sample undergoing deformation and referred to as peak strain energy, serves as a measure of the material's

toughness (Maher and Ho 1994; Soltani *et al.* 2019). Unlike strength and stiffness, the development of toughness, similar to ductility, was consistently in favor of the JF inclusions, and displayed a monotonically-increasing trend with respect to JF content (see the E_u values in Figure 3). An increase in toughness warrants an increase in the peak UC strength and/or the axial strain at failure (Mirzababaei *et al.* 2013, 2018). With regard to JF-reinforcement, both q_u and ε_u contribute to the development of toughness; however, the greater the JF content the less prominent the strength's contribution and hence the more significant the role of ductility. The natural soil resulted in E_u = 2.36 kJ/m^3, while the samples reinforced with F_c = 0.5%, 1% and 1.5% resulted in higher values of E_u = 4.49 kJ/m^3, 6.11 kJ/m^3 and 8.32 kJ/m^3, respectively.

3.4.2. Effect of JF + GBFS on UC Strength

Typical stress–strain curves for the natural soil ($F_0S_0T_0$) and various GBFS-treated samples — $F_xS_yT_z$ where x = {0}, y = {3, 9}, and z = {7, 28} — are provided in Figure 4a. Unlike the JF-reinforced samples (see Figure 3), the stress–strain responses for all GBFS-treated composites were seemingly strain-softening and hence accompanied by brittle failures. In general, the greater the GBFS content and/or the longer the curing period, the higher the developed strength and stiffness, and the more prominent the strain-softening character. Stress–strain curves for the natural soil ($F_0S_0T_0$) and various JF-reinforced samples treated with 6% GBFS — $F_xS_yT_z$ where x = {0, 0.5, 1.0, 1.5}, y = {6}, and z = {7} — are provided in Figure 4b. Much like the natural soil reinforced with JF (see Figure 3), for any given GBFS content, an increase in JF content progressively transitioned the stress–strain locus towards a strain-hardening character. In this case, the greater the JF content the more pronounced the strain-hardening effect and hence the more ductile the failures.

Figures 5a and 5b illustrate the variations of peak UC strength against JF content for the natural soil and various GBFS-treated samples tested at 7 and 28 days of curing, respectively. Much like the natural soil reinforced with JF, for any given GBFS content and curing time, the peak UC strength increased with JF content up to F_c = 1%; beyond 1% JF, the effect of JF-reinforcement adversely influenced strength development in the composite. For instance, the sample $F_0S_6T_{28}$ resulted in q_u = 191.32 kPa, while the inclusions of 0.5%, 1% and 1.5% JF, with the same 6% GBFS content and the same 28-day curing condition, resulted in q_u = 250.08 kPa, 327.42 kPa and 302.76 kPa, respectively. Moreover, for any given JF content, the greater the GBFS content and/or the longer the curing period, the higher the developed peak UC strength, following a monotonically-increasing trend. The sample $F_{1.0}S_0T_0$, for instance, exhibited a peak

UC strength of q_u = 138.21 kPa. As a result of 3%, 6% and 9% GBFS inclusions, along with the same 1% JF content and a 7-day curing condition, the peak UC strength increased to 203.56 kPa, 273.68 kPa and 330.06 kPa, respectively. Similar mix designs cured for T_c = 28 days exhibited significant improvements over their 7-day counterparts, as the aforementioned values increased to 248.65 kPa, 327.42 kPa and 443.21 kPa, respectively. The ASTM D4609–08 standard suggests a minimum improvement of 345 kPa in the natural soil's peak UC strength (at T_c = 28 days) as a criterion for characterizing an effective stabilization scheme (Soltani *et al.* 2017). As demonstrated in Figure 5b, the sample $F_{1.0}S_9T_{28}$ promotes a 361.06 kPa improvement in the peak UC strength and hence satisfies the aforementioned criterion.

The deformability index, a measure of the material's ductility, was also calculated for various JF + GBFS mix designs, and the results are provided in Figures 6a and 6b for the samples tested at T_c = 7 and 28 days, respectively. Similar to the natural soil reinforced with JF, for any given GBFS content and curing time, the greater the JF content the higher the deformability index, following a monotonically-increasing trend. For any given JF content, however, the greater the GBFS content and/or the longer the curing period, the lower the developed ductility. The deformability index for various JF + GBFS blends was cross-checked with that of the natural soil (or I_D = 1) to arrive at the optimum cases. In this regard, nine cases (out of 28) manage to satisfy the $I_D \geq 1$ criterion, and thus are deemed as optimum with respect to ductility improvement. The nine optimum cases and their corresponding I_D values include $F_{0.5}S_3T_7$ (I_D = 1.10), $F_{1.0}S_3T_7$ (I_D = 1.34), $F_{1.5}S_3T_7$ (I_D = 1.68), $F_{1.0}S_3T_{28}$ (I_D = 1.09), $F_{1.5}S_3T_{28}$ (I_D = 1.34), $F_{1.0}S_6T_7$ (I_D = 1.16), $F_{1.5}S_6T_7$ (I_D = 1.32), $F_{1.5}S_6T_{28}$ (I_D = 1.10), and $F_{1.5}S_9T_7$ (I_D = 1.08).

Figures 7a and 7b illustrate the variations of E_{50} against JF content for the natural soil and various GBFS-treated samples tested at 7 and 28 days of curing, respectively. The variations of E_{50} exhibited a trend similar to that observed for the peak UC strength given in Figure 5. As such, for any given JF content, the development of stiffness was in favor of both the GBFS content and the curing time. As typical cases, the samples $F_{1.0}S_0T_0$, $F_{1.0}S_3T_7$, $F_{1.0}S_3T_{28}$, $F_{1.0}S_9T_7$ and $F_{1.0}S_9T_{28}$ resulted in E_{50} = 3.70 MPa, 5.39 MPa, 7.81 MPa, 12.30 MPa and 18.92 MPa, respectively. Moreover, for any given GBFS content and curing time, stiffness enhancements were only notable for samples with up to 1% JF inclusions. In this regard, the samples $F_0S_6T_{28}$, $F_{0.5}S_6T_{28}$, $F_{1.0}S_6T_{28}$ and $F_{1.5}S_6T_{28}$, for instance, resulted in E_{50} = 8.25 MPa, 9.47 MPa, 11.21 MPa and 10.23 MPa, respectively.

Figures 8a and 8b illustrate the variations of peak strain energy, a measure of the material's toughness, against JF content for the natural soil and various GBFS-treated samples tested at 7 and 28 days of curing, respectively. The development of toughness was in favor of both the JF content and the GBFS treatments (i.e., GBFS content and/or curing time). For any given GBFS content and curing time, the greater the JF content the higher the peak strain energy, following a monotonically-increasing trend. For instance, the samples $F_0S_6T_{28}$, $F_{0.5}S_6T_{28}$, $F_{1.0}S_6T_{28}$ and $F_{1.5}S_6T_{28}$ resulted in peak strain energies of E_u = 3.99 kJ/m^3, 6.30 kJ/m^3, 9.71 kJ/m^3 and 10.70 kJ/m^3, respectively. Similarly, for any given JF content, the greater the GBFS content and/or the longer the curing period, the higher the developed toughness. As typical cases, the sample $F_{1.0}S_0T_0$ resulted in E_u = 6.11 kJ/m^3, while the aforementioned value increased to 8.02 kJ/m^3, 8.22 kJ/m^3, 8.78 kJ/m^3 and 9.88 kJ/m^3 for $F_{1.0}S_3T_7$, $F_{1.0}S_3T_{28}$, $F_{1.0}S_9T_7$ and $F_{1.0}S_9T_{28}$, respectively.

Figures 9a and 9b illustrate the variations of E_{50} and E_u against q_u for various JF + GBFS mix designs, respectively. The variations of E_{50} were situated within the $0.054q_u < E_{50} < 0.025q_u$ domain (E_{50} in MPa, and q_u in kPa). For E_u, however, a broader domain in the form of $0.063q_u < E_u < 0.018q_u$ (E_u in kJ/m^3, and q_u in kPa) was noted. The former, the E_{50}, exhibited a rather strong correlation with q_u. On the contrary, the peak strain energy was poorly correlated with the peak UC strength. In this regard, simple correlative models in the forms of $E_{50} = 0.038q_u$ (with R^2 = 0.836) and $E_u = 0.029q_u$ (with R^2 = 0.449) can be derived; the former can be implemented for indirect estimations of E_{50}.

3.4.3. Stabilization Mechanisms and Microstructure Analysis

The JF inclusions are able to amend the soil fabric through improvements achieved in two aspects: **(i)** frictional resistance generated at the soil–fiber interface, owing to the fiber's rough surface texture; and **(ii)** mechanical interlocking of soil particles and fibers (Tang *et al.* 2007, 2010; Wang *et al.* 2017; Gowthaman *et al.* 2018; Mirzababaei *et al.* 2018; Soltani *et al.* 2018; Wei *et al.* 2018; Soltani *et al.* 2019). The interfacial frictional resistance is a function of the soil–fiber contact area, with greater contact levels providing a higher resistance to bear the external loads. Consequently, this amending mechanism can be ascribed to the fiber content, meaning that the greater the number of included fiber units, i.e., increase in fiber content, the greater the contact levels achieved between the soil particles and fibers, and thus the higher the generated interfacial frictional resistance against UC loading. The second amending mechanism, the mechanical interlocking of soil particles and fibers, is achieved during sample

preparation/compaction, and induces the composite's adhesion by immobilizing the soil particles undergoing shearing. Quite clearly, the more effective/pronounced the achieved mechanical interlocking the higher the permanence against UC loading. Consequently, this amending mechanism is in line with the fiber content, and more importantly the fiber's elongated form factor. In general, the greater the number of included fiber units, i.e., increase in fiber content, the greater the number of interlocked or enwrapped soil aggregates, and thus the higher the developed peak UC strength. It should be noted that the soil–fiber amending mechanisms, as described above, only hold provided that the fiber units do not cluster (or adhere to each other) during mixture preparation and compaction (Prabakar and Sridhar 2002; Estabragh *et al.* 2017; Yadav and Tiwari 2017; Soltani *et al.* 2019). At high fiber contents, the behavior of the composite, at some points, may be governed by a dominant fiber-to-fiber interaction; this effect, commonly referred to as fiber-clustering, leads to a notable improvement in the sample's ductility/deformability and toughness (see Figures 6 and 8) while offsetting the desired soil-to-fiber interaction capable of improving the sample's peak UC strength and stiffness. Fiber-clustering effects were evident for all samples containing 1.5% JF, as the previously-improved peak UC strength and stiffness manifested a notable decrease compared with similar mix designs containing 1% JF (see Figures 5 and 7).

Calcium-based binders, in this case GBFS, initiate a series of short- and long-term chemical reactions in the soil–water medium, which alter the soil fabric into a unitary mass of improved mechanical performance. Short-term chemical reactions consist of cation exchange and flocculation–agglomeration; their amending roles are often negligible when paired with neutrally-charged soil particles such as gravels, sands and silts. For fine-grained soils containing a notable fraction of negatively-charged clay particles, however, short-term reactions lead to significant improvements in the soil's plasticity/workability, early-age strength, swelling potential and consolidation capacity (Locat *et al.* 1990; Sivapullaiah *et al.* 1996; Mallela *et al.* 2004; Soltani *et al.* 2017). During short-term reactions, higher-valence cations substitute those of lower valence, and cations of larger ionic radius replace smaller cations of the same valence; the order of substitution follows the Hofmeister (or Lyotropic) series, i.e., $Na^+ < K^+ << Mg^{2+} < Ca^{2+}$ (Grim 1953). GBFS-treatment supplies the clay–water medium with additional calcium cations (Ca^{2+}), which immediately substitute cations of lower valence (e.g., sodium Na^+) and/or same-valence cations of smaller ionic radius (e.g., magnesium Mg^{2+}) in the vicinity of the clay particles. These cation exchanges lead to a decrease in the thickness of the Diffused Double Layers (DDLs), owing to the development of strong

van der Waals bonds between adjacent clay particles in the matrix, which in turn promote aggregation and flocculation of the clay particles (Little 1987; Mallela *et al.* 2004; Firoozi and Olgun 2017). Long-term chemical reactions, commonly referred to as pozzolanic reactions, are strongly time- and often temperature-dependent, meaning that their commencement and evolution require a certain and often long period of curing. During pozzolanic reactions, ionized calcium (Ca^{2+}) and hydroxide (OH^{-}) units, released from the water–binder complex, gradually react with silicate (SiO_2) and aluminate (Al_2O_3) units in the soil, thereby leading to the formation of strong cementation products/gels, namely Calcium–Silicate–Hydrates (CSH), Calcium–Aluminate–Hydrates (CAH) and Calcium–Aluminate–Silicate–Hydrates (CASH); these products encourage further solidification and flocculation of the soil particles, which in turn accommodate the development of a dense, uniform matrix coupled with enhanced strength performance (Mallela *et al.* 2004; Sharma and Sivapullaiah 2016; Firoozi *et al.* 2017; Sotani *et al.* 2017). It should be noted that the short- and long-term amending reactions, as described above, are generally in favor of a higher binder content; this general perception also complies with the results outlined in Figures 5, 7 and 8.

The microstructure analysis was carried out using an SEM characterization scheme developed by Soltani *et al.* (2018). Figures 10a–10d illustrate SEM micrographs for the samples $F_0S_0T_0$ (natural soil), $F_{1.0}S_0T_0$, $F_0S_6T_{28}$ and $F_{1.0}S_6T_{28}$, respectively. The microstructure of the natural soil sample manifested a partly-dense, non-uniform matrix, accompanied by a notable number of large inter- and intra-assemblage pore-spaces, respectively, formed between and within the soil aggregates; such morphological features warrant the existence of an edge-to-edge dispersed fabric (see Figure 10a). The microstructure of the JF-reinforced sample or $F_{1.0}S_0T_0$ exhibited a partly-dense but more uniform matrix, accompanied by a limited number of small intra-assemblage pore-spaces mainly distributed along the soil–fiber connection interface. In essence, the fiber units acted as physical anchors within the matrix, interlocking the neighboring soil aggregates and hence withstanding compressive stresses during shearing (see Figure 10b). As a result of GBFS-treatment (see sample $F_0S_6T_{28}$ in Figure 10c), the microstructure became even more uniform in nature, indicating aggregation and flocculation of the soil particles and hence the development of a fully-dense matrix with a dominant edge-to-face flocculated fabric. Prevalent cementation products were clearly visible between and within the soil aggregates, which portrayed a major role in eliminating the inter- and intra-assemblage pore-spaces in the matrix. As a result of JF-reinforcement and GBFS-treatment (see sample $F_{1.0}S_6T_{28}$ in Figure 10d), the soil–fiber connection interface was markedly improved, as evident with the presence

of fully-clothed fibers strongly embedded between and within the soil aggregates, which in turn led to a further improvement in the composite's strength and stiffness.

3.5. Modeling

3.5.1. Model Development

For a given type of soil reinforced with JF and/or treated with GBFS, the independent variables governing the peak UC strength q_u (in kPa), as evident with the experimental results discussed in Section 4, can be categorized as: **(i)** JF content F_c (in %); **(ii)** GBFS content S_c (in %); and **(iii)** curing time T_c (in days). Therefore, the peak UC strength problem for various JF + GBFS blends can be expressed as:

$$q_u = f(F_c, S_c, T_c) \tag{6}$$

where f = an unknown functional expression which is to be obtained through trial and error.

A suitable regression model can be characterized as one that maintains a perfect balance between simplicity, i.e., ease of application, and accuracy, i.e., acceptable goodness of fit and low forecast error. As such, any suggested functional expression for f should involve a simple algebraic structure, constructed by a minimal number of model/fitting parameters (or regression coefficients), capable of arriving at a reliable estimate of the problem at hand (Soltani and Mirzababaei 2018; Soltani *et al.* 2019). The multivariable quadratic function, as demonstrated in Equation (7) for the JF + GBFS peak UC strength problem, often serves as a suitable starting point to initiate the trial and error stage, and thus identify statistically-meaningful functional components capable of constructing a regression model which is both simple in structure and accurate in terms of predictive capacity (Estabragh *et al.* 2016; Shahbazi *et al.* 2017; Tran *et al.* 2018; Soltani and Mirzababaei 2018).

$$q_u = \beta_0 + \beta_1 F_c + \beta_2 S_c + \beta_3 T_c + \beta_4 F_c^2 + \beta_5 S_c^2 + \beta_6 T_c^2 + \beta_7 F_c S_c + \beta_8 F_c T_c + \beta_9 S_c T_c \tag{7}$$

where β_0 to β_9 = model/fitting parameters (or regression coefficients); and β_0 = peak UC strength of the natural soil, since setting $F_c = 0$, $S_c = 0$ and $T_c = 0$ leads to $q_u = \beta_0$.

The model proposed in Equation (7) was fitted to the experimental peak UC strength data (presented in Figure 5) by means of the least-squares optimization technique. Routine statistical tests, namely Fisher's F–test and Student's t–test, were then carried out to examine the model's statistical significance. In addition, statistical fit-measure indices, such as the coefficient of

determination R^2 (dimensionless), the root-mean-squared error RMSE (in kPa), the normalized root-mean-squared error NRMSE (in %) and the mean-absolute-percentage error MAPE (in %), were adopted to assess the model's predictive capacity (Wu and Jiang 2013; Soltani *et al.* 2018):

$$\mathrm{RMSE} = \sqrt{\frac{1}{N}\sum_{b=1}^{N}\left[\left(q_u{}^{A}\right)_b - \left(q_u{}^{P}\right)_b\right]^2} \tag{8}$$

$$(\%)\ \mathrm{NRMSE} = \frac{\mathrm{RMSE}}{\left(q_u{}^{A}\right)_{max} - \left(q_u{}^{A}\right)_{min}} \times 100 \tag{9}$$

$$(\%)\ \mathrm{MAPE} = \frac{1}{N}\sum_{b=1}^{N}\left|1 - \frac{\left(q_u{}^{P}\right)_b}{\left(q_u{}^{A}\right)_b}\right| \times 100 \tag{10}$$

where $q_u{}^{A}$ = actual peak UC strength, as presented in Figure 5; $q_u{}^{P}$ = predicted peak UC strength; b = index of summation; and N = number of experimental data points used for model development (N = 28, as outlined in Table 5).

The regression analysis outputs with respect to Equation (7) are summarized in Table 6. The high R^2 (= 0.964) and low RMSE (= 17.28 kPa), NRMSE (= 4.78%) or MAPE (= 6.19%) values warrant a strong agreement between actual and predicted peak UC strength data. The R^2 index merely surpassed 0.95, thus indicating that leastwise 95% of the variations in experimental observations are captured and further explained by the proposed regression model. The NRMSE index was found to be slightly less than 5%, thus signifying a maximum offset of 5% associated with the predictions. However, the *P*–value associated with some of the regression components, namely S_c, T_c, $S_c{}^2$, $T_c{}^2$ and F_cT_c, was found to be greater than 5%, implying that these components are statistically-insignificant and hence make no or little contribution towards the predictions. Statistically-insignificant terms can be eliminated to accommodate the derivation of a simplified model with unanimously-significant regression components (Tran *et al.* 2018). As such, Equation (7) can be simplified as:

$$q_u = \beta_0 + \beta_1 F_c + \beta_4 F_c{}^2 + \beta_7 F_c S_c + \beta_9 S_c T_c \tag{11}$$

The regression analysis outputs with respect to Equation (11) are summarized in Table 7. The simplified model proposed in Equation (11) resulted in R^2 = 0.951, RMSE = 20.00 kPa, NRMSE = 5.54% and MAPE = 7.28%, which are on par with that observed for Equation (7). In essence, Equation (11) suggests a more practical path towards predicting the peak UC strength while maintaining a performance similar to that offered by the more complex Equation

(7). Moreover, the *P*–values associated with all of the regression components were unanimously less than 5% (see Regression Outputs in Table 7), thus corroborating their statistical significance (and contribution) towards the predictions. Figure 11 illustrates the variations of predicted, by Equation (11), against actual peak UC strength data, along with the corresponding 95% prediction bands/intervals, for various JF + GBFS blends. Despite the existence of some scatter, all data points cluster around the line of equality and firmly position themselves between the 95% upper and 95% lower prediction bands, thereby indicating no particular outliers associated with the predictions. The proposed regression model given in Equation (11) contains a total of four fitting parameters, i.e., β_1, β_4, β_7 and β_9 (β_0 is equal to the peak UC strength of the natural soil), all of which can be calibrated by little experimental effort, as well as simple explicit calculations, and hence implemented for preliminary design assessments, predictive purposes and/or JF + GBFS optimization studies. Assuming that the peak UC strength of the natural soil (or β_0) is at hand, the four fitting parameters can be adequately calibrated by a total of four UC tests carried out on four arbitrary JF + GBFS mix designs.

3.5.2. Sensitivity Analysis

The partial derivative sensitivity analysis technique, as commonly adopted in the literature (Estabragh *et al.* 2016; Soltani 2017; Soltani *et al.* 2018), was carried out on Equation (11) to quantify the relative impacts of the independent variables, namely F_c, S_c and T_c, on the dependent variable q_u. The overall relative impact, both positive and negative, of an independent variable, i.e., $x_a = F_c$, S_c or T_c, on the dependent variable q_u, commonly referred to as sensitivity, can be defined as:

$$S(x_a) = \frac{\sigma(x_a)}{N\sigma(q_u)} \times \sum_{b=1}^{N} \left| D_{ab} \right| \quad \ni \quad D_a = \frac{dq_u}{dx_a} \tag{12}$$

where D_a = partial derivative of q_u or Equation (11) with respect to $x_a = F_c$, S_c or T_c; $\sigma(x_a)$ = standard deviation of x_a data; $\sigma(q_u)$ = standard deviation of predicted q_u data; b = index of summation; and N = number of observations (N = 28, as outlined in Table 5).

The partial derivative term, $D_a = dq_u/dx_a$ in Equation (12), measures the likelihood of q_u increasing or decreasing as a result of an increase in x_a. As such, the likelihood of increase or decrease in q_u as a result of an increase in x_a can be, respectively, defined as:

$$(\%)\ P_P(x_a) = \frac{M_P(x_a)}{N} \times 100 \tag{13}$$

$$(\%)\ P_{\mathrm{N}}(x_a) = \frac{M_{\mathrm{N}}(x_a)}{N} \times 100 \tag{14}$$

where $M_{\mathrm{P}}(x_a)$ = number of observations where $D_a \geq 0$; and $M_{\mathrm{N}}(x_a)$ = number of observations where $D_a < 0$.

The positive and negative impacts of an independent variable, i.e., $x_a = F_{\mathrm{c}}$, S_{c} or T_{c}, on the dependent variable q_{u} can be, respectively, defined as:

$$\forall x_a \ni D_a \geq 0\ ,\ S_{\mathrm{P}}(x_a) = \frac{\sigma(x_a)}{N\sigma(q_{\mathrm{u}})} \times \sum_{b=1}^{N} \left| D_{ab} \right| \ni D_a = \frac{dq_{\mathrm{u}}}{dx_a} \tag{15}$$

$$\forall x_a \ni D_a < 0\ ,\ S_{\mathrm{N}}(x_a) = \frac{\sigma(x_a)}{N\sigma(q_{\mathrm{u}})} \times \sum_{b=1}^{N} \left| D_{ab} \right| \ni D_a = \frac{dq_{\mathrm{u}}}{dx_a} \tag{16}$$

It should be noted that $S_{\mathrm{P}}(x_a)$ and $S_{\mathrm{N}}(x_a)$ are, respectively, positive and negative fractions of the sensitivity parameter, $S(x_a)$ or Equation (12), meaning that for any given x_a, $S(x_a) = S_{\mathrm{P}}(x_a) + S_{\mathrm{N}}(x_a)$.

The principal objective of any introduced soil stabilization scheme is to accommodate an increase in the peak UC strength, and as such, the variations of the positive-sensitivity parameter, $S_{\mathrm{P}}(x_a)$ or Equation (15), is of interest for further analysis. The positive-sensitivity parameter can be expressed in terms of percentage to facilitate a more practical comparison between the independent variables (Soltani 2017):

$$(\%)\ F_{\mathrm{P}}(x_a) = \frac{S_{\mathrm{P}}(x_a)}{\sum_{a=1}^{K} S_{\mathrm{P}}(x_a)} \times 100 \tag{17}$$

where $F_{\mathrm{P}}(x_a)$ = positive contribution offered by an increase in x_a resulting in an increase in q_{u} (in %); and K = number of independent variables ($K = 3$, namely F_{c}, S_{c} and T_{c}).

The sensitivity analysis results with respect to Equation (11) are summarized in Table 8. The likelihood of increase in the peak UC strength as a result of an increase in JF content was found to be 71%, thus indicating that JF-reinforcement, where $0.5\% \leq F_{\mathrm{c}} \leq 1.5\%$, exhibits favorable improvements only up to a particular/optimum fiber content, beyond of which marginal improvements or adverse effects, owing to fiber-clustering, can be expected (see the discussions in Section 4.3). As for GBFS content and curing time, the likelihood of increase was found to be 100% for both variables, thus indicting that GBFS-treatment, where $3\% \leq S_{\mathrm{c}} \leq 9\%$, consistently leads to favorable improvements which can be further enhanced by means of

curing. The positive contribution offered by an increase in JF content resulting in an increase in the peak UC strength was obtained as 35%. For GBFS content and curing time, however, the positive contribution was found to be 38% and 27%, respectively. These results imply that for a given JF + GBFS blend without curing, F_c and S_c would theoretically portray an equally-significant role towards strength development. With curing, however, the overall contribution offered by GBFS-treatment profoundly outweighs that of JF-reinforcement, as $F_P(S_c) + F_P(T_c) = 65\% >> F_P(F_c) = 35\%$.

3.6. Conclusions

The following conclusions can be drawn from this study:

- For any given GBFS content and curing time, the greater the JF content the higher the developed strength and stiffness up to F_c = 1%; beyond 1% JF, the effect of JF-reinforcement adversely influenced the development of strength and stiffness. The composite's ductility and toughness, however, were consistently in favor of JF-reinforcement, meaning that the greater the JF content the higher the developed ductility and toughness.
- For any given JF content, the greater the GBFS content and/or the longer the curing period, the higher the developed strength, stiffness and toughness, following monotonically-increasing trends. The composite's ductility, however, was adversely influenced by GBFS-treatment, meaning that the greater the GBFS content and/or the longer the curing period, the lower the developed ductility.
- The addition of GBFS to JF-reinforced samples improved the soil–fiber connection interface or bonding, as the fiber units became fully embedded between and within the soil aggregates; this in turn led to a further improvement in the composite's strength and stiffness. The ASTM D4609–08 strength criterion was used to assess the efficiency and hence applicability of the proposed JF + GBFS mix designs. In this regard, the sample $F_{1.0}S_9T_{28}$ managed to satisfy ASTM's criterion and hence can be taken as the optimum design choice.
- A non-linear, multivariable regression model was developed to quantify the peak UC strength q_u as a function of the composite's basic index properties, i.e., JF content F_c, GBFS content S_c, and curing time T_c. The predictive capacity of the suggested model was examined and further validated by statistical techniques. A sensitivity analysis was also carried out to quantify the relative impacts of the independent regression variables, namely

F_c, S_c and T_c, on the dependent variable q_u. The proposed regression model contained a limited number of fitting parameters, all of which can be calibrated by little experimental effort, as well as simple explicit calculations, and hence implemented for preliminary design assessments, predictive purposes and/or JF + GBFS optimization studies.

Author Contributions

Conceptualization, J.Z., A.D. and M.B.J.; Methodology, J.Z., A.S. and A.D.; Validation, J.Z. and A.S.; Formal analysis, J.Z. and A.S.; Investigation, J.Z.; Writing—original draft preparation, J.Z. and A.S.; Writing—review and editing, A.D. and M.B.J.; Visualization, A.S.; Supervision, A.D. and M.B.J.; Project administration, A.D. and M.B.J.; Funding acquisition, A.D. and M.B.J.

Acknowledgments:

This research was made possible through the provision of an Australian Government Research Training Program Scholarship; this support is gratefully acknowledged.

Conflicts of Interest

The authors declare no conflict of interest.

References

Alazigha, D. P.; Indraratna, B.; Vinod, J. S.; Ezeajugh, L. E. The swelling behaviour of lignosulfonate-treated expansive soil. *Proc. Inst. Civ. Eng. - Gr. Improv.* **2016**, *169*, 182–193, doi:10.1680/jgrim.15.00002.

Ang, E. C.; Loehr, J. E. Specimen size effects for fiber-reinforced silty clay in unconfined compression. *Geotech. Test. J.* **2003**, *26*, 191–200, doi:10.1520/gtj11320j.

Arpitha, G. R.; Sanjay, M. R.; Senthamaraikannan, P.; Barile, C.; Yogesha, B. Hybridization effect of sisal/glass/epoxy/filler based woven fabric reinforced composites. *Exp. Tech.* **2017**, *41*, 577–584, doi:10.1007/s40799-017-0203-4.

Ballantine, R. W.; Rossouw, A. J. *Stabilization of Soils*; PPC Lime Ltd: Pretoria, Gauteng, South Africa, 1989; pp. 25–27, 42–51.

Cabalar, A. F.; Cevik, A. Triaxial behavior of sand–mica mixtures using genetic programming. *Expert Syst. Appl.* **2011**, *38*, 10358–10367, doi:10.1016/j.eswa.2011.02.051.

Ekblad, J.; Isacsson, U. Influence of water and mica content on resilient properties of coarse granular materials. *Int. J. Pavement Eng.* **2008**, *9*, 215–227, doi:10.1080/10298430701551193.

Estabragh, A. R.; Javadi, A. A. Critical state for overconsolidated unsaturated silty soil. *Can. Geotech. J.* **2008**, *45*, 408–420, doi:10.1139/t07-105.

Estabragh, A. R.; Naseh, M.; Beytolahpour, I.; Javadi, A. A. Strength of a clay soil and soil–cement mixture with resin. *Proc. Inst. Civ. Eng. - Gr. Improv.* **2013**, *166*, 108–114, doi:10.1680/grim.12.00014.

Estabragh, A. R.; Pereshkafti, M. R. S.; Parsaei, B.; Javadi, A. A. Stabilised expansive soil behaviour during wetting and drying. *Int. J. Pavement Eng.* **2013**, *14*, 418–427, doi:10.1080/10298436.2012.746688.

Estabragh, A. R.; Ranjbari, S.; Javadi, A. A. Properties of clay soil and soil cement reinforced with polypropylene fibers. *ACI Mater. J.* **2017**, *114*, 195–205, doi:10.14359/51689469.

Estabragh, A. R.; Soltani, A.; Javadi, A. A. Models for predicting the seepage velocity and seepage force in a fiber reinforced silty soil. *Comput. Geotech.* **2016**, *75*, 174–181, doi:10.1016/j.compgeo.2016.02.002.

Firoozi, A. A.; Olgun, C. G.; Firoozi, A. A.; Baghini, M. S. Fundamentals of soil stabilization. *Int. J. Geo-Engineering* **2017**, *8*, 1–16, doi:10.1186/s40703-017-0064-9.

Fleet, M. E. *Rock-Forming Minerals. Volume 3A, Micas*, 2nd ed.; The Geological Society of London: London, England, UK, 2003; pp. 1–40, 178–180, 512–515, ISBN:1862391424.

Frempong, E. M. A comparative assessment of sand and lime stabilization of residual micaceous compressible soils for road construction. *Geotech. Geol. Eng.* **1995**, *13*, 181–198, doi:10.1007/bf00422209.

Frempong, E. M. Geotechnical properties of some residual micaceous soils in the Kumasi Metropolitan area (Ghana). *Bull. Int. Assoc. Eng. Geol.* **1994**, *49*, 47–54, doi:10.1007/bf02595000.

Galán, E.; Ferrell, R. E. Genesis of clay minerals. *Dev. Clay Sci.* **2013**, *5*, 83–126, doi:10.1016/B978-0-08-098258-8.00003-1.

Gilboy, G. The compressibility of sand–mica mixtures. *Proc. Am. Soc. Civ. Eng.* **1928**, *54*, 555–568.

Gowthaman, S.; Nakashima, K.; Kawasaki, S. A state-of-the-art review on soil reinforcement technology using natural plant fiber materials: Past findings, present trends and future directions. *Materials* **2018**, *11*, 1–23, doi:10.3390/ma11040553.

Grim, R. E. *Clay Mineralogy*, 1st ed.; McGraw-Hill: New York, NY, USA, 1953; pp. 126–155.

Harris, W. G.; Parker, J. C.; Zelazny, L. W. Effects of mica content on engineering properties of sand. *Soil Sci. Soc. Am. J.* **1984**, *48*, 501–505, doi:10.2136/sssaj1984.03615995004800030006x.

Harvey, J. C. *Geology for Geotechnical Engineers*, 1st ed.; Cambridge University Press: Cambridge, Cambridgeshire, England, UK, 1982, ISBN:9780521288620.

Hight, D. W.; Georgiannou, V. N.; Martin, P. L.; Mundegar, A. K. Flow slides in micaceous sand. In *Problematic Soils: Proceedings of the International Symposium on Problematic Soils, IS-Tōhoku '98, Sendai, Japan, 28–30 October*; Yanagisawa, E., Moroto, N., Mitachi, T., Eds.; A.A. Balkema: Rotterdam, South Holland, Netherlands, 1998; Volume 1, pp. 945–960, ISBN:9054109971.

Keramatikerman, M.; Chegenizadeh, A.; Nikraz, H. Effect of GGBFS and lime binders on the engineering properties of clay. *Appl. Clay Sci.* **2016**, *132–133*, 722–730, doi:10.1016/j.clay.2016.08.029.

Kim, Y. T.; Kim, H. J.; Lee, G. H. Mechanical behavior of lightweight soil reinforced with waste fishing net. *Geotext. Geomembranes* **2008**, *26*, 512–518, doi:10.1016/j.geotexmem.2008.05.004.

Kosmatka, S. H.; Kerkhoff, B.; Panarese, W. C. Portland, blended, and other hydraulic cements. In *Design and Control of Concrete Mixtures, Engineering Bulletin 001*, 14th ed.; Portland Cement Association: Skokie, IL, USA, 2002; pp. 21–56, ISBN:0893122173.

Lee, J. S.; Guimaraes, M.; Santamarina, J. C. Micaceous sands: Microscale mechanisms and macroscale response. *J. Geotech. Geoenvironmental Eng.* **2007**, *133*, 1136–1143, doi:10.1061/(asce)1090-0241(2007)133:9(1136).

Little, D. L. *Fundamentals of the Stabilization of Soil with Lime, Bulletin 332*; The National Lime Association: Arlington, VA, USA, 1987.

Locat, J.; Bérubé, M. A.; Choquette, M. Laboratory investigations on the lime stabilization of sensitive clays: Shear strength development. *Can. Geotech. J.* **1990**, *27*, 294–304, doi:10.1139/t90-040.

Maher, M. H.; Ho, Y. C. Mechanical properties of kaolinite/fiber soil composite. *J. Geotech. Eng.* **1994**, *120*, 1381–1393, doi:10.1061/(asce)0733-9410(1994)120:8(1381).

Mallela, J.; Von Quintus, H.; Smith, K. L. *Consideration of Lime-Stabilized Layers in Mechanistic-Empirical Pavement Design*; The National Lime Association: Arlington, VA, USA, 2004; Available online: http://lime.org/documents/other/MechEmpPavement.pdf (accessed on 8 January 2019).

McCarthy Jr., D. F.; Leonard, R. J. Compaction and compression characteristics of micaceous fine sands and silts. In *Highway Research Record 22*; Transportation Research Board: Washington, DC, USA, 1963; pp. 23–37; Available online: http://onlinepubs.trb.org/Onlinepubs/hrr/1963/22/22-003.pdf (accessed on 8 January 2019).

Miller, G. A.; Azad, S. Influence of soil type on stabilization with cement kiln dust. *Constr. Build. Mater.* **2000**, *14*, 89–97, doi:10.1016/s0950-0618(00)00007-6.

Mirzababaei, M.; Arulrajah, A.; Horpibulsuk, S.; Aldavad, M. Shear strength of a fibre-reinforced clay at large shear displacement when subjected to different stress histories. *Geotext. Geomembranes* **2017**, *45*, 422–429, doi:10.1016/j.geotexmem.2017.06.002.

Mirzababaei, M.; Arulrajah, A.; Haque, A.; Nimbalkar, S.; Mohajerani, A. Effect of fiber reinforcement on shear strength and void ratio of soft clay. *Geosynth. Int.* **2018**, *25*, 471–480, doi:10.1680/jgein.18.00023.

Mirzababaei, M.; Arulrajah, A.; Horpibulsuk, S.; Soltani, A.; Khayat, N. Stabilization of soft clay using short fibers and poly vinyl alcohol. *Geotext. Geomembranes* **2018**, *46*, 646–655, doi:10.1016/j.geotexmem.2018.05.001.

Mirzababaei, M.; Miraftab, M.; Mohamed, M.; McMahon, P. Unconfined compression strength of reinforced clays with carpet waste fibers. *J. Geotech. Geoenvironmental Eng.* **2013**, *139*, 483–493, doi:10.1061/(asce)gt.1943-5606.0000792.

Mirzababaei, M.; Yasrobi, S. S.; Al-Rawas, A. A. Effect of polymers on swelling potential of expansive soils. *Proc. Inst. Civ. Eng. - Gr. Improv.* **2009**, *162*, 111–119, doi:10.1680/grim.2009.162.3.111.

Moore, C. A. Effect of mica on K_0 compressibility of two soils. *J. Soil Mech. Found. Div.* **1971**, *97*, 1275–1291.

Mshali, M. R.; Visser, A. T. Influence of mica on unconfined compressive strength of a cement-treated weathered granite gravel. *J. South African Inst. Civ. Eng.* **2012**, *54*, 71–77.

Mshali, M. R.; Visser, A. T. Influence of Mica on Compactability and Moisture Content of Cement–Treated Weathered Granite Gravel. In *Proceedings of the 33rd Southern African Transport Conference (SATC 2014)*; Minister of Transport, South Africa: Pretoria, Gauteng, South Africa, 2014; pp. 546–555, ISBN:9781920017613.

Olgun, M. The effects and optimization of additives for expansive clays under freeze–thaw conditions. *Cold Reg. Sci. Technol.* **2013**, *93*, 36–46, doi:10.1016/j.coldregions.2013.06.001.

Onyejekwe, S.; Ghataora, G. S. Soil stabilization using proprietary liquid chemical stabilizers: Sulphonated oil and a polymer. *Bull. Eng. Geol. Environ.* **2015**, *74*, 651–665, doi:10.1007/s10064-014-0667-8.

Park, S. S. Unconfined compressive strength and ductility of fiber-reinforced cemented sand. *Constr. Build. Mater.* **2011**, *25*, 1134–1138, doi:10.1016/j.conbuildmat.2010.07.017.

Phanikumar, B. R.; Nagaraju, T. V. Engineering behaviour of expansive clays blended with cement and GGBS. *Proc. Inst. Civ. Eng. - Gr. Improv.* **2018**, *171*, 167–173, doi:10.1680/jgrim.17.00054.

Prabakar, J.; Sridhar, R. S. Effect of random inclusion of sisal fibre on strength behaviour of soil. *Constr. Build. Mater.* **2002**, *16*, 123–131, doi:10.1016/s0950-0618(02)00008-9.

Qu, J.; Li, C.; Liu, B.; Chen, X.; Li, M.; Yao, Z. Effect of random inclusion of wheat straw fibers on shear strength characteristics of Shanghai cohesive soil. *Geotech. Geol. Eng.* **2013**, *31*, 511–518, doi:10.1007/s10706-012-9604-4.

Qu, J.; Zhao, D. Stabilising the cohesive soil with palm fibre sheath strip. *Road Mater. Pavement Des.* **2016**, *17*, 87–103, doi:10.1080/14680629.2015.1064010.

Radovic, M.; Lara-Curzio, E.; Riester, L. Comparison of different experimental techniques for determination of elastic properties of solids. *Mater. Sci. Eng. A* **2004**, *368*, 56–70, doi:10.1016/j.msea.2003.09.080.

Schmidt, K. Effects of mica content on cyclic resistance of poorly-graded sand. In *Geotechnical Earthquake Engineering and Soil Dynamics IV, GSP 181*; Zeng, D., Manzari, M. T., Hiltunen, D. R., Eds.; ASCE: Sacramento, CA, USA, 2008; pp. 1–8, ISBN:9780784409756, doi:10.1061/9780784409756.

Seethalakshmi, P.; Sachan, A. Effect of successive impact loading on compactability, microstructure, and compressibility behavior of micaceous sand. *Transp. Infrastruct. Geotechnol.* **2018**, *5*, 114–128, doi:10.1007/s40515-018-0052-3.

Seethalakshmi, P.; Sachan, A. Effect of mica content on pore pressure and stress-strain response of micaceous sand using energy dissipation and different failure mechanisms. *Int. J. Geotech. Eng.* **2018**, doi:10.1080/19386362.2018.1530169.

Sekhar, D. C.; Nayak, S. Utilization of granulated blast furnace slag and cement in the manufacture of compressed stabilized earth blocks. *Constr. Build. Mater.* **2018**, *166*, 531–536, doi:10.1016/j.conbuildmat.2018.01.125.

Shahbazi, M.; Rowshanzamir, M.; Abtahi, S. M.; Hejazi, S. M. Optimization of carpet waste fibers and steel slag particles to reinforce expansive soil using response surface methodology. *Appl. Clay Sci.* **2017**, *142*, 185–192, doi:10.1016/j.clay.2016.11.027.

Sharma, A. K.; Sivapullaiah, P. V. Ground granulated blast furnace slag amended fly ash as an expansive soil stabilizer. *Soils Found.* **2016**, *56*, 205–212, doi:10.1016/j.sandf.2016.02.004.

Sivakumar Babu, G. L.; Vasudevan, A. K. Strength and stiffness response of coir fiber-reinforced tropical soil. *J. Mater. Civ. Eng.* **2008**, *20*, 571–577, doi:10.1061/(asce)0899-1561(2008)20:9(571).

Sivapullaiah, P. V.; Prashanth, J. P.; Sridharan, A. Effect of fly ash on the index properties of black cotton soil. *Soils Found.* **1996**, *36*, 97–103, doi:10.3208/sandf.36.97.

Soltani, A. Discussion of “Optimization of carpet waste fibers and steel slag particles to reinforce expansive soil using response surface methodology” by M. Shahbazi, M. Rowshanzamir, S.M. Abtahi, S.M. Hejazi [Appl. Clay Sci., doi:10.1016/j.clay.2016.11.027]. *Appl. Clay Sci.* **2017**, doi:10.1016/j.clay.2017.07.020.

Soltani, A.; Deng, A.; Taheri, A. Swell–compression characteristics of a fiber–reinforced expansive soil. *Geotext. Geomembranes* **2018**, *46*, 183–189, doi:10.1016/j.geotexmem.2017.11.009.

Soltani, A.; Deng, A.; Taheri, A.; Mirzababaei, M. A sulphonated oil for stabilisation of expansive soils. *Int. J. Pavement Eng.* **2017**, doi:10.1080/10298436.2017.1408270.

Soltani, A.; Deng, A.; Taheri, A.; Mirzababaei, M.; Nikraz, H. Interfacial shear strength of rubber-reinforced clays: A dimensional analysis perspective. *Geosynth. Int.* **2019**, doi:10.1680/jgein.18.00045.

Soltani, A.; Deng, A.; Taheri, A.; Mirzababaei, M. Rubber powder–polymer combined stabilization of South Australian expansive soils. *Geosynth. Int.* **2018**, *25*, 304–321, doi:10.1680/jgein.18.00009.

Soltani, A.; Deng, A.; Taheri, A.; Sridharan, A. Consistency limits and compaction characteristics of clay soils containing rubber waste. *Proc. Inst. Civ. Eng. - Geotech. Eng.* **2018**, doi:10.1680/jgeen.18.00042.

Soltani, A.; Deng, A.; Taheri, A.; Sridharan, A. Swell–shrink–consolidation behavior of rubber–reinforced expansive soils. *Geotech. Test. J.* **2018**, doi:10.1520/gtj20170313.

Soltani, A.; Estabragh, A. R.; Taheri, A.; Deng, A.; Meegoda, J. N. Experiments and dimensional analysis of contaminated clay soils. *Environ. Geotech.* **2018**, doi:10.1680/jenge.18.00018.

Soltani, A.; Mirzababaei, M. Discussion on “Effects of lime addition on geotechnical properties of sedimentary soil in Curitiba, Brazil” [J Rock Mech Geotech Eng 10 (2018) 188–194]. *J. Rock Mech. Geotech. Eng.* **2018**, doi:10.1016/j.jrmge.2018.08.008.

Soltani, A.; Mirzababaei, M. Comment on “Compaction and strength behavior of tire crumbles–fly ash mixed with clay” by A. Priyadarshee, A. Kumar, D. Gupta, and P. Pushkarna. *J. Mater. Civ. Eng.* **2018**, accepted.

Soltani, A.; Taheri, A.; Deng, A.; Nikraz, H. Tyre rubber and expansive soils: Two hazards, one solution. *Proc. Inst. Civ. Eng. - Constr. Mater.* **2019**, doi:10.1680/jcoma.18.00075.

Soltani, A.; Taheri, A.; Khatibi, M.; Estabragh, A. R. Swelling potential of a stabilized expansive soil: A comparative experimental study. *Geotech. Geol. Eng.* **2017**, *35*, 1717–1744, doi:10.1007/s10706-017-0204-1.

Sridharan, A.; Nagaraj, H. B. Compressibility behaviour of remoulded, fine-grained soils and correlation with index properties. *Can. Geotech. J.* **2000**, *37*, 712–722, doi:10.1139/t99-128.

Tang, C. S.; Shi, B.; Gao, W.; Chen, F.; Cai, Y. Strength and mechanical behavior of short polypropylene fiber reinforced and cement stabilized clayey soil. *Geotext. Geomembranes* **2007**, *25*, 194–202, doi:10.1016/j.geotexmem.2006.11.002.

Tang, C. S.; Shi, B.; Zhao, L. Z. Interfacial shear strength of fiber reinforced soil. *Geotext. Geomembranes* **2010**, *28*, 54–62, doi:10.1016/j.geotexmem.2009.10.001.

Tran, K. Q.; Satomi, T.; Takahashi, H. Improvement of mechanical behavior of cemented soil reinforced with waste cornsilk fibers. *Constr. Build. Mater.* **2018**, *178*, 204–210, doi:10.1016/j.conbuildmat.2018.05.104.

Tubey, L. W. *A Laboratory Investigation to Determine the Effect of Mica on the Properties of Soils and Stabilized Soils, Research Note 4077*; Road Research Laboratory (RRL): Wokingham, Berkshire, England, UK, 1961.

Tubey, L. W.; Bulman, J. N. Micaceous soils: Methods of determining mica content and the use of routine tests in the evaluation of such soils. *Proc. Aust. Road Res. Board (ARRB)* **1964**, *2*, 880–901.

Tubey, L. W.; Webster, D. C. *The Effects of Mica on the Roadmaking Properties of Materials, Supplementary Report 408*; Transport and Road Research Laboratory (TRL): Crowthorne, Berkshire, England, UK, 1978, ISBN:03051315.

Vakili, M. V.; Chegenizadeh, A.; Nikraz, H.; Keramatikerman, M. Investigation on shear strength of stabilised clay using cement, sodium silicate and slag. *Appl. Clay Sci.* **2016**, *124–125*, 243–251, doi:10.1016/j.clay.2016.02.019.

Wang, Y. X.; Guo, P. P.; Ren, W. X.; Yuan, B. X.; Yuan, H. P.; Zhao, Y. L.; Shan, S. B.; Cao, P. Laboratory investigation on strength characteristics of expansive soil treated with jute fiber reinforcement. *Int. J. Geomech.* **2017**, *17*, 04017101:1–04017101:12, doi:10.1061/(asce)gm.1943-5622.0000998.

Wei, J.; Kong, F.; Liu, J.; Chen, Z.; Kanungo, D. P.; Lan, X.; Jiang, C.; Shi, X. Effect of sisal fiber and polyurethane admixture on the strength and mechanical behavior of sand. *Polymers* **2018**, *10*, 1–15, doi:10.3390/polym10101121.

Weinert, H. H. *The Natural Road Construction Materials of Southern Africa*, 1st ed.; H&R Academica: Cape Town, Western Cape, South Africa, 1980, ISBN:0860740470.

Winterkorn, H. F.; Pamukcu, S. Soil stabilization and grouting. In *Foundation Engineering Handbook*, 2nd ed.; Fang, H. Y., Ed.; Springer: Boston, MA, USA, 1991; pp. 317–378, ISBN:9781461539285, doi:10.1007/978-1-4615-3928-5_9.

Wu, Y. F.; Jiang, C. Quantification of bond-slip relationship for externally bonded FRP-to-concrete joints. *J. Compos. Constr.* **2013**, *17*, 673–686, doi:10.1061/(asce)cc.1943-5614.0000375.

Yadav, J. S.; Tiwari, S. K. Effect of waste rubber fibres on the geotechnical properties of clay stabilized with cement. *Appl. Clay Sci.* **2017**, *149*, 97–110, doi:10.1016/j.clay.2017.07.037.

Yin, C.; Zhang, W.; Jiang, X.; Huang, Z. Effects of initial water content on microstructure and mechanical properties of lean clay soil stabilized by compound calcium-based stabilizer. *Materials* **2018**, *11*, 1–18, doi:10.3390/ma11101933.

Zhao, Y.; Soltani, A.; Taheri, A.; Karakus, M.; Deng, A. Application of slag–cement and fly ash for strength development in cemented paste backfills. *Minerals* **2019**, *9*, 1–19, doi:10.3390/min9010022.

List of Tables

Table 1. Physical and mechanical properties of K, GM and MC.

Table 2. Chemical compositions of K and GM (as supplied by the manufacturers).

Table 3. Physical and mechanical properties of JF (as supplied by the distributor).

Table 4. Physical properties and chemical composition of GBFS (as supplied by the manufacturer).

Table 5. Mix designs and their properties.

Table 6. Summary of the regression analysis outputs with respect to Equation (7).

Table 7. Summary of the regression analysis outputs with respect to Equation (11).

Table 8. Summary of the sensitivity analysis results with respect to Equation (11).

Table 1. Physical and mechanical properties of K, GM and MC.

Properties	K	GM	MC	Standard designation
Specific gravity of solids, G_s	2.69	2.80	2.73	ASTM D854–14
Clay fraction [< 2 μm] (%)	51	—	39	ASTM D422–07
Silt fraction [2–75 μm] (%)	48	—	55	ASTM D422–07
Fines fraction [< 75 μm] (%)	99	93	94	ASTM D422–07
Sand fraction [0.075–4.75 mm] (%)	1	7	6	ASTM D422–07
Natural water content, w_n (%)	2.14	0.41	1.67	ASTM D2216–10
Liquid limit, LL (%)	44.67	—	48.67	AS 1289.3.9.1–15
Plastic limit, PL (%)	23.72	—	36.94	AS 1289.3.2.1–09
Plasticity index, PI (%)	20.95	—	11.28	AS 1289.3.3.1–09
Linear shrinkage, LS (%)	7.06	—	8.84	AS 1289.3.4.1–08
Shrinkage index, SI (%) [1]	37.61	—	39.83	Sridharan and Nagaraj [65]
USCS classification	CI [2]	—	MI [3]	ASTM D2487–11
Optimum water content, w_{opt} (%)	19.84	—	23.52	ASTM D698–12
Maximum dry density, ρ_{dmax} (g/cm^3)	1.63	—	1.56	ASTM D698–12
Unconfined compression strength, q_u (kPa) [4]	137.62	—	85.14	ASTM D2166–16
Splitting tensile strength, q_t (kPa) [4]	21.76	—	14.62	ASTM C496–17

[1] SI = LL – LS; [2] Clay with intermediate plasticity; [3] Silt with intermediate plasticity; and [4] Tested at standard Proctor optimum condition.

Table 2. Chemical compositions of K and GM (as supplied by the manufacturers).

Properties	**K**	**GM**
SiO_2 (%)	64.9	49.5
Al_2O_3 (%)	22.2	29.2
K_2O (%)	2.7	8.9
TiO_2 (%)	1.4	0.8
Fe_2O_3 (%)	1.0	4.6
MgO (%)	0.6	0.7
Na_2O (%)	0.2	0.5
CaO (%)	0.1	0.4
Acidity, pH [20% slurry]	7.4	7.8
Oil absorption (mL/100 g)	34.0	36.0
Loss on ignition, LOI [at 1000 ^oC] (%)	6.5	< 6
Specific surface area, SSA (m^2/g)	11.2	5.3

Table 3. Physical and mechanical properties of JF (as supplied by the distributor).

Properties	**Value**
Specific gravity, G_s	1.30–1.46
Length, F_L (mm)	15
Diameter, F_D (μm)	30–40
Aspect ratio, $F_{AR} = F_L/F_D$	375–500
Young's modulus (GPa)	10–30
Tensile strength (MPa)	400–900
Tensile elongation at break (%)	1.5–1.8
Water absorption (%)	12

Table 4. Physical properties and chemical composition of GBFS (as supplied by the manufacturer).

Properties	**Value**
Specific gravity of solids, G_s	2.87
Fines fraction [< 75 μm] (%)	96
Sand fraction [0.075–4.75 mm] (%)	4
Natural water content, w_n (%)	< 1
Acidity, pH [20% slurry]	9.6
Loss on ignition, LOI [at 1000 ^oC] (%)	< 3
Specific surface area, SSA (m^2/g)	0.7
CaO (%)	44.7
SiO_2 (%)	27.1
Al_2O_3 (%)	13.6
MgO (%)	5.1
Fe_2O_3 (%)	3.5
TiO_2 (%)	1.7
K_2O (%)	0.7
Na_2O (%)	0.2

Table 5. Mix designs and their properties.

Group	Designation	JF content (%)	GBFS content (%)
Control [1]	$F_0S_0T_0$	0	0
JF-reinforced	$F_{0.5}S_0T_0$	0.5	0
	$F_{1.0}S_0T_0$	1.0	0
	$F_{1.5}S_0T_0$	1.5	0
GBFS-treated	$F_0S_3T_{7,28}$	0	3
	$F_0S_6T_{7,28}$	0	6
	$F_0S_9T_{7,28}$	0	9
JF + GBFS	$F_{0.5}S_3T_{7,28}$	0.5	3
	$F_{1.0}S_3T_{7,28}$	1.0	3
	$F_{1.5}S_3T_{7,28}$	1.5	3
	$F_{0.5}S_6T_{7,28}$	0.5	6
	$F_{1.0}S_6T_{7,28}$	1.0	6
	$F_{1.5}S_6T_{7,28}$	1.5	6
	$F_{0.5}S_9T_{7,28}$	0.5	9
	$F_{1.0}S_9T_{7,28}$	1.0	9
	$F_{1.5}S_9T_{7,28}$	1.5	9

[1] Natural soil.

Table 6. Summary of the regression analysis outputs with respect to Equation (7).

Fit-Measure Indices

R [1]	R^2	Adjusted R^2	RMSE (kPa)	NRMSE (%)	MAPE (%)
0.982	0.964	0.946	17.28	4.78	6.19

[1] Coefficient of correlation.

Analysis of Variance (ANOVA)

Source of variation	DF [1]	SS [2]	MS [3]	*F*–value	Significance *F*
Regression	9	2.20×10^5	2.44×10^4	52.62	4.26×10^{-11} < 5% (S)
Residual	18	8.36×10^3	4.64×10^2		
Total	27	2.28×10^5			

[1] Degree of freedom; [2] Sum of squares; [3] Mean squares; and (S) = Significant.

Regression Outputs

Variable	Coefficient	SE [1]	*t*–value	*P*–value
Intercept	$\beta_0 = 64.75$	16.19	4.00	8.42×10^{-4} < 5% (S)
F_c	$\beta_1 = 171.31$	28.76	5.96	1.23×10^{-5} < 5% (S)
S_c	$\beta_2 = 2.43$	13.06	0.19	8.55×10^{-1} > 5% (NS)
T_c	$\beta_3 = 1.48$	6.68	0.22	8.27×10^{-1} > 5% (NS)
F_c^2	$\beta_4 = -85.99$	16.29	–5.28	5.10×10^{-5} < 5% (S)
S_c^2	$\beta_5 = 0.26$	1.04	0.25	8.02×10^{-1} > 5% (NS)
T_c^2	$\beta_6 = -0.04$	0.20	–0.22	8.31×10^{-1} > 5% (NS)
$F_c \times S_c$	$\beta_7 = 6.65$	2.53	2.63	1.70×10^{-2} < 5% (S)
$F_c \times T_c$	$\beta_8 = -0.17$	0.68	–0.25	8.09×10^{-1} > 5% (NS)
$S_c \times T_c$	$\beta_9 = 0.61$	0.17	3.55	2.28×10^{-3} < 5% (S)

[1] Standard error; (S) = Significant; and (NS) = Not Significant.

Table 7. Summary of the regression analysis outputs with respect to Equation (11).

Fit-Measure Indices

R [1]	R^2	Adjusted R^2	RMSE (kPa)	NRMSE (%)	MAPE (%)
0.976	0.951	0.943	20.00	5.54	7.28

[1] Coefficient of correlation.

Analysis of Variance (ANOVA)

Source of variation	DF [1]	SS [2]	MS [3]	*F*–value	Significance *F*
Regression	4	2.17×10^5	5.43×10^4	111.49	1.04×10^{-14} < 5% (S)
Residual	23	1.12×10^4	4.87×10^2		
Total	27	2.28×10^5			

[1] Degree of freedom; [2] Sum of squares; [3] Mean squares; and (S) = Significant.

Regression Outputs

Variable	Coefficient	SE [1]	*t*–value	*P*–value
Intercept	$\beta_0 = 89.14$	9.70	9.19	3.69×10^{-9} < 5% (S)
F_c (%)	$\beta_1 = 148.90$	27.51	5.41	1.69×10^{-5} < 5% (S)
F_c^2	$\beta_4 = -85.99$	16.68	–5.16	3.17×10^{-5} < 5% (S)
$F_c \times S_c$	$\beta_7 = 10.52$	1.69	6.22	2.40×10^{-6} < 5% (S)
$S_c \times T_c$	$\beta_9 = 0.65$	0.06	11.08	1.07×10^{-10} < 5% (S)

[1] Standard error; and (S) = Significant.

Table 8. Summary of the sensitivity analysis results with respect to Equation (11).

Variable, x_a	**$D_a = dq_u/dx_a$**	**$S(x_a)$**	**$P_P(x_a)$ (%)**	**$P_N(x_a)$ (%)**	**$S_P(x_a)$**	**$S_N(x_a)$**	**$F_P(x_a)$ (%)**
JF content, F_c	$\beta_1 + 2\beta_4 F_c + \beta_7 S_c$	0.639	71	29	0.548	0.090	35
GBFS content, S_c	$\beta_7 F_c + \beta_9 T_c$	0.605	100	0	0.605	0	38
Curing time, T_c	$\beta_9 S_c$	0.427	100	0	0.427	0	27

List of Figures

Figure 1. JF at different magnification ratios: **(a)** Raw fibers (no magnification); **(b)** Processed fibers (no magnification); and **(c)** Processed fibers (1,500× magnification).

Figure 2. Variations of dry density along the height of the compacted samples: **(a)** $F_0S_0T_0$; **(b)** $F_{1.0}S_0T_0$; **(c)** $F_0S_6T_0$; and **(d)** $F_{1.0}S_6T_0$.

Figure 3. Stress–strain curves for the natural soil and various JF-reinforced samples, i.e., $F_xS_yT_z$ where x = {0, 0.5, 1.0, 1.5}, y = {0}, and z = {0}.

Figure 4. Typical stress–strain curves for the natural soil ($F_0S_0T_0$) and various stabilized samples: **(a)** $F_xS_yT_z$ where x = {0}, y = {3, 9}, and z = {7, 28}; and **(b)** $F_xS_yT_z$ where x = {0, 0.5, 1.0, 1.5}, y = {6}, and z = {7}.

Figure 5. Variations of peak UC strength q_u against JF content for the natural soil and various GBFS-treated samples: **(a)** T_c = 7 days; and **(b)** T_c = 28 days.

Figure 6. Variations of deformability index I_D against JF content for the natural soil and various GBFS-treated samples: **(a)** T_c = 7 days; and **(b)** T_c = 28 days.

Figure 7. Variations of E_{50} against JF content for the natural soil and various GBFS-treated samples: **(a)** T_c = 7 days; and **(b)** T_c = 28 days.

Figure 8. Variations of peak strain energy E_u against JF content for the natural soil and various GBFS-treated samples: **(a)** T_c = 7 days; and **(b)** T_c = 28 days.

Figure 9. Variations of **(a)** E_{50} and **(b)** peak strain energy E_u against peak UC strength q_u for various JF + GBFS blends.

Figure 10. SEM micrographs for the tested samples: **(a)** $F_0S_0T_0$ (natural soil); **(b)** $F_{1.0}S_0T_0$; **(c)** $F_0S_6T_{28}$; and **(d)** $F_{1.0}S_6T_{28}$.

Figure 11. Variations of predicted, by Equation (11), against actual peak UC strength data for various JF + GBFS blends.

Figure 1. JF at different magnification ratios: **(a)** Raw fibers (no magnification); **(b)** Processed fibers (no magnification); and **(c)** Processed fibers (1,500× magnification).

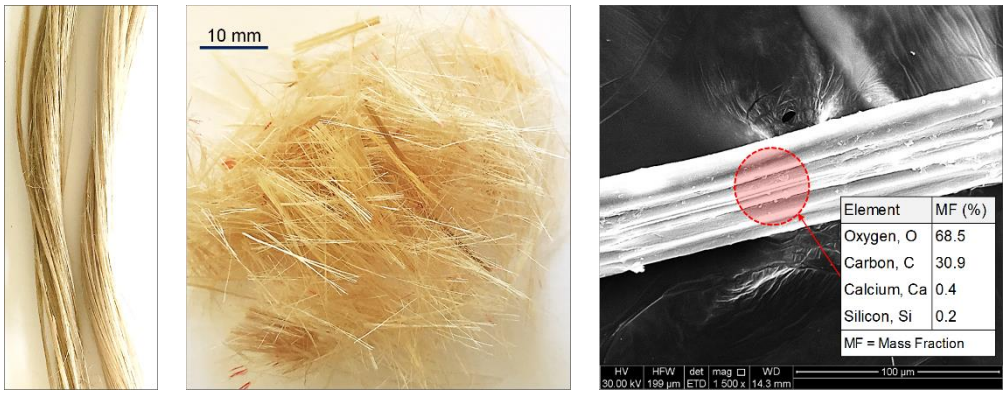

(a) **(b)** **(c)**

Figure 2. Variations of dry density along the height of the compacted samples: **(a)** $F_0S_0T_0$; **(b)** $F_{1.0}S_0T_0$; **(c)** $F_0S_6T_0$; and **(d)** $F_{1.0}S_6T_0$.

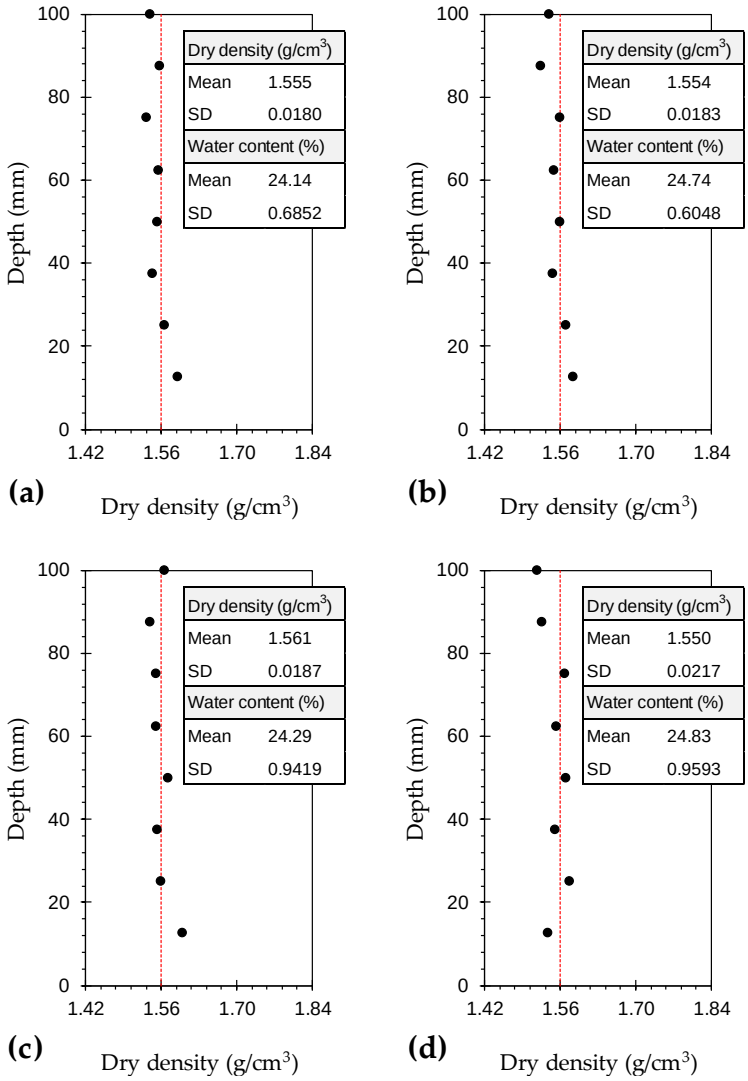

Figure 3. Stress–strain curves for the natural soil and various JF-reinforced samples, i.e., $F_xS_yT_z$ where x = {0, 0.5, 1.0, 1.5}, y = {0}, and z = {0}.

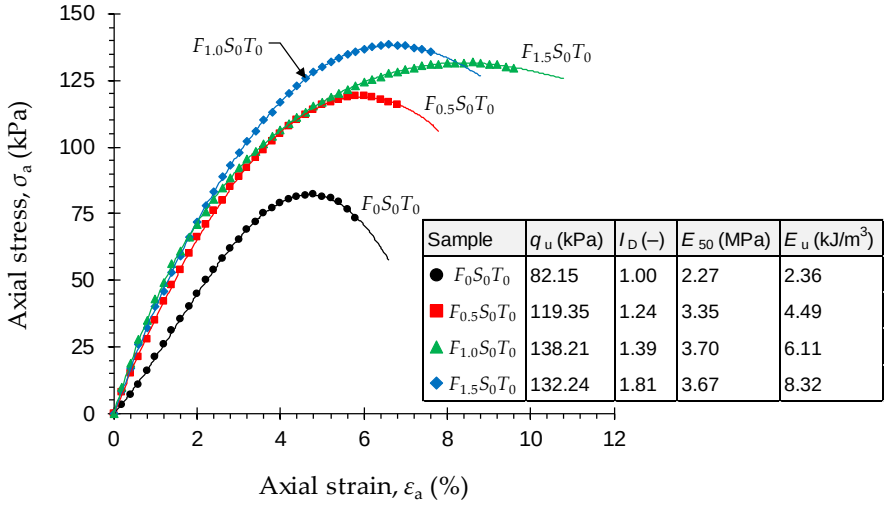

Sample	q_u (kPa)	I_D (–)	E_{50} (MPa)	E_u (kJ/m^3)
$F_0S_0T_0$	82.15	1.00	2.27	2.36
$F_{0.5}S_0T_0$	119.35	1.24	3.35	4.49
$F_{1.0}S_0T_0$	138.21	1.39	3.70	6.11
$F_{1.5}S_0T_0$	132.24	1.81	3.67	8.32

Figure 4. Typical stress–strain curves for the natural soil ($F_0S_0T_0$) and various stabilized samples: **(a)** $F_xS_yT_z$ where x = {0}, y = {3, 9}, and z = {7, 28}; and **(b)** $F_xS_yT_z$ where x = {0, 0.5, 1.0, 1.5}, y = {6}, and z = {7}.

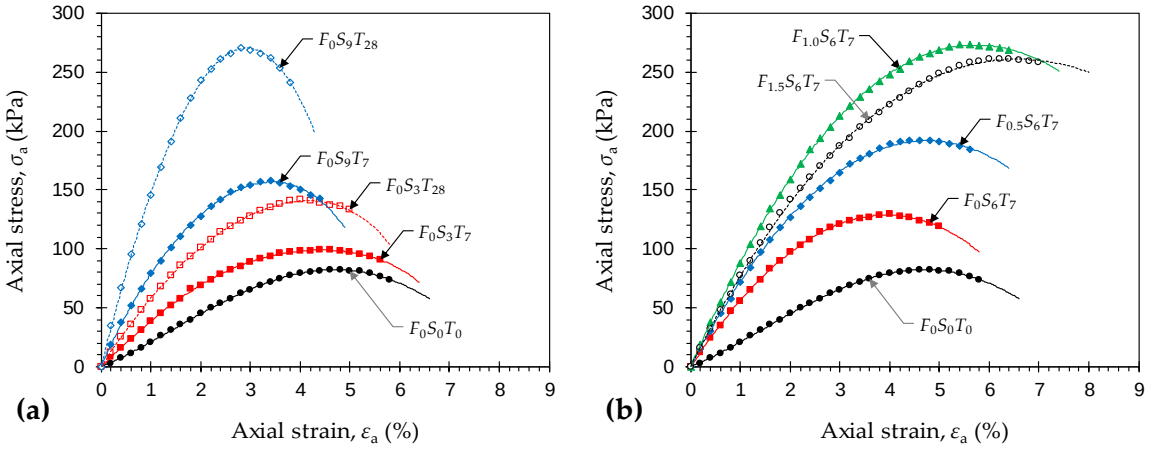

Figure 5. Variations of peak UC strength q_u against JF content for the natural soil and various GBFS-treated samples: **(a)** T_c = 7 days; and **(b)** T_c = 28 days.

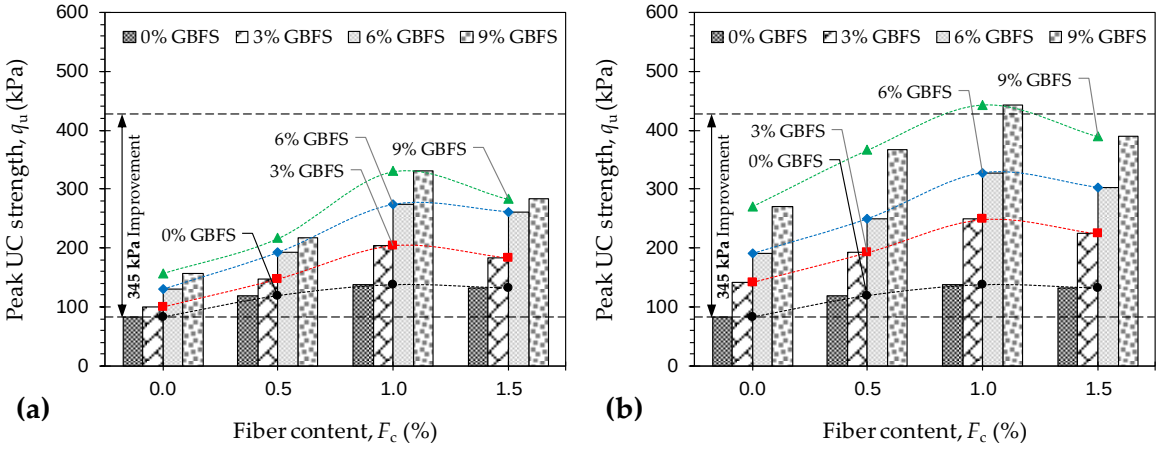

Figure 6. Variations of deformability index I_D against JF content for the natural soil and various GBFS-treated samples: **(a)** T_c = 7 days; and **(b)** T_c = 28 days.

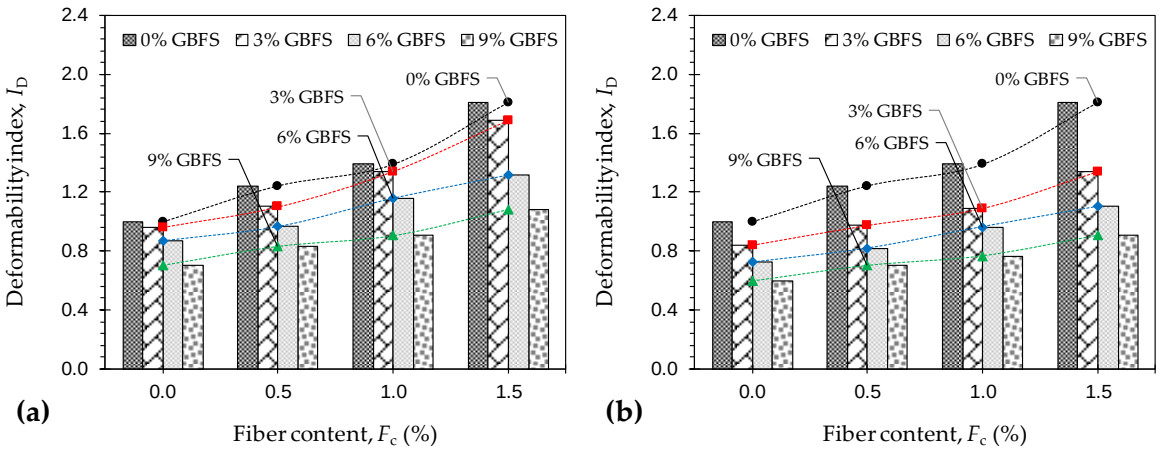

Figure 7. Variations of E_{50} against JF content for the natural soil and various GBFS-treated samples: **(a)** T_c = 7 days; and **(b)** T_c = 28 days.

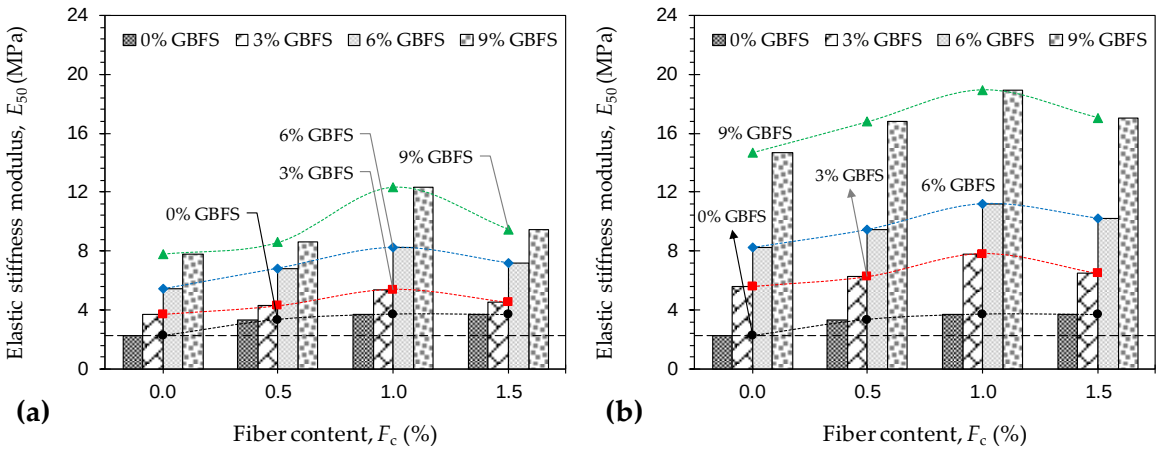

Figure 8. Variations of peak strain energy E_u against JF content for the natural soil and various GBFS-treated samples: **(a)** T_c = 7 days; and **(b)** T_c = 28 days.

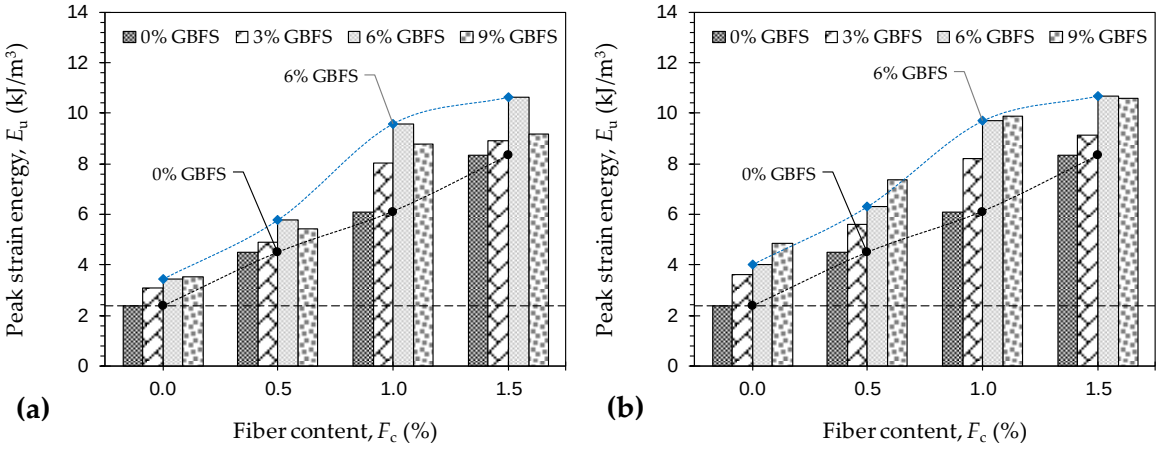

Figure 9. Variations of **(a)** E_{50} and **(b)** peak strain energy E_u against peak UC strength q_u for various JF + GBFS blends.

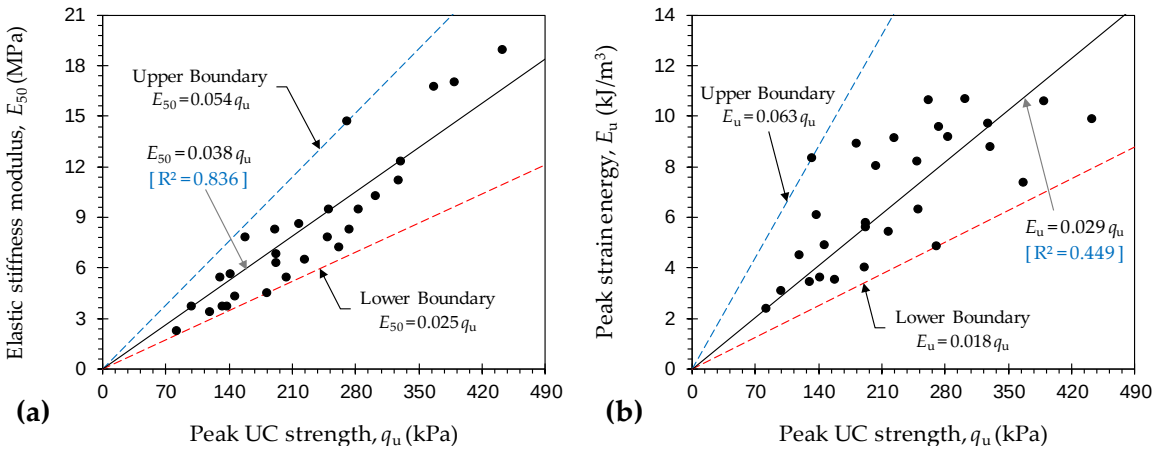

Figure 10. SEM micrographs for the tested samples: **(a)** $F_0S_0T_0$ (natural soil); **(b)** $F_{1.0}S_0T_0$; **(c)** $F_0S_6T_{28}$; and **(d)** $F_{1.0}S_6T_{28}$.

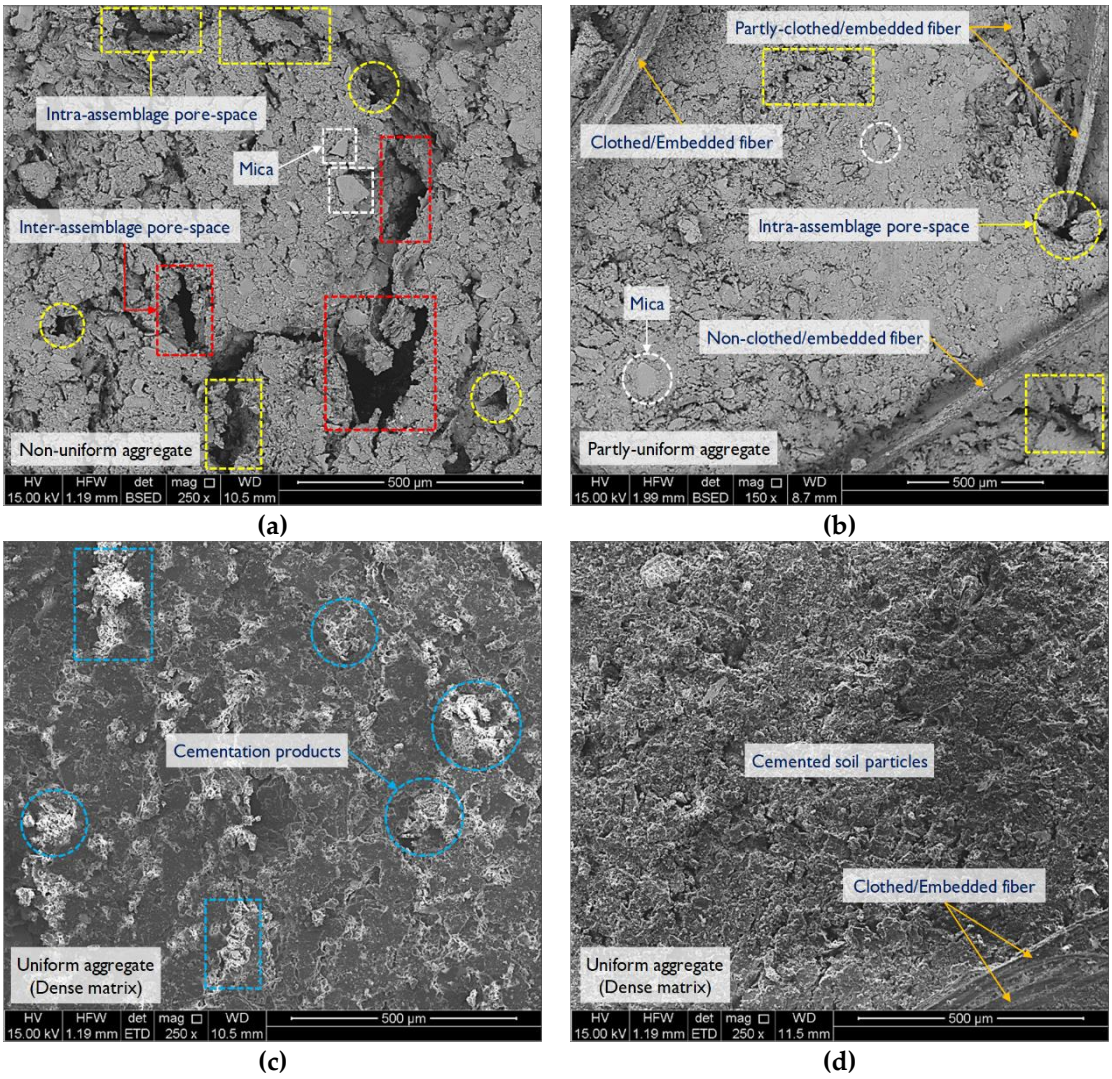

Figure 11. Variations of predicted, by Equation (11), against actual peak UC strength data for various JF + GBFS blends.

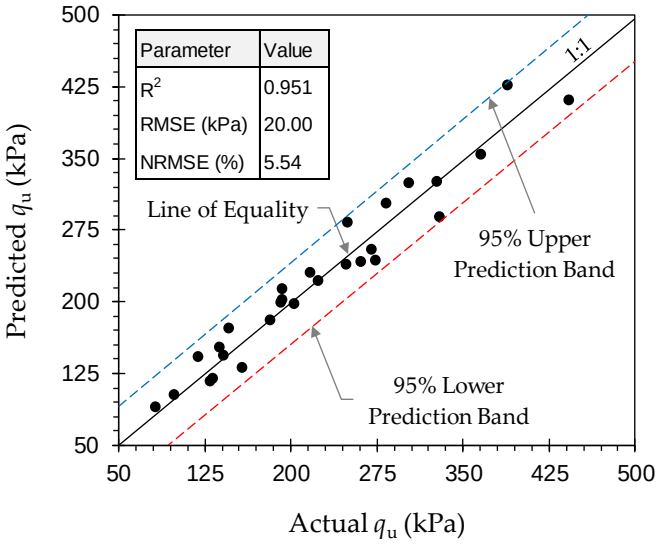

Statement of Authorship

Title of Paper	Mechanical Performance of Jute-Reinforced Micaceous Clay Composites Treated with Ground-Granulated Blast-Furnace Slag
Publication Status	■Published ☐Accepted for Publication ☐Submitted for Publication ☐Unpublished and Unsubmitted work written in manuscript style
Publication Details	**Zhang J**, Soltani A, Deng A, Jaksa M **(2019)** Mechanical Performance of Jute-Reinforced Micaceous Clay Composites Treated with Ground-Granulated Blast-Furnace Slag. ***Materials***, 12(4), 576:1-23. http://doi.org/10.3390/ma12040576

Principal Author

Name of Principal Author (Candidate)	Jiahe Zhang (**Email**: Jiahe.Zhang@adelaide.edu.au)		
Contribution to the Paper	Overall paper preparation		
Overall percentage (%)	85%		
Certification:	This paper reports on original research I conducted during the period of my Higher Degree by Research candidature and is not subject to any obligations or contractual agreements with a third party that would constrain its inclusion in this thesis. I am the primary author of this paper.		
Signature		Date	01/05/2019

Co-Author Contributions

By signing the Statement of Authorship, each author certifies that:

i. the candidate's stated contribution to the publication is accurate (as detailed above);
ii. permission is granted for the candidate in include the publication in the thesis; and
iii. the sum of all co-author contributions is equal to 100% less the candidate's stated contribution.

Name of Co-Author	An Deng **Senior Lecturer**, School of Civil, Environmental and Mining Engineering, The University of Adelaide, Adelaide, SA 5005, Australia (**Email**: An.Deng@adelaide.edu.au)		
Contribution to the Paper	Methodology, paper review and revision		
Signature		Date	1/05/2019

Name of Co-Author	Mark Jaksa **Professor**, School of Civil, Environmental and Mining Engineering, The University of Adelaide, Adelaide, SA 5005, Australia (**Email**: Mark.Jaksa@adelaide.edu.au)		
Contribution to the Paper	Paper review and revision		
Signature		Date	2/05/2019

Name of Co-Author	Amin Soltani Former: **Research Academic**, School of Civil, Environmental and Mining Engineering, The University of Adelaide, Adelaide, SA 5005, Australia (**Email**: Amin.Soltani@adelaide.edu.au) Current: **Research Fellow in Geotechnical Engineering**, Department of Infrastructure Engineering, Melbourne School of Engineering, the University of Melbourne, Parkville VIC 3010, (Email: Amin.Soltani@unimel.edu.au)		
Contribution to the Paper	Paper review and revision		
Signature		Date	2/05/2019

Published copy

materials

MDPI

Article

Mechanical Performance of Jute Fiber-Reinforced Micaceous Clay Composites Treated with Ground-Granulated Blast-Furnace Slag

Jiahe Zhang, Amin Soltani *, An Deng * and Mark B. Jaksa

School of Civil, Environmental and Mining Engineering, The University of Adelaide, Adelaide, SA 5005, Australia; Jiahe.Zhang@adelaide.edu.au (J.Z.); Mark.Jaksa@adelaide.edu.au (M.B.J.)

* Correspondence: Amin.Soltani@adelaide.edu.au (A.S.); An.Deng@adelaide.edu.au (A.D.)

Received: 14 January 2019; Accepted: 12 February 2019; Published: 14 February 2019

check for updates

Abstract: The combined capacity of Jute Fibers (JF), the reinforcement, and Ground-Granulated Blast-Furnace Slag (GBFS), the binder, was examined as a sustainable solution towards ameliorating the inferior engineering properties of micaceous clays. A total of sixteen JF + GBFS mix designs, i.e., JF (% by total mass) = {0, 0.5, 1.0, 1.5} and GBFS (% by total mass) = {0, 3, 6, 9}, were tested for unconfined compression (UC) strength; for those mix designs containing GBFS, curing was allowed for 7 and 28 days prior to testing. Scanning electron microscopy (SEM) studies were also carried out to observe the evolution of fabric in response to JF, GBFS and JF + GBFS amendments. The greater the JF content the higher the developed strength and stiffness up to 1% JF, beyond of which the effect of JF-reinforcement led to some adverse results. The JF inclusions, however, consistently improved the ductility and toughness of the composite. The addition of GBFS to the JF-reinforced samples improved the soil–fiber connection interface, and thus led to further improvements in the composite's strength, stiffness and toughness. The mix design "1% JF + 9% GBFS" managed to satisfy ASTM's strength criterion and hence was deemed as the optimum choice in this investigation. Finally, a non-linear, multivariable regression model was developed and validated to quantify the peak UC strength as a function of the composite's index properties. The proposed model contained a limited number of fitting parameters, all of which can be calibrated by little experimental effort, and thus implemented for preliminary design assessments.

Keywords: micaceous clay; jute fibers; ground-granulated blast-furnace slag; unconfined compression; strength; stiffness; scanning electron microscopy; multivariable regression

1. Introduction

Soils are the most common and readily accessible of all materials encountered in construction operations. Most soils, however, are characterized as problematic, as their intrinsic mechanical features, e.g., strength and bearing capacity, are often less than ideal for common civil engineering applications [1,2]. Meanwhile, shortage of land for development, as well as increasing costs associated with construction and raw materials, necessitates maximum utilization of local materials, one being problematic soils; among others, micaceous soils have been less publicized and hence demand further attention. The mica group of sheet silicates are among the most widely distributed minerals around the world; they naturally occur in igneous, sedimentary and certain metamorphic rocks [3,4]. Common physical features of mica include its unique platy structure, high elasticity (owing to its soft, spongy fabric) and nearly perfect basal cleavage; the latter, the nearly perfect cleavage, is attributed to the hexagonal sheet-like arrangement of mica atoms [5,6]. The presence of excessive mica minerals such as muscovite in weathered soils, particularly sands, adversely influence the soil's mechanical

properties. Mica minerals, although rather resilient, may gradually recover their initial shape due to the elastic rebound (or springy action), thereby reducing the efficiency of compactive effort and hence compromising the performance of facilities founded on micaceous soils [7]. During loading, i.e., compression, tension or shearing, mica minerals tend to rotate and orient themselves in a somewhat parallel fashion, which in turn leads to low strength resistance in micaceous soils [8]. Therefore, micaceous soils are characterized by poor compactibility, high compressibility and low shear strength, all of which present significant challenges for road construction, building foundations, earth dams and other geotechnical engineering systems [9–21]. Consequently, micaceous soils demand engineering solutions to alleviate the associated socio-economic impacts on human life.

Common solutions to counteract the adversities associated with problematic soils, and most likely micaceous clays, include soil replacement or attempting to amend the low-graded soil by means of stabilization [22]. The former involves replacing a portion of the problematic host soil with suitable quarried/burrowed materials capable of satisfying the desired mechanical performance; this approach is often impractical due to long-haul distances, as well as other economic considerations [23]. The latter, soil stabilization, refers to any chemical, physical, biological or combined practice of altering the soil fabric to meet the intended engineering criteria [24]. The chemical stabilization scheme makes use of chemical binders and/or additives—Portland cements, limes, fly ashes and slags, and more recently non-conventional agents such as polymers, resins and sulfonated oils—which initiate a series of short- and long-term chemical reactions in the soil–water medium, thereby amending the soil fabric into a coherent matrix of improved mechanical performance [23,25–37]. Physical stabilization often involves the placement of random or systematically-engineered reinforcements in the soil regime, thus engendering a spatial three-dimensional reinforcement network in favor of weaving/interlocking the soil particles into a unitary mass of induced strength resistance and improved ductility. Common reinforcements include fibers and geogrids of natural (e.g., bamboo, coir, hemp, jute and sisal) or synthetic (e.g., nylon, polyester, polyethylene, polypropylene and steel) origin, and more recently other sustainable geosynthetics such as waste textiles and recycled tire rubbers, all of which have been well documented in the literature [22,38–50]. Recent studies indicate that the use of chemical agents, particularly cementitious binders such as Portland cement and lime, alongside physical reinforcements may significantly improve the soil–reinforcement connection interface or bonding, thereby promoting further fabric enhancements [1,51–59].

A sustainable soil stabilization scheme can be characterized as one that maintains a perfect balance between infrastructure performance and the social, economic and ecological processes required to maintain human equity, diversity, and the functionality of natural systems. Traditional stabilization agents including cementitious binders and synthetic reinforcements, although proven effective, are not financially competitive in terms of materials procurement, labor and equipment usage. Furthermore, these solutions often suffer from serious environmental drawbacks attributed to their significant energy and carbon emissions footprints [22,60]. As such, the transition towards sustainable soil stabilization necessitates utilizing natural reinforcements and/or industrial by-products as part of the infrastructure system, and more specifically as replacements for traditional stabilization materials. Although the adverse effects of mica content on soils, particularly gravels and sands, have been well documented in the literature, systematic stabilization studies on micaceous soils, and micaceous clays in particular, are still limited [12,61–63]. More importantly, the adopted stabilization materials have been limited to Portland cement and lime, while sustainable agents commonly practiced for other problematic soils, e.g., natural fibers and industrial by-products such as fly ashes and slags, have not yet been examined and hence demand further attention.

The present study examines the combined capacity of Jute Fibers (JF), the reinforcement, and Ground-Granulated Blast-Furnace Slag (GBFS), the binder, as a sustainable solution towards ameliorating the inferior engineering characteristics of micaceous clays. A series of unconfined compression (UC) tests were carried out on various mix designs to evaluate the effects of JF-reinforcement and/or GBFS-treatment on the strength, ductility, stiffness and toughness of the

micaceous clay. Scanning electron microscopy (SEM) studies were also carried out to observe the evolution of soil fabric in response to JF, GBFS and JF + GBFS amendments. Finally, a non-linear, multivariable regression model was developed and validated to quantify the peak UC strength as a function of the composite's index properties. A sensitivity analysis was also carried out to quantify the relative impacts of the independent regression variables, namely JF content, GBFS content and curing time, on the composite's strength.

2. Materials

2.1. Micaceous Clay

Commercially-available Kaolin (K) and Ground Mica (GM), sourced from local distributors, were used to artificially prepare a desired Micaceous Clay (MC) blend for further experimental work. The choice of GM content for the MC blend was selected as 20% (by dry mass of K), as it represents an upper boundary prerequisite to simulate adverse mechanical attributes commonly exhibited by natural micaceous clays, i.e., compactability issues and low shear strength/bearing capacity [10,11,16]. The artificial MC blend manifested the same typical texture, sheen and friability features as natural micaceous clays commonly reported in the literature, and thus may well provide a basis for systematic stabilization studies. The physical and mechanical properties of K, GM and the MC blend (hereafter simply referred to as natural soil) were determined as per relevant ASTM and Australian (AS) standards, and the results are summarized in Table 1. The conventional gradation analysis, carried out in accordance with ASTM D422–07, indicated a clay fraction (<2 μm) of 51%, along with 48% silt (2–75 μm) and 1% sand (0.075–4.75 mm) for K. As a result of 20% GM inclusion, the aforementioned values changed to 39%, 55% and 6%, respectively. The liquid limit and plasticity index were measured as LL = 44.67% and PI = 20.95% for K, and LL = 48.67% and PI = 11.28% for MC, from which these soils were, respectively, characterized as *clay with intermediate plasticity* (CI) and *silt with intermediate plasticity* (MI) in accordance with the Unified Soil Classification System (USCS). The standard Proctor compaction test (ASTM D698–12) indicated optimum water contents of w_{opt} = 19.84% and 23.52%, along with maximum dry densities of ρ_{dmax} = 1.63 g/cm^3 and 1.56 g/cm^3, for K and MC, respectively. Such trends can be attributed to the spongy nature (i.e., elastic/rebound response to compaction energy) and high water demand of the mica mineral [12,20,64].

Table 1. Physical and mechanical properties of K, GM and MC.

Properties	K	GM	MC	Standard Designation
Specific gravity of solids, G_s	2.69	2.80	2.73	ASTM D854–14
Clay fraction [<2 μm] (%)	51	-	39	ASTM D422–07
Silt fraction [2–75 μm] (%)	48	-	55	ASTM D422–07
Fines fraction [<75 μm] (%)	99	93	94	ASTM D422–07
Sand fraction [0.075–4.75 mm] (%)	1	7	6	ASTM D422–07
Natural water content, w_n (%)	2.14	0.41	1.67	ASTM D2216–10
Liquid limit, LL (%)	44.67	-	48.67	AS 1289.3.9.1–15
Plastic limit, PL (%)	23.72	-	36.94	AS 1289.3.2.1–09
Plasticity index, PI (%)	20.95	-	11.28	AS 1289.3.3.1–09
Linear shrinkage, LS (%)	7.06	-	8.84	AS 1289.3.4.1–08
Shrinkage index, SI (%) [1]	37.61	-	39.83	Sridharan and Nagaraj [65]
USCS classification	CI [2]	-	MI [3]	ASTM D2487–11
Optimum water content, w_{opt} (%)	19.84	-	23.52	ASTM D698–12
Maximum dry density, ρ_{dmax} (g/cm^3)	1.63	-	1.56	ASTM D698–12
Unconfined compression strength, q_u (kPa) [4]	137.62	-	85.14	ASTM D2166–16
Splitting tensile strength, q_t (kPa) [4]	21.76	-	14.62	ASTM C496–17

[1] SI = LL–LS; [2] Clay with intermediate plasticity; [3] Silt with intermediate plasticity; and [4] Tested at standard Proctor optimum condition.

The chemical compositions of K and GM, as supplied by the manufacturers, are outlined in Table 2. The chemical composition of both K and GM is mainly dominated by silicon dioxide (SiO_2) and aluminum trioxide (Al_2O_3) with mass fractions of 64.9% and 22.2% for K, and 49.5% and 29.2%

for GM, respectively. The pH for slurries of K and GM was, respectively, found to be 7.4 and 7.8, from which both materials were classified as neutral substances. Other material properties included a specific surface area of SSA = 11.2 m^2/g and 5.3 m^2/g for K and GM, respectively.

Table 2. Chemical compositions of K and GM (as supplied by the manufacturers).

Properties	K	GM
SiO_2 (%)	64.9	49.5
Al_2O_3 (%)	22.2	29.2
K_2O (%)	2.7	8.9
TiO_2 (%)	1.4	0.8
Fe_2O_3 (%)	1.0	4.6
MgO (%)	0.6	0.7
Na_2O (%)	0.2	0.5
CaO (%)	0.1	0.4
Acidity, pH [20% slurry]	7.4	7.8
Oil absorption (mL/100 g)	34.0	36.0
Loss on ignition, LOI [at 1000 °C] (%)	6.5	<6
Specific surface area, SSA (m^2/g)	11.2	5.3

2.2. *Jute Fibers*

Commercially-available Jute Fibers (JF), manufactured from *Corchorus capsularis* (a shrub species in the Malvaceae family), was used as the reinforcing agent. Its biochemical composition, as commonly reported in the literature, consists of 56–71% cellulose, 29–35% hemicellulose and 11–14% lignin [66]. The raw fibers had a diameter of F_D = 30–40 μm; they were cut into segments of approximately F_L = 15 mm, thus resulting in an aspect ratio of $F_{AR} = F_L/F_D$ = 375–500 (see Figure 1a,b). The scanning electron microscopy (SEM) technique was used to observe the fiber's surface morphology, and the results are illustrated in Figure 1c. The fiber's surface embodies a highly-irregular shape comprising of a series of peaks and troughs of varying heights, depths and spacing, thus signifying a rough surface texture. Such surface features may potentially promote adhesion and/or induce frictional resistance at the soil–fiber interface, and thus amend the soil fabric into a coherent matrix of induced strength and improved ductility (see Section 4.3). The physical and mechanical properties of JF, as supplied by the distributor, are provided in Table 3. The specific gravity of JF was found to be 1.30–1.46, which is approximately two-fold less than that of the MC blend.

(a) (b) (c)

Figure 1. JF at different magnification ratios: (**a**) Raw fibers (no magnification); (**b**) Processed fibers (no magnification); and (**c**) Processed fibers (1500× magnification).

Table 3. Physical and mechanical properties of JF (as supplied by the distributor).

Properties	Value
Specific gravity, G_s	1.30–1.46
Length, F_L (mm)	15
Diameter, F_D (μm)	30–40
Aspect ratio, $F_{AR} = F_L/F_D$	375–500
Young's modulus (GPa)	10–30
Tensile strength (MPa)	400–900
Tensile elongation at break (%)	1.5–1.8
Water absorption (%)	12

2.3. Ground-Granulated Blast-Furnace Slag

A large quantity of Ground-Granulated Blast-Furnace Slag (GBFS) was sourced from a local manufacturer in South Australia, and was used as the cementitious binder. The physical properties and chemical composition of GBFS, as supplied by the manufacturer, are outlined in Table 4. The particles of GBFS were mainly finer than 75 μm in size; its fines and sand fractions were found to be 96% and 4%, respectively. Other properties included a basic pH of 9.6 and a specific surface area of SSA = 0.7 m^2/g; the latter is approximately two-fold greater than that of ordinary Portland cement [67]. The chemical composition of GBFS is mainly dominated by calcium oxide or lime (CaO) and silicon dioxide (SiO_2) with mass fractions of 44.7% and 27.1%, respectively. The former, the calcium oxide, acts as a precursor agent, initiating a series of short- and long-term chemical reactions in the soil–water medium, i.e., cation exchange, flocculation–agglomeration and pozzolanic reactions, thereby amending the soil fabric into a unitary mass of enhanced mechanical performance (see Section 4.3).

Table 4. Physical properties and chemical composition of GBFS (as supplied by the manufacturer).

Properties	Value
Specific gravity of solids, G_s	2.87
Fines fraction [<75 μm] (%)	96
Sand fraction [0.075–4.75 mm] (%)	4
Natural water content, w_n (%)	<1
Acidity, pH [20% slurry]	9.6
Loss on ignition, LOI [at 1000 °C] (%)	<3
Specific surface area, SSA (m^2/g)	0.7
CaO (%)	44.7
SiO_2 (%)	27.1
Al_2O_3 (%)	13.6
MgO (%)	5.1
Fe_2O_3 (%)	3.5
TiO_2 (%)	1.7
K_2O (%)	0.7
Na_2O (%)	0.2

3. Experimental Program

3.1. Mix Designs and Sample Preparations

In this study, a total of sixteen mix designs consisting of one control (natural soil), three JF-reinforced, three GBFS-treated and nine JF + GBFS blends were examined (see Table 5). Hereafter, the following coding system is adopted to designate the various mix designs:

$$F_xS_yT_z \quad (1)$$

where F_x = x% JF; S_y = y% GBFS; and T_z = z days of curing.

Table 5. Mix designs and their properties.

Group	Designation	JF Content (%)	GBFS Content (%)
Control [1]	$F_0S_0T_0$	0	0
JF-reinforced	$F_{0.5}S_0T_0$	0.5	0
	$F_{1.0}S_0T_0$	1.0	0
	$F_{1.5}S_0T_0$	1.5	0
GBFS-treated	$F_0S_3T_{7,28}$	0	3
	$F_0S_6T_{7,28}$	0	6
	$F_0S_9T_{7,28}$	0	9
JF + GBFS	$F_{0.5}S_3T_{7,28}$	0.5	3
	$F_{1.0}S_3T_{7,28}$	1.0	3
	$F_{1.5}S_3T_{7,28}$	1.5	3
	$F_{0.5}S_6T_{7,28}$	0.5	6
	$F_{1.0}S_6T_{7,28}$	1.0	6
	$F_{1.5}S_6T_{7,28}$	1.5	6
	$F_{0.5}S_9T_{7,28}$	0.5	9
	$F_{1.0}S_9T_{7,28}$	1.0	9
	$F_{1.5}S_9T_{7,28}$	1.5	9

[1] Natural soil.

The JF, GBFS and water contents were, respectively, defined as:

$$(\%)\ F_c = \frac{m_{JF}}{m_{JF} + m_{GBFS} + m_{MC}} \times 100 \quad (2)$$

$$(\%)\ S_c = \frac{m_{GBFS}}{m_{GBFS} + m_{JF} + m_{MC}} \times 100 \quad (3)$$

$$(\%)\ w_c = \frac{m_W}{m_{JF} + m_{GBFS} + m_{MC}} \times 100 \quad (4)$$

where F_c = JF content; S_c = GBFS content; w_c = water content; m_{JF} = mass of JF; m_{GBFS} = mass of GBFS; m_{MC} = mass of micaceous clay (or natural soil); and m_W = mass of water.

The natural soil, JF and GBFS were blended in dry form as per the selected mix designs outlined in Table 5. Mixing was carried out for approximately 5 min to gain visible homogeneity of the ingredients. The required volume of water corresponding to a water content of w_c = 23.52%, the standard Proctor optimum water content of the natural soil (ASTM D698–12), was added to each blend and thoroughly mixed by hand for approximately 15 min. Extensive care was taken to pulverize the clumped particles, targeting homogeneity of the mixtures. A special split mold, similar to that described in the literature, was designed and fabricated from stainless steel to accomplish static compaction [33,43,49]. The mold consisted of three segments, namely the top collar, the middle section, and the bottom collar. The middle section measures 50 mm in diameter and 100 mm in height, and accommodates the sample for the unconfined compression test (see Section 3.2). The moist blends were statically compacted in the mold in five layers; each layer achieved a dry density of ρ_d = 1.56 g/cm^3 (i.e., the standard Proctor maximum dry density of the natural soil, obtained as per ASTM D698–12). The surface of the first to fourth compacted layers was scarified to ensure adequate bonding between adjacent layers of the mixture. Samples containing GBFS were enclosed in multiple layers of cling wrap and transferred to a humidity chamber, maintained at 70% relative humidity and a temperature of 25 ± 2 °C, where curing was allowed for 7 and 28 days prior to testing,

To ensure uniformity of fabric and hence consistency in behavior, the variations of dry density and water content should be measured along the height of the compacted samples [68]. In this regard, typical cases including $F_0S_0T_0$ (natural soil), $F_{1.0}S_0T_0$, $F_0S_6T_0$ and $F_{1.0}S_6T_0$ were examined, and the results are provided in Figure 2. The variations of both dry density and water content were found to

be marginal, as evident with the low standard deviations (SD), thus corroborating the suitability of the adopted sample preparation technique.

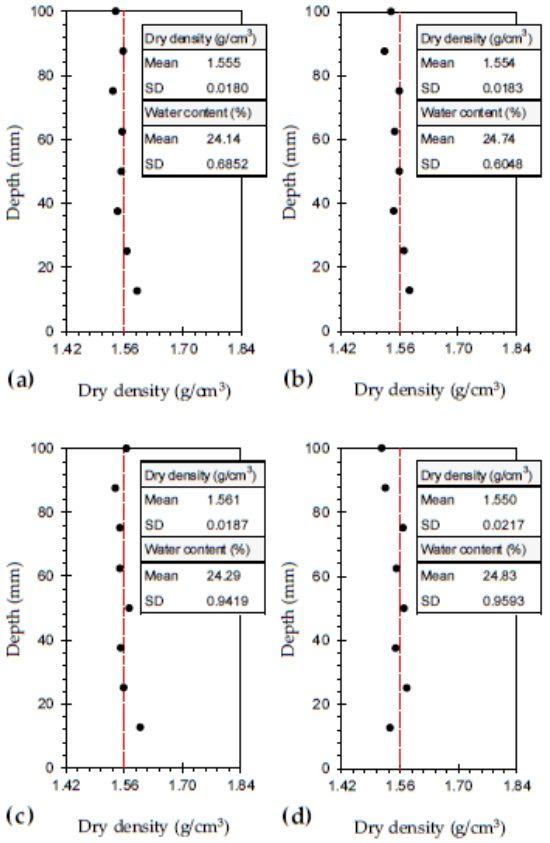

Figure 2. Variations of dry density along the height of the compacted samples: (**a**) $F_0S_0T_0$; (**b**) $F_{1.0}S_0T_0$; (**c**) $F_0S_6T_0$; and (**d**) $F_{1.0}S_6T_0$.

3.2. Unconfined Compression Test

Unconfined compression (UC) tests were carried out in accordance with ASTM D2166–16. The prepared samples (see Section 3.1) were axially compressed at a constant displacement rate of 1 mm/min (equivalent to 1%/min), as commonly adopted in the literature [22,33,69]. Axial strains and the corresponding axial stresses were recorded at various time intervals to a point at which the maximum axial stress required for sample failure, denoted as the peak UC strength, was achieved. On account of the two curing times adopted for the samples containing GBFS, a total of 28 UC tests, i.e., one for control (natural soil), three for JF-reinforced, six for GBFS-treated and eighteen for JF + GBFS blends, were conducted to address the sixteen mix designs outlined in Table 5. To ensure sufficient accuracy, triplicate samples were tested for typical mix designs, i.e., $F_0S_0T_0$ (natural soil), $F_{1.0}S_0T_0$, $F_0S_6T_{28}$ and $F_{1.0}S_6T_{28}$. In this regard, the standard deviation (SD) and the coefficient of variation (CV) for the triplicate peak UC strength data were found to range between SD = 3.74 kPa and 11.19 kPa, and CV = 3.23% and 5.15%; these low values corroborate the repeatability of the adopted sample preparation technique, as well as the implemented UC testing procedure.

3.3. Scanning Electron Microscopy Studies

The scanning electron microscopy (SEM) technique was implemented to investigate the evolution of fabric in response to JF, GBFS and JF + GBFS amendments. SEM imaging was carried out by means of the Philips XL20 (Amsterdam, The Netherlands) scanning electron microscope. Apparatus specifications included a resolution of 4 µm and a maximum magnification ratio of 50,000×. In this regard, typical mix designs consisting of $F_0S_0T_0$ (natural soil), $F_{1.0}S_0T_0$, $F_0S_6T_{28}$ and $F_{1.0}S_6T_{28}$ were examined. The desired samples, prepared as per Section 3.1, were first air-dried for approximately 14 days. The desiccated samples were then carefully fractured into small cubic-shaped pieces measuring approximately 1000 mm^3 in volume, and were further subjected to SEM imaging at various magnification ratios ranging from 250× to 20,000×.

4. Results and Discussion

4.1. Effect of JF on UC Strength

Stress–strain curves for the natural soil and various JF-reinforced samples—$F_xS_yT_z$ where x = {0, 0.5, 1.0, 1.5}, y = {0}, and z = {0}—are provided in Figure 3. The stress–strain relationship for the natural soil sample demonstrated a rise–fall response with a visually-detectable peak point, thereby indicating a strain-softening behavior accompanied by a brittle sample failure. As a result of JF-reinforcement, the stress–strain locus progressively transitioned towards a strain-hardening character. In this case, the greater the JF content the more prominent the strain-hardening effect and hence the less dramatic (or the more ductile) the failures.

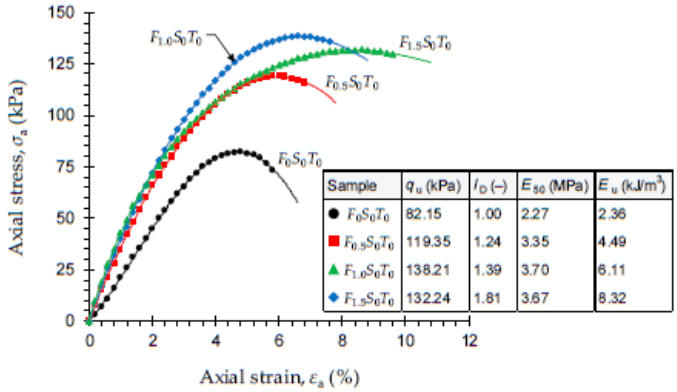

Figure 3. Stress–strain curves for the natural soil and various JF-reinforced samples, i.e., $F_xS_yT_z$ where x = {0, 0.5, 1.0, 1.5}, y = {0}, and z = {0}.

As demonstrated in Figure 3, the greater the JF content the higher the peak UC strength up to F_c = 1%, beyond of which JF-reinforcement was found to adversely influence strength development in the composite. The natural soil exhibited a peak UC strength of q_u = 82.15 kPa, while the samples reinforced with F_c = 0.5% and 1% resulted in higher values of q_u = 119.35 kPa and 138.21 kPa, respectively. The higher JF inclusion of 1.5% changed the peak UC strength to 132.24 kPa, which still holds a notable advantage over the natural soil, as well as the sample reinforced with 0.5% JF. The axial strain at failure, denoted as ε_u, is an indication of the material's ductility; higher ε_u values manifest a more ductile (or a less brittle) character. Improvement in ductility is often quantified by means of the deformability index I_D [70]:

$$I_D = \frac{{\varepsilon_u}^S}{{\varepsilon_u}^N} \quad (5)$$

where $\varepsilon_u{}^S$ = axial strain at failure for the stabilized soil sample; and $\varepsilon_u{}^N$ = axial strain at failure for the control (or natural soil) sample.

The deformability index exhibited a monotonically-increasing trend with JF content, thus indicating that the greater the JF content the more ductile the sample's response to compression. By definition, the natural soil corresponds to a deformability index of unity ($\varepsilon_u{}^N$ = 4.73%). As a result of JF-reinforcement, the deformability index exhibited a monotonically-increasing trend, and resulted in I_D = 1.24, 1.39 and 1.81 ($\varepsilon_u{}^S$ = 5.88%, 6.57% and 8.55%) for F_c = 0.5%, 1% and 1.5%, respectively.

The secant modulus at 50% of the peak UC strength, denoted as E_{50}, is a measure of the material's stiffness in the elastic compression domain [22,71]. The variations of E_{50}, as given in Figure 3, exhibited a trend similar to that observed for the peak UC strength, peaking at F_c = 1% and then slightly decreasing for the higher JF content of 1.5%. The natural soil and samples reinforced with 0.5%, 1% and 1.5% JF resulted in E_{50} = 2.27 MPa, 3.35 MPa, 3.70 MPa and 3.67 MPa, respectively. The area under a typical stress–strain curve up to the peak point, defined as the energy stored by a sample undergoing deformation and referred to as peak strain energy, serves as a measure of the material's toughness [22,72]. Unlike strength and stiffness, the development of toughness, similar to ductility, was consistently in favor of the JF inclusions, and displayed a monotonically-increasing trend with respect to JF content (see the E_u values in Figure 3). An increase in toughness warrants an increase in the peak UC strength and/or the axial strain at failure [41,57]. With regard to JF-reinforcement, both q_u and ε_u contribute to the development of toughness; however, the greater the JF content the less prominent the strength's contribution and hence the more significant the role of ductility. The natural soil resulted in E_u = 2.36 kJ/m^3, while the samples reinforced with F_c = 0.5%, 1% and 1.5% resulted in higher values of E_u = 4.49 kJ/m^3, 6.11 kJ/m^3 and 8.32 kJ/m^3, respectively.

4.2. Effect of JF + GBFS on UC Strength

Typical stress–strain curves for the natural soil ($F_0S_0T_0$) and various GBFS-treated samples—$F_xS_yT_z$ where x = {0}, y = {3, 9}, and z = {7, 28}—are provided in Figure 4a. Unlike the JF-reinforced samples (see Figure 3), the stress–strain responses for all GBFS-treated composites were seemingly strain-softening and hence accompanied by brittle failures. In general, the greater the GBFS content and/or the longer the curing period, the higher the developed strength and stiffness, and the more prominent the strain-softening character. Stress–strain curves for the natural soil ($F_0S_0T_0$) and various JF-reinforced samples treated with 6% GBFS—$F_xS_yT_z$ where x = {0, 0.5, 1.0, 1.5}, y = {6}, and z = {7}—are provided in Figure 4b. Much like the natural soil reinforced with JF (see Figure 3), for any given GBFS content, an increase in JF content progressively transitioned the stress–strain locus towards a strain-hardening character. In this case, the greater the JF content the more pronounced the strain-hardening effect and hence the more ductile the failures.

Figure 5a,b illustrate the variations of peak UC strength against JF content for the natural soil and various GBFS-treated samples tested at 7 and 28 days of curing, respectively. Much like the natural soil reinforced with JF, for any given GBFS content and curing time, the peak UC strength increased with JF content up to F_c = 1%; beyond 1% JF, the effect of JF-reinforcement adversely influenced strength development in the composite. For instance, the sample $F_0S_6T_{28}$ resulted in q_u = 191.32 kPa, while the inclusions of 0.5%, 1% and 1.5% JF, with the same 6% GBFS content and the same 28-day curing condition, resulted in q_u = 250.08 kPa, 327.42 kPa and 302.76 kPa, respectively. Moreover, for any given JF content, the greater the GBFS content and/or the longer the curing period, the higher the developed peak UC strength, following a monotonically-increasing trend. The sample $F_{1.0}S_0T_0$, for instance, exhibited a peak UC strength of q_u = 138.21 kPa. As a result of 3%, 6% and 9% GBFS inclusions, along with the same 1% JF content and a 7-day curing condition, the peak UC strength increased to 203.56 kPa, 273.68 kPa and 330.06 kPa, respectively. Similar mix designs cured for T_c = 28 days exhibited significant improvements over their 7-day counterparts, as the aforementioned values increased to 248.65 kPa, 327.42 kPa and 443.21 kPa, respectively. The ASTM D4609–08 standard suggests a minimum improvement of 345 kPa in the natural soil's peak UC strength (at T_c = 28 days)

as a criterion for characterizing an effective stabilization scheme [34]. As demonstrated in Figure 5b, the sample $F_{1.0}S_9T_{28}$ promotes a 361.06 kPa improvement in the peak UC strength and hence satisfies the aforementioned criterion.

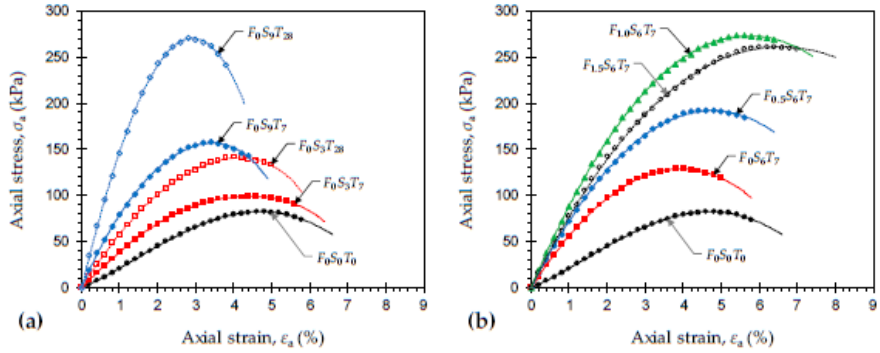

Figure 4. Typical stress–strain curves for the natural soil ($F_0S_0T_0$) and various stabilized samples: (**a**) $F_xS_yT_z$ where x = {0}, y = {3, 9}, and z = {7, 28}; and (**b**) $F_xS_yT_z$ where x = {0, 0.5, 1.0, 1.5}, y = {6}, and z = {7}.

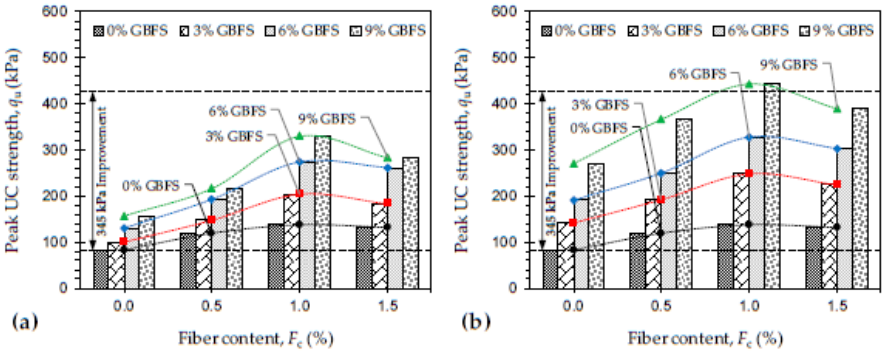

Figure 5. Variations of peak UC strength q_u against JF content for the natural soil and various GBFS-treated samples: (**a**) T_c = 7 days; and (**b**) T_c = 28 days.

The deformability index, a measure of the material's ductility, was also calculated for various JF + GBFS mix designs, and the results are provided in Figure 6a,b for the samples tested at T_c = 7 and 28 days, respectively. Similar to the natural soil reinforced with JF, for any given GBFS content and curing time, the greater the JF content the higher the deformability index, following a monotonically-increasing trend. For any given JF content, however, the greater the GBFS content and/or the longer the curing period, the lower the developed ductility. The deformability index for various JF + GBFS blends was cross-checked with that of the natural soil (or I_D = 1) to arrive at the optimum cases. In this regard, nine cases (out of 28) manage to satisfy the $I_D \geq 1$ criterion, and thus are deemed as optimum with respect to ductility improvement. The nine optimum cases and their corresponding I_D values include $F_{0.5}S_3T_7$ (I_D = 1.10), $F_{1.0}S_3T_7$ (I_D = 1.34), $F_{1.5}S_3T_7$ (I_D = 1.68), $F_{1.0}S_3T_{28}$ (I_D = 1.09), $F_{1.5}S_3T_{28}$ (I_D = 1.34), $F_{1.0}S_6T_7$ (I_D = 1.16), $F_{1.5}S_6T_7$ (I_D = 1.32), $F_{1.5}S_6T_{28}$ (I_D = 1.10), and $F_{1.5}S_9T_7$ (I_D = 1.08).

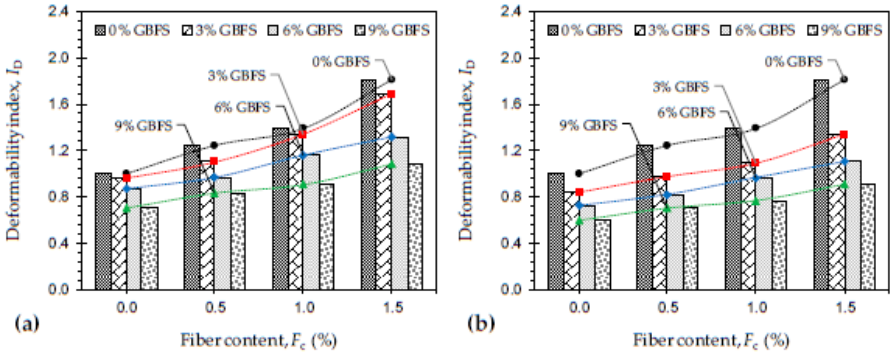

Figure 6. Variations of deformability index I_D against JF content for the natural soil and various GBFS-treated samples: (**a**) T_c = 7 days; and (**b**) T_c = 28 days.

Figure 7a,b illustrate the variations of E_{50} against JF content for the natural soil and various GBFS-treated samples tested at 7 and 28 days of curing, respectively. The variations of E_{50} exhibited a trend similar to that observed for the peak UC strength given in Figure 5. As such, for any given JF content, the development of stiffness was in favor of both the GBFS content and the curing time. As typical cases, the samples $F_{1.0}S_0T_0$, $F_{1.0}S_3T_7$, $F_{1.0}S_3T_{28}$, $F_{1.0}S_9T_7$ and $F_{1.0}S_9T_{28}$ resulted in E_{50} = 3.70 MPa, 5.39 MPa, 7.81 MPa, 12.30 MPa and 18.92 MPa, respectively. Moreover, for any given GBFS content and curing time, stiffness enhancements were only notable for samples with up to 1% JF inclusions. In this regard, the samples $F_0S_6T_{28}$, $F_{0.5}S_6T_{28}$, $F_{1.0}S_6T_{28}$ and $F_{1.5}S_6T_{28}$, for instance, resulted in E_{50} = 8.25 MPa, 9.47 MPa, 11.21 MPa and 10.23 MPa, respectively.

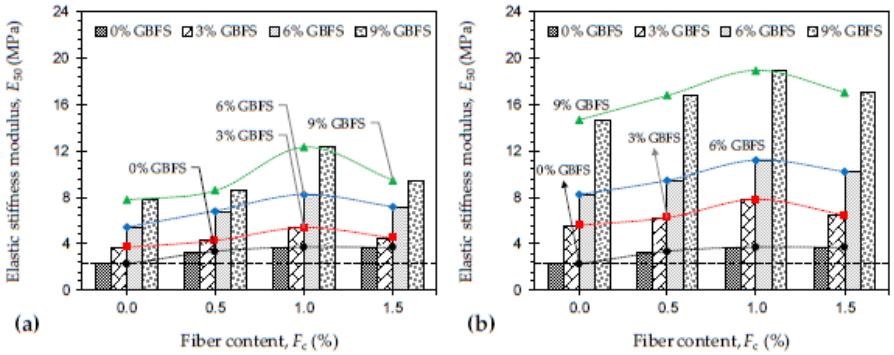

Figure 7. Variations of E_{50} against JF content for the natural soil and various GBFS-treated samples: (**a**) T_c = 7 days; and (**b**) T_c = 28 days.

Figure 8a,b illustrate the variations of peak strain energy, a measure of the material's toughness, against JF content for the natural soil and various GBFS-treated samples tested at 7 and 28 days of curing, respectively. The development of toughness was in favor of both the JF content and the GBFS treatments (i.e., GBFS content and/or curing time). For any given GBFS content and curing time, the greater the JF content the higher the peak strain energy, following a monotonically-increasing trend. For instance, the samples $F_0S_6T_{28}$, $F_{0.5}S_6T_{28}$, $F_{1.0}S_6T_{28}$ and $F_{1.5}S_6T_{28}$ resulted in peak strain energies of E_u = 3.99 kJ/m^3, 6.30 kJ/m^3, 9.71 kJ/m^3 and 10.70 kJ/m^3, respectively. Similarly, for any given JF content, the greater the GBFS content and/or the longer the curing period, the higher the developed toughness. As typical cases, the sample $F_{1.0}S_0T_0$ resulted in E_u = 6.11 kJ/m^3, while the aforementioned

value increased to 8.02 kJ/m^3, 8.22 kJ/m^3, 8.78 kJ/m^3 and 9.88 kJ/m^3 for $F_{1.0}S_3T_7$, $F_{1.0}S_3T_{28}$, $F_{1.0}S_9T_7$ and $F_{1.0}S_9T_{28}$, respectively.

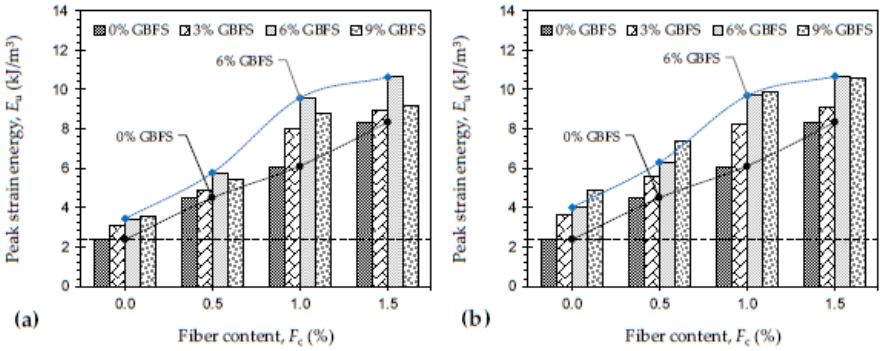

Figure 8. Variations of peak strain energy E_u against JF content for the natural soil and various GBFS-treated samples: (**a**) T_c = 7 days; and (**b**) T_c = 28 days.

Figure 9a,b illustrate the variations of E_{50} and E_u against q_u for various JF + GBFS mix designs, respectively. The variations of E_{50} were situated within the $0.054q_u < E_{50} < 0.025q_u$ domain (E_{50} in MPa, and q_u in kPa). For E_u, however, a broader domain in the form of $0.063q_u < E_u < 0.018q_u$ (E_u in kJ/m^3, and q_u in kPa) was noted. The former, the E_{50}, exhibited a rather strong correlation with q_u. On the contrary, the peak strain energy was poorly correlated with the peak UC strength. In this regard, simple correlative models in the forms of $E_{50} = 0.038q_u$ (with $R^2 = 0.836$) and $E_u = 0.029q_u$ (with $R^2 = 0.449$) can be derived; the former can be implemented for indirect estimations of E_{50}.

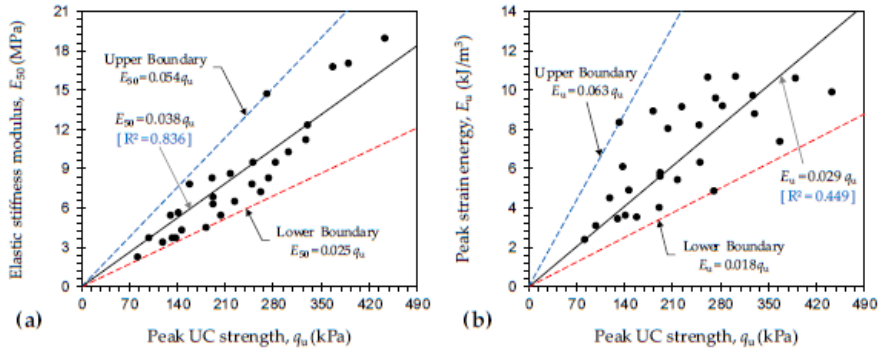

Figure 9. Variations of (**a**) E_{50} and (**b**) peak strain energy E_u against peak UC strength q_u for various JF + GBFS blends.

4.3. Stabilization Mechanisms and Microstructure Analysis

The JF inclusions are able to amend the soil fabric through improvements achieved in two aspects: (**i**) frictional resistance generated at the soil–fiber interface, owing to the fiber's rough surface texture; and (**ii**) mechanical interlocking of soil particles and fibers [1,22,40,45,48,51,57,66]. The interfacial frictional resistance is a function of the soil–fiber contact area, with greater contact levels providing a higher resistance to bear the external loads. Consequently, this amending mechanism can be ascribed to the fiber content, meaning that the greater the number of included fiber units, i.e., increase in fiber content, the greater the contact levels achieved between the soil particles

and fibers, and thus the higher the generated interfacial frictional resistance against UC loading. The second amending mechanism, the mechanical interlocking of soil particles and fibers, is achieved during sample preparation/compaction, and induces the composite's adhesion by immobilizing the soil particles undergoing shearing. Quite clearly, the more effective/pronounced the achieved mechanical interlocking the higher the permanence against UC loading. Consequently, this amending mechanism is in line with the fiber content, and more importantly the fiber's elongated form factor. In general, the greater the number of included fiber units, i.e., increase in fiber content, the greater the number of interlocked or enwrapped soil aggregates, and thus the higher the developed peak UC strength. It should be noted that the soil–fiber amending mechanisms, as described above, only hold provided that the fiber units do not cluster (or adhere to each other) during mixture preparation and compaction [22,54,56,73]. At high fiber contents, the behavior of the composite, at some points, may be governed by a dominant fiber-to-fiber interaction; this effect, commonly referred to as fiber-clustering, leads to a notable improvement in the sample's ductility/deformability and toughness (see Figures 6 and 8) while offsetting the desired soil-to-fiber interaction capable of improving the sample's peak UC strength and stiffness. Fiber-clustering effects were evident for all samples containing 1.5% JF, as the previously-improved peak UC strength and stiffness manifested a notable decrease compared with similar mix designs containing 1% JF (see Figures 5 and 7).

Calcium-based binders, in this case GBFS, initiate a series of short- and long-term chemical reactions in the soil–water medium, which alter the soil fabric into a unitary mass of improved mechanical performance. Short-term chemical reactions consist of cation exchange and flocculation–agglomeration; their amending roles are often negligible when paired with neutrally-charged soil particles such as gravels, sands and silts. For fine-grained soils containing a notable fraction of negatively-charged clay particles, however, short-term reactions lead to significant improvements in the soil's plasticity/workability, early-age strength, swelling potential and consolidation capacity [33,74–76]. During short-term reactions, higher-valence cations substitute those of lower valence, and cations of larger ionic radius replace smaller cations of the same valence; the order of substitution follows the Hofmeister (or Lyotropic) series, i.e., $Na^+ < K^+ << Mg^{2+} < Ca^{2+}$ [77]. GBFS-treatment supplies the clay–water medium with additional calcium cations (Ca^{2+}), which immediately substitute cations of lower valence (e.g., sodium Na^+) and/or same-valence cations of smaller ionic radius (e.g., magnesium Mg^{2+}) in the vicinity of the clay particles. These cation exchanges lead to a decrease in the thickness of the Diffused Double Layers (DDLs), owing to the development of strong van der Waals bonds between adjacent clay particles in the matrix, which in turn promote aggregation and flocculation of the clay particles [76,78,79]. Long-term chemical reactions, commonly referred to as pozzolanic reactions, are strongly time- and often temperature-dependent, meaning that their commencement and evolution require a certain and often long period of curing. During pozzolanic reactions, ionized calcium (Ca^{2+}) and hydroxide (OH^-) units, released from the water–binder complex, gradually react with silicate (SiO_2) and aluminate (Al_2O_3) units in the soil, thereby leading to the formation of strong cementation products/gels, namely Calcium–Silicate–Hydrates (CSH), Calcium–Aluminate–Hydrates (CAH) and Calcium–Aluminate–Silicate–Hydrates (CASH); these products encourage further solidification and flocculation of the soil particles, which in turn accommodate the development of a dense, uniform matrix coupled with enhanced strength performance [31,33,76,79]. It should be noted that the short- and long-term amending reactions, as described above, are generally in favor of a higher binder content; this general perception also complies with the results outlined in Figures 5, 7 and 8.

The microstructure analysis was carried out using an SEM characterization scheme developed by Soltani et al. [58]. Figure 10a–d illustrate SEM micrographs for the samples $F_0S_0T_0$ (natural soil), $F_{1.0}S_0T_0$, $F_0S_6T_{28}$ and $F_{1.0}S_6T_{28}$, respectively. The microstructure of the natural soil sample manifested a partly-dense, non-uniform matrix, accompanied by a notable number of large inter- and intra-assemblage pore-spaces, respectively, formed between and within the soil aggregates; such morphological features warrant the existence of an edge-to-edge dispersed fabric (see Figure 10a). The microstructure of the JF-reinforced sample or $F_{1.0}S_0T_0$ exhibited a partly-dense but more uniform

matrix, accompanied by a limited number of small intra-assemblage pore-spaces mainly distributed along the soil–fiber connection interface. In essence, the fiber units acted as physical anchors within the matrix, interlocking the neighboring soil aggregates and hence withstanding compressive stresses during shearing (see Figure 10b). As a result of GBFS-treatment (see sample $F_0S_6T_{28}$ in Figure 10c), the microstructure became even more uniform in nature, indicating aggregation and flocculation of the soil particles and hence the development of a fully-dense matrix with a dominant edge-to-face flocculated fabric. Prevalent cementation products were clearly visible between and within the soil aggregates, which portrayed a major role in eliminating the inter- and intra-assemblage pore-spaces in the matrix. As a result of JF-reinforcement and GBFS-treatment (see sample $F_{1.0}S_6T_{28}$ in Figure 10d), the soil–fiber connection interface was markedly improved, as evident with the presence of fully-clothed fibers strongly embedded between and within the soil aggregates, which in turn led to a further improvement in the composite's strength and stiffness.

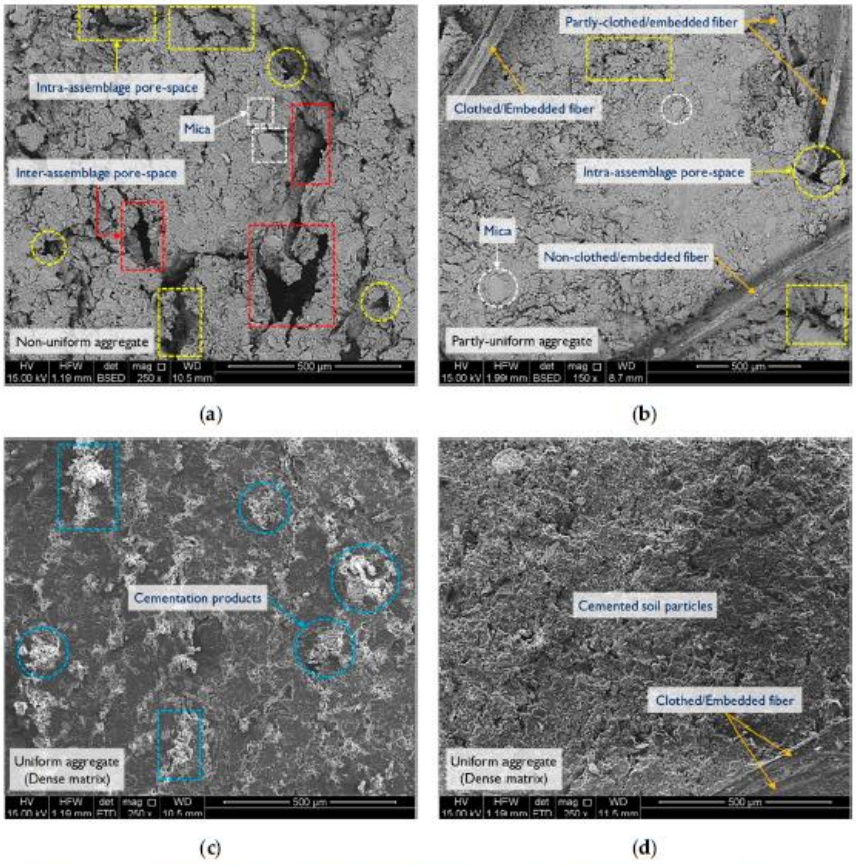

Figure 10. SEM micrographs for the tested samples: (**a**) $F_0S_0T_0$ (natural soil); (**b**) $F_{1.0}S_0T_0$; (**c**) $F_0S_6T_{28}$; and (**d**) $F_{1.0}S_6T_{28}$.

5. Modeling

5.1. Model Development

For a given type of soil reinforced with JF and/or treated with GBFS, the independent variables governing the peak UC strength q_u (in kPa), as evident with the experimental results discussed in Section 4, can be categorized as: **(i)** JF content F_c (in %); **(ii)** GBFS content S_c (in %); and **(iii)** curing time T_c (in days). Therefore, the peak UC strength problem for various JF + GBFS blends can be expressed as:

$$q_u = f(F_c, S_c, T_c) \tag{6}$$

where f = an unknown functional expression which is to be obtained through trial and error.

A suitable regression model can be characterized as one that maintains a perfect balance between simplicity, i.e., ease of application, and accuracy, i.e., acceptable goodness of fit and low forecast error. As such, any suggested functional expression for f should involve a simple algebraic structure, constructed by a minimal number of model/fitting parameters (or regression coefficients), capable of arriving at a reliable estimate of the problem at hand [50,80]. The multivariable quadratic function, as demonstrated in Equation (7) for the JF + GBFS peak UC strength problem, often serves as a suitable starting point to initiate the trial and error stage, and thus identify statistically-meaningful functional components capable of constructing a regression model which is both simple in structure and accurate in terms of predictive capacity [43,55,59,81].

$$q_u = \beta_0 + \beta_1 F_c + \beta_2 S_c + \beta_3 T_c + \beta_4 {F_c}^2 + \beta_5 {S_c}^2 + \beta_6 {T_c}^2 + \beta_7 F_c S_c + \beta_8 F_c T_c + \beta_9 S_c T_c \tag{7}$$

where β_0 to β_9 = model/fitting parameters (or regression coefficients); and β_0 = peak UC strength of the natural soil, since setting $F_c = 0$, $S_c = 0$ and $T_c = 0$ leads to $q_u = \beta_0$.

The model proposed in Equation (7) was fitted to the experimental peak UC strength data (presented in Figure 5) by means of the least-squares optimization technique. Routine statistical tests, namely Fisher's F–test and Student's t–test, were then carried out to examine the model's statistical significance. In addition, statistical fit-measure indices, such as the coefficient of determination R^2 (dimensionless), the root-mean-squared error RMSE (in kPa), the normalized root-mean-squared error NRMSE (in %) and the mean-absolute-percentage error MAPE (in %), were adopted to assess the model's predictive capacity [82,83]:

$$\text{RMSE} = \sqrt{\frac{1}{N}\sum_{b=1}^{N}\left[\left({q_u}^A\right)_b - \left({q_u}^P\right)_b\right]^2} \tag{8}$$

$$(\%)\ \text{NRMSE} = \frac{\text{RMSE}}{\left({q_u}^A\right)_{max} - \left({q_u}^A\right)_{min}} \times 100 \tag{9}$$

$$(\%)\ \text{MAPE} = \frac{1}{N}\sum_{b=1}^{N}\left|1 - \frac{\left({q_u}^P\right)_b}{\left({q_u}^A\right)_b}\right| \times 100 \tag{10}$$

where ${q_u}^A$ = actual peak UC strength, as presented in Figure 5; ${q_u}^P$ = predicted peak UC strength; b = index of summation; and N = number of experimental data points used for model development ($N = 28$, as outlined in Table 5).

The regression analysis outputs with respect to Equation (7) are summarized in Table 6. The high R^2 (=0.964) and low RMSE (=17.28 kPa), NRMSE (=4.78%) or MAPE (=6.19%) values warrant a strong agreement between actual and predicted peak UC strength data. The R^2 index merely surpassed 0.95, thus indicating that leastwise 95% of the variations in experimental observations are captured and further explained by the proposed regression model. The NRMSE index was found to be slightly less than 5%, thus signifying a maximum offset of 5% associated with the predictions. However,

the *P*-value associated with some of the regression components, namely S_c, T_c, ${S_c}^2$, ${T_c}^2$ and F_cT_c, was found to be greater than 5%, implying that these components are statistically-insignificant and hence make no or little contribution towards the predictions. Statistically-insignificant terms can be eliminated to accommodate the derivation of a simplified model with unanimously-significant regression components [59]. As such, Equation (7) can be simplified as:

$$q_u = \beta_0 + \beta_1 F_c + \beta_4 {F_c}^2 + \beta_7 F_c S_c + \beta_9 S_c T_c \quad (11)$$

Table 6. Summary of the regression analysis outputs with respect to Equation (7).

Fit-Measure Indices

R [1]	R^2	Adjusted R^2	RMSE (kPa)	NRMSE (%)	MAPE (%)
0.982	0.964	0.946	17.28	4.78	6.19

[1] Coefficient of correlation.

Analysis of Variance (ANOVA)

Source of Variation	DF [1]	SS [2]	MS [3]	*F*-Value	Significance *F*
Regression	9	2.20×10^5	2.44×10^4	52.62	4.26×10^{-11} < 5% (S)
Residual	18	8.36×10^3	4.64×10^2		
Total	27	2.28×10^5			

[1] Degree of freedom; [2] Sum of squares; [3] Mean squares; and (S) = Significant.

Regression Outputs

Variable	Coefficient	SE [1]	*t*-Value	*p*-Value
Intercept	$\beta_0 = 64.75$	16.19	4.00	8.42×10^{-4} < 5% (S)
F_c	$\beta_1 = 171.31$	28.76	5.96	1.23×10^{-5} < 5% (S)
S_c	$\beta_2 = 2.43$	13.06	0.19	8.55×10^{-1} > 5% (NS)
T_c	$\beta_3 = 1.48$	6.68	0.22	8.27×10^{-1} > 5% (NS)
${F_c}^2$	$\beta_4 = -85.99$	16.29	−5.28	5.10×10^{-5} < 5% (S)
${S_c}^2$	$\beta_5 = 0.26$	1.04	0.25	8.02×10^{-1} > 5% (NS)
${T_c}^2$	$\beta_6 = -0.04$	0.20	−0.22	8.31×10^{-1} > 5% (NS)
$F_c \times S_c$	$\beta_7 = 6.65$	2.53	2.63	1.70×10^{-2} < 5% (S)
$F_c \times T_c$	$\beta_8 = -0.17$	0.68	−0.25	8.09×10^{-1} > 5% (NS)
$S_c \times T_c$	$\beta_9 = 0.61$	0.17	3.55	2.28×10^{-3} < 5% (S)

[1] Standard error; (S) = Significant; and (NS) = Not Significant.

The regression analysis outputs with respect to Equation (11) are summarized in Table 7. The simplified model proposed in Equation (11) resulted in R^2 = 0.951, RMSE = 20.00 kPa, NRMSE = 5.54% and MAPE = 7.28%, which are on par with that observed for Equation (7). In essence, Equation (11) suggests a more practical path towards predicting the peak UC strength while maintaining a performance similar to that offered by the more complex Equation (7). Moreover, the *p*-values associated with all of the regression components were unanimously less than 5% (see Regression Outputs in Table 7), thus corroborating their statistical significance (and contribution) towards the predictions. Figure 11 illustrates the variations of predicted, by Equation (11), against actual peak UC strength data, along with the corresponding 95% prediction bands/intervals, for various JF + GBFS blends. Despite the existence of some scatter, all data points cluster around the line of equality and firmly position themselves between the 95% upper and 95% lower prediction bands, thereby indicating no particular outliers associated with the predictions. The proposed regression model given in Equation (11) contains a total of four fitting parameters, i.e., β_1, β_4, β_7 and β_9 (β_0 is equal to the peak UC strength of the natural soil), all of which can be calibrated by little experimental effort, as well as simple explicit calculations, and hence implemented for preliminary design assessments, predictive purposes and/or JF + GBFS optimization studies. Assuming that the peak UC strength of

the natural soil (or β_0) is at hand, the four fitting parameters can be adequately calibrated by a total of four UC tests carried out on four arbitrary JF + GBFS mix designs.

Table 7. Summary of the regression analysis outputs with respect to Equation (11).

Fit-Measure Indices

R [1]	R^2	Adjusted R^2	RMSE (kPa)	NRMSE (%)	MAPE (%)
0.976	0.951	0.943	20.00	5.54	7.28

[1] Coefficient of correlation.

Analysis of Variance (ANOVA)

Source of Variation	DF [1]	SS [2]	MS [3]	*F*-Value	Significance *F*
Regression	4	2.17×10^5	5.43×10^4	111.49	1.04×10^{-14} < 5% (S)
Residual	23	1.12×10^4	4.87×10^2		
Total	27	2.28×10^5			

[1] Degree of freedom; [2] Sum of squares; [3] Mean squares; and (S) = Significant.

Regression Outputs

Variable	Coefficient	SE [1]	*t*-Value	*p*-Value
Intercept	$\beta_0 = 89.14$	9.70	9.19	3.69×10^{-9} < 5% (S)
F_c (%)	$\beta_1 = 148.90$	27.51	5.41	1.69×10^{-5} < 5% (S)
F_c [2]	$\beta_4 = -85.99$	16.68	−5.16	3.17×10^{-5} < 5% (S)
$F_c \times S_c$	$\beta_7 = 10.52$	1.69	6.22	2.40×10^{-6} < 5% (S)
$S_c \times T_c$	$\beta_9 = 0.65$	0.06	11.08	1.07×10^{-10} < 5% (S)

[1] Standard error; and (S) = Significant.

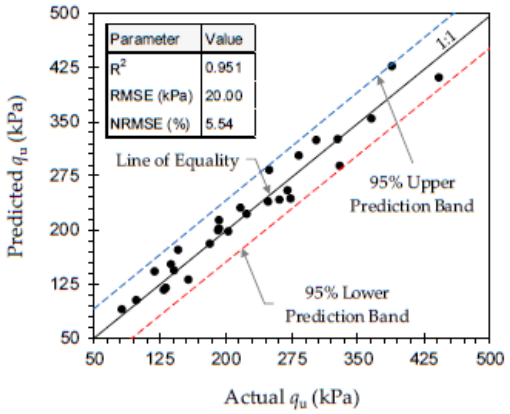

Figure 11. Variations of predicted, by Equation (11), against actual peak UC strength data for various JF + GBFS blends.

5.2. Sensitivity Analysis

The partial derivative sensitivity analysis technique, as commonly adopted in the literature [43,82,84], was carried out on Equation (11) to quantify the relative impacts of the independent variables, namely F_c, S_c and T_c, on the dependent variable q_u. The overall relative impact, both positive and negative, of an independent variable, i.e., $x_a = F_c$, S_c or T_c, on the dependent variable q_u, commonly referred to as sensitivity, can be defined as:

$$S(x_a) = \frac{\sigma(x_a)}{N\sigma(q_u)} \times \sum_{b=1}^{N} |D_{ab}| \ni D_a = \frac{dq_u}{dx_a} \tag{12}$$

where D_a = partial derivative of q_u or Equation (11) with respect to $x_a = F_c$, S_c or T_c; $\sigma(x_a)$ = standard deviation of x_a data; $\sigma(q_u)$ = standard deviation of predicted q_u data; b = index of summation; and N = number of observations ($N = 28$, as outlined in Table 5).

The partial derivative term, $D_a = dq_u/dx_a$ in Equation (12), measures the likelihood of q_u increasing or decreasing as a result of an increase in x_a. As such, the likelihood of increase or decrease in q_u as a result of an increase in x_a can be, respectively, defined as:

$$(\%)\ P_P(x_a) = \frac{M_P(x_a)}{N} \times 100 \tag{13}$$

$$(\%)\ P_N(x_a) = \frac{M_N(x_a)}{N} \times 100 \tag{14}$$

where $M_P(x_a)$ = number of observations where $D_a \geq 0$; and $M_N(x_a)$ = number of observations where $D_a < 0$.

The positive and negative impacts of an independent variable, i.e., $x_a = F_c$, S_c or T_c, on the dependent variable q_u can be, respectively, defined as:

$$\forall x_a \ni D_a \geq 0\ ,\ S_P(x_a) = \frac{\sigma(x_a)}{N\sigma(q_u)} \times \sum_{b=1}^{N} |D_{ab}| \ \ni\ D_a = \frac{dq_u}{dx_a} \tag{15}$$

$$\forall x_a \ni D_a < 0\ ,\ S_N(x_a) = \frac{\sigma(x_a)}{N\sigma(q_u)} \times \sum_{b=1}^{N} |D_{ab}| \ \ni\ D_a = \frac{dq_u}{dx_a} \tag{16}$$

It should be noted that $S_P(x_a)$ and $S_N(x_a)$ are, respectively, positive and negative fractions of the sensitivity parameter, $S(x_a)$ or Equation (12), meaning that for any given x_a, $S(x_a) = S_P(x_a) + S_N(x_a)$.

The principal objective of any introduced soil stabilization scheme is to accommodate an increase in the peak UC strength, and as such, the variations of the positive-sensitivity parameter, $S_P(x_a)$ or Equation (15), is of interest for further analysis. The positive-sensitivity parameter can be expressed in terms of percentage to facilitate a more practical comparison between the independent variables [84]:

$$(\%)\ F_P(x_a) = \frac{S_P(x_a)}{\sum_{a=1}^{K} S_P(x_a)} \times 100 \tag{17}$$

where $F_P(x_a)$ = positive contribution offered by an increase in x_a resulting in an increase in q_u (in %); and K = number of independent variables ($K = 3$, namely F_c, S_c and T_c).

The sensitivity analysis results with respect to Equation (11) are summarized in Table 8. The likelihood of increase in the peak UC strength as a result of an increase in JF content was found to be 71%, thus indicating that JF-reinforcement, where $0.5\% \leq F_c \leq 1.5\%$, exhibits favorable improvements only up to a particular/optimum fiber content, beyond of which marginal improvements or adverse effects, owing to fiber-clustering, can be expected (see the discussions in Section 4.3). As for GBFS content and curing time, the likelihood of increase was found to be 100% for both variables, thus indicting that GBFS-treatment, where $3\% \leq S_c \leq 9\%$, consistently leads to favorable improvements which can be further enhanced by means of curing. The positive contribution offered by an increase in JF content resulting in an increase in the peak UC strength was obtained as 35%. For GBFS content and curing time, however, the positive contribution was found to be 38% and 27%, respectively. These results imply that for a given JF + GBFS blend without curing, F_c and S_c would theoretically portray an equally-significant role towards strength development. With curing, however, the overall contribution

offered by GBFS-treatment profoundly outweighs that of JF-reinforcement, as $F_P(S_c) + F_P(T_c) = 65\% >> F_P(F_c) = 35\%$.

Table 8. Summary of the sensitivity analysis results with respect to Equation (11).

Variable, x_a	$D_a = dq_u/dx_a$	$S(x_a)$	$P_P(x_a)$ (%)	$P_N(x_a)$ (%)	$S_P(x_a)$	$S_N(x_a)$	$F_P(x_a)$ (%)
JF content, F_c	$\beta_1 + 2\beta_4 F_c + \beta_7 S_c$	0.639	71	29	0.548	0.090	35
GBFS content, S_c	$\beta_7 F_c + \beta_9 T_c$	0.605	100	0	0.605	0	38
Curing time, T_c	$\beta_9 S_c$	0.427	100	0	0.427	0	27

6. Conclusions

The following conclusions can be drawn from this study:

- For any given GBFS content and curing time, the greater the JF content the higher the developed strength and stiffness up to F_c = 1%; beyond 1% JF, the effect of JF-reinforcement adversely influenced the development of strength and stiffness. The composite's ductility and toughness, however, were consistently in favor of JF-reinforcement, meaning that the greater the JF content the higher the developed ductility and toughness.
- For any given JF content, the greater the GBFS content and/or the longer the curing period, the higher the developed strength, stiffness and toughness, following monotonically-increasing trends. The composite's ductility, however, was adversely influenced by GBFS-treatment, meaning that the greater the GBFS content and/or the longer the curing period, the lower the developed ductility.
- The addition of GBFS to JF-reinforced samples improved the soil–fiber connection interface or bonding, as the fiber units became fully embedded between and within the soil aggregates; this in turn led to a further improvement in the composite's strength and stiffness. The ASTM D4609–08 strength criterion was used to assess the efficiency and hence applicability of the proposed JF + GBFS mix designs. In this regard, the sample $F_{1.0}S_9T_{28}$ managed to satisfy ASTM's criterion and hence can be taken as the optimum design choice.
- A non-linear, multivariable regression model was developed to quantify the peak UC strength q_u as a function of the composite's basic index properties, i.e., JF content F_c, GBFS content S_c, and curing time T_c. The predictive capacity of the suggested model was examined and further validated by statistical techniques. A sensitivity analysis was also carried out to quantify the relative impacts of the independent regression variables, namely F_c, S_c and T_c, on the dependent variable q_u. The proposed regression model contained a limited number of fitting parameters, all of which can be calibrated by little experimental effort, as well as simple explicit calculations, and hence implemented for preliminary design assessments, predictive purposes and/or JF + GBFS optimization studies.

Author Contributions: Conceptualization, J.Z., A.D. and M.B.J.; Methodology, J.Z., A.S. and A.D.; Validation, J.Z. and A.S.; Formal analysis, J.Z. and A.S.; Investigation, J.Z.; Writing—original draft preparation, J.Z. and A.S.; Writing—review and editing, A.D. and M.B.J.; Visualization, A.S.; Supervision, A.D. and M.B.J.; Project administration, A.D. and M.B.J.; Funding acquisition, A.D. and M.B.J.

Acknowledgments: This research was made possible through the provision of an Australian Government Research Training Program Scholarship; this support is gratefully acknowledged.

Conflicts of Interest: The authors declare no conflict of interest.

References

1. Wei, J.; Kong, F.; Liu, J.; Chen, Z.; Kanungo, D.P.; Lan, X.; Jiang, C.; Shi, X. Effect of sisal fiber and polyurethane admixture on the strength and mechanical behavior of sand. *Polymers* **2018**, *10*, 1121. [CrossRef]
2. Yin, C.; Zhang, W.; Jiang, X.; Huang, Z. Effects of initial water content on microstructure and mechanical properties of lean clay soil stabilized by compound calcium-based stabilizer. *Materials* **2018**, *11*, 1933. [CrossRef] [PubMed]

3. Harvey, J.C. *Geology for Geotechnical Engineers*, 1st ed.; Cambridge University Press: Cambridge, Cambridgeshire, UK, 1982; ISBN 9780521288620.
4. Galán, E.; Ferrell, R.E. Genesis of clay minerals. *Dev. Clay Sci.* **2013**, *5*, 83–126. [CrossRef]
5. Frempong, E.M. Geotechnical properties of some residual micaceous soils in the Kumasi Metropolitan area (Ghana). *Bull. Int. Assoc. Eng. Geol.* **1994**, *49*, 47–54. [CrossRef]
6. Fleet, M.E. *Rock-Forming Minerals. Volume 3A, Micas*, 2nd ed.; The Geological Society of London: London, UK, 2003; pp. 1–40, 178–180, 512–515. ISBN 1862391424.
7. Weinert, H.H. *The Natural Road Construction Materials of Southern Africa*, 1st ed.; H&R Academica: Cape Town, Western Cape, South Africa, 1980; ISBN 0860740470.
8. Harris, W.G.; Parker, J.C.; Zelazny, L.W. Effects of mica content on engineering properties of sand. *Soil Sci. Soc. Am. J.* **1984**, *48*, 501–505. [CrossRef]
9. Gilboy, G. The compressibility of sand–mica mixtures. *Proc. Am. Soc. Civ. Eng.* **1928**, *54*, 555–568.
10. Tubey, L.W. *A Laboratory Investigation to Determine the Effect of Mica on the Properties of Soils and Stabilized Soils, Research Note 4077*; Road Research Laboratory (RRL): Wokingham, Berkshire, UK, 1961.
11. McCarthy, D.F., Jr.; Leonard, R.J. Compaction and compression characteristics of micaceous fine sands and silts. In *Highway Research Record 22*; Transportation Research Board: Washington, DC, USA, 1963; pp. 23–37. Available online: http://onlinepubs.trb.org/Onlinepubs/hrr/1963/22/22-003.pdf (accessed on 8 January 2019).
12. Tubey, L.W.; Bulman, J.N. Micaceous soils: Methods of determining mica content and the use of routine tests in the evaluation of such soils. *Proc. Aust. Road Res. Board (ARRB)* **1964**, *2*, 880–901.
13. Moore, C.A. Effect of mica on K_0 compressibility of two soils. *J. Soil Mech. Found. Div.* **1971**, *97*, 1275–1291.
14. Tubey, L.W.; Webster, D.C. *The Effects of Mica on the Roadmaking Properties of Materials, Supplementary Report 408*; Transport and Road Research Laboratory (TRL): Crowthorne, Berkshire, UK, 1978; ISBN 03051315.
15. Hight, D.W.; Georgiannou, V.N.; Martin, P.L.; Mundegar, A.K. Flow slides in micaceous sand. In *Problematic Soils: Proceedings of the International Symposium on Problematic Soils, IS-Tōhoku '98, Sendai, Japan, 28–30 October*; Yanagisawa, E., Moroto, N., Mitachi, T., Eds.; A.A. Balkema: Rotterdam, South Holland, The Netherlands, 1998; Volume 1, pp. 945–960. ISBN 9054109971.
16. Lee, J.S.; Guimaraes, M.; Santamarina, J.C. Micaceous sands: Microscale mechanisms and macroscale response. *J. Geotech. Geoenviron. Eng.* **2007**, *133*, 1136–1143. [CrossRef]
17. Ekblad, J.; Isacsson, U. Influence of water and mica content on resilient properties of coarse granular materials. *Int. J. Pavement Eng.* **2008**, *9*, 215–227. [CrossRef]
18. Schmidt, K. Effects of mica content on cyclic resistance of poorly-graded sand. In *Geotechnical Earthquake Engineering and Soil Dynamics IV, GSP 181*; Zeng, D., Manzari, M.T., Hiltunen, D.R., Eds.; ASCE: Sacramento, CA, USA, 2008; pp. 1–8. ISBN 9780784409756.
19. Cabalar, A.F.; Cevik, A. Triaxial behavior of sand–mica mixtures using genetic programming. *Expert Syst. Appl.* **2011**, *38*, 10358–10367. [CrossRef]
20. Seethalakshmi, P.; Sachan, A. Effect of successive impact loading on compactability, microstructure, and compressibility behavior of micaceous sand. *Transp. Infrastruct. Geotechnol.* **2018**, *5*, 114–128. [CrossRef]
21. Seethalakshmi, P.; Sachan, A. Effect of mica content on pore pressure and stress-strain response of micaceous sand using energy dissipation and different failure mechanisms. *Int. J. Geotech. Eng.* **2018**. [CrossRef]
22. Soltani, A.; Taheri, A.; Deng, A.; Nikraz, H. Tyre rubber and expansive soils: Two hazards, one solution. *Proc. Inst. Civ. Eng. Constr. Mater.* **2019**. [CrossRef]
23. Estabragh, A.R.; Naseh, M.; Beytolahpour, I.; Javadi, A.A. Strength of a clay soil and soil–cement mixture with resin. *Proc. Inst. Civ. Eng. Gr. Improv.* **2013**, *166*, 108–114. [CrossRef]
24. Winterkorn, H.F.; Pamukcu, S. Soil stabilization and grouting. In *Foundation Engineering Handbook*, 2nd ed.; Fang, H.Y., Ed.; Springer: Boston, MA, USA, 1991; pp. 317–378. ISBN 9781461539285.
25. Miller, G.A.; Azad, S. Influence of soil type on stabilization with cement kiln dust. *Constr. Build. Mater.* **2000**, *14*, 89–97. [CrossRef]
26. Mirzababaei, M.; Yasrobi, S.S.; Al-Rawas, A.A. Effect of polymers on swelling potential of expansive soils. *Proc. Inst. Civ. Eng. Gr. Improv.* **2009**, *162*, 111–119. [CrossRef]
27. Estabragh, A.R.; Pereshkafti, M.R.S.; Parsaei, B.; Javadi, A.A. Stabilised expansive soil behaviour during wetting and drying. *Int. J. Pavement Eng.* **2013**, *14*, 418–427. [CrossRef]

28. Onyejekwe, S.; Ghataora, G.S. Soil stabilization using proprietary liquid chemical stabilizers: Sulphonated oil and a polymer. *Bull. Eng. Geol. Environ.* **2015**, *74*, 651–665. [CrossRef]
29. Alazigha, D.P.; Indraratna, B.; Vinod, J.S.; Ezeajugh, L.E. The swelling behaviour of lignosulfonate-treated expansive soil. *Proc. Inst. Civ. Eng. Gr. Improv.* **2016**, *169*, 182–193. [CrossRef]
30. Keramatikerman, M.; Chegenizadeh, A.; Nikraz, H. Effect of GGBFS and lime binders on the engineering properties of clay. *Appl. Clay Sci.* **2016**, *132–133*, 722–730. [CrossRef]
31. Sharma, A.K.; Sivapullaiah, P.V. Ground granulated blast furnace slag amended fly ash as an expansive soil stabilizer. *Soils Found.* **2016**, *56*, 205–212. [CrossRef]
32. Vakili, M.V.; Chegenizadeh, A.; Nikraz, H.; Keramatikerman, M. Investigation on shear strength of stabilised clay using cement, sodium silicate and slag. *Appl. Clay Sci.* **2016**, *124–125*, 243–251. [CrossRef]
33. Soltani, A.; Taheri, A.; Khatibi, M.; Estabragh, A.R. Swelling potential of a stabilized expansive soil: A comparative experimental study. *Geotech. Geol. Eng.* **2017**, *35*, 1717–1744. [CrossRef]
34. Soltani, A.; Deng, A.; Taheri, A.; Mirzababaei, M. A sulphonated oil for stabilisation of expansive soils. *Int. J. Pavement Eng.* **2017**. [CrossRef]
35. Phanikumar, B.R.; Nagaraju, T.V. Engineering behaviour of expansive clays blended with cement and GGBS. *Proc. Inst. Civ. Eng. Gr. Improv.* **2018**, *171*, 167–173. [CrossRef]
36. Sekhar, D.C.; Nayak, S. Utilization of granulated blast furnace slag and cement in the manufacture of compressed stabilized earth blocks. *Constr. Build. Mater.* **2018**, *166*, 531–536. [CrossRef]
37. Zhao, Y.; Soltani, A.; Taheri, A.; Karakus, M.; Deng, A. Application of slag–cement and fly ash for strength development in cemented paste backfills. *Minerals* **2019**, *9*, 22. [CrossRef]
38. Kim, Y.T.; Kim, H.J.; Lee, G.H. Mechanical behavior of lightweight soil reinforced with waste fishing net. *Geotext. Geomembr.* **2008**, *26*, 512–518. [CrossRef]
39. Sivakumar Babu, G.L.; Vasudevan, A.K. Strength and stiffness response of coir fiber-reinforced tropical soil. *J. Mater. Civ. Eng.* **2008**, *20*, 571–577. [CrossRef]
40. Tang, C.S.; Shi, B.; Zhao, L.Z. Interfacial shear strength of fiber reinforced soil. *Geotext. Geomembr.* **2010**, *28*, 54–62. [CrossRef]
41. Mirzababaei, M.; Miraftab, M.; Mohamed, M.; McMahon, P. Unconfined compression strength of reinforced clays with carpet waste fibers. *J. Geotech. Geoenviron. Eng.* **2013**, *139*, 483–493. [CrossRef]
42. Qu, J.; Li, C.; Liu, B.; Chen, X.; Li, M.; Yao, Z. Effect of random inclusion of wheat straw fibers on shear strength characteristics of Shanghai cohesive soil. *Geotech. Geol. Eng.* **2013**, *31*, 511–518. [CrossRef]
43. Estabragh, A.R.; Soltani, A.; Javadi, A.A. Models for predicting the seepage velocity and seepage force in a fiber reinforced silty soil. *Comput. Geotech.* **2016**, *75*, 174–181. [CrossRef]
44. Qu, J.; Zhao, D. Stabilising the cohesive soil with palm fibre sheath strip. *Road Mater. Pavement Des.* **2016**, *17*, 87–103. [CrossRef]
45. Wang, Y.X.; Guo, P.P.; Ren, W.X.; Yuan, B.X.; Yuan, H.P.; Zhao, Y.L.; Shan, S.B.; Cao, P. Laboratory investigation on strength characteristics of expansive soil treated with jute fiber reinforcement. *Int. J. Geomech.* **2017**, *17*, 04017101:1–04017101:12. [CrossRef]
46. Mirzababaei, M.; Arulrajah, A.; Horpibulsuk, S.; Aldavad, M. Shear strength of a fibre-reinforced clay at large shear displacement when subjected to different stress histories. *Geotext. Geomembr.* **2017**, *45*, 422–429. [CrossRef]
47. Mirzababaei, M.; Arulrajah, A.; Haque, A.; Nimbalkar, S.; Mohajerani, A. Effect of fiber reinforcement on shear strength and void ratio of soft clay. *Geosynth. Int.* **2018**, *25*, 471–480. [CrossRef]
48. Soltani, A.; Deng, A.; Taheri, A. Swell–compression characteristics of a fiber–reinforced expansive soil. *Geotext. Geomembr.* **2018**, *46*, 183–189. [CrossRef]
49. Soltani, A.; Deng, A.; Taheri, A.; Sridharan, A. Swell–shrink–consolidation behavior of rubber–reinforced expansive soils. *Geotech. Test. J.* **2018**. [CrossRef]
50. Soltani, A.; Deng, A.; Taheri, A.; Mirzababaei, M.; Nikraz, H. Interfacial shear strength of rubber-reinforced clays: A dimensional analysis perspective. *Geosynth. Int.* **2019**. [CrossRef]
51. Tang, C.S.; Shi, B.; Gao, W.; Chen, F.; Cai, Y. Strength and mechanical behavior of short polypropylene fiber reinforced and cement stabilized clayey soil. *Geotext. Geomembr.* **2007**, *25*, 194–202. [CrossRef]
52. Arpitha, G.R.; Sanjay, M.R.; Senthamaraikannan, P.; Barile, C.; Yogesha, B. Hybridization effect of sisal/glass/epoxy/filler based woven fabric reinforced composites. *Exp. Tech.* **2017**, *41*, 577–584. [CrossRef]

53. Olgun, M. The effects and optimization of additives for expansive clays under freeze–thaw conditions. *Cold Reg. Sci. Technol.* **2013**, *93*, 36–46. [CrossRef]
54. Estabragh, A.R.; Ranjbari, S.; Javadi, A.A. Properties of clay soil and soil cement reinforced with polypropylene fibers. *ACI Mater. J.* **2017**, *114*, 195–205. [CrossRef]
55. Shahbazi, M.; Rowshanzamir, M.; Abtahi, S.M.; Hejazi, S.M. Optimization of carpet waste fibers and steel slag particles to reinforce expansive soil using response surface methodology. *Appl. Clay Sci.* **2017**, *142*, 185–192. [CrossRef]
56. Yadav, J.S.; Tiwari, S.K. Effect of waste rubber fibres on the geotechnical properties of clay stabilized with cement. *Appl. Clay Sci.* **2017**, *149*, 97–110. [CrossRef]
57. Mirzababaei, M.; Arulrajah, A.; Horpibulsuk, S.; Soltani, A.; Khayat, N. Stabilization of soft clay using short fibers and poly vinyl alcohol. *Geotext. Geomembr.* **2018**, *46*, 646–655. [CrossRef]
58. Soltani, A.; Deng, A.; Taheri, A.; Mirzababaei, M. Rubber powder–polymer combined stabilization of South Australian expansive soils. *Geosynth. Int.* **2018**, *25*, 304–321. [CrossRef]
59. Tran, K.Q.; Satomi, T.; Takahashi, H. Improvement of mechanical behavior of cemented soil reinforced with waste cornsilk fibers. *Constr. Build. Mater.* **2018**, *178*, 204–210. [CrossRef]
60. Soltani, A.; Deng, A.; Taheri, A.; Sridharan, A. Consistency limits and compaction characteristics of clay soils containing rubber waste. *Proc. Inst. Civ. Eng. Geotech. Eng.* **2018**. [CrossRef]
61. Frempong, E.M. A comparative assessment of sand and lime stabilization of residual micaceous compressible soils for road construction. *Geotech. Geol. Eng.* **1995**, *13*, 181–198. [CrossRef]
62. Mshali, M.R.; Visser, A.T. Influence of mica on unconfined compressive strength of a cement-treated weathered granite gravel. *J. S. Afr. Inst. Civ. Eng.* **2012**, *54*, 71–77.
63. Mshali, M.R.; Visser, A.T. Influence of Mica on Compactability and Moisture Content of Cement–Treated Weathered Granite Gravel. In *Proceedings of the 33rd Southern African Transport Conference (SATC 2014)*; Minister of Transport, South Africa: Pretoria, Gauteng, South Africa, 2014; pp. 546–555. ISBN 9781920017613.
64. Ballantine, R.W.; Rossouw, A.J. *Stabilization of Soils*; PPC Lime Ltd.: Pretoria, Gauteng, South Africa, 1989; pp. 25–27, 42–51.
65. Sridharan, A.; Nagaraj, H.B. Compressibility behaviour of remoulded, fine-grained soils and correlation with index properties. *Can. Geotech. J.* **2000**, *37*, 712–722. [CrossRef]
66. Gowthaman, S.; Nakashima, K.; Kawasaki, S. A state-of-the-art review on soil reinforcement technology using natural plant fiber materials: Past findings, present trends and future directions. *Materials* **2018**, *11*, 553. [CrossRef] [PubMed]
67. Kosmatka, S.H.; Kerkhoff, B.; Panarese, W.C. Portland, blended, and other hydraulic cements. In *Design and Control of Concrete Mixtures, Engineering Bulletin 001*, 14th ed.; Portland Cement Association: Skokie, IL, USA, 2002; pp. 21–56. ISBN 0893122173.
68. Estabragh, A.R.; Javadi, A.A. Critical state for overconsolidated unsaturated silty soil. *Can. Geotech. J.* **2008**, *45*, 408–420. [CrossRef]
69. Ang, E.C.; Loehr, J.E. Specimen size effects for fiber-reinforced silty clay in unconfined compression. *Geotech. Test. J.* **2003**, *26*, 191–200. [CrossRef]
70. Park, S.S. Unconfined compressive strength and ductility of fiber-reinforced cemented sand. *Constr. Build. Mater.* **2011**, *25*, 1134–1138. [CrossRef]
71. Radovic, M.; Lara-Curzio, E.; Riester, L. Comparison of different experimental techniques for determination of elastic properties of solids. *Mater. Sci. Eng. A* **2004**, *368*, 56–70. [CrossRef]
72. Maher, M.H.; Ho, Y.C. Mechanical properties of kaolinite/fiber soil composite. *J. Geotech. Eng.* **1994**, *120*, 1381–1393. [CrossRef]
73. Prabakar, J.; Sridhar, R.S. Effect of random inclusion of sisal fibre on strength behaviour of soil. *Constr. Build. Mater.* **2002**, *16*, 123–131. [CrossRef]
74. Locat, J.; Bérubé, M.A.; Choquette, M. Laboratory investigations on the lime stabilization of sensitive clays: Shear strength development. *Can. Geotech. J.* **1990**, *27*, 294–304. [CrossRef]
75. Sivapullaiah, P.V.; Prashanth, J.P.; Sridharan, A. Effect of fly ash on the index properties of black cotton soil. *Soils Found.* **1996**, *36*, 97–103. [CrossRef]
76. Mallela, J.; Von Quintus, H.; Smith, K.L. *Consideration of Lime-Stabilized Layers in Mechanistic-Empirical Pavement Design*; The National Lime Association: Arlington, VA, USA, 2004; Available online: http://lime.org/documents/other/MechEmpPavement.pdf (accessed on 8 January 2019).

77. Grim, R.E. *Clay Mineralogy*, 1st ed.; McGraw-Hill: New York, NY, USA, 1953; pp. 126–155.
78. Little, D.L. *Fundamentals of the Stabilization of Soil with Lime, Bulletin 332*; The National Lime Association: Arlington, VA, USA, 1987.
79. Firoozi, A.A.; Olgun, C.G.; Firoozi, A.A.; Baghini, M.S. Fundamentals of soil stabilization. *Int. J. Geo-Eng.* **2017**, *8*, 1–16. [CrossRef]
80. Soltani, A.; Mirzababaei, M. Discussion on "Effects of lime addition on geotechnical properties of sedimentary soil in Curitiba, Brazil" [J Rock Mech Geotech Eng 10 (2018) 188–194]. *J. Rock Mech. Geotech. Eng.* **2018**. [CrossRef]
81. Soltani, A.; Mirzababaei, M. Comment on "Compaction and strength behavior of tire crumbles–fly ash mixed with clay" by A. Priyadarshee, A. Kumar, D. Gupta, and P. Pushkarna. *J. Mater. Civ. Eng.* **2018**. accepted.
82. Soltani, A.; Estabragh, A.R.; Taheri, A.; Deng, A.; Meegoda, J.N. Experiments and dimensional analysis of contaminated clay soils. *Environ. Geotech.* **2018**. [CrossRef]
83. Wu, Y.F.; Jiang, C. Quantification of bond-slip relationship for externally bonded FRP-to-concrete joints. *J. Compos. Constr.* **2013**, *17*, 673–686. [CrossRef]
84. Soltani, A. Discussion of "Optimization of carpet waste fibers and steel slag particles to reinforce expansive soil using response surface methodology" by M. Shahbazi, M. Rowshanzamir, S.M. Abtahi, S.M. Hejazi [Appl. Clay Sci., doi:10.1016/j.clay.2016.11.027]. *Appl. Clay Sci.* **2017**. [CrossRef]

Chapter 4

Mechanical Behavior of Micaceous Clays stabilized by Lime, Slag-lime with Fibers

Jiahe Zhang [1,*] , An Deng [2] , Mark B. Jaksa [3]

[1] **PhD Student** — School of Civil, Environmental and Mining Engineering, The University of Adelaide, Adelaide SA 5005, Australia | **Email:** Jiahe.Zhang@adelaide.edu.au

[2] **Senior Lecturer** — School of Civil, Environmental and Mining Engineering, The University of Adelaide, Adelaide SA 5005, Australia | **Email:** An.Deng@adelaide.edu.au ; **ORCID:** 0000-0002-3897-9803

[3] **Professor** — School of Civil, Environmental and Mining Engineering, The University of Adelaide, Adelaide SA 5005, Australia | **Email:** Mark.Jaksa@adelaide.edu.au

* Corresponding Author.

Zhang J, Deng A and Jaksa M **(2019)** Mechanical behavior of micaceous soils stabilized by lime and slag-lime with fibers. x(x):x-x, http://doi.org/x[3]

Abstract

Micaceous soils are considered to be a class of problematic soils due to its low strength and weak ductility, which has been shown to cause severe damage to highways and other engineering infrastructure. The present study focuses on the investigation of the combined capacity of jute fibers with lime or slag-lime as sustainable solutions to improve the mechanical behavior of micaceous soils. A total of 53 groups of soils were prepared at various fiber proportions (0.5%, 1.0% and 1.5%), lime content (3%, 6% and 9%), and slag-lime (3%, 6% and 9%), and unconfined compressive tests were carried out after 7 and 28 days curing. The test results indicated that the unconfined compressive strength and stiffness were increased with

[3] Unpublished and unsubmitted work written in a manuscript style

the addition of up to 1% fiber, beyond which the strength decreased, while the toughness and ductility of the composite were consistently improved by the inclusion of fibers. The addition of chemical binders, i.e. lime or slag-lime, had a significantly positive influence on strength and stiffness of the fiber-reinforced soils, and the improvement depended on the fiber and chemical binder proportions and the extent of curing. Though the improvement of strength was significant, the trend was dominated by the inclusion of the fibers; that is, the threshold of strength improvement was considered to be 1% of fibers, with further inclusion leading to an adverse effect on strength.

Keywords: Micaceous clay; jute fibers; hydrated lime; slag-lime; unconfined compression; strength; stiffness

4.1. Introduction

Mica is a mineral widely occurring in igneous, sedimentary and certain metamorphic rocks (Harvey 1982; Galán and Ferrell 2013). The mineral exhibits a unique platy structure and high elasticity and, if weathered from the parent rocks, affects the mechanical behavior of soils which include mica. Micaceous soils are widely distributed around the world, especially in some countries, such as South Africa (Paige-Green and Semmelink 2002), Malawi (Netterberg et al. 2011), Nigeria (Gogo 1984) and the U.K. (Northmore 1996). Owing to its soft, spongy fabric properties, micaceous soils may deform significantly at stress levels typically associated with soils, thereby affecting the bulk compressibility (Moore 1971; Harries et al. 1984). Given the platy nature of mica and clay particles, they tend to rotate and orient themselves, during compression or shearing, in a somewhat parallel fashion, resulting in low strength resistance (Harris et al. 1984). Low strength, high compressibility and poor compactibility of micaceous soils are significant issues for road subgrades, building foundations, earth dams and embankments, as well as other engineering applications. To meet the design requirements of such infrastructure, stabilization of micaceous soils, aiming to improve the mechanical properties, is explored.

Chemical stabilization involves the mixing of cementitious agents with soils, causing a chemical reaction with the water-soil system. Chemical additives such as cement, lime, fly ash, and other chemical compounds have been used in soil stabilization for decades with varying degrees of success (Ingles and Metcalf 1972; Al-Rawas et al. 2002; Sharma and Sivapullaiah 2016). Mechanical stabilization, on the other hand, involves reinforcing the soil with natural or synthetic fibers or similar for improving the mechanical behavior of soils. The traditional methods of mechanical stabilization consist of placing inclusions such as strips, bars, grids or geotextiles within the soils and the inclusions are usually oriented in a preferred direction or layers. The distribution of fibers can also be random and discrete, which seeks to reduce the presence of potential planes of weakness that can develop parallel to the oriented reinforcement (Maher and Gray 1990).

The purpose of this study is to investigate different chemical cementitious binders and their combined influence with natural fibers in the stabilization of the inferior engineering characteristics of micaceous soils. The additives investigated include lime and slag-lime, with

fibers. Lime has been widely used for decades in relation to roadways, railways, foundation layers and others (Wilkinson et al. 2010). The addition of lime to clay soils can facilitate cementitious reactions, resulting in the significant improvement of strength and stiffness (Bell 1996; Rajasekaran and Narasimha Rao 2000; Consoli et al. 2011). The cementation is mainly attributed to pozzolanic reactions and can increase the long-term performance of the stabilized soils (Rogers et al. 2006; Khattab et al. 2007). Introducing slag into the lime-clay hydration reaction can undoubtedly modify the original reaction process. The lime will provide the required alkaline environment for slag activation and hydration, forming crystalline cementitious products, which accelerates the bridging effect between the slag-lime and clay particles (James et al. 2008). Previous research has reported that the combination of these two materials can be more beneficial when used as stabilization agents than using them individually, resulting in significant improvement in soil strength (Kamon and Nontananandh 1991; Wild et al. 1998; Rajasekaran 2005). Moreover, utilizing the slag, not only improves problematic soils in a cost-efficient and environmentally-friendly manner, but also mitigates disposal burdens caused by the industrial waste material. The improvement from adopting the chemical technique alone is significant, but it generally results in the brittle behavior of the treated soils (Wang et al. 2003; Basha et al. 2005). Incorporating fibers within soils is another effective technique for enhancing soil strength, as the use of random discrete fibers mimics the presence of plant roots which contributes to the stability of the soil. More importantly, fiber-reinforced soils exhibit greater toughness and ductility, and offer a relatively higher level of residual strength (Tang et al. 2007). As no studies on the joint activation of chemical additives and fibers as stabilizing agents for micaceous clays have been published to date, this study can potentially achieve the optimal benefits for stabilizing problematic micaceous soils. This study seeks to investigate the effectiveness of lime, slag-lime as well as those combined with fibers in relation to the stabilization of micaceous soils. The influence of binders on unconfined compressive strength, ductility and stiffness are examined in order to evaluate the performance of the treated soils.

4.2. Materials

4.2.1. Micaceous clay

This investigation was carried out on artificially mixed micaceous soil containing 80% kaolinite and 20% ground mica, both of which were sourced from local distributors. The choice of 20% of mica was selected to form the micaceous clays, as it represents the upper boundary

prerequisite to simulate the low strength and high compressibility exhibited by natural micaceous clays (Tubey 1961; McCarthy and Leonard 1963). The artificial soil–mica blends manifested the same typical texture, sheen and friability properties as the natural micaceous soils commonly reported in the literature, and thus provide a basis for relevant comparison. The physical and mechanical properties of the artificial micaceous clay were determined as per relevant ASTM and Australian standards, as summarized in Table **1**. The liquid limit and plasticity index were, respectively, measured as 48.7% and 36.9%, from which the soil was characterized as a *silt with intermediate plasticity* (MI) in accordance with the Unified Soil Classification System (USCS). Furthermore, the standard Proctor optimum water content and maximum dry density were obtained as 23.5% and 1.56 g/cm^3, respectively.

4.2.2. Jute fibers

The mechanical binder used in this study were jute fibers, which were manufactured from *Corchorus capsularis* (a shrub sprcies in the Malvaceae family). This type of fiber consists of 56–71% cellulose, 29–35% hemicellulose and 11–14% lignin, as commonly reported in the literature (Gowthaman et al. 2018). The jute fibers have a highly rough surface texture, which likely promotes adhesion and induces frictional resistance between the fibers and soils. The diameter of the fibers is typically 30–40 μm, and the length was cut into segments of approximately 15 mm. Detailed physical and mechanical properties are summarized in **Table 2**.

4.2.3. Cementitious binders

Commercially-available hydrated lime and slag-lime, sourced from the local distributors, were used as the cementitious binders in this study. The chemical characteristics of two binders are provided in **Table 3**. From the table, it can be seen that both lime and slag-lime have appreciable amounts of ionized calcium (Ca^{2+}), which facilitates the occurence of time-dependent pozzolanic reactions (James et al. 2008).

4.3. Overview of Experimentation

4.3.1. Sample preparation

The samples were prepared to attain the target and consistent values of dry density and water content. To achieve this, for the artificial micaceous soils, the standard compaction test was carried out according to ASTM D698-12. Sample were then expected, within the experimental

errors, to be of the same density and water content for all the mix designs. All the samples were prepared by the static compaction technique for the unconfined compressive (UC) strength tests. The mixes were designated using the convention of $F_xB_yT_z$, where $F_x = x$% fiber, with x = 0.5, 1.0 and 1.5; $B_y = y$% chemical binders, with $B = L$ for lime or SL for slag-lime, and y = 3, 6 and 9; and T_z is the sample curing time. The untreated artificial micaceous soils were denoted as $MF_0B_0T_0$. For example, $F_{0.5}SL_6T_{28}$ represents the natural soil mixed with 0.5% fiber and 6% slag-lime with 28 days of curing time. Table **4** summarizes the details of the different soil mixtures adopted in the study.

In the preparation of all soil mixtures, if fibers were solely used to reinforce the micaceous soils, the desired fiber content was added manually and incrementally to the soil, ensuring that all of the fibers were evenly distributed in order to achieve uniform mixtures. The corresponding optimum water contents were subsequently added to the mixtures. If the lime or slag-lime was used alone, the required volume of water was added to the soil prior to the addition of binders, enabling effective hydration of these chemical binders. If both chemical and mechanical binders were used, the inclusions were added in the order of fibers, water and the chemical binders. All of the mix designs were prepared manually, and care was taken to prepare homogenous mixtures at each stage. After compaction, the samples were wrapped with plastic film and then placed in a curing chamber for 7 or 28 days until tested.

4.3.2. Unconfined compression test

Unconfined compressive (UC) tests were carried out on the soil mixtures in accordance with ASTM D2166–16. The prepared samples, measuring 50 mm in diameter and 100 mm in height, were axially compressed at a constant displacement rate of 1 mm/min, as commonly adopted by Ang (2003). Axial strains and the corresponding axial stresses were recorded at regular time intervals until the maximum axial stress required for sample failure, and its corresponding axial strain, were achieved. To ensure the accuracy of the UC tests, triplicate samples were tested for typical samples, i.e., F_0T_0, $F_{1.5}T_0$, $F_{0.5}L_6T_7$, $F_{1.5}L_3T_{28}$, $F_{1.0}SL_9T_7$, $F_{1.5}SL_3T_{28}$. In this regard, the standard deviation (SD) and the coefficient of variation (CV) for the triplicate UC strength values were found to be in the range between SD = 4.82 kPa and 13.39 kPa, and CV = 4.15% and 6.07%. These low values corroborate the repeatability of the adopted sample preparation technique, as well as the implemented UC testing procedure.

4.4. Results and Discussion

4.4.1. Effect of fibers on UC strength

To examine the effect of fibers on the strength of micaceous soils, a series of UC strength tests were carried out on samples of micaceous soils. The samples were prepared at ρ_{dmax} =1.56 g/m^3, and ω_{opt}=23.52%, as shown in Table 1. The fiber contents were 0.5%, 1.0% and 1.5%.

Stress-strain curves for the fiber-reinforced soils obtained from the UC tests are provided in Figure 1. For the untreated artificial micaceous soil, the stress-strain locus exhibited a strain-softening behavior, and thus a more dramatic failure after reaching peak strength. Due to the fiber inclusion, the soils showed a more ductile behavior and a greater residual strength than the untreated micaceous soils. Interestingly, the soils reached their largest peak strength at a fiber content of 1.0% and slightly decreased in strength with the inclusion of 1.5% of fibers. The natural micaceous soil resulted in a peak UC strength of q_u = 82.7 kPa, while the inclusion of 0.5%, 1.0% and 1.5% of fiber yielded values of q_u = 118.0 kPa, 136.0 kPa, 127.4 kPa, respectively. Moreover, the strain at peak strength, ε_u, was also positively related to the fiber proportion, thereby suggesting the improvement in both the soil's strength and ductility when fibers were added to the micaceous soils. As a typical case, the untreated micaceous soil resulted in ε_u = 4.73%, while the inclusion of 1.5% fiber resulted in ε_u = 8.55%, which indicates a nearly two-fold improvement in the soil's ductility.

The results of the elastic stiffness modulus, E_{50}, defined as the secant modulus at 50% of the peak UC strength (Radovic et al. 2004; Iyengar et al. 2013), are shown in **Figure 2.** The variations of E_{50} follow a trend similar to that observed for q_u, with the increasing values of E_{50} up to 1.0% of fiber inclusion. All fiber-reinforced samples exhibited higher E_{50} values compared to that of the untreated micaceous soil, indicating the improvement of material stiffness as the result of fiber inclusion. The untreated micaceous soil resulted in E_{50} = 2.27 MPa, while the inclusion of 0.5%, 1.0% and 1.5% fibers resulted in E_{50} = 3.35, 3.70 and 3.67 MPa, respectively. The area under a typical UC stress-strain curve up to the failure point or (ε_u, q_u) is defined as the strain energy at peak (or energy adsorption capacity). The strain energy serves as a measure of the material's toughness (Maher and Ho 1994; Mirzababaei et al. 2013). The variation of E_u, as shown in Figure 2, exhibits an increasing tendency with respect to fiber inclusion, and this trend is different to the developments of strength and stiffness, as discussed above. Higher strain energy at peak values manifests an increase in either the axial failure strain

or the peak UC strength (or both). As a typical case, the untreated micaceous soil resulted in E_u = 2.36 kJ/m^3, while the inclusion of 1.0% fiber resulted in E_u = 6.11 kJ/m^3, which indicates almost a threefold improvement in the soil's energy adsorption capacity (or toughness).

4.4.2. Effect of fibers and lime on UC strength

A series of experiments was carried out on fiber-reinforced micaceous soils treated by two different cementitious binders, slag and slag-lime with a curing period of 7 and 28 days. **Figure 3(a)** shows the strengths of the combinations of fiber and lime reinforced soils from which it can be observed that the addition of lime significantly improves the strength of micaceous clays. Specifically, the untreated micaceous clay results in a q_u = 82.7 kPa, while the inclusion of 3% lime yields a q_u = 196.6 kPa after 7 days curing and q_u = 245.3 kPa after 28 days, improving the strength by 138% and 197% respectively. For a given amount of lime and fibers, the peak UC strength increases with a longer curing time. For example, for a lime content of 6%, the peak strength for 1.5% fiber inclusion is 348.7 kPa at Day 7 and 426.0 kPa at Day 28. At any given curing time and fiber content, the greater the lime content, the higher the peak UC strength. For example, the sample $F_{0.5}L_3T_7$ exhibited a peak UC strength of q_u = 226.7 kPa, while the inclusion of 6% and 9% of lime, at the same curing time of 7 days, resulted in q_u = 286.7 and 365.9 kPa, respectively. Similarly, for any given lime content and fiber content, the increase in curing time promotes a major increase in the UC strength for the mix designs. Moreover, the UC strength rose with increased fiber content up to 1% and then decreased with 1.5% fibers. For example, the UC strengths were 452.9 kPa for the no-fiber sample, 496.3 kPa for 0.5% fibers, 593.2 kPa for 1.0% fibers and 542.9 kPa for 1.5% fibers, where the lime content was 9% lime and the curing time was 28 days throughout. Therefore, 1% fiber inclusion is considered to be the optimum from the perspective of strength gain. The ASTM D4609-08 standard suggests that a minimum strength of 345 kPa improvement in any soils' peak UC strength is the criterion for an effective stabilization scheme. As demonstrated in **Figure 3(a)**, the samples $F_{0,\,0.5,\,1.0,\,1.5}L_9T_{28}$, $F_{1.0}L_9T_7$, $F_{1.0}L_6T_{28}$, and $F_{1.5}L_9T_7$ satisfy this strength criterion.

Figure 3(b) presents the variations of axial strain at peak strength, ε_u, against fiber content for different lime contents tested at 7 and 28 days. The axial strain at failure demonstrates a different trend to that of the peak UC strength. Specifically, the greater the lime content/curing time, the lower the sample's ductility. With the variation of fiber inclusions, the axial strain at peak strength did not fluctuate as markedly as was observed with UC strength. Instead, ε_u grew

with the increasing fiber content, indicating improvement in the soil's ductility with fiber inclusion.

The elastic stiffness modulus, E_{50}, was calculated and then compared against fiber content, as shown in **Figure 4(a)**. For a given fiber content, the value of E_{50} increased with the lime content and curing time, indicating an improvement in the material stiffness. Moreover, the variations on E_{50} at different fiber contents after 7 days curing is insignificant, while samples that were cured for 28 days resulted in much greater variations in E_{50}. Additionally, the soil treated with 9% lime showed a significant improvement in the stiffness at each fiber content, when compared with the soils treated with 3% or 6% lime. The samples $ML_3F_{0.5}T_{28}$, $ML_3F_{1.0}T_{28}$ and $ML_3F_{1.5}T_{28}$, resulted in E_{50} = 34.7, 52.5 and 88.6 MPa respectively.

Figure 4(b) illustrates the variations of peak strain energy, against fiber content for the untreated micaceous soils and various lime-treated soils tested after 7 and 28 days curing. For any given lime content and curing period, the greater the fiber content, the higher the peak strain energy. It should be noted that, at the lowest fiber content for a given curing time, the peak strain energy rises with increasing lime content, while at higher fiber contents (1.0% and 1.5%), 6% lime results in higher peak strain energies. For example, the samples $F_{1.5}L_3T_{28}$, $F_{1.5}L_6T_{28}$, $F_{1.5}L_9T_{28}$ resulted in peak strain energies of E_u = 11.3, 11.5 and 11.0 kJ/m^3, respectively.

4.4.3. Effect of fibers and slag-lime on UC strength

Figure 5(a) presents the relationship between the peak UC strength and fiber content after 7 and 28 days curing. As can be observed, slag-lime, as the chemical binder, significantly improves the strength of the soils. For example, the sample $F_{1.0}SL_6T_{28}$, exhibited the greatest q_u = 1,287.3 kPa, which is more than ten-times that of the untreated micaceous soils. At any given fiber content, the strength increases with higher slag-lime content/curing time, at a greater rate. Similarly, the inclusion of fibers promotes improvement in strength, however, an excessive fiber content (more than 1% fibers) will decrease soil strength.

The axial strain at failure was again obtained for various fiber-slag-lime mixtures, and the results are summarized in **Figure 5(b)**, for the samples tested after 7 and 28 days curing. Similar to the fiber with lime-treated samples, the greater the slag-lime content and the longer the curing time, the lower the material ductility. The results again demonstrated that the inclusion of fibers greatly reduces the brittleness of the chemically treated soils, thus improving the workability of such soils.

Figure 6(a) presents the variation of elastic stiffness modulus, E_{50}, against fiber content for the slag-lime treated soils tested after 7 and 28 days curing. Similarly, the variations in E_{50} follow a trend similar to that observed in fiber-lime treated soils, where the peak E_{50} occurs at a fiber content of 0.5%, and the value then gradually decreases with increasing fiber content. For example, the samples, $MF_{0,\ 0.5,1.0,1.5}SL_3T_{28}$ yielded UC strengths of 28.3, 75.1, 54.6 and 46.0 MPa, respectively. Figure **6(b)** shows the variations of peak strain energy against fiber content for the samples treated with slag-lime and tested at various curing periods. The improvement in toughness with respect to an increase in binder content and/or curing time can be attributed to an increase in the peak UC strength and/or the axial strain at failure. The rise in peak strain energy, which, as demonstrated in **Figure 4(b)**, was due to a greater fiber and slag-lime content and/or a shorter curing time, indicates that the improvement in q_u dominates the exhibited reduction in ε_u in the mix designs. The samples $F_{0.5}SL_3T_{28}$ and $F_{0.5}SL_9T_{28}$ resulted in peak strain energies of E_u = 6.6 and 8.2 kJ/m^3, respectively, increased to 9.3 and 11.0 kJ/m^3 for $F_{1.5}SL_3T_{28}$ and $F_{1.5}SL_9T_{28}$, and E_u = 8.3 and 8.6 kJ/m^3 for $F_{0.5}SL_3T_7$ and $F_{0.5}SL_9T_7$, respectively.

4.4.4. Discussion

It is observed that the presence of fibers promotes the UC strength of micaceous soils. This strength gain is influenced by the internal friction resistance between the soil particles and the fibers, which in turn, is a function of the soil-fiber contact area. Therefore, a greater number of fibers within the soil will lead to larger frictional resistance between the soil particles and the fibers, which results in increased UC strength. Moreover, as the study by Zhang et al. (2019) showed that, with respect to the amount of voids and cracks associated with micaceous soils, some fibers can bridge across these cracks and voids, and this leads to enhanced shear strength and toughness (Tang et. al 2007; Tang et. al 2010; Wang et. al 2017; Mirzababaei et. al 2018; Zhang et al. 2019). However, when the proportion of fibers within the soil is too great the fibers are not evenly distributed and are present in clumps. As a result the improvement in soil strength and toughness is modest or diminishes.

Calcium-based chemical binders, such as lime, initiates a chemical reaction, which is commonly referred to as pozzolanic reaction in the soil-water medium, which improves the strength and toughness of micaceous clays. During pozzolanic reactions, ionized calcium (Ca^{2+}) and hydroxide (OH^-) units, are released from the water-binder complex. These ions gradually react with the silicate (SiO_2), and aluminate (Al_2O_3) units in the soils, thereby forming a strong cementation gel of calcium-aluminate-silicate-hydrates (CASH), and in some cases calcium-

silicate-hydrates (CSH) and calcium-aluminate-hydrates (CAH). These products promote further solidification and flocculation of the particles, which accommodate the development of a dense, uniform matrix with strong performance (Mallela et al. 2004, Sharma and Sivapullaiah 2016; Firoozi et al. 2017). Owing to the time-dependent nature of pozzolanic reactions, the stabilization by lime is a long-term process, indicating the longer the curing time, the greater the improvement of the UC strength of soils. In addition, the formation of cementitious compounds in the soil matrix leads to an increase in the bonding and interlocking forces between the soil particles, due to the rough surface and high rigidity of the cementitious compounds, which further improves the strength and roughness of soils. Introducing slag into the clay-lime hydration reaction undoubtedly results in a systematic increase in strength when compared with lime-treated soils. This is indicated by the slag hydration, which is activated by the lime. Particularly, this is a more rapid reaction than the traditional lime-clay reactions discussed above. Moreover, lime will also provide the required alkaline environment for slag activation and hydration, forming crystalline cementitious products, which accelerates the bridging effect between slag-lime and clay particles (James et al. 2008). The inclusion of fibers further enhances the UC strength of cementitious binder-treated soils. This is because the effective contact areas of fibers and lime-treated or lime-slag treated soils are quite large due to the smaller pores in the cementitious binder-treated soils. Thus, the total effective friction between soils and fibers in the cementitious binder-treated soil is greater, resulting in the larger UC strength and stronger performance (Cai et al. 2006).

4.5. Conclusions

The effects of jute fiber, lime and slag-lime on the unconfined compressive strength of artificially created micaceous clays were studied. It is shown from the test results that the addition solely of fibers, or mixtures of fibers with lime or slag-lime, increased the unconfined compressive (UC) strength and stiffness of micaceous clays.

The inclusion of fibers can increase the UC strength of micaceous soils, and the greater the fiber proportion the higher the measured strength and stiffness. However, the largest peak strength was obtained at a fiber content of 1.0%, with a slight decrease when 1.5% fibers were included. At any given fiber proportion, the UC strength of the reinforced soil increased with the addition of lime or slag-lime, with the improvement being more significant with the inclusion of slag-lime. The greater the cementitious binders and/or the longer the curing time, the higher the

developed strength, stiffness and toughness. However, the ductility of the samples decreased with the cementitious binders and/or the longer curing period.

Stabilization by adding fibers and slag-lime has been shown to be the most effective method for improving the low strength and high brittleness of micaceous clays. This stabilization scheme has been shown to meet the ASTM strength requirements of 345.0 kPa. In fact, the majority of mix designs examined in this study satisfied the ASTM standard and were considered to be appropriate for the purposes of stabilization of micaceous clays.

Acknowledgments

This research was made possible through the provision of an Australian Government Research Training Program Scholarship; this support is gratefully acknowledged.

Conflicts of Interest

The authors wish to confirm that there are no known conflicts of interest associated with this publication, and there has been no significant financial support for this work that could have influenced its outcome.

References

Al-Rawas, A. A. (2002). Microfabric and mineralogical studies on the stabilization of an expansive soil using cement by-pass dust and some types of slags. *Canadian Geotechnical Journal*, *39*(5), 1150–1167. http://doi.org/10.1139/t02-046

Ang, E. C., & Erik Loehr, J. (2003). Specimen size effects for fiber-reinforced silty clay in unconfined compression. *Geotechnical Testing Journal*, *26*(2), 191–200.

Basha, E. A., Hashim, R., Mahmud, H. B., & Muntohar, A. S. (2005). Stabilization of residual soil with rice husk ash and cement. *Construction and Building Materials*, *19*(6), 448–453. http://doi.org/10.1016/j.conbuildmat.2004.08.001

Bell, F. G. (1996). Lime stabilization of clay minerals and soils. *Engineering Geology*, *42*, 223–237.

Cai, Y., Shi, B., Ng, C. W. W., & Tang, C. (2006). Effect of polypropylene fibre and lime admixture on engineering properties of clayey soil. *Engineering Geology*, *87*(3–4), 230–240. http://doi.org/10.1016/j.enggeo.2006.07.007

Consoli, N. C., Lopes, L. da S., Festugato, L., & Cruz, R. C. (2011). Variables Controlling Stiffness and Strength of Lime-Stabilized Soils. *Journal of Geotechnical and Geoenvironmental Engineering*, *137*(6), 628–632. http://doi.org/10.1061/(ASCE)GT

Firoozi, A. A., Guney Olgun, C., Firoozi, A. A., & Baghini, M. S. (2017). Fundamentals of soil stabilization. *International Journal of Geo-Engineering*, *8*(1). http://doi.org/10.1186/s40703-017-0064-9

Galán, E., & Ferrell, R. E. **(**2013**).** Chapter 3 – Genesis of clay minerals. *Developments in Clay Science*, 83–126. http://doi.org/10.1016/b978-0-08-098258-8.00003-1

Gogo, J. O. (1984). Compaction and strength characteristics of decomposed mica schist. *In: Proceedings of the 8th Regional Conference for Africa on Soil Mechanics and Foundation Engineering*. Harare, Zimbabwe, 275–284. ISBN:9061915325

Gowthaman, S., Nakashima, K., & Kawasaki, S. (2018). A state-of-the-art review on soil reinforcement technology using natural plant fiber materials: Past findings, present trends and future directions. *Materials*, *11*(4). http://doi.org/10.3390/ma11040553

Harris, W.G., Parker, J.C. & Zelazny L.W. (1984). Effects of mica content on engineering properties of sand. *Soil Science Society America Journal*. 48(3), 501–5. http://doi.org/10.2136/sssaj1984.03615995004800030006x

Harvey, J.C. (1982). Geology for Geotechnical Engineers (1st Ed). Cambridge, CambridgeshireEngland, UK: Cambridge University Press. ISBN:9780521288620

Ingles, O. G., & Metcalf, J. B. (1972). Soil stabilization : *principles and practice*. Sydney: Butterworths.

Iyengar, S.R., Masad, E., Rodriguez, A.K., Bazzi, H.S., Little, D. & Hanley, H.J.M. (2013) Pavement subgrade stabilization using polymers: Characterization and performance. *Journal of Materials in Civil Engineering* 25(4): 472–483, http://doi.org/10.1061/(asce)mt.1943-5533.0000612

James, R., Kamruzzaman, A. H. M., Haque, A., & Wilkinson, A. (2008). Behaviour of lime – slag-treated clay. *Proceedings of the Institution of Civil Engineers - Ground Improvement*, *161*(4), 207–216. http://doi.org/10.1680/grim.2008.161.4.207

Kamon, M., & Nontananandh, S. (1991). Combining Industrial Wastes with Lime for Soil Stabilization. *Journal of Geotechnical Engineering*, *117*(1), 1–17. http://doi.org/10.1061/(asce)0733-9410(1991)117:1(1)

Khattab, S. A., Al-Mukhtar, M., & Fleureau, J. M. (2007). Long-Term Stability Characteristics of a Lime-Treated. *Journal of Materials in Civil Engineering*, *19*(4), 358–366.

Maher, M. H., & Gray, D. H. (1990). Static Response of Sands Reinforced with Randomly Distributed Fibers. *Journal of Geotechnical Engineering*, *116*(11), 1661–1677.

Maher, M.H., & Ho, Y.C. (1994). Mechanical properties of kaolinite/fiber soil composite. *Journal of Geotechnical Engineering* 120(8): 1381–1393, http://doi.org/10.1061/(asce)0733-9410(1994)120:8(1381)

Mallela, J., Von Quintus, H., & Smith, K. L. (2004). *Consideration of lime-stabilized layers in mechanistic-empirical pavement design*. The National Lime Asscociation: Arlington, VA, USA.

Mirzababaei, M., Miraftab, M., Mohamed, M., & McMahon, P. (2013) Unconfined compression strength of reinforced clays with carpet waste fibers. *Journal of Geotechnical and Geoenvironmental Engineering* 139(3): 483–493, http://doi.org/10.1061/(asce)gt.1943-5606.0000792

Mirzababaei, M., Arulrajah, A., Haque, A., Nimbalkar, S., & Mohajerani, A. (2018). Effect of fiber reinforcement on shear strength and void ratio of soft clay. *Geosynthetics International*, *25*(4), 471–480. http://doi.org/10.1680/jgein.18.00023

McCarthy, D.F., & Jr. Leonard, R.J. (1963). Compaction and compression characteristics of micaceous fine sands and silts. *In Highway Research Record 22*; Transportation Research Board: Washington, DC, USA. 23–37

Moore C.A. (1971). Effect of mica on K0 compressibility of two soils. *Journal of the Soil Mechanics and Foundations Division* 97(SM9): 1275–1291.

Netterberg, F., Hefer, A., & Preez, H.D. (2011). Cracking and staining of an airport asphalt. *In: Proceedings of the 10th Conference on Asphalt Pavements for South Africa (CAPSA 11): Roads of the Future. KwaZulu KwaZulu–Natal*, South Africa: International Road Federation (IRF), 1–17.

Northmore, K.J., Bell, F.G., & Culshaw, M.G. (1996). The engineering properties and behaviour of the brickearth of south Essex. *Q J Eng Geol Hydrogeol*.; 29(2):147–61. http://doi.org/10.1144/gsl.qjegh.1996.029.p2.04

Paige-Green P, Semmelink CJ. (2002). Road compaction problems related to the presence of biotite. *In: Proceedings of the 9th Congress of the International Association of Engineering Geology and the Environment*. Durban, KwaZulu–Natal, South Africa, 2605–2610.

Radovic, M., Lara-Curzio, E., & Riester, L. (2004) Comparison of different experimental techniques for determination of elastic properties of solids. *Materials Science and Engineering: A* 368(1–2): 56–70, http://doi.org/10.1016/j.msea.2003.09.080.

Rajasekaran, G., & Narasimha Rao, S. (2000). Strength characteristics of lime-treated marine clay. *Proceedings of the Institution of Civil Engineers - Ground Improvement*, *4*(3), 127–136.

Rajasekaran, G. (2005). Sulphate attack and ettringite formation in the lime and cement stabilized marine clays. *Ocean Engineering*, *32*(8–9), 1133–1159. http://doi.org/10.1016/j.oceaneng.2004.08.012

Rogers, C. D. F., Boardman, D. I., & Papadimitriou, G. (2006). Stress Path Testing of Realistically Cured Lime and Lime / Cement Stabilized Clay. *Journal of Materials in Civil Engineering*, *18*(2), 259–266.

Sharma, A. K., & Sivapullaiah, P. V. (2016). Ground granulated blast furnace slag amended fly ash as an expansive soil stabilizer. *Soils and Foundations*, *56*(2), 205–212. http://doi.org/10.1016/j.sandf.2016.02.004

Tang, C., Shi, B., Gao, W., Chen, F., & Cai, Y. (2007). Strength and mechanical behavior of short polypropylene fiber reinforced and cement stabilized clayey soil. *Geotextiles and Geomembranes*, *25*(3), 194–202. http://doi.org/10.1016/j.geotexmem.2006.11.002

Tang, C. S., Shi, B., & Zhao, L. Z. (2010). Interfacial shear strength of fiber reinforced soil. *Geotextiles and Geomembranes*, *28*(1), 54–62. http://doi.org/10.1016/j.geotexmem.2009.10.001

Tubey, L.W. (1961). *A Laboratory Investigation to Determine the Effect of Mica on the Properties of Soils and Stabilized Soils*. Research Note 4077, Road Research Laboratory (RRL), Wokingham, Berkshire, UK.

Wang, Q., Chen, H.E., & Cai, K.Y. (2003). Quantitative evaluation of microstructure features of soil contained some cement. *Rock and Soil Mechanics* 24 (Sup. 1), 12–16.

Wild, S., Kinuthia, J. M., Jones, G. I., & Higgins, D. D. (1998). Effects of partial substitution of lime with ground granulated blast furnace slag (GGBS) on the strength properties of lime-stabilised sulphate-bearing clay soils. *Engineering Geology*, *51*(1), 37–53. http://doi.org/10.1016/s0013-7952(98)00039-8

Wilkinson, A., Haque, A., Kodikara, J., Adamson, J., & Christie, D. (2010). Improvement of Problematic Soils by Lime Slurry Pressure Injection: Case Study. *Journal of Geotechnical Engineering*, (10), 1459–1468.

Zhang, J., Soltani, A., Deng, A., & Jaksa, M. B. (2019). Mechanical Performance of Jute Fiber-Reinforced Micaceous Clay Composites Treated with Ground-Granulated Blast-Furnace Slag. *Materials*, *12*(4), 576:1-23. http://doi.org/10.3390/ma12040576

List of Tables

Table 1. Physical and mechanical properties of the used soil.

Table 2. The physical and chemical composition of jute fibers (as provided by the distributor).

Table 3. The chemical composition of hydrated lime and slag-lime (as provided by the distributor).

Table 4. Soil mixtures and associated notations

Table 1. Physical and mechanical properties of the used soil.

Properties	Value/Description	Standard designation
Specific gravity, G_{ss}	2.73	ASTM D854–14
Grain–size distribution		
Clay (< 2 μm) (%)	39	ASTM D422–07
Silt (2–75 μm) (%)	55	
Sand (0.075–4.75 mm) (%)	6	
Consistency limits and classification		
Liquid limit, w_L (%)	48.7	AS 1289.3.9.1–15
Plastic limit, w_P (%)	36.9	AS 1289.3.2.1–09
Plasticity index, I_P (%)	11.3	AS 1289.3.3.1–09
USCS classification	MI[†]	ASTM D2487–11
Compaction characteristics		
Optimum water content, w_{opt} (%)	23.5	ASTM D698–12
Maximum dry density, ρ_{dmax} (g/m^3)	1.56	

Note:
[†]silt with intermediate plasticity.

Table 2. The physical and chemical composition of jute fibers (as provided by the distributor).

Properties	**Value**
Physical/mechanical properties	
Fiber type	Single fiber
Specific gravity, G_s	1.30–1.46
Length, *FL* (mm)	15
Diameter, *FD* (μm)	30–40
Aspect ratio, *FAR* = *FL*/*FD*	375–500
Young's modulus (GPa)	10–30
Tensile strength (MPa)	400–900
Tensile elongation at break (%)	1.5–1.8

Table 3. The chemical composition of hydrated lime and slag-lime (as provided by the distributor).

Properties	Slag-lime	Lime
Chemical composition		
$Ca(OH)_2$ (%)	0.98	85–95
Na_2O (%)	–	–
MgO (%)	0.87	–
$Mg(OH)_2$ (%)	–	0.5–1.5
Al_2O_3 (%)	7.12	0–2
SiO_2 (%)	21.45	1–2
SO_3 (%)	0.05	–
CI (%)	0.06	–
K_2O (%)	1.01	–
Cao (%)	45.32	–
TiO_2 (%)	0.55	–
Cr_2O_3 (%)	0.14	–
MnO (%)	11.21	–
Fe_2O_3 (%)	10.67	0–0.7
CuO (%)	0.07	–
ZnO (%)	0.13	–
Ga_2O_3 (%)	0.004	–
Rb_2O (%)	0.005	–
SrO (%)	0.012	–
PbO (%)	0.02	–

Table 4. Soil mixtures and associated notations

Designation	Fiber content, F (%)	Lime content, L (%)	Designation	Fiber content, F (%)	Slag-lime content, SL (%)
Fiber-reinorced					
F_0T_0	0	-	-	-	-
$F_{0.5}T_0$	0.5	-	-	-	-
$F_{1.0}T_0$	1.0	-	-	-	-
$F_{1.5}T_0$	1.5	-	-	-	-
Lime, and lime + fiber-reinforced			**Slag-lime, and slag-lime + fiber-reinforced**		
$F_0L_3T_{7,28}$	0	3	$F_0SL_3T_{7,28}$	3	0
$F_0L_6T_{7,28}$	0	6	$F_0SL_6T_{7,28}$	6	0
$F_0L_9T_{7,28}$	0	9	$F_0SL_9T_{7,28}$	9	0
$F_{0.5}L_3T_{7,28}$	0.5	3	$F_{0.5}SL_3T_{7,28}$	3	0
$F_{0.5}L_6T_{7,28}$	0.5	6	$F_{0.5}SL_6T_{7,28}$	6	0
$F_{0.5}L_9T_{7,28}$	0.5	9	$F_{0.5}SL_9T_{7,28}$	9	0
$F_{1.0}L_3T_{7,28}$	1.0	3	$F_{1.0}SL_3T_{7,28}$	3	0
$F_{1.0}L_6T_{7,28}$	1.0	6	$F_{1.0}SL_6T_{7,28}$	6	0
$F_{1.0}L_9T_{7,28}$	1.0	9	$F_{1.0}SL_9T_{7,28}$	9	0
$F_{1.5}L_3T_{7,28}$	1.5	3	$F_{1.5}SL_3T_{7,28}$	3	0
$F_{1.5}L_6T_{7,28}$	1.5	6	$F_{1.5}SL_6T_{7,28}$	6	0
$F_{1.5}L_9T_{7,28}$	1.5	9	$F_{1.5}SL_9T_{7,28}$	9	0

List of Figures

Figure 1. UC stress-strain curves for the natural soil and fiber-reinforced samples

Figure 2. Elastic stiffness modulus E_{50} and strain energy E_u for the natural soil and fiber-reinforced samples

Figure 3. Variations in (a) Peak UC strength q_u and (b) axial strain at failure ε_u against fiber content for different lime contents after 7 and 28 days curing

Figure 4. Variation in (a) Elastic stiffness modulus E_{50} (b) Strain energy E_u against fiber content for the lime-treated soils after 7 and 28 days curing

Figure 5. Variations in (a) Peak UC strength q_u and (b) axial strain at failure ε_u against fiber content for different slag-lime content after 7 and 28 days curing

Figure 6. Variation in (a) Elastic stiffness modulus E_{50} (b) Strain energy E_u against fiber content for the slag-lime-treated soils after 7 and 28 days curing

Figure 1. UC stress-strain curves for the natural soil and fiber-reinforced samples

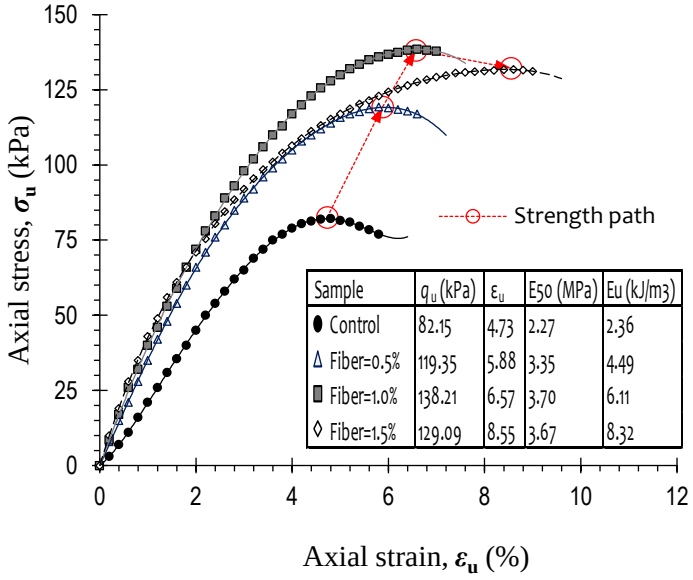

Figure 2. Elastic stiffness modulus E_{50} and strain energy E_u for the natural soil and fiber-reinforced samples

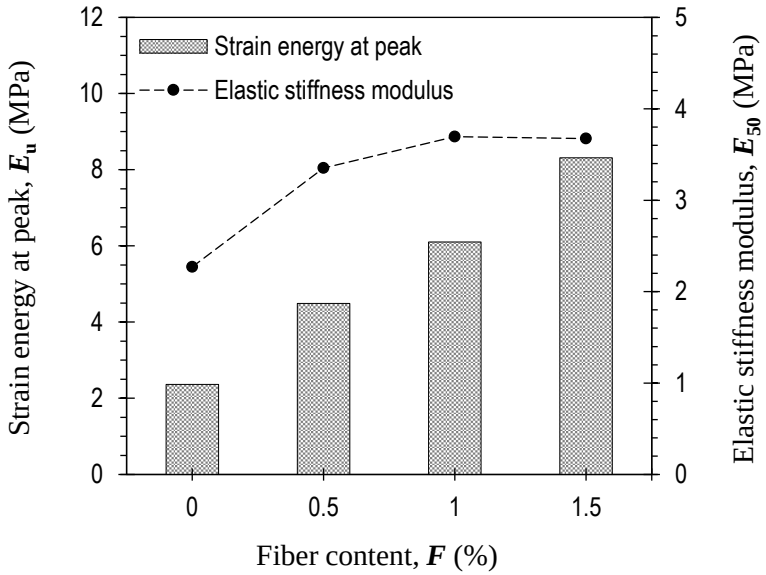

Figure 3. Variations in (a) Peak UC strength q_u and (b) axial strain at failure ε_u against fiber content for different lime contents after 7 and 28 days curing

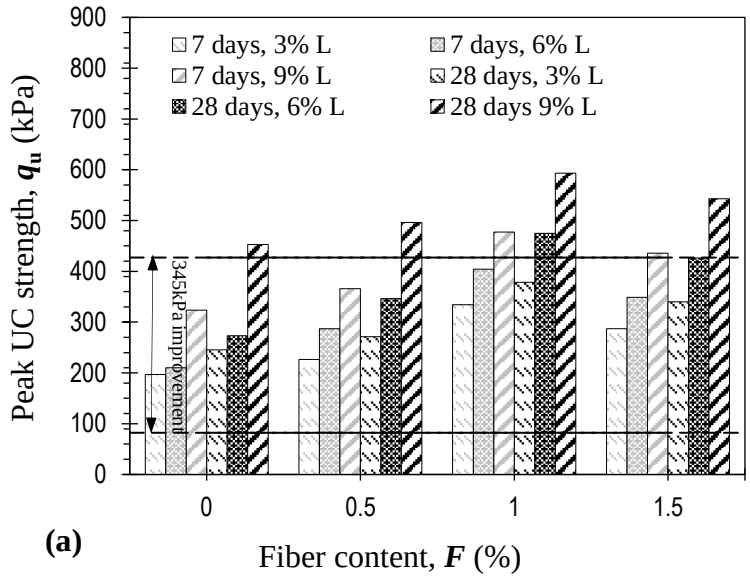

(a)

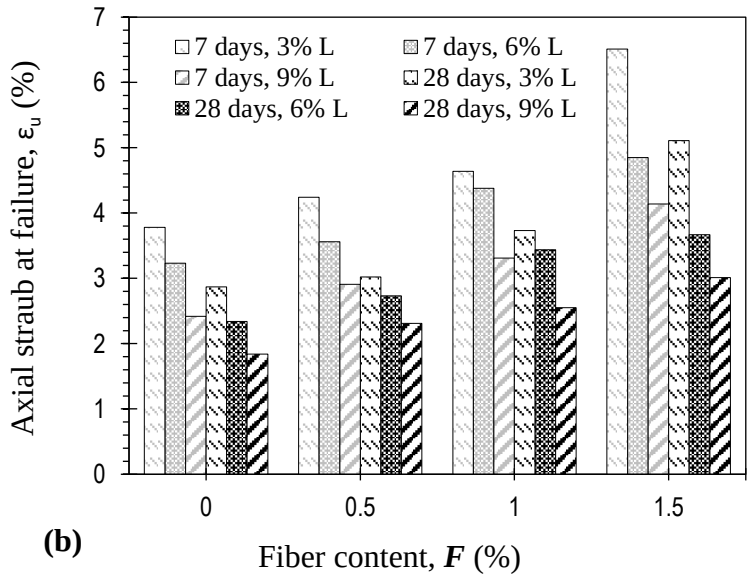

(b)

Figure 4. Variation in (a) Elastic stiffness modulus E_{50} (b) Strain energy E_u against fiber content for the lime-treated soils after 7 and 28 days curing

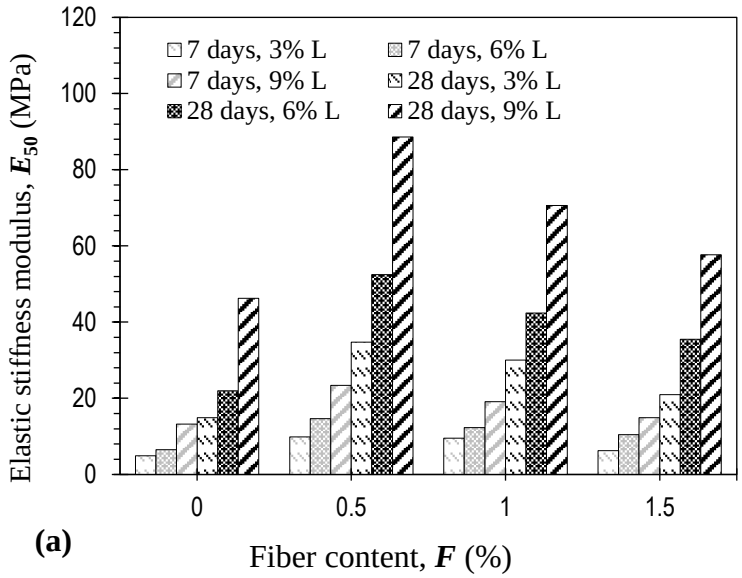

(a)

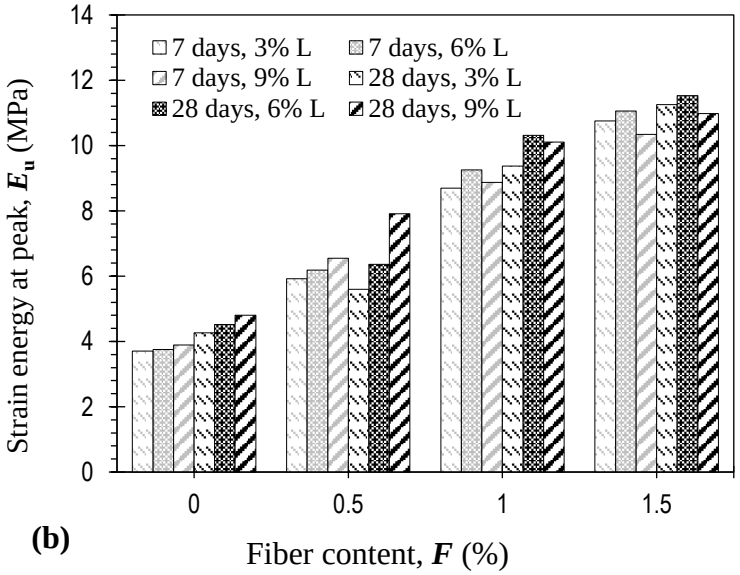

(b)

Figure 5. Variations in (a) Peak UC strength q_u and (b) axial strain at failure ε_u against fiber content for different slag-lime content after 7 and 28 days curing

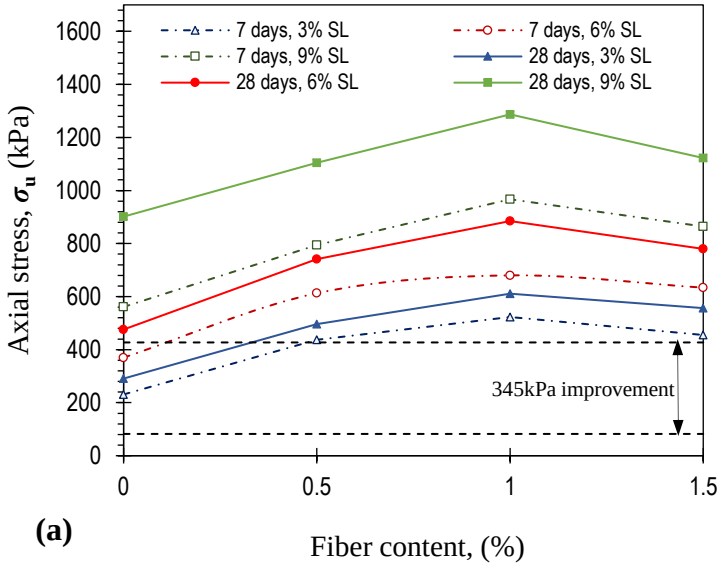

(a)

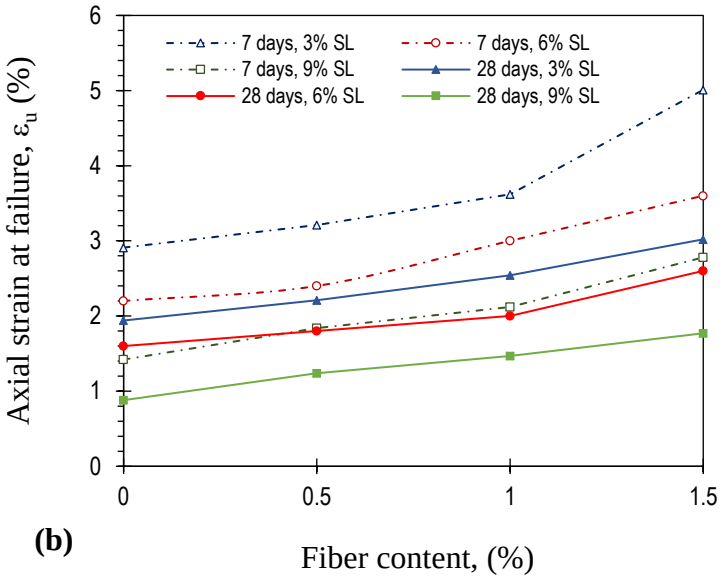

(b)

Figure 6. Variation in (a) Elastic stiffness modulus E_{50} (b) Strain energy E_u against fiber content for the slag-lime-treated soils after 7 and 28 days curing

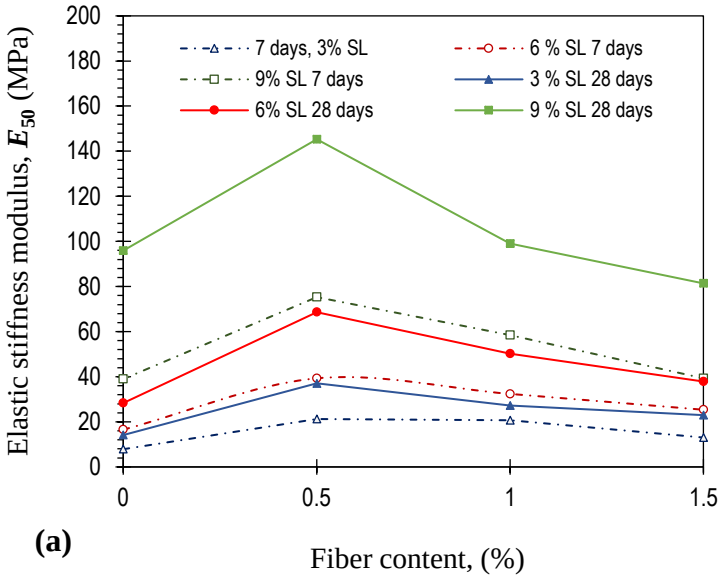

(a)

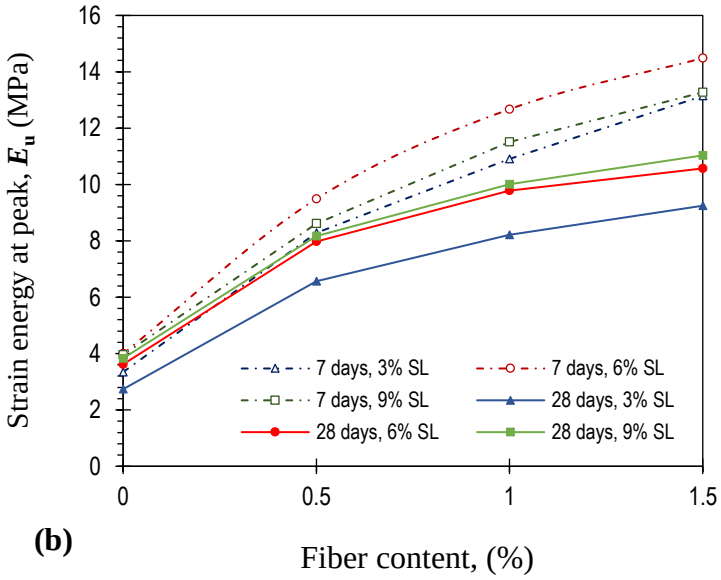

(b)

Statement of Authorship

Title of Paper	Mechanical behavior of micaceous soils stabilized by lime and slag-lime with fibers
Publication Status	☐Published ☐Accepted for Publication ☐Submitted for Publication ■Unpublished and Unsubmitted work written in manuscript style
Publication Details	**Zhang J**, Deng A, Jaksa M **(2019)** Mechanical behavior of micaceous soils stabilized by lime and slag-lime with fibers. x(x):x-x, http://doi.org/x

Principal Author

Name of Principal Author (Candidate)	Jiahe Zhang (**Email**: Jiahe.Zhang@adelaide.edu.au)		
Contribution to the Paper	Overall paper preparation		
Overall percentage (%)	85%		
Certification:	This paper reports on original research I conducted during the period of my Higher Degree by Research candidature and is not subject to any obligations or contractual agreements with a third party that would constrain its inclusion in this thesis. I am the primary author of this paper.		
Signature		Date	01/05/2019

Co-Author Contributions

By signing the Statement of Authorship, each author certifies that:

i. the candidate's stated contribution to the publication is accurate (as detailed above);
ii. permission is granted for the candidate in include the publication in the thesis; and
iii. the sum of all co-author contributions is equal to 100% less the candidate's stated contribution.

Name of Co-Author	An Deng **Senior Lecturer**, School of Civil, Environmental and Mining Engineering, The University of Adelaide, Adelaide, SA 5005, Australia (**Email**: An.Deng@adelaide.edu.au)		
Contribution to the Paper	Methodology, paper review and revision		
Signature		Date	1/05/2019

Name of Co-Author	Mark Jaksa **Professor**, School of Civil, Environmental and Mining Engineering, The University of Adelaide, Adelaide, SA 5005, Australia (**Email**: Mark.Jaksa@adelaide.edu.au)		
Contribution to the Paper	Paper review and revision		
Signature		Date	2/05/2019

Chapter 5

Optimization of slag and fiber/polymeric agent to reinforce micaceous soils using response surface methodology

Jiahe Zhang [1,*] , An Deng [2] , Mark B. Jaksa [3]

[1] **PhD Student** — School of Civil, Environmental and Mining Engineering, The University of Adelaide, Adelaide SA 5005, Australia | **Email:** Jiahe.Zhang@adelaide.edu.au

[2] **Senior Lecturer** — School of Civil, Environmental and Mining Engineering, The University of Adelaide, Adelaide SA 5005, Australia | **Email:** An.Deng@adelaide.edu.au ; **ORCID:** 0000-0002-3897-9803

[3] **Professor** — School of Civil, Environmental and Mining Engineering, The University of Adelaide, Adelaide SA 5005, Australia | **Email:** Mark.Jaksa@adelaide.edu.au

* Corresponding Author.

Zhang J, Deng A and Jaksa M **(2019)** Optimization of slag and fiber/polymeric agent to reinforce micaceous soils using response surface methodology. x(x):x-x, http://doi.org/x.[4]

Abstract

Micaceous soil is classified as a problematic soil due to its low strength and weak ductility. In this paper, the combined capacity of granulated blast furnace slag (GBFS), fiber and a polymer-agent were examined as additives to improve the inferior engineering properties of micaceous soils. A three-factor central composite design (CCD), combined with the response surface methodology (RSM), was employed to design the experiments as well as to optimize the content of slag-fiber or slag-polymer composites to achieve the desired strengths. Four independent

[4] Unpublished and unsubmitted work written in a manuscript style

variables were examined, including the mica content (0–30%) for forming various percentages of micaceous soils, slag (3–15%) and fiber content (0.25–1.25%), and polymer concentration (0.1–0.5 g/l), to optimize the geotechnical characteristics of the stabilized soils. The additives were transformed into coded values and a second-order quadratic model was subsequently derived to predict the responses of the stabilized soils. The significance of the independent variables, the validation of the models and their interactions were assessed by the analysis of variance (ANOVA) and *t*-test statistics. In the optimization process, the micaceous soils were stabilized using the binders of slag and fiber or slag and the polymer agent (Polycom) at different percentages (10%, 20%, and 30%). The results showed that both binders are effective in improving the strength of the soil to achieve appropriate standards.

Keywords: Geotechnical engineering; central composite design (CCD); strength and testing of materials; micaceous clay

5.1. Introduction

The need to expand urban areas to satisfy growing population and industrial activities requires more land. However, naturally occurring soils, such as micaceous soils, sometimes fail to meet the construction quality requirement, e.g. strength and bearing capacity, and if untreated are unsuitable for common engineering applications (Zhang et al. 2019). The treatment for micaceous soils, in order to improve their design characteristics, has attracted modest research attention and hence further work is needed. Mica minerals are amongst the most widely distributed around the world and naturally occur in igneous, sedimentary and certain metamorphic rocks (Harvey 1982; Galán and Ferrell 2013). When mica minerals are present in soils due to the weathering process, their unique characteristics may significantly affect the mechanical properties of such soils. Micaceous soils are distributed worldwide, being a particular issue in some countries, such as South Africa (Paige-Green and Semmelink 2002), Malawi (Netterberg et al. 2011), Nigeria (Gogo 1984) and the U.K. (Northmore 1996). Due to the extremely elastic properties of mica minerals, micaceous soils may deform significantly under applied load which affects the compressibility of such soils. Mica minerals, although somewhat resilient, may recover their initial shape due to elastic rebound (springy action), thus reducing the efficiency of compactive effort and/or potentially compromising the performance of facilities constructed on micaceous clays (Weinert 1980). When such soils are unloaded, elastic rebound is likely to occur, resulting in volumetric expansion. Given the platy nature of the shapes of the mica and clay particles, during compression or shearing, they tend to rotate and orient themselves in a somewhat parallel fashion, resulting in low strength resistance (Harris et al. 1984). Due to the high compressibility, poor compactibility and low shear strength, the construction of building foundations, road constructions and other geotechnical engineering systems on micaceous soils is problematic. The improvement of certain desired properties such as unconfined compression strength and ductility can be undertaken through soil stabilization.

Chemical stabilization generally includes the agents, such as cement, limes, fly ashes, slags and more recently, non-conventional agents, such as polymers and resins. The addition of such binders into the soils fabric creates a series of short- and long-term chemical reactions in the soil–water system and thus results in materials having lower compressibility and higher strength in comparison with their natural counterparts (Ingles and Metcalf 1972; Al-Rawas et al. 2002; Basha et al. 2005; Falah 2018). An alternative technique involves mechanical stabilization, whereby soils are reinforced with natural or synthetic fibers, thus improving the mechanical

behavior of soils. The traditional methods of mechanical stabilization consist of placing strips, bars, grids or geotextiles within the soils and the inclusions are usually oriented in a preferred direction and/or in layers. The fiber distribution can also be random and discrete, which minimizes the potential for planes of weakness that can develop parallel to the reinforcement orientation (Maher and Gray 1990; Ranjan 1996; Hejazi et al. 2012; Wang et al. 2017). Recent studies indicate that the combination of both chemical agents (cementitious binders, such as cement and lime) and mechanical agents, significantly improves the soil–binder bonding, thereby enhancing the behavior of the soil. (Tang et al. 2007; Consoli et al. 2010; Estabragh et al. 2017; Shahbazi et al. 2017; Yadav and Tiwari 2017; Qudoos et al. 2018).

The purpose of this study is to investigate the effective percentage and contribution ratio of each additive (slag, fiber and polymer) in order to develop sustainable solutions for improving the engineering characteristics of different micaceous soils. A series of unconfined compression (UC) strength tests were carried out and then analyzed by the performance of optimization software, which is explained in detail below.

5.2. Materials and methods

5.2.1. Soils

The soil adopted in the experimental program was a mixture of two commercially available clays: kaolinite and sodium-activated bentonite. They were blended at percentages of 85% and 15%, respectively, by weight. The physical and mechanical properties of the soil, determined using the relevant ASTM and Australian standards, are summarized in **Table 1**. The liquid limit and plasticity index were, respectively, measured as 44% and 22%, from which the soil was characterized as a clay of intermediate plasticity (CI), in accordance with the Unified Soil Classification System (USCS). Furthermore, the standard Proctor compaction test, carried out as per ASTM D698-12, indicated that optimum water content was 25.2%, corresponding to a maximum dry unit weight of 14.6 kN/m^3.

5.2.2. Ground Mica

Commercially available ground mica, sourced from a local distributor, was used to artificially prepare the micaceous clay blends. The physical properties and chemical composition of the ground mica, as provided by the supplier, are summarized in **Table 2**. The product appeared as a white powder with the particle size being silt-to-clay (< 75 μm). The specific gravity of the

ground mica was found to be G_s^M = 2.80. The chemical composition of the ground mica, provided by the supplier, was found to be dominated by silicon dioxide (SiO_2) and aluminum trioxide (Al_2O_3) with mass fractions of 49.5% and 29.2%, respectively. In terms of acidity, the ground mica slurry was classified as a neutral substance, corresponding to a pH of 7.8.

5.2.3. Ground-Granulated Blast-Furnace Slag

The Ground-Granulated Blast-Furnace Slag (GBFS) was sourced from a local manufacturer and was used as the cementitious binder. The physical properties and chemical composition, provided by the manufacturer, are shown in **Table 3**. The particle sizes of GBFS are mainly finer than 75 μm, consisting of 96% of such particles. The specific gravity and pH value of GBFS were 2.87 and 9.6, respectively. The chemical composition is mainly dominated by CaO and SiO_2 with the contents of 44.7% and 27.1%, respectively.

5.2.4. Fibers

Polypropylene fiber was used as the mechanical reinforced material in this research. This type of fiber has been widely used in previous studies (e.g. Yetimoglu et al. 2005; Olgun 2013 Estabragh et al. 2017). The diameter of the raw fiber was in the range of 20 to 30 μm, and was cut into segments of approximately 10 mm in length. Polypropylene fiber has advantageous properties, such as being hydrophobic, noncorrosive and resistant to alkalis, chemicals and chlorides. The physical and engineering properties, provided by the manufacturer, are given in **Table 4**.

5.2.5. Polymeric agent

A commercially manufactured polymer agent, known as Polycom, was used as the chemical binder in this research. This type of polymer is referred to as a polyacrylamide or PAM (–$CH_2CHCONH_2$–), which is a water-soluble, anionic synthetic polymer formed from acrylamide subunits. Polycom has been successfully implemented in several Australian roadway construction projects in a variety of soils (Andrews and Sharp 2010; Camarena 2013; Georgees et al. 2015). Polycom presents in a granular form and is diluted with water (200 g of Polycom into 1 kl of water, as per the manufacturer's specification). Other properties include a specific gravity (at 25 °C) of 0.8 and a pH (at 25 °C) of 6.9.

5.2.6. Response surface modelling

Response surface methodology (RSM) is an empirical statistical and mathematical tool which can identify and fit quantitative, experimental data to determine regression models and operational conditions (Myer et al. 2009). The main objective of RSM is to determine the optimal sets of operational variables in order to obtain the desired response. The effect of an individual variable can be assessed while the other variables may vary at the same time (Singh et al. 2011). The RSM approach has been widely applied in chemical engineering and more recently in civil engineering (Shahbazi et al. 2018).

Central composite design (CCD), which is a standard implementation of RSM, has been used to fit a second-order model and subsequently to optimize the desired outcome. The advantage of this method is that an optimal number of experiments is required and a detailed understanding of the interraltionship between the various variables is not needed as the mathematical model is entirely empirical (Sahu et al. 2009). Generally, the CCD design consists of the sum of 2^n factorial runs, $2n$ axial runs, and n_c center runs, ($2^n + 2n + n_c$), where n is the number of independent variables in the experiment. The factorial runs, 2^n, the axial runs, $2n$ (±α, 0, 0, … ,0), (0, ± α, 0, … , 0), …, (0, 0, …, ±α), the center runs, n_c (0, 0, 0, …, 0), and the replicates of the center runs are determined by the number of variables during the design process, usually between 3 and 10 (Myer et al. 2009).

In CCD, the process involves the design of the experiments, the estimation of the coefficients in the mathematical model, prediction of the response and validation of the model. The response model may be expressed as

$$Y = f(X_1, X_2, X_3, \ldots, X_n) \pm e \quad (1)$$

where Y is the response of the experiment, X_i are the independent variables and e represents the experimental errors. In this system, the independent variables are considered to be continuous and the experimental errors can be neglected. The form of the function is unknown and it may be complex, based on the relationship between the independent variables and the response. Therefore, RSM aims at identifying a suitable polynomial relationship between the independent variables and the response surface (Gunaraj and Murugan, 1999). In some cases, a higher-order polynomial, such as a quadratic model, may be applied and expressed as:

$$Y = \beta_0 + \sum_{i=1}^{n} \beta_i X_i + \sum_{i=1}^{n} \beta_{ii} X_1^2 + \sum_{i=1}^{n} \sum_{j=1}^{n} \beta_{ij} X_{ij} X_i X_j + e \quad (2)$$

where Y is the predicted response, β_0 is a constant, β_i are the linear coefficients, β_{ii} the quadratic coefficients, β_{ij} the interaction coefficients, X_i and X_j are the coded values of the independent process variables, and e is the residual error between the predicted and actual values.

RSM aids in the investigation of the response over the entire variable space and the identification of the region where it achieves its optimal performance. The analysis of variance (ANOVA) and the *t*-test are also used to examine the adequacy and statistical parameters of the model. The model parameters are evaluated by the *P* value (probability) with a 95% confidence level.

5.2.7. Sample preparations and experimental tests

The soils were mixed with the mica and additives according to the designed runs from the CCD, shown in **Table 5**. For the purpose of sample preparation, it was found to be necessary to establish the target values (soil mixtures of 85% kaolinite and 15% bentonite, in **Section 2.1**) of dry density and water content, and the samples were then expected, within an appropriate experimental error range, to be of the same density and water content for all the mix designs. All the moist samples were mixed manually and thoroughly for about 5 minutes to ensure the mixtures were homogenous. The prepared samples were then carefully sealed using plastic cling film and placed into a fog room and cured for 14 days. As a result, the moisture was evenly distributed throughout the soils samples, which led to the full pozzolanic reaction of the slag.

UC tests were conducted in accordance with the ASTM D2166-16. The test samples were prepared at the target optimum moisture content, as provided in **Table 1**, with the dimensions of 50 mm in diameter and 100 mm in height. The samples were then axially compressed with a displacement rate of 1 mm/minute (equivalent to 1%/min), as commonly adopted by Ang (2003) and Soltani et al. (2019). The load with respect to time was recorded continuously until the sample failed, enabling the UC peak strength to be determined.

5.3. Results and discussion

5.3.1. Determination of the regression model and statistical analysis

The CCD approach was adopted for investigating the individual and interaction effects of the variables on the UC strength of the samples. The two design sets, together with the results, are provided in **Table 5**. The ANOVA analysis is considered to be essential to test the fitness and

significance of the model, and the ANOVA results for the two sets of quadratic models are provided in **Table 6**. Two proposed statistical models were suggested to be highly significant, as evident from Fisher's *F*-test with very low probability value (<0.0001). The fitness of the models was assessed using R^2 and adj-R^2 between the experimental values and those predicted by the models (**Figure 1**). As can be seen, the resulting R^2 values are high, indicating that the predicted UC strengths of the two models are accurate representations of the measured values. Further, it can be observed that the R^2 and adj-R^2 values are similar in both UCS responses (99.3–99.9%), confirming that the predictions from both models equally reflect the measurements. Moreover, the two models have a very low variation, as is evident from the coefficients of variation, *CV*, which is the ratio of the standard deviation to the mean. Thus, the quadratic regression model is considered as the optimal model with respect to the three different variables and the corresponding responses. These models are expressed by Eqs. (3) and (4), as follows:

$$UCS_{SF} = 301.77 - 50.40A_1 + 139.50B_1 + 43.64C_1 - 25.98A_1B_1 - 16.04A_1C_1 + 15.23B_1C_1 - 28.61A_1^2 + 10.53B_1^2 - 19.23C_1^2 \quad (3)$$

$$UCS_{SP} = 312.67 - 35.30A_2 + 137.00B_2 + 31.50C_2 - 15.75A_2B_2 - 2.5A_2C_2 + 19.50B_2C_2 - 20.68A_2^2 + 32.82B_2^2 - 84.68C_2^2 \quad (4)$$

Where UCS_{SF} and UCS_{SP} are the unconfined compressive strength of slag-fiber treated soils and slag-polycom treated soils, A_1 and A_2 are the mica contents, B_1 and B_2 are the slag contents, C_1 is the fiber content and C_2 is the Polycom concentration.

5.3.2. Effect of addition of slag and fiber on the UCS of micaceous soils

Three-dimensional (3D) response surface plots, as a function of two factors, while maintaining the other factor at a fixed level, are more effective in analyzing both the response and the interactive effects of these two factors (Adinarayana and Ellaiah 2002). In addition, 3D response surfaces and their corresponding contour plots can facilitate the direct investigation of the effects of the design variables on the responses (Wu et al. 2009). As a consequence, **Figure 2(a)** shows the 3D response surface and the corresponding contour plot as a function of the combined slag content and mica content at a constant fiber content (0.75%). It is shown that the peak UC strength is inversely dependent on the mica content, with higher mica contents exhibiting lower UC strength. Conversely, slag significantly contributes to increasing the UC strength of the material. If the contents of both slag and mica increase simultaneously, UC

strength also increased due to the positive effect of slag on the strength was larger. When the slag and mica contents changed in opposite senses (i.e. slag content increased and mica content decreased), the UC strength increased. Overall, these variations arise from the interactive effects between the additives, as specified in Eq. (3).

The combined effect of fiber and mica content on the UC strength of the composite material is shown in **Figure 2(b)**. It can be seen that the fiber content improves the UC strength of the soils, while the improvement rate is less significant when compared with that obtained by using slag. The presence of mica again shows an adverse effect on the UC strength of the soil. It is important that, initially the improvement in the UC strength of the composite material with the addition of fibers is effective, but beyond 0.9%, the change in UC strength is not noticeable.

The relationship between slag and fiber content, at constant of mica content, is presented in **Figure 2(c)**. It can be observed that the UC strength increases with both slag and fiber within the tested ranges. It is evident that the slag is more effective than the fiber in increasing the UC strength. In addition, when the fiber content is 1.25% (i.e. the maximum dosage tested), the effectiveness of the slag on improving the UC strength is most significant.

The above variations suggest that micaceous soils have relative low strength compared with the natural clay soils. If compressed, mica particles tend to rotate and orient themselves into a somewhat parallel fashion due to the unique platy structure, thus resulting in low strength resistance (Harris et al. 1984). The reason for the slag effectively improving the strength is the initiation of chemical reactions in the soil-water medium. The chemical reactions consist of cation exchange and flocculation-agglomeration, and occur in the fine-grained soils, while the reactions are often negligible when paired with neutrally-charged soil particles, such as silts, gravels, and sands (Locat 1990; Sivapullaiah 1996; Mallela 2004). The reason is that the fine-grained soils, like clays, contain a notable amount of negative charges. During the short-term reactions, higher-valence cations substitute those of lower valence, and cations of larger ionic radius replace smaller cations of the same valence, and the order of substitution follows the Hofmeister series, i.e. $Na^+ < K^+ < Mg^{2+} < Ca^{2+}$ (Grim, 1953). The slag contains additional calcium cations (Ca^{2+}), which immediately substitute cations of lower valence (e.g. Na^+), and/or the same valence cations of smaller ionic radius (e.g., Mg^{2+}) in the vicinity of the clay particles (Zhang et al. 2019). Due to the development of the strong van der Waals bonds between adjacent clay particles in the matrix, these cation exchanges lead to a decrease in the thickness of the diffused double layers, leading to the aggregation and flocculation of the clay particles

(Little 1987; Mallela et. al 2004; Firoozi et. al 2017). Another reaction, referred to as pozzolanic activity, is depends greatly on the time of curing. During pozzolanic reactions, ionized calcium (Ca^{2+}) and hydroxide (OH^{-}) units, are released from the water-binder complex. These ions gradually react with silicate (SiO_2), and aluminate (Al_2O_3) unites in the soil, thereby forming strong cementation gels, namely calcium-silicate-hydrates (CSH), calcium-aluminate-hydrates (CAH) and calcium-aluminate-silicate-hydrates (CASH). These products promote further solidification and flocculation of the particles, which lead to the development of a dense, uniform matrix, thus improving strength (Mallela et al. 2004, Sharma and Sivapullaiah 2016; Firoozi et al. 2017). On the other hand, fiber also promotes increase in the strength of soils to some degree, which results from two phenomena: (i) the frictional resistance generated at the soil-fiber interface, due to the roughness of the fiber's surface, and (ii) the mechanical interlocking of the soil particles and fibers (Tang et al. 2007; 2010; Wang et al. 2017; Mirzababaei et al. 2018; Zhang et al. 2019). The internal frictional resistance between the soil and the fibers is a function of the soil-fiber contact area. Therefore, a greater number of fibers in the soil will lead to the larger contact levels between the soil particles and the fibers, thus resulting in higher frictional resistance. The mechanical interlocking of soils and fibers are achieved during the sample preparation phase (e.g. soil compaction), and this process induces adhesion of the mixtures by immobilizing the soil particles undergoing loading. It should be noted that, in the preparation of the fiber-soil mixture, care needs to be taken to prevent the formation of fiber clusters (Prabakar and Sridhar 2002; Estabragh et al. 2017; Yadav and Tiwari 2017). The addition of fibers into slag-treated soils further enhances the strength of such soils. This is because the effective contact area between the fibers and clay particles, in the fiber-slag treated soils, is greater than that in the soils reinforced solely with fibers due to the smaller pores in the slag-treated soils. Thus, the total effective friction between the soils and the fibers in the fiber-slag treated soil is greater, resulting in a greater UC strength and stronger toughness (Cai et al. 2006).

5.3.3. Effect of addition of slag and polymer on the UCS of micaceous soils

Figure 3(a) shows the interactive influence of slag and mica on the UC strength of the soils at a constant dosage of Polycom (0.3 g/l). As can be observed, the increase of slag content, at a constant dosage of Polycom, contributes to a significant increase in the UC strength of the composite, while mica again has an adverse effect. This observation is consistent with the soils treated with slag at a constant content of fibers, but with a less noticable improvement. The plot for the combined effect of the Polycom and mica at a constant slag content (9%) is shown in

Figure 3(b). It can be seen that the UC strength increases with a greater concentration of Polycom up to 0.3 g/l, beyond which additional Polycom has a slightly adverse effect on strength. The combined effect of slag and Polycom on micaceous clays is shown in Figure **3(c)**. It can be seen that both slag and Polycom have a positive effect on strength improvement. Considering 0.3 g/l of Polycom to be a threshold for strength increase, the maximum UC strength was observed at 15% of slag content, with Polycom concentration of 0.3 g/l.

From the above results, Polycom, as the chemical binder, has a positive effect on improving the strength of the composite soil. Different types of polymers have different stabilization mechanisms to attract/adsorb to the clay particles. Positively charged polymers are electrostatically attracted to the negatively charged clay surface, and non-ionic polymers achieve the adsorption through van der Waals forces and/or hydrogen bonding (Theng 1982; Wallace et al. 1986; Miller et al. 1998). Polycom is an anionic polymer which, although it tends to be repelled by the negatively charged clay particles, attraction can still take place with the presence of cations acting as bridges. The degree of the adsorption is dependent on the amount and type of exchangeable cations, clay content, pH and the size of the polymer molecules (Theng 1982; Lu et al. 2002; Rabiee et al. 2013). The role of Polycom in improving the strength of the composite can be attributed to its ability to form ionic bonds, thereby holding clay particles together through the cationic bridging mechanism. This results in the occurrence of the flocculation of the clay particles, which further improves the density of the composite. Moreover, Polycom also acts as the bridging agent, which enhances the interlocking of the slag-clay flocculation, thus promoting a more significant improvement in the UC strength of the composite.

5.3.4. Optimization study

One of the primary aims of this study was to determine the optimum stabilization solutions for different micaceous soils using various combinations of stabilizers. As ASTM D 4609 states "if the UCS value reaches 345.0 kPa in any soil, the stabilization procedure has been effective". The target UCS values for the micaceous soils was set to be 345.0 kPa with the treatment of slag and fiber or slag and Polycom. The optimization study was applied to soils of three mica contents, i.e. M_c = 10%, 20% and 30%. Hereafter, the coding system M*i* (where *i* = mica content) is adopted to designate the various mix designs. As such, 'M0' refers to the natural soil with no mica inclusion, and 'M30', for example, refers to a soil–mica blend containing 30% mica by dry weight of soil. The UC strength was then measured according to the procedure

described in **Section 2.3**. The criterion for the response parameter (i.e. the UCS value) was set as 345.0 kPa for all scenarios, and the optimization suggested a series of solutions with different dosages and desirabilities. For instance, for a soil with a mica content M20 (= 20%), 11 solutions for slag–fiber stabilization, and 5 solutions for the slag–Polycom stabilization were suggested. Of the suggested solutions, two solutions with the highest desirability for each scenario were chosen and are summarized in **Table 7**.

Confirmation tests on M10 were conducted using the suggested optimal additive proportions. The optimization and test results are provided in **Table 8**. As can be observed, excellent agreement was obtained, with a modest UCS prediction bias of 4.13% for the slag–fiber system and 6.42% for the slag–fiber system. Furthermore, the UC strengths obtained by the confirmation tests are higher than the corresponding optimization values, which suggests that the model is slightly conservative .

5.4. Conclusions

In this study, response surface methodology (RSM) was used to evaluate the changes in the unconfined compression strength (UCS) of micaceous soils, as a function of the dosage of various additives. The additives included two combinations: (i) slag and fiber, (ii) slag and Polycom. Based on the findings and results, the following conclusions are drawn:

1) RSM, together with the central composite design (CCD) method, is a method suitable for enabling the optimization of the additive dosage for soil stabilization.

2) Both combinations of additives were able to stabilize the micaceous soils. The additives exhibited varied effects on the stabilization. Slag exhibited a noticeable synergistic effect and greatly contributed to the stabilization of micaceous soils with the presence of fiber or Polycom.

3) Models were developed as a tool to predict the UCS of the micaceous soils which were stabilized by the two combinations of additives. Excellent agreement was obtained between the model prediction results and actual test measurements, for the samples tested in this study.

4) The RSM-based optimization was successful in determining the additive dosages in terms of the targeted UCS value, and based on the developed models, identified the most efficient dosage for improving the UCS of micaceous soils.

5) The performance of the model optimization was verified by additional laboratory tests. The test results agreed very well with the predicted results, suggesting that the optimization process was successful.

Acknowledgments

This research was made possible through the provision of an Australian Government Research Training Program Scholarship; this support is gratefully acknowledged.

Conflicts of Interest

The authors wish to confirm that there are no known conflicts of interest associated with this publication, and there has been no significant financial support for this work that could have influenced its outcome.

References

Adinarayana, K., & Ellaiah, P. (2002). Response surface optimization of the critical medium components for the production of alkaline protease by a newly isolated Bacillus sp. *Journal of Pharmacy and Pharmaceutical Sciences*, *5*(3), 272–278.

Al-Rawas, A. A. (2002). Microfabric and mineralogical studies on the stabilization of an expansive soil using cement by-pass dust and some types of slags. *Canadian Geotechnical Journal*, *39*(5), 1150–1167. http://doi.org/10.1139/t02-046

Andrews, R. & Sharp, K. (2010). A protocol for conducting field trials for best value management of unsealed roads. *Proceedings of the 24th ARRB Conference–Building on 50 Years of Road and Transport Research*, ARRB, Melbourne, VIC, Australia, pp. 1–14.

Ang, E. C., & Erik Loehr, J. (2003). Specimen size effects for fiber-reinforced silty clay in unconfined compression. *Geotechnical Testing Journal*, *26*(2), 191–200.

Basha, E. A., Hashim, R., Mahmud, H. B., & Muntohar, A. S. (2005). Stabilization of residual soil with rice husk ash and cement. *Construction and Building Materials*, *19*(6), 448–453. http://doi.org/10.1016/j.conbuildmat.2004.08.001

Camarena, S. (2013). Sustainable road maintenance and construction utilising new technologies. *Proceedings of the IPWEA International Public Works Conference*, IPWEA, Darwin, NT, Australia, pp. 1–11.

Consoli, N. C., Arcari Bassani, M. A., & Festugato, L. (2010). Effect of fiber-reinforcement on the strength of cemented soils. *Geotextiles and Geomembranes*, *28*(4), 344–351. http://doi.org/10.1016/j.geotexmem.2010.01.005

Estabragh, A. R., Ranjbari, S., & Javadi, A. A. (2017). Properties of a Clay Soil and Soil Cement Reinforced with Polypropylene Fibers. *ACI Materials Journal*, *114*(2), 195–206. http://doi.org/10.14359/51689469

Falah, M., Pouya, K. R., Tolooiyan, A., & Mackenzie, K. (2018). Structural behaviour of an Australian silty clay (Coode Island silt) stabilised by treatment with slag lime. *Applied Clay Science*, *157*(October 2017), 198–203. http://doi.org/10.1016/j.clay.2018.02.045

Firoozi, A. A., Guney Olgun, C., Firoozi, A. A., & Baghini, M. S. (2017). Fundamentals of soil stabilization. *International Journal of Geo-Engineering*, *8*(1). http://doi.org/10.1186/s40703-017-0064-9

Galán, E., & Ferrell, R. E. **(**2013**).** Chapter 3 – Genesis of clay minerals. *Developments in Clay Science*, 83–126. http://doi.org/10.1016/b978-0-08-098258-8.00003-1

Georgees, R. N., Hassan, R. A., Evans, R. P. & Jegatheesan, P. (2015). Effect of the use of a polymeric stabilizing additive on unconfined compressive strength of soils. *Transportation Research Record*, 2473, 200–208, https://doi.org/10.3141/2473-23.

Gogo, J. O. (1984). Compaction and strength characteristics of decomposed mica schist. *In: Proceedings of the 8th Regional Conference for Africa on Soil Mechanics and Foundation Engineering*. Harare, Zimbabwe, 275–284. ISBN:9061915325

Gunaraj, V., & Murugan, N. (1999). Application of response surface methodology for predicting weld bead quality in submerged arc welding of pipes. *Journal of Materials Processing Technology*, *88*(1), 266–275. http://doi.org/10.1016/S0924-0136(98)00405-1

Harris, W.G., Parker, J.C. & Zelazny L.W. (1984). Effects of mica content on engineering properties of sand. *Soil Science Society America Journal*. 48(3), 501–5. http://doi.org/10.2136/sssaj1984.03615995004800030006x

Harvey, J.C. (1982). Geology for Geotechnical Engineers (1st Ed). Cambridge, CambridgeshireEngland, UK: Cambridge University Press. ISBN:9780521288620

Hejazi, S. M., Sheikhzadeh, M., Abtahi, S. M., & Zadhoush, A. (2012). A simple review of soil reinforcement by using natural and synthetic fibers. *Construction and Building Materials*, *30*, 100–116. http://doi.org/10.1016/j.conbuildmat.2011.11.045

Ingles, O. G., & Metcalf, J. B. (1972). *Soil stabilization : principles and practice*. Sydney: Butterworths.

Little, D.L. (1987). *Fundamentals of the Stabilization of Soil with Lime*, The National Lime Association: Arlington, VA, USA.

Maher, M. H., & Gray, D. H. (1990). Static response of sand reinforced with randomly distributed fibers. *Journal of Geotechnical Engineering*, *116*(11), 1661–1677.

Mallela, J., Von Quintus, H., & Smith, K. L. (2004). *Consideration of lime-stabilized layers in mechanistic-empirical pavement design*. The National Lime Asscociation: Arlington, VA, USA.

Wallace, A.,Wallace, G. A. & Cha,W. J. (1986). Mechanisms involved in soil conditioning by polymers. *Soil Science*, 141, No. 5, 381–386, https://doi.org/10.1097/00010694-198605000-00017.

Mirzababaei, M., Miraftab, M., Mohamed, M., & McMahon, P. (2012). Unconfined Compression Strength of Reinforced Clays with Carpet Waste Fibers. *Journal of Geotechnical and Geoenvironmental Engineering*, *139*(3), 483–493. http://doi.org/10.1061/(asce)gt.1943-5606.0000792

Myer, R. H., Montgomery, D. C., & Anderson-Cook, C. M. (2009). *Response surface methodology: process and product optimization using designed experiments* (3rd ed.). Wiley.

Lu, J. H., Wu, L. & Letey, J. (2002). Effects of soil and water properties on anionic polyacrylamide sorption. *Soil Science Society of America Journal*, 66, No. 2, 578–584, https://doi.org/10.2136/sssaj2002.5780.

Netterberg F, Hefer A & Preez HD. (2011). Cracking and staining of an airport asphalt. *In: Proceedings of the 10th Conference on Asphalt Pavements for South Africa (CAPSA 11): Roads of the Future*. KwaZulu KwaZulu–Natal, South Africa: International Road Federation (IRF). p. 1–17.

Northmore K.J., Bell F.G. & Culshaw M.G. (1996). The engineering properties and behaviour of the brickearth of south Essex. *Quarterly Journal Engineering Geology Hydrogeology*. 29(2):147–61. http://doi.org/10.1144/gsl.qjegh.1996.029.p2.04

Paige-Green P, Semmelink CJ. (2002). Road compaction problems related to the presence of biotite. *In: Proceedings of the 9th Congress of the International Association of Engineering Geology and the Environment*. Durban, KwaZulu–Natal, South Africa, 2605–2610.

Prabakar, J., & Sridhar, R. S. (2002). Effect of random inclusion of sisal fibre on strength behaviour of soil. *Construction and Building Materials*, *16*(2), 123–131. http://doi.org/10.1016/S0950-0618(02)00008-9

Olgun, M. (2013). Effects of polypropylene fiber inclusion on the strength and volume change characteristics of cement-fly ash stabilized clay soil. *Geosynthetics International*, *20*(4), 263–275.

Qudoos, A., Kim, H. G., Atta-ur-Rehman, & Ryou, J. S. (2018). Effect of mechanical processing on the pozzolanic efficiency and the microstructure development of wheat straw ash blended cement composites. *Construction and Building Materials*, *193*, 481–490. http://doi.org/10.1016/j.conbuildmat.2018.10.229

Shahbazi, M., Rowshanzamir, M., Abtahi, S. M., & Hejazi, S. M. (2017). Optimization of carpet waste fibers and steel slag particles to reinforce expansive soil using response surface methodology. *Applied Clay Science*, *142*, 185–192. http://doi.org/10.1016/j.clay.2016.11.027

Soltani, A., Taheri, A., Deng, A., & Nikraz, H. (2019). Tyre rubber and expansive soils: two hazards, one solution. *Proceedings of the Institution of Civil Engineers - Construction Materials*, 1–37. http://doi.org/10.1680/jcoma.18.00075

Tang, C., Shi, B., Gao, W., Chen, F., & Cai, Y. (2007). Strength and mechanical behavior of short polypropylene fiber reinforced and cement stabilized clayey soil. *Geotextiles and Geomembranes*, *25*(3), 194–202. http://doi.org/10.1016/j.geotexmem.2006.11.002

Tang, C. S., Shi, B., & Zhao, L. Z. (2010). Interfacial shear strength of fiber reinforced soil. *Geotextiles and Geomembranes*, *28*(1), 54–62. http://doi.org/10.1016/j.geotexmem.2009.10.001

Theng, B. K. G. (1982). Clay–polymer interactions: summary and perspectives. *Clays and Clay Minerals*, 30, No. 1, 1–10, https://doi.org/10.1346/ccmn.1982.0300101.

Sahu, J. N., Acharya, J., & Meikap, B. C. (2009). Response surface modeling and optimization of chromium(VI) removal from aqueous solution using Tamarind wood activated carbon in batch process. *Journal of Hazardous Materials*, *172*(2–3), 818–825. http://doi.org/10.1016/j.jhazmat.2009.07.075

Sharma, A. K., & Sivapullaiah, P. V. (2016). Ground granulated blast furnace slag amended fly ash as an expansive soil stabilizer. *Soils and Foundations*, *56*(2), 205–212. http://doi.org/10.1016/j.sandf.2016.02.004

Singh, K. P., Gupta, S., Singh, A. K., & Sinha, S. (2011). Optimizing adsorption of crystal violet dye from water by magnetic nanocomposite using response surface modeling approach. *Journal of Hazardous Materials*, *186*(2–3), 1462–1473. http://doi.org/10.1016/j.jhazmat.2010.12.032

Wallace, A.,Wallace, G. A. & Cha,W. J. (1986). Mechanisms involved in soil conditioning by polymers. *Soil Science*, 141, No. 5, 381–386, https://doi.org/10.1097/00010694-198605000-00017.

Wang, Y., Guo, P., Ren, W., Yuan, W., Yuan, H., Zhao, Y. & Cao, P. (2017). Laboratory Investigation on Strength Characteristics of Expansive Soil Treated with Jute Fiber Reinforcement. *International Journal of Geomechanics*, *17*(11), 04017101. http://doi.org/10.1061/(asce)gm.1943-5622.0000998

Weinert H.H. (1980). *The Natural Road Construction Materials of Southern Africa* (1st Ed). Cape Town, Western Cape, South Africa: H&R Academica; ISBN:0860740470

Wu, D., Zhou, J., & Li, Y. (2009). Effect of the sulfidation process on the mechanical properties of a CoMoP/Al2O3 hydrotreating catalyst. *Chemical Engineering Science*, *64*(2), 198–206. http://doi.org/10.1016/j.ces.2008.10.014

Rabiee, A., Gilani, M., Jamshidi, H. & Baharvand, H. (2013). Synthesis and characterization of a calcium– and sodium–containing acrylamide-based polymer and its effect on soil strength. *Journal of Vinyl and Additive Technology*, 19, No. 2, 140–146, https://doi.org/10.1002/vnl.21310.

Ranjan, G., Vasan, R. M., & Charan, H. D. (1996). Probabilistic analysis of randomly distributed fiber-reinforced soil. *Journal of Geotechnical Engineering*, *122*(6), 419–426.

Yadav, J. S., & Tiwari, S. K. (2017). Effect of waste rubber fibres on the geotechnical properties of clay stabilized with cement. *Applied Clay Science*, *149*(May), 97–110. http://doi.org/10.1016/j.clay.2017.07.037

Yetimoglu, T., Inanir, M., & Inanir, O. E. (2005). A study on bearing capacity of randomly distributed fiber-reinforced sand fills overlying soft clay. *Geotextiles and Geomembranes*, *23*, 174–183. http://doi.org/10.1016/j.geotexmem.2004.09.004

Zhang, J., Soltani, A., Deng, A., & Jaksa, M. B. (2019). Mechanical Performance of Jute Fiber-Reinforced Micaceous Clay Composites Treated with Ground-Granulated Blast-Furnace Slag. *Materials*, *12*(4), 576:1-23. http://doi.org/10.3390/ma12040576

List of Tables

Table 1. Physical and mechanical properties of the mixtures of soils.

Table 2. The physical and chemical composition of ground mica (as provided by the supplier).

Table 3. The physical and chemical composition of GBFS (as supplied by the manufacturer).

Table 4. The physical and chemical composition of polypropylene fiber (as given by the distributor).

Table 5. Experimental design and corresponding response.

Table 6. Statistical factors for the stabilization system models.

Table 7. Optimum additive ratios and responses for micaceous soils.

Table 8. The confirmation test result for M10.

Table 1. Physical and mechanical properties of the mixtures of soils.

Properties	Value/Description	Standard designation
Specific gravity (soil), G_s[S]	2.71	ASTM D854–14
Grain–size distribution		
Clay (< 2 μm) (%)	53	ASTM D422–07
Silt (2–75 μm) (%)	46	
Fine Sand (0.075–0.425 mm) (%)	1	
Consistency limits and classification		
Liquid limit, w_L (%)	44	AS 1289.3.9.1–15
Plastic limit, w_P (%)	22	AS 1289.3.2.1–09
Plasticity index, I_P (%)	31	AS 1289.3.3.1–09
USCS classification	CH[†]	ASTM D2487–11
Compaction characteristics		
Optimum water content, w_{opt} (%)	25.2	ASTM D698–12
Maximum dry unit weight, γ_{dmax} (kN/m^3)	14.6	

Note: [†]clay of high plasticity.

Table 2. The physical and chemical composition of ground mica (as provided by the supplier).

Properties	Value/Description
Basic/Physical properties	
Specific gravity (mica), G_s^M	2.80
Particle diameter D_{90} (μm)	53.60
Appearance	Fine (< 75 μm) white powder
Hardness (Mohs)	2.50
Oil absorption (ml/100 g)	36.00
Water content, w (%)	0.41
Acidity, pH	7.80
Chemical formulation	$K\{Al_2[AlSi_3O_{10}](OH)_2\}$
Major chemical composition	
Al_2O_3 (%)	29.17
CaO (%)	0.38
Fe_2O_3 (%)	4.62
K_2O (%)	8.85
MgO (%)	0.67
Na_2O (%)	0.45
SiO_2 (%)	49.53
TiO_2 (%)	0.83

Table 3. The physical and chemical composition of GBFS (as supplied by the manufacturer).

Properties	Value/Description
Basic/Physical properties	
Specific gravity, G_s^{GBFS}	2.87
Fine fraction [< 75 μm](%)	96
Coarse fraction [0.074-4.75mm]	4
Specific surface area, *SSA* (m^2/g)	0.7
Water content, *w* (%)	<1
Acidity, pH	9.6
Loss on ignition, LOI [at 1000 ºC] (%)	< 3
Main chemical composition	
CaO (%)	44.7
SiO_2 (%)	27.1
Al_2O_3 (%)	13.6
MgO (%)	5.1
Fe_2O_3 (%)	3.5
TiO_2 (%)	1.7
K_2O (%)	0.7
Na_2O (%)	0.2

Table 4. The physical and chemical composition of polypropylene fiber (as given by the distributor).

Properties	Value
Physical/mechanical properties	
Fiber type	Single fiber
Specific gravity, G_s^F	0.94
Length, *FL* (mm)	10
Diameter, *FD* (μm)	20–30
Aspect ratio, *FAR* = *FL*/*FD*	375–500
Young's modulus (GPa)	2–3
Tensile strength (MPa)	320–400
Tensile elongation at rupture (%)	25

Table 5. Experimental design and corresponding response.

Run	Slag–Fiber System				Slag–Polycom System			
	Mica (A_1: %)	Slag (B_1: %)	Fiber (C_1: %)	UCS (kPa)	Mica (A_2: %)	Slag (B_2: %)	Fiber (C_2: g/l)	UCS (kPa)
1	15	9	0.75	299.12	15	9	0.3	313.42
2	15	9	0.25	240.26	0	15	0.1	370.75
3	30	3	0.25	80.54	0	15	0.5	480.30
4	15	9	0.75	299.12	30	9	0.3	247.44
5	0	15	1.25	560.87	0	9	0.3	336.74
6	0	9	0.75	325.69	15	3	0.3	204.83
7	15	15	0.75	462.51	15	9	0.3	313.42
8	15	9	0.75	299.12	15	9	0.3	313.42
9	15	3	0.75	170.01	30	3	0.5	98.13
10	15	9	1.25	332.74	0	3	0.5	136.64
11	0	3	1.25	185.83	15	9	0.3	313.42
12	30	9	0.75	228.55	15	9	0.3	313.42
13	15	9	0.75	299.12	15	9	0.1	199.47
14	15	9	0.75	299.12	15	15	0.3	486.11
15	30	15	1.25	358.09	0	3	0.1	107.93
16	0	15	0.25	395.35	15	9	0.3	313.42
17	15	9	0.75	299.12	30	3	0.1	76.35
18	30	3	1.25	120.98	15	9	0.5	256.67
19	30	15	0.25	290.74	30	15	0.1	279.12
20	0	3	0.25	115.20	30	15	0.5	376.75

Table 6. Statistical factors for the stabilization system models.

Statistical factors	Response models	
	Slag-fiber system	Slag-Polycom system
R^2	0.9966	0.9989
Adj-R^2	0.9936	0.9979
SD	0.048	0.032
CV	3.28	1.92
P value (prob > ***F***)	<0.0001	<0.0001

Table 7. Optimum additive ratios and responses for micaceous soils.

Results						
Mica (%)	UCS (kPa)	Target UCS (kPa)	Slag (%)	Fiber (%)	Polycom (g/l)	Desirability
0	101.93	446.93	11.68	1.25	/	0.890
0	101.93	446.93	11.79	1.20	/	0.887
0	101.93	446.93	12.80	/	0.35	0.854
0	101.93	446.93	12.79	/	0.38	0.852
10	83.41	428.41	11.96	1.25	/	0.883
10	83.41	428.41	12.056	1.19	/	0.880
10	83.41	428.41	12.71	/	0.35	0.860
10	83.41	428.41	12.75	/	0.38	0.859
20	66.33	411.33	12.63	1.30	/	0.853
20	66.33	411.33	12.65	1.30	/	0.853
20	66.33	411.33	12.81	/	0.35	0.856
20	66.33	411.33	12.53	/	0.38	0.853
30	54.04	399.04	12.90	1.30	/	0.761
30	54.04	399.04	12.88	1.24	/	0.761
30	54.04	399.04	13.001	/	0.350	0.809
30	54.04	399.04	13.378	/	0.374	0.806

Table 8. The confirmation test result for M10.

Run	Additives				Results	
Solutions	Mica (%)	Slag (%)	Fiber (%)	Polycom (g/l)	UCS (kPa)	Desirability
Optimization	10	11.96	1.25	/	428.41	0.883
Test	10	11.96	1.25	/	446.10	
UCS difference					17.69	
Optimization	10	12.71	/	0.35	428.41	0.860
Test	10	12.71	/	0.35	455.91	
UCS difference					27.50	

List of Figures

Figure 1. Predicted UCS values versus actual UCS measurements for (a) slag–fiber stabilized micaceous soil samples, and (b) slag–polymer stabilized micaceous soil samples.

Figure 2. 3D response surface plots for the interactive effect of the constituents on UCS at constant additive proportions: (a) fiber = 0.75%, (b) slag = 9%, and (c) mica = 15%.

Figure 3. 3D response surface plots for the interactive effect of variables on UCS at constant additive proportions: (a) Polycom = 0.3 g/l, (b) slag = 9%, and (c) mica = 15%.

Figure 1. Predicted UCS values versus actual UCS measurements for (a) slag–fiber stabilized micaceous soil samples, and (b) slag–polymer stabilized micaceous soil samples.

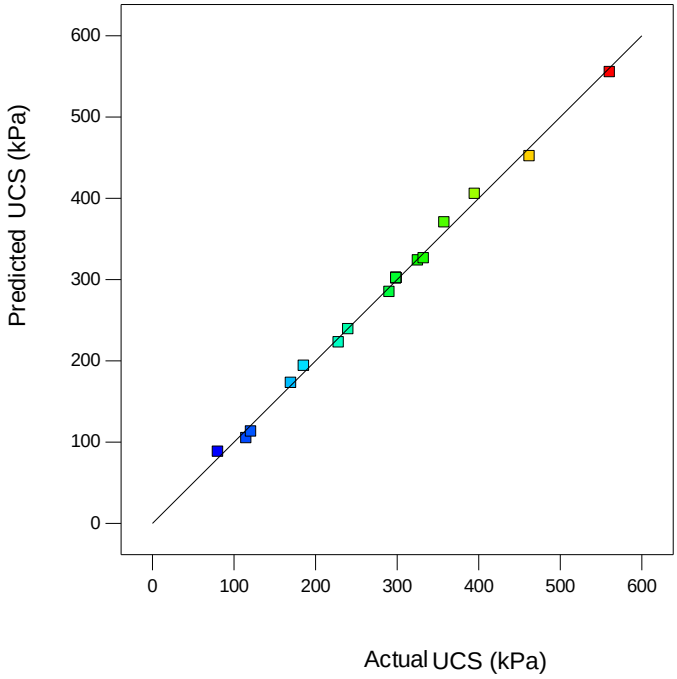

(a)

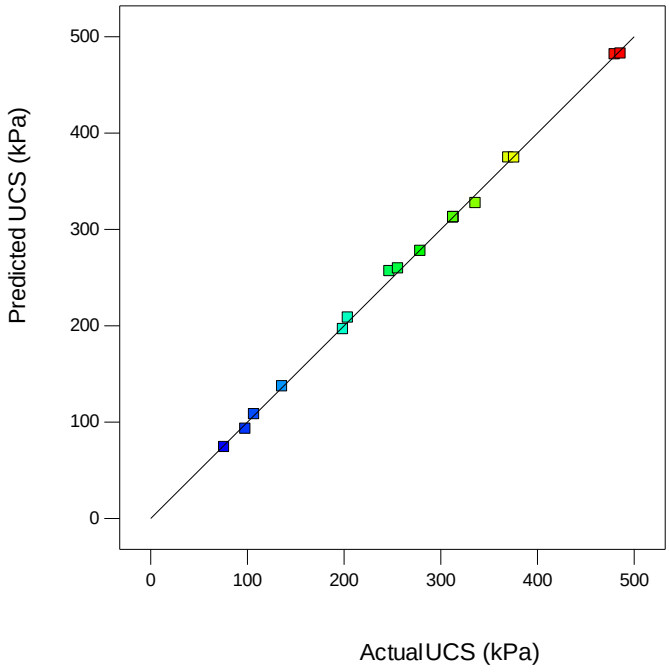

(b)

Figure 2. 3D response surface plots for the interactive effect of the constituents on UCS at constant additive proportions: (a) fiber = 0.75%, (b) slag = 9%, and (c) mica = 15%.

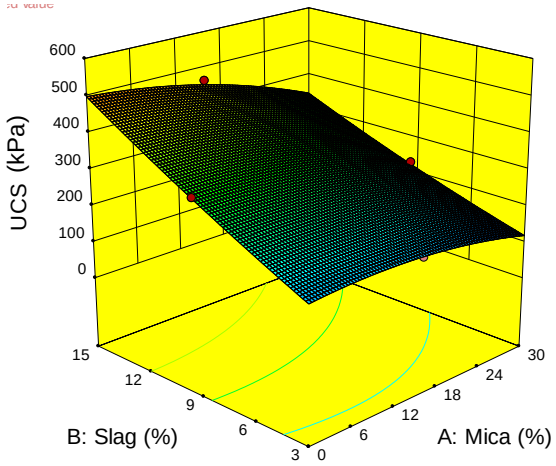

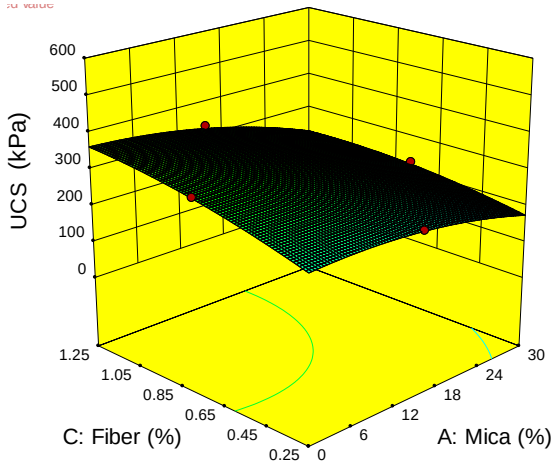

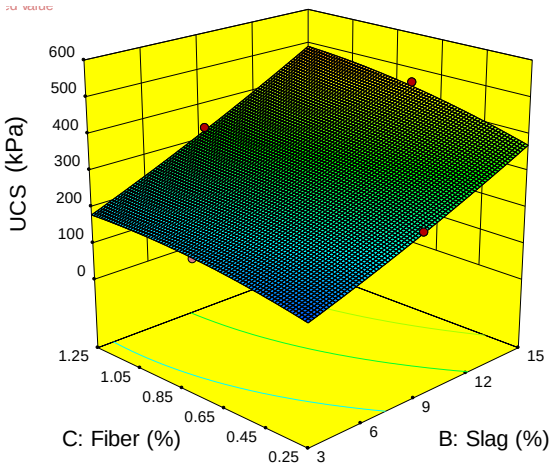

Figure 3. 3D response surface plots for the interactive effect of variables on UCS at constant additive proportions: (a) Polycom = 0.3 g/l, (b) slag = 9%, and (c) mica = 15%.

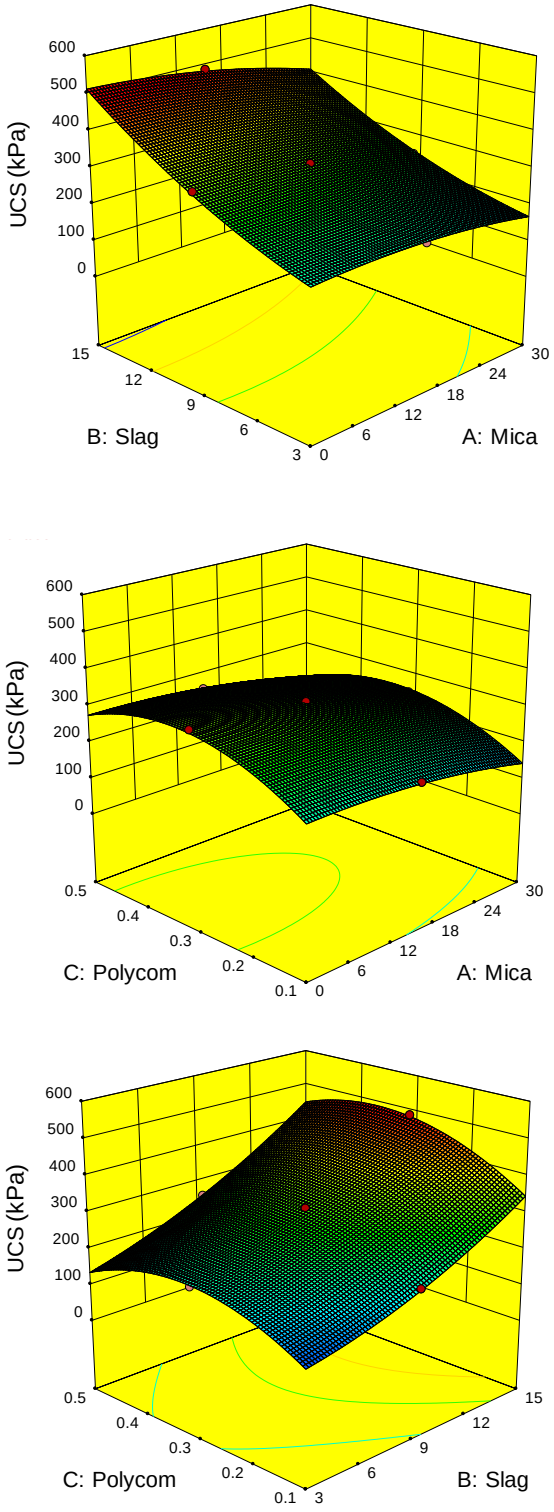

Statement of Authorship

Title of Paper	Optimization of slag and fiber/polymeric agent to reinforce micaceous soils using response surface methodology
Publication Status	☐ Published ☐ Accepted for Publication ☐ Submitted for Publication ■ Unpublished and Unsubmitted work written in manuscript style
Publication Details	**Zhang J**, Deng A, Jaksa M **(2019)** Optimization of slag and fiber/polymeric agent to reinforce micaceous soils using response surface methodology, x(x):x-x, http://doi.org/x

Principal Author

Name of Principal Author (Candidate)	Jiahe Zhang (**Email**: Jiahe.Zhang@adelaide.edu.au)		
Contribution to the Paper	Overall paper preparation		
Overall percentage (%)	85%		
Certification:	This paper reports on original research I conducted during the period of my Higher Degree by Research candidature and is not subject to any obligations or contractual agreements with a third party that would constrain its inclusion in this thesis. I am the primary author of this paper.		
Signature		Date	01/05/2019

Co-Author Contributions

By signing the Statement of Authorship, each author certifies that:

i. the candidate's stated contribution to the publication is accurate (as detailed above);
ii. permission is granted for the candidate in include the publication in the thesis; and
iii. the sum of all co-author contributions is equal to 100% less the candidate's stated contribution.

Name of Co-Author	An Deng **Senior Lecturer**, School of Civil, Environmental and Mining Engineering, The University of Adelaide, Adelaide, SA 5005, Australia (**Email**: An.Deng@adelaide.edu.au)		
Contribution to the Paper	Methodology, paper review and revision		
Signature		Date	1/05/2019

Name of Co-Author	Mark Jaksa **Professor**, School of Civil, Environmental and Mining Engineering, The University of Adelaide, Adelaide, SA 5005, Australia (**Email**: Mark.Jaksa@adelaide.edu.au)		
Contribution to the Paper	Paper review and revision		
Signature		Date	2/05/2019